Analytical Solutions for some Chemical Transport Processes in Porous Media

Alexandros Viktor Angelos Stamatiou, MSci

Submitted for the degree of Doctor of Philosophy.

Heriot-Watt University
Institute of Petroleum Engineering
August 2018

Abstract

Flow and transport through porous media is applicable in many areas of industrial and geoscientific importance, e.g. flow through packed bed reactors in chemical engineering, reactive transport in porous membranes in biology, flow of chemicals through porous rocks in enhanced oil recovery (EOR) and in chemical treatments. Most mathematical models for the transport of chemicals in porous media are formulated as systems of several partial differential equations. Very often, these systems are so complex that they can only be solved numerically and, in general, analytical solutions to these equations cannot be found. In this thesis, we will examine two models for which analytical solutions are available. The first of these is the well-known polymer flood model in enhanced oil recovery, which describes the displacement of oil by polymer-enriched water. An analytical solution for this problem exists in the literature in the form of a "solution algorithm". In this work, we have applied this algorithm to reveal all possible solution profiles that can occur under certain assumptions, which the original authors of the algorithm did not present. However, the main emphasis of this PhD thesis lies in the construction of analytical solutions to several (simplifications of) models describing the transport of scale inhibitor in oil reservoirs. These chemicals are employed to slow down the formation and deposition of mineral scale. The most complex model considered here assumes both kinetic precipitation/dissolution and kinetic adsorption/desorption of scale inhibitor into an aqueous phase flowing at constant velocity. This general model consists of a system of three partial differential equations and must be solved numerically, but there are two important sub-cases for which analytical solutions can be found. The first of these only considers the kinetic precipitation mechanism. The second, much more complicated case assumes kinetic precipitation together with equilibrium adsorption. Both problems consist of two first-order partial differential equations relating the mobile phase concentration (C) and the amount of scale inhibitor precipitate (Π). The central idea for the construction of analytical solutions is the existence of an "invariant" relationship between C and Π. Together with the method of characteristics, this relationship enables us to build solution profiles consisting of several different regions. A key feature of these profiles is the motion

of a boundary point, $x = \alpha_{\Pi}(t)$, which divides the domain into a region where there is precipitate ($\Pi > 0$) and a region where the precipitate has been completely used up by the dissolution process ($\Pi = 0$). The velocity of this boundary point in relation to the concentration flux velocity is of importance when determining the corresponding concentration level. Knowledge of C on the boundary is another essential building block in the development of the solution. In treating the various cases, a powerful solution method emerges which may be applicable to the analysis of other chemical transport models in which one of the unknown quantities can be completely depleted, thereby altering the underlying system of first-order partial differential equations. It appears that this work is the first in which this solution methodology has been brought to bear on this type of internal moving boundary problem; it has certainly never been applied in any problem in oilfield chemistry or enhanced oil recovery.

Dedication

For my beloved mother, Andrea Elisabeth Stamatiou-Von Ilsemann.

Acknowledgements

I would like to express enormous gratitude to my advisor, Professor Ken Sorbie, for his continuous commitment and belief in my work throughout these years. This academic and personal journey would not have been possible to complete without his invaluable guidance. I would also like to thank Clariant Oil Services for introducing me to Professor Sorbie and for providing funding towards the research. Finally, I want to mention Heriot Watt University for granting me the opportunity to study there and my fiancee, parents and friends for their unwavering support.

Contents

Chapter 1

Introduction

Chemical transport processes in porous media occur in a range of geological and industrial settings, such as enhanced oil recovery (EOR) in petroleum reservoirs, the movement of fluids in aquifers and in packed bed reactors in chemical engineering. All of these applications rely on the formulation of accurate mathematical models describing the governing physical processes. Typically, these models consist of one or more partial differential equations (PDE). These are often difficult or impossible to solve analytically and numerical methods must be employed to describe the evolution of the models. In this PhD, we mainly focus on understanding the transport of a chemical scale inhibitor in an oil reservoir. The set of equations modelling this process will be simplified to the extent that analytical solutions can be found. Essential mathematical concepts such as the method of characteristics, weak solutions and shock conditions will be outlined in Chapter 2, along with a brief discussion of the numerical methods employed in this work.

A major problem for the petroleum industry is the formation and deposition of scale minerals on the downhole equipment and reservoir rock surfaces in contact with formation brine. The most common scaling substances are calcium carbonate ($CaCO_3$), calcium sulphate ($CaSO_4$) and barium sulphate ($BaSO_4$). Precipitation of these salts occurs when their concentration exceeds their solubility in the formation brine. Causes for this supersaturation include evaporation of water, a reduction in temperature and the mixing of different waters during production ([1], [2]). The salt particles (crystals) accumulate on the tubing and in the pore spaces of the near-wellbore formation and thereby cause a significant reduction in volumetric

flow rates. This results in a rapid decline of oil production, which is illustrated in Figure 1.1 for an oil field in Prudhoe Bay, Alaska ([3]). One-off chemical treatments to clean the well can restore productivity, but often only for a short period of time. For a more permanent resolution of the problem, the well is treated with scale inhibitors. These chemicals prevent the formation of scale crystals at the nucleation stage. Scale inhibitor concentrations of as small as 5ppm can already be sufficient to accomplish this ([4]).

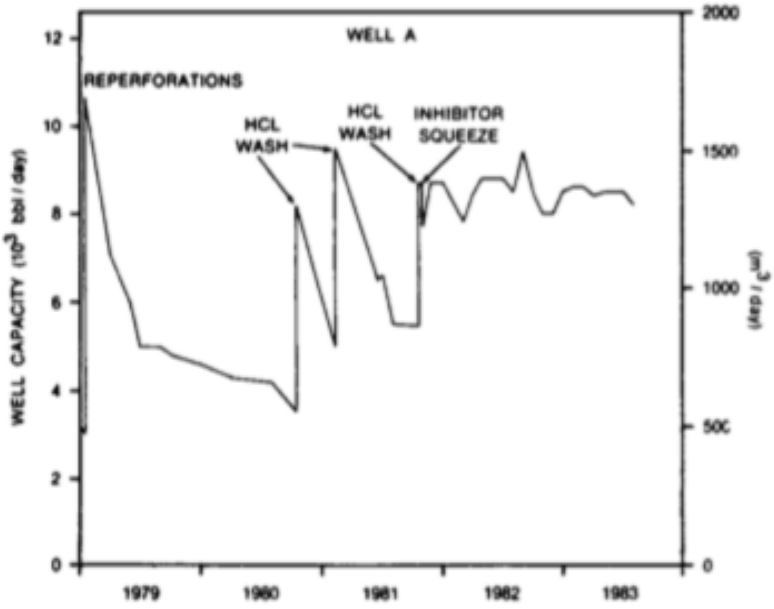

Figure 1.1: *Plot showing decline in oil production at the Prudhoe Bay field due to scale deposition. Scale inhibitor treatments restore productivity levels more permanently then one-off well-cleaning treatments.*

For the scale inhibitor (SI) to be effective in reducing scale problems, it must be present inside the pore spaces of the rock formation surrounding a producing well. This is achieved in a so-called scale inhibitor squeeze treatment ([5], [6]). A schematic of this procedure is shown in Figure 1.2. Production is brought to a hold and a scale inhibitor solution is injected into the well. It is then pushed out further into the nearby formation by an overflush with water containing no scale inhibitor. After this, the well is shut-in for a period of time to allow the scale inhibitor to "settle" inside the pore spaces. It is widely agreed that the scale inhibitor is retained in the rock formation by the two main mechanisms of adsorption and precipitation. When production is re-started following the shut-in, the SI chemical then desorbs or dissolves into the aqueous phase (formation brine) at a concentration which is

sufficient to prevent the formation of scale crystals (threshold concentrion). Ideally, the desorption/dissolution is a slow process as this will increase the lifetime of a squeeze treatment and hence minimise costs.

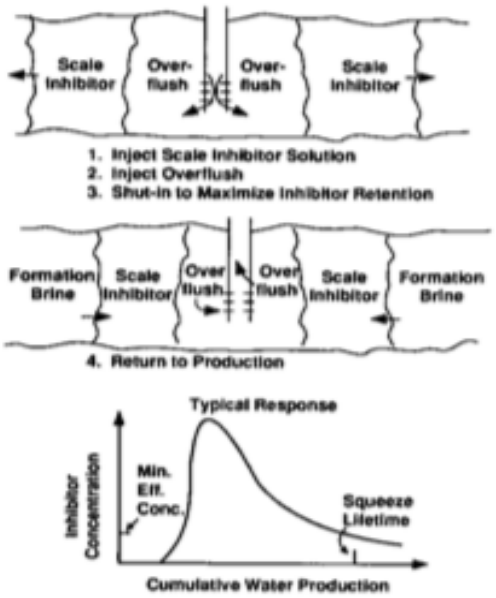

Figure 1.2: *Schematic of a SI squeeze treatment in the field.*

In order make field predictions and optimise a squeeze treatment, mathematical models are extremely useful. The development of such models requires a correct description of the adsorption/desorption and precipitation/dissolution processes encountered in oil reservoirs. *Adsorption* is said to take place if the scale inhibitor molecules in the liquid phase pass onto a surface. Desorption is the reverse process by which the molecules are released from the surface back into the liquid phase. Both mechanisms occur simultaneously and, away from equilibrium, the rates of adsorption and desorption are different. In such a *kinetic* process, the *net adsorption rate* and consequential change in concentration of the scale inhibitor can be modelled by the following pair of rate laws ([7], [8], [9],[10]):

$$\frac{d\Gamma}{dt} = r_a \left[\Gamma_{eq}(C(t)) - \Gamma(t)\right] \tag{1.1}$$

$$\frac{dC}{dt} = -\frac{1-\phi}{\phi}\frac{d\Gamma}{dt} \tag{1.2}$$

Here, ϕ is the porosity of the rock (fraction of rock-volume), r_a an adsorption rate

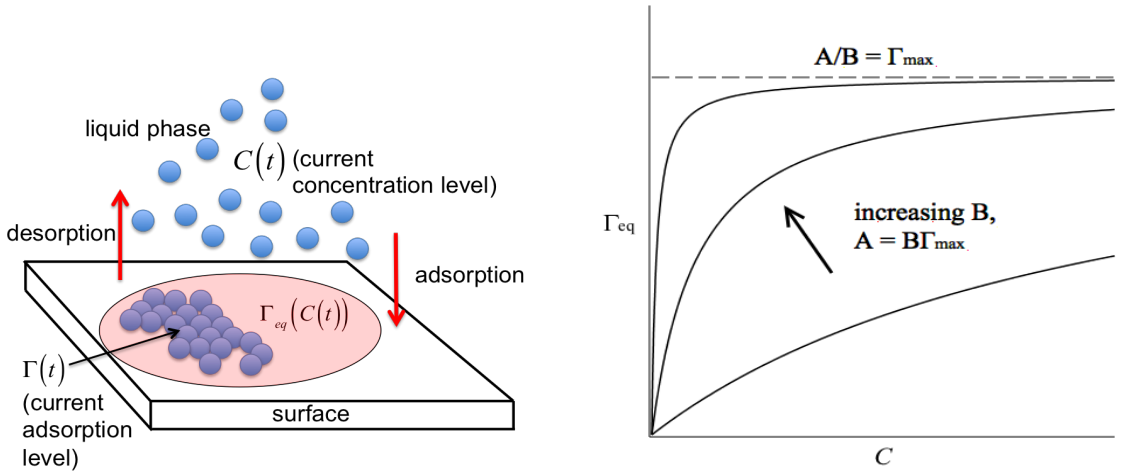

Figure 1.3: *Schematic of the adsorption/desorption process (left) and plots of the Langmuir isotherm (right) for different values of the parameter B.*

constant (in s^{-1}), $\Gamma(t)$ is the current level of adsorption and $C(t)$ is the current concentration level (both expressed in ppm). Furthermore, the function $\Gamma_{eq}(C)$ is the adsorption isotherm, an expression which (under constant temperature) tells us what the adsorption level *would be* if $C(t)$ were the equilibrium concentration level (i.e. if $d\Gamma/dt = 0$). Figure 1.3 shows a schematic of the situation at time t, where $\Gamma(t) < \Gamma_{eq}(C(t))$ and hence $d\Gamma/dt > 0$. In this scenario, adsorption prevails as the inhibitor molecules in the liquid phase are pushed to occupy the number of vacant sites predicted by the isotherm. On the other hand, desorption dominates ($d\Gamma/dt < 0$) if the number of adsorbed molecules exceeds the predicted available space. Given enough time, the system will always come to equilibrium, so that $\Gamma = \Gamma_{eq}(C)$ eventually. More complex kinetic rate laws than equations (1.1)-(1.2) can be proposed ([11]) and it largely depends on the specific circumstances (type of rock, scale inhibitor, etc.) which formulation is more applicable. Another matter of debate is the correct form of the adsorption isotherm itself. Many different theoretical expressions for $\Gamma_{eq}(C)$ exist, ranging from simple one-parameter linear models to generalised Langmuir-type isotherms having five parameters ([12]). In the vast majority of the literature on oilfield scale inhibitors, the two-parameter Freundlich and Langmuir isotherms are employed, but sometimes it becomes necessary to use a combination of isotherms reflecting the mixed mineral composition of the rock. In this work, we will assume a Langmuir-type adsorption/desorption process, where the isotherm is of the form

$$\Gamma_{eq}(C) = \frac{AC}{1 + BC} \tag{1.3}$$

The ratio $A/B = \Gamma_{max}$ is the adsorption capacity of the rock. Keeping this constant and increasing B results in a steeper isotherm (see Figure 1.3). Significant levels of adsorption then occur already at relatively low equilibrium concentrations.

Precipitation of scale inhibitor from the liquid phase occurs through the formation of a sparingly soluble calcium / inhibitor complex, which is then retained in the pore spaces as an actual solid or separate gel-like liquid. This process has been modelled using a solubility product ([13], [14], [15]), which relates the precipitation level Π to the concentrations of the individual components (calcium and scale inhibitor) in the aqueous phase. A simpler model that is frequently used ([16], [17]) asserts that the rate of precipitation depends on the scale inhibitor concentration as follows:

$$\frac{d\Pi}{dt} = -\kappa \left[C_s - C\right] \cdot \left[H\left(\Pi\right) + H\left(C - C_s\right) - H\left(\Pi\right) H\left(C - C_s\right)\right] \tag{1.4}$$

$$\frac{dC}{dt} = -\frac{d\Pi}{dt} \tag{1.5}$$

In equation (1.4), κ is the dissolution rate constant (in s^{-1}), which is related to temperature via the Arrhenuis equation ([18]). The scale inhibitor solubility C_s generally depends on field conditions such as temperature and pH ([19]), but here we will simply assume that there is a critical temperature T_{cp} such that C_s is infinite for $T < T_{cp}$ and constant for $T \geq T_{cp}$. The combination of the Heaviside step functions $H\left(\Pi\right)$, $H\left(C - C_s\right)$ in the rate equation ensures that (i) precipitation can only take place if $C > C_s$ and (ii) *no* dissolution takes place if $\Pi \leq 0$.

The two retention mechanisms must now be embedded in a transport equation for flow in porous media. Before any field predictions are made, a mathematical model is tested against data obtained from coreflood experiments in which the field conditions are simulated. In such an experiment, a rock-core of length L (cm), cross-sectional area A (cm^2) and porosity ϕ is saturated with a solution containing scale inhibitor at some concentration $C = C_i$ (see Figure 1.4). If the temperature is raised above T_{cp} and if $C_i > C_s$, a scale inhibitor precipitate forms. At the same time, scale inhibitor adsorption/desorption takes place in accordance with equation (1.1).

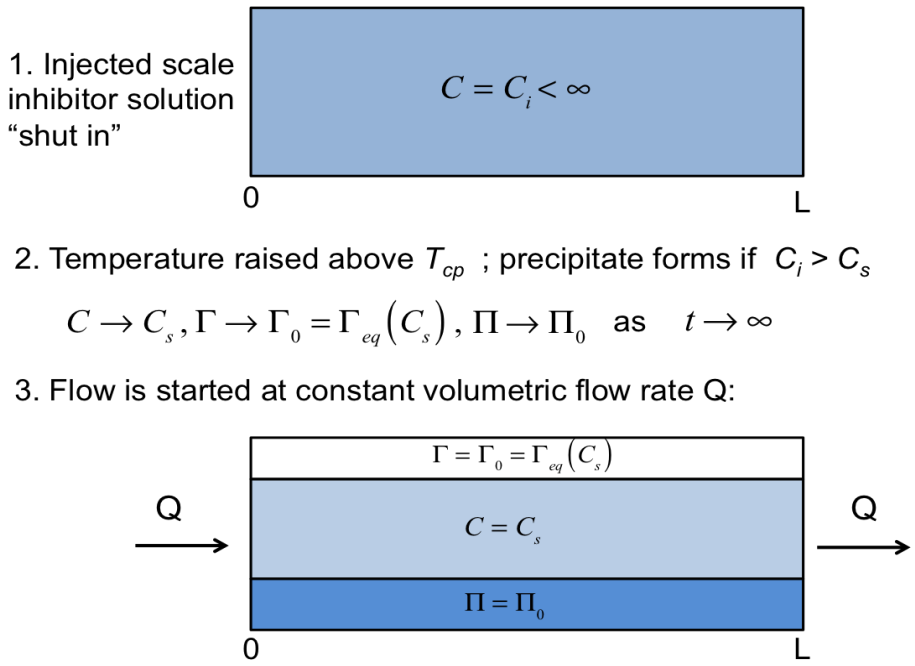

Figure 1.4: *Illustration of the consecutive stages in a core-flood experiment*

The interaction of these processes eventually leads to an equilibrium situation where $d\Gamma/dt = d\Pi/dt = 0$. Throughout the core, the levels of concentration, adsorption and precipitation then are $C = C_s$, $\Gamma = \Gamma_0 = \Gamma_{eq}(C_s)$ and $\Pi = \Pi_0$, where Π_0 to some extent depends on the injected concentration C_i. After a shut-in period during which this equilibrium is reached, water containing no scale inhibitor (i.e. $C = 0$) is injected into the core at a steady volumetric flow rate Q $(cm^3 s^{-1})$. This translates into a constant horizontal fluid velocity $v = Q/A\phi$ $(cm\ s^{-1})$. Assuming isothermal conditions and homogenous adsorption/precipitation properties throughout the rock core, equations (1.1), (1.2), (1.4) and (1.5) can be combined with the one dimensional advection-dispersion equation to describe the flow stage:

$$\frac{\partial C}{\partial t} + v\frac{\partial C}{\partial x} = D\frac{\partial^2 C}{\partial x^2} - \frac{\partial \Pi}{\partial t} - \frac{1-\phi}{\phi}\frac{\partial \Gamma}{\partial t} \tag{1.6}$$

$$\frac{\partial \Pi}{\partial t} = -\kappa\left[C_s - C\right] \cdot \left[H\left(\Pi\right) + H\left(C - C_s\right) - H\left(\Pi\right) H\left(C - C_s\right)\right] \tag{1.7}$$

$$\frac{\partial \Gamma}{\partial t} = r_a\left[\Gamma_{eq}(C) - \Gamma\right] \tag{1.8}$$

The unknowns C, Π, Γ are now functions of both x and t. In this formulation, D is the dispersion/diffusion coefficient, which is a measure of the extent to which molecules tend to diffuse from areas of high concentration to areas of low

concentration. This happens in both directions and, broadly speaking, causes the solution to "smooth out". The rock core can be represented mathematically by the domain $\Omega := \{(x,t) \in \mathbb{R}^2 : 0 \leq x \leq L, t \geq 0\}$ with U-shaped boundary $\partial\Omega := \{t = 0\} \cup \{x = 0\} \cup \{x = L\}$. In order to solve equations (1.6)-(1.8) on Ω, we need initial/boundary conditions on $\partial\Omega$. For the situation shown in Figure 1.4, we have

$$C(x,0) = C_s \ , \ \Pi(x,0) = \Pi_0 \ , \ \Gamma(x,0) = \Gamma_{eq}(C_s) \tag{1.9}$$

Furthermore, we will demand that

$$C = 0 \text{ at } x = 0 \quad \text{and} \quad \frac{\partial C}{\partial x} = 0 \text{ at } x = L \quad \text{for} \quad t > 0 \tag{1.10}$$

The first boundary condition in equation (1.10) reflects the physical assumption that the concentration at the inlet ($x = 0$) drops to zero immediately after the flow with fresh water ($C = 0$) is started and remains so for all time. The second condition implies zero concentration gradient across the exit boundary.

Having established this linear model for scale inhibitor transport, we now begin to investigate to what extent equations (1.6)-(1.10) can be solved analytically. The first simplification will be to assume that adsorption/desorption is an *equilibrium process*, for which $r_a \to \infty$. That is, for a given mobile phase concentration $C(x,t)$, the adsorption level instantaneously becomes $\Gamma(x,t) = \Gamma_{eq}(C(x,t))$. Then, by the chain rule, $\partial\Gamma/\partial t = \Gamma'_{eq}(C)\partial C/\partial t$ and the system of three equations reduces to a system of two equations:

$$\left[1 + \frac{1-\phi}{\phi}\frac{d\Gamma_{eq}}{dC}\right]\frac{\partial C}{\partial t} + v\frac{\partial C}{\partial x} = D\frac{\partial^2 C}{\partial x^2} - \frac{\partial \Pi}{\partial t} \tag{1.11}$$

$$\frac{\partial \Pi}{\partial t} = -\kappa\left[C_s - C\right] \cdot \left[H\left(\Pi\right) + H\left(C - C_s\right) - H\left(\Pi\right)H\left(C - C_s\right)\right] \tag{1.12}$$

In a pure precipitation process ($\Gamma_{eq} = 0$), the advection-dispersion equation (1.11) becomes linear and has a source term $\kappa\left(C_s - C\right)$ if $C < C_s$ and $\Pi > 0$, a sink term $-\kappa\left(C_s - C\right)$ if $C > C_s$ (independent of Π) and no sink/source if $C = C_s$ or $C < C_s$ and $\Pi \leq 0$. As shown in [20], all these variants of equation (1.11) have analytical solutions satisfying the conditions given by equations (1.9)-(1.10). More complicated problems, in which the coefficients are functions of x and t, can also be solved

analytically (e.g. [21], [22]). In general, these solutions have much simpler forms if a semi-infinite domain is considered ($L \to \infty$), as this does not involve superposition of solutions due to reflection at the exit boundary. For this reason, analytical solutions on the finite domain are often derived by extending it to a semi-infinite domain and translating the boundary condition from $x = L$ to $x = \infty$. Next to the advantage of obtaining simpler algebraic expressions, this also removes the necessity of specifying the solution at $x = L$ in situations where it is unclear what the correct physical assumptions should be.

Although analytical solutions are available in the linear case that arises for pure precipitation, the formulas are very complex. To find $\Pi(x, t)$ using equation (1.12), these expressions need to be integrated. Moreover, if, during a dissolution process ($C < C_s$), there is some region of Ω in which $\Pi = 0$, the source term disappears and we have to deal with different second order equations in different regions. In order to gain an understanding of the interaction between such sub-domains, we will make a further simplification by setting $D = 0$ (no dispersion), which turns equations (1.11) and (1.12) into a pair of first order quasilinear PDEs. The theory for such equations is outlined in Chapter 2, where we introduce the method of characteristics and the notion of a weak solution. Then, in Chapter 3, we solve the case with $\Gamma_{eq} = 0$ (no adsorption). This is quite straightforward while $\Pi > 0$. The resulting transport equation with constant coefficients and a source term has a well-known general solution and this is specified using equation (1.9) and the first boundary condition in equation (1.10). However, the problem becomes more complicated when the uniform layer of precipitate initially present in the system begins to "run out". This first happens at the inlet ($x = 0$) and leads to the emergence of a moving boundary point (denoted α_Π), which divides the interval $0 \leq x \leq L$ into a region where $\Pi = 0$ and a region where $\Pi > 0$. The velocity of this boundary, $d\alpha_\Pi/dt$, is *constant* and *lower* than the fluid velocity v and it can be derived by assuming the invariance of a certain relationship between the unknowns C and Π. Since the boundary moves slower than the fluid, it can be inferred that $C = 0$ at $x = \alpha_\Pi(t)$, which constitutes a boundary condition for the specification of a new analytical solution in the $\Pi > 0$ region. With constant boundary velocity, this new solution is a travelling wave, which is joined to the previously existing solution to form a composite solution consisting of several analytical components. As we shall

see later, the whole procedure is best understood in terms of characteristic curves on Ω and a (straight-line) boundary curve dividing Ω into the sub-domains Ω_+ (where $\Pi(x,t) > 0$) and Ω_0 (where $\Pi(x,t) = 0$).

Chapter 4 addresses the same set of equations as Chapter 3, but the assumption of a constant flow rate (fluid velocity) is relaxed. We will look at a problem without adsorption ($\Gamma_{eq} = 0$), constant initial data and the addition of a shut-in phase $t_1 \leq t < t_2$ during which flow is halted (i.e. $v = 0$). The constant fluid velocities v_1, v_2 before and after the shut-in phase are allowed to be different. Such processes are often performed in core-flooding experiments and, as such, exact solutions are a valuable tool for design and prediction purposes. It is also possible to choose velocities of different sign to model what is happening during a squeeze treatment in the field, when the outward flow in the placement stage is opposite to the inward flow in the production stage. However, for illustrative purposes we will assume here that $v_1 > 0$, $v_2 > 0$. As before, the finite amount of precipitate will begin to run out at the inlet, resulting in the moving boundary point α_Π, the trajectory of which separates the domains Ω_+ and Ω_0. Due to the shut-in period and the degree of freedom in the choice of velocities, this boundary curve is no longer a straight line. In fact, we can have $d\alpha_\Pi/dt > v$ in some area of Ω and $d\alpha_\Pi/dt \leq v$ in another. We will see how this velocity (and therefore the boundary curve itself) arises as a result of an "invariant" relationship together with knowledge of C on the boundary. A constant interaction between Ω_+ and Ω_0 takes place. The boundary curve $x = \alpha_\Pi(t)$ is *formed* by the solutions in two domains, while at the same time it *defines* these solutions. Six main cases will be identified. One of these cases is worked out in complete detail and it will be shown explicitly that the resulting "hand-built", composite solution satisfies mass balance.

The analysis of the shut-in problem in Chapter 4 motivates the solution for the pure precipitation problem with constant fluid velocity v and *arbitrary* initial data $C(x,0) = C_s(x)$, $\Pi(x,0) = \Pi_0(x)$. Such conditions may arise as a result of an uneven initial concentration distribution $C_i(x)$ (see Figure 1.4) at the placement stage and/or a short shut-in period. Generalising the contents of Chapter 3 in this way, the existence of an invariant relationship is precisely explained and proved in section 4.8. The theoretical construction of the solution is also discussed here.

In Chapter 5 we widen the discussion and consider the coupled precipitation / equilibrium adsorption problem. As in Chapter 3, we assume a single constant fluid velocity v and initial/boundary conditions given by equations (1.9) and (1.10). If $\kappa = 0$ (no precipitation/dissolution occurs), equations (1.11)-(1.12) reduce to a quasilinear, homogenous PDE. Such equations can be solved easily using the method of characteristics. Depending on the initial/boundary conditions and the nature of the coefficients, the solution typically consists of a combination of constant states, rarefaction waves and shock waves (see Chapter 2 and Appendix A). With equations (1.9)-(1.10) providing the data and the Langmuir isotherm defined by equation (1.3), the solution of equation (1.11) is a single rarefaction wave between the two constant states $C = 0$ and $C = C_s$. However, the problem is much harder if $\kappa \neq 0$, due to the resulting non-homogeneity of the equation when $\Pi > 0$. A complete explicit or even implicit solution is not available in this case, but it will be shown that the evolution of the system may be described in an original way by the introduction of an auxiliary parameter. Inspired by the discussion in previous chapters, the idea of an invariant relationship between the unknowns is also pursued here. Once the precipitate begins to run out, this relation will allow us to determine the motion of the boundary point α_Π and hence construct a composite solution on the entire domain. Three qualitatively different cases can be identified, depending on the initial level of precipitate Π_0 in relation to the solubility C_s and the adsorbed quantity $\Gamma_0 = \Gamma_{eq}(C_s)$. Two of these cases are characterised by a long "adsorption tail", which is often observed in experimental data. Thus, the analytical solution developed in this chapter can serve as a valuable tool for making predictions about the lifetime of the squeeze treatments simulated in the rock-core (see the discussion in section 6.2). As mentioned before in the case of pure precipitation, it may also be desirable to extend the scope of the precipitation/adsorption problem to include arbitrary initial data. This turns out to be relatively straightforward for an arbitrary initial precipitate distribution $\Pi_0(x)$, but is a more complex issue for an initial concentration distribution $C_s(x)$.

For the purpose of making field predictions, equations (1.6)-(1.8) must be put into a form that applies to an isotropic, radial model around a producing well (see Figure 1.5). The near-well region in which the scale inhibitor is placed can be represented

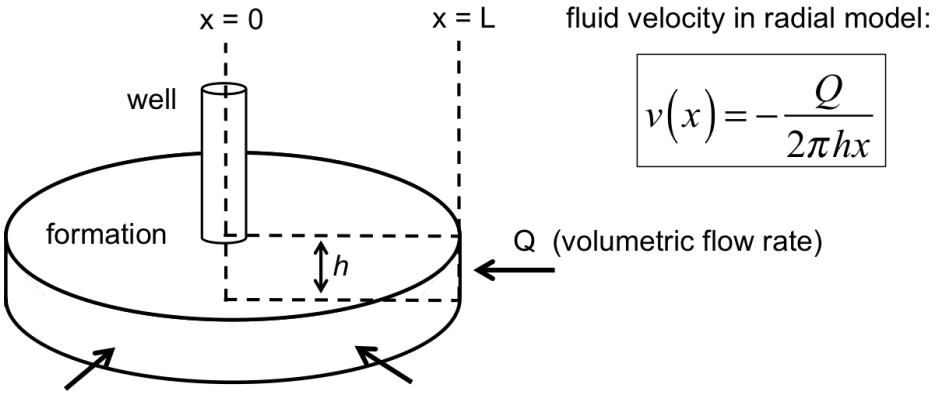

Figure 1.5: *Schematic of the scale inhibitor region around a producing well.*

as a disc of thickness h and radius L. As before in the linear model, the formation rock is assumed to be homogenous and there is no vertical flow or variation in the concentration, precipitation and adsorption. Fresh water ($C = 0$) is injected from surrounding injector wells and flows towards the producing well at volumetric flow rate Q. The schematic of Figure 1.4 is then obtained by considering a cross-section extending from the centre of the disc. The radial distance from the well is measured by $x \in [0, L]$. For the case with zero dispersion ($D = 0$), the only modification with respect to the linear model equations is the fluid velocity, which now is $v(x) = -Q/(2\pi hx)$. This inward flow requires the boundary condition $C = 0$ to be set at $x = L$. In [23], [24], pure equilibrium adsorption/desorption cases were solved analytically, describing both the placement phase (outward flow) and the subsequent production phase (inward flow). An extension of these solutions to the coupled adsorption/precipitation model is complicated by several factors. Firstly, the uniform initial conditions observed in the core-flood experiment are not necessarily a reflection of reality. During the placement phase in the field (radial model), a scale inhibitor solution is injected and over-flushed with fresh water. Adsorption / precipitation takes place during the flow away from the well and this can result in an uneven distribution of concentration, adsorption and precipitate, even after the system is allowed to equilibrate in a shut-in phase. What is more, the temperature near the well is often too low for precipitation to occur, i.e. $T < T_{cp}$. In typical reservoir conditions, the temperature is higher further away from the well, so that precipitate forms only in a certain region of the radial domain. Even if we were to assume the uniform initial distributions seen in the linear case, the analogous construction of a practical analytical solution to the radial case might well be beyond reach, because of complications in determining the concentration of the boundary

curve $x = \alpha_\Pi(t)$ (this will be become evident in Chapters 4-5). However, the solution of the linear model still tells us a great deal about what is going on in a radial setting. Indeed, the only difference comes from the fact that the monotone increasing velocity causes the solution regions of the linear model to stretch considerably as they come closer to the producing well.

Another approach to solving the Cauchy problems in Chapters 3-5 would be to notice that we are dealing with strictly hyperbolic systems of first-order PDEs for C and Π with eigenvalues 0 and v. These lead to two families of characteristic curves on which the solution can be developed by solving a related system of ordinary differential equations (see section 2.4). The non-homogeneity of these systems and the difficulty in dealing with the discontinuous function H (and the consequential breakdown of the standard theory) makes this a very daunting task. Even if we were to replace H with one of its smooth approximations ([25]), the resulting pair of ordinary differential equations is hard (if not impossible) to solve. For similar reasons, an analytical solution to the sub-case with no precipitation ($\kappa = 0$) and kinetic adsorption ($r_a < \infty$) remains at large, which also implies that there is no analytical solution available for the full system of equations (1.6)-(1.8) with $D = 0$. However, the solutions of the two limiting cases $r_a = 0$ and $r_a \to \infty$ serve as nice reference "boundaries" for numerical solutions of this general system. They also allow us to make some informed guesses about the behaviour of the "true" solution.

In contrast to non-homogenous systems, there is a rich literature for analytical solution techniques of homogenous, strictly hyperbolic systems and in particular for systems of conservation laws. Famous examples include the shallow water equations, the Euler equations for the flow of an incompressible gas and the equations for the chromatography of two solutes ([26]). In Appendix B we look at the EOR-related problem of polymer flooding. In oil reservoirs, water is injected to recover the oil by a frontal displacement mechanism dominated at the macroscopic scale by viscous forces. Two phase water/oil displacement, under certain simplifications, is described in 1D by the well-known Buckley-Leverett equation ([27]-[29]). This displacement is governed by the mobility ratio (M) which depends on the viscosity ratio (μ_o/μ_w). When $\mu_o >> \mu_w$, M is high and this leads to an inefficient frontal displacement of oil by water. To remedy this situation, the injected water phase may

be viscosified by adding a relatively small concentration (typically between 200-2000 ppm) of a polymer ([30]). This process is modelled by a pair of conservation laws relating the normalised water saturation (s) and the polymer concentration (c):

$$\frac{\partial s}{\partial t} + \frac{\partial}{\partial x} f_w(s, c) = 0 \tag{1.13}$$

$$\frac{\partial}{\partial t}[s \cdot c + a(c)] + \frac{\partial}{\partial x}[c \cdot f_w(s, c)] = 0 \tag{1.14}$$

In these equations, $f_w(s, c)$ is the fractional flow of water and $a(c)$ an adsorption isotherm. Under fairly general assumptions about the shape of these functions, Johansen and Winther ([31]) proved existence and uniqueness of a solution of the Riemann problem for the system of equations (1.13)-(1.14). They did so by explicitly constructing solution sequences made up of so-called s-waves (in which c is constant) and c-waves (in which c varies). We will apply their solution algorithm to find all possible solution profiles of the model with a particular fractional flow function. The emphasis here is very much on the calculation of a catalogue of numerical examples. This body of work was carried during my first year of PhD and was very much part of the orientation process.

Chapter 2

Methodolgy

2.1 Introduction

In this chapter we give a brief overview of the theory of first-order partial differential equations (PDE). Sections 2.2-2.4 outline the analytical solution techniques available for solving scalar quasi-linear PDEs, which are covered in many standard texts (e.g. [32], [33]). The notion of "weak solution" is introduced as an alternative to a "classical" smooth solution of a PDE. Many of the concepts developed for the scalar case carry over to systems of quasi-linear PDEs, which are discussed in Section 2.5. However, analytical solutions for systems are only available in special cases, such as Riemann problems for systems conservation laws ([34]-[36]). The vast majority of (systems of) PDEs can only be solved numerically. A brief discussion of these numerical methods is given in Section 2.6 (see also [37]-[39]).

2.2 The method of characteristics for scalar PDE

The general form of a first-order quasi-linear PDE is

$$a\left(x,t,u\right)\frac{\partial u}{\partial x}+b\left(x,t,u\right)\frac{\partial u}{\partial t}=c\left(x,t,u\right) \tag{2.1}$$

where the coefficients a, b, c are continuously differentiable (C^1) functions of their arguments. Equation (2.1) is called *linear* if the coefficients are functions of the independent variables x, t only, *semi-linear* if the source term c depends additionally on u and *quasi-linear* if a or b (or both) depend on u. In a *Cauchy problem*, the

dependent variable u is prescribed on a curve C_0 in the x-t plane. A C^1 function $u(x,t)$ which satisfies equation (2.1) as well as these *Cauchy data* data is said to be a *classical* solution.

The strategy for solving the Cauchy problem is based on a geometrical idea. Suppose that a classical solution $u(x,t)$ exists on a domain $\Omega \subset \mathbb{R}^2$. This can be represented as a *solution surface* $z = u(x,t)$ in $\Omega \times \mathbb{R} \subset \mathbb{R}^3$. Now consider the vector field $\mathbf{V} : \Omega \times \mathbb{R} \to \mathbb{R}^3$ given by

$$\mathbf{V}(x,t,z) = (a(x,t,z),\ b(x,t,z),\ c(x,t,z)) \tag{2.2}$$

The key observation is to note that u solves equation (2.1) at $(x,t) \in \Omega$ if and only if the vector $\mathbf{V}(x,t,u(x,t))$ is tangent to the surface. Indeed, the outward normal vector to the surface is $\mathbf{N}(x,t,u(x,t)) = (\partial u/\partial x, \partial u/\partial t, -1)$ and equation (2.1) says that $\mathbf{N}(x,t,u(x,t)) \cdot \mathbf{V}(x,t,u(x,t)) = 0$. This suggests that a solution of the Cauchy problem may be "built up" using the vector field $\mathbf{V}$. The starting point in this process is to describe the plane curve C_0 by a parameter $r \in [r_1, r_2]$. The specification of u on C_0 then yields the parametrised Cauchy data curve $\Sigma_0 \subset \mathbb{R}^3$:

$$\Sigma_0 := \{(x_0(r), t_0(r), u_0(r)),\ r \in \mathbb{R}\} \tag{2.3}$$

Let us assume that x_0, t_0 and u_0 are C^1 functions, so that the curve Σ_0 is continuous and does not have any sharp edges (i.e. no discontinuities in the derivatives). Next, consider the following autonomous system of ordinary differential equations:

$$\frac{dx}{ds} = a(x,t,z) \tag{2.4}$$

$$\frac{dt}{ds} = b(x,t,z) \tag{2.5}$$

$$\frac{dz}{ds} = c(x,t,z) \tag{2.6}$$

Now, a parameter value $r^* \in [r_1, r_2]$ corresponds to a point $P(r^*) \in \Sigma_0$ and the Cauchy-Picard theorem ([40]) ensures the existence of $\epsilon = \epsilon(r^*) > 0$ and a unique solution $\gamma(s, r^*) : (-\epsilon, \epsilon) \to \mathbb{R}^3$ of equations (2.4)-(2.6) such that $\gamma(0, r^*) = P(r^*)$. Such a solution curve is called a *characteristic*. By varying r we obtain a one-parameter family of characteristics,

$$\gamma(s,r) = (x(s,r), t(s,r), z(s,r)) \tag{2.7}$$

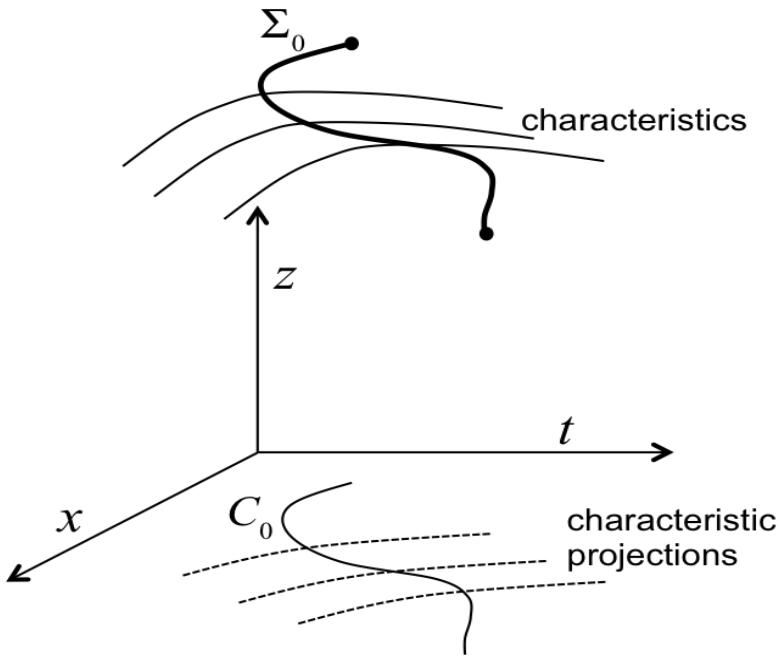

Figure 2.1: *A non-characteristic initial data curve* Σ_0.

By another result in the theory of ODEs, the family $\gamma(s, r)$ is differentiable with respect to both s and r. It actually constitutes a parametric surface Σ with tangent vectors $\partial\gamma/\partial s$ and $\partial\gamma/\partial r$, containing the curve Σ_0. Note that, *if* we can express s and r as C^1 functions of x, t, we can describe the surface as the graph $z = u(x, t)$, where u is some C^1 function which solves equation (2.1):

$$c = \frac{dz}{ds} = \frac{d}{ds}u(x,t) = \frac{\partial x}{\partial s}\frac{\partial u}{\partial x} + \frac{\partial t}{\partial s}\frac{\partial u}{\partial x} = a\frac{\partial u}{\partial x} + b\frac{\partial u}{\partial x} \tag{2.8}$$

Given a point $P = (x_0, t_0, u_0) \in \Sigma_0$, the Inverse Function Theorem implies that, in a neighbourhood of the *projection* of P, i.e. $(x_0, t_0) \in C_0 \subset \mathbb{R}^2$, the C^1 transformation $(x, t) \to (s, r)$ has a unique C^1 inverse, provided that the Jacobian of the transformation is non-zero, i.e.

$$J = a(x_0, t_0, 0) \cdot \frac{dt_0}{dr} - b(x_0, t_0, 0) \cdot \frac{dx_0}{dr} \neq 0 \tag{2.9}$$

Although this criterion is about the projection vector $(a(P), b(P)) \in \mathbb{R}^2$ of $\mathbf{V}(P)$, it still follows that if Σ_0 is not tangent to the characteristic through P, then there exists a unique classical solution $u(x, t)$ of equation (2.1) in a neighbourhood of P. A Cauchy data curve which is nowhere tangent to a characteristic is called *non-characteristic* (see Figure 2.1). If the data curve is tangent to a characteristic, the Jacobian in equation (2.9) vanishes and the classical solution breaks down. Isolated

points of tangency can cause a blow-up in the solution, which is a point at which the partial derivatives become infinite (we will see examples of this behaviour in Chapters 4 and 5).

Example 2.1: Consider the following Cauchy problem:

$$\frac{\partial u}{\partial t} + v\frac{\partial u}{\partial x} = 0 \ , \ \ u(x,0) = u_0(x), \ -\infty < x < \infty \tag{2.10}$$

The general solution of equations (2.4)-(2.6) in this case is $x(s) = vs+\beta_1$, $t(s) = s+\beta_2$, $z(s) = \beta_3$ for $-\infty < s < \infty$ and arbitrary $(\beta_1, \beta_2, \beta_3) \in \mathbb{R}^3$. The curve C_0 (the x-axis) is parametrised, which yields the initial data curve $\Sigma_0 := \{(r, 0, u_0(r)), \ r \in \mathbb{R}\}$. Application of Σ_0 leads to the characteristic curves $x(s,r) = vs + r$, $t(s,r) = s$, $z(s,r) = u_0(r)$ defining a surface Σ containing Σ_0. It is clear that z remains constant along a characteristic curve. Since there is a *global* inverse transformation $(s,r) \to (x,t)$ given by $s = t$ and $r = x - vt$, we can describe Σ by $z = u_0(x - vt)$ for all $(x,t) \in \mathbb{R}^2$. Graphically, this solution may be visualised as the propagation of the initial profile $u_0(x)$ along the x-axis at constant speed v.

As we will see later, the simple solution form encountered in Example 2.1 may also be a (local) solution of other PDEs and we therefore give it a special name:

Definition: A solution $u(x,t)$ of a PDE is called a *travelling wave solution* if, in principle, it can be put in the form $u(x,t) = f(x - vt)$ for some function f. Its main feature is that all solution values travel at the same constant speed v, thus preserving the initial "shape" of f.

2.3 Characteristic projections

For linear and semi-linear PDEs, equations (2.4) and (2.5) are independent of equation (2.6) and the family of *characteristic projections* $(x(s,r), t(s,r)) \subset \mathbb{R}^2$ passing through $C_0 \subset \mathbb{R}^2$ can be calculated *a priori* without any knowledge of u. They may be obtained directly by solving $dx/dt = a(x,t)/b(x,t)$. This generally leads to a non-intersecting family of plane curves along which z can be found using the data prescribed on C_0 and equation (2.6) with x or t as a parameter. This relatively

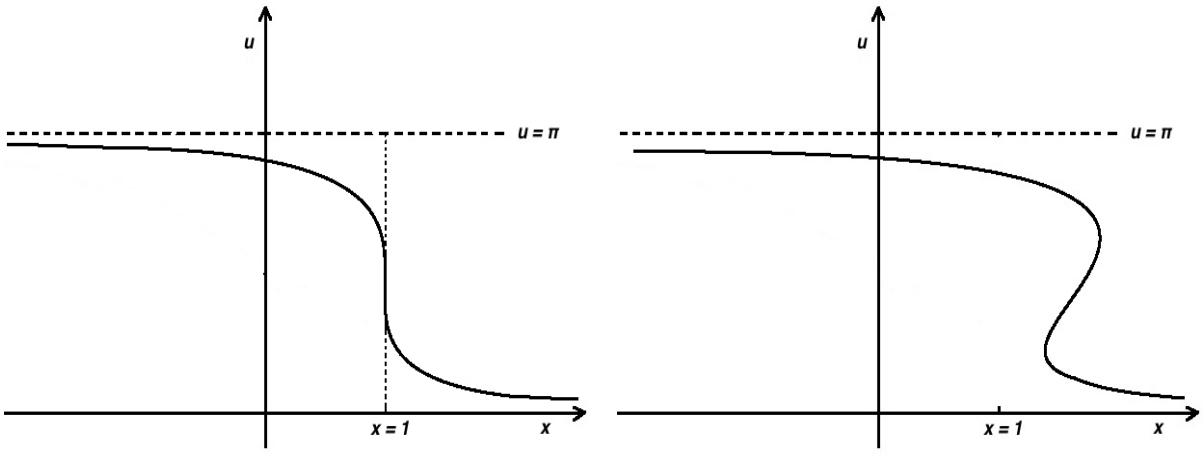

(a) $t = 1$ (b) $t > 1$

Figure 2.2: *Sketch of the solution in Example 2.2.*

simple procedure breaks down for quasi-linear equations. The characteristic projections in this case can only be found *after* Σ (the solution surface) is determined, because equations (2.4)-(2.6) are now all dependent on each other. The initial data curve Σ_0 becomes hugely significant here, as demonstrated in the next example.

Example 2.2: Consider the Cauchy problem given by

$$\frac{\partial u}{\partial t} + u\frac{\partial u}{\partial x} = 0 \ , \ \ u(x,0) = u_0(x) = \frac{\pi}{2} - tan^{-1}(x), \ x \in \mathbb{R} \tag{2.11}$$

The characteristic system of ODEs is $dx/ds = z$, $dt/ds = 1$, $dz/ds = 0$. Using the initial data curve $\Sigma_0 := \{(r, 0, u_0(r)), \ r \in \mathbb{R}\}$, we find $z(s, r) = u_0(r)$, which means that z is constant along characteristics. The characteristic projections then are given by $x(r, s) = u_0(r)s + r$ and $t(r, s) = s$. Taking partial derivatives with respect to x (keeping $t = s$ fixed), we obtain $r_x = (1 + u_0'(r)s)^{-1}$ and hence

$$\frac{\partial z}{\partial x} = \frac{\partial r}{\partial x}u'(r) = \frac{u'(r)}{1 + u_0'(r)s} = \frac{1}{s - (1 + r^2)} \tag{2.12}$$

This shows that $z_x < 0$ for $s < 1 + r^2$ and $z_x > 0$ for $s > 1 + r^2$, with $z_x \to \infty$ at $s = 1+r^2$. Since $z(s, r) = u_0(r)$ is smooth, this shows that the surface begins to fold over on itself for $s = t \geq 1$. Where this happens, the projections of three different characteristics will intersect in a single point lying in the region bounded by the plane curves $x = u_0(\pm\sqrt{t-1})t \pm \sqrt{t-1}$. A classical solution of the Cauchy problem on

$-\infty < x < \infty$ therefore only exists for $t < 1$. For $t \geq 1$, the solution becomes multivalued, which does not make sense if u represents some physical quantity like concentration, density. This raises the question as to whether an alternative form of "solution" can be introduced which allows for discontinuities in u or its derivatives.

2.4 Weak solutions

Example 2.2 shows that even for smooth initial data curves Σ_0, a classical solution may be very short-lived. This issue becomes even more apparent when Σ_0 has discontinuities or edges, as is often the case in physical systems. For instance, if $u_0(x) = H(-x)$ were used as initial data in Example 2.2, the surface would fold over immediately. To address such problems, a new, *weaker* definition of solution is needed, one which incorporates possible discontinuities in the quantities u, $\partial u/\partial x$ and $\partial u/\partial t$. This concept relies on the possibility of re-writing equation (2.1) in divergence form:

$$\frac{\partial}{\partial x} P\left(x,t,u\right) + \frac{\partial}{\partial t} Q\left(x,t,u\right) = R\left(x,t,u\right) \tag{2.13}$$

The most rigorous way to proceed from here is to view equation (2.13) in a *distributional* sense ([35],[36]). The solution u is then a "distribution" or "generalised function". For a more direct approach, consider a domain $D \subset \mathbb{R}^2$ bounded by C_0 and an arbitrary curve γ (see Figure 2.3). We now multiply equation (2.13) by a *test function*, a smooth function $\psi(x,t)$ such that $\psi = 0$ on γ. Using the fact that $\psi P_x = (\psi P)_x - \psi_x P$ and $\psi Q_t = (\psi Q)_t - \psi_t Q$, the equation becomes

$$\frac{\partial}{\partial x}(\psi P) + \frac{\partial}{\partial t}(\psi Q) = P\frac{\partial \psi}{\partial x} + Q\frac{\partial \psi}{\partial t} + \psi R \tag{2.14}$$

Green's Theorem applied to the region D then yields

$$\int\int_D \left[P\frac{\partial \psi}{\partial x} + Q\frac{\partial \psi}{\partial t} + \psi R\right] dtdx = \int_{C_0} \psi\left[Pdt - Qdx\right] \tag{2.15}$$

Definition: A *weak solution* of the Cauchy problem for equation (2.13) is a function $u(x,t)$ which satisfies equation (2.15) for all test functions $\psi(x,t)$.

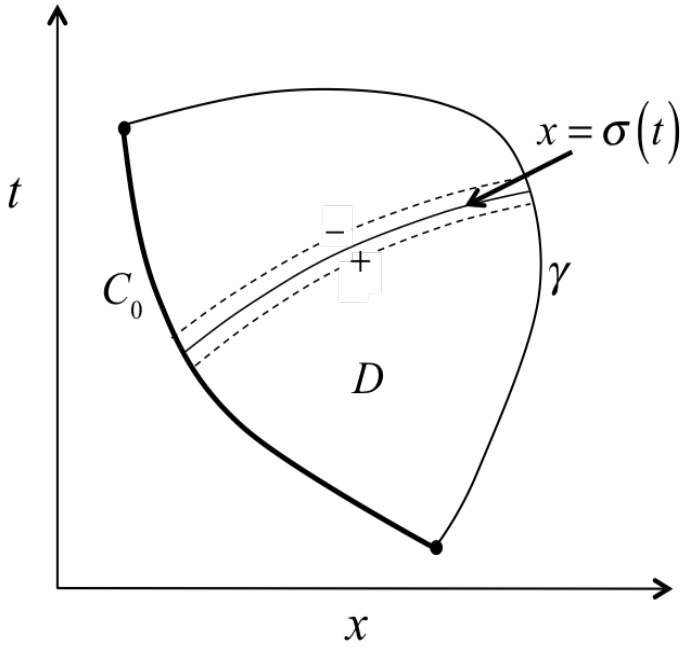

Figure 2.3: *A domain D enclosed by C_0 and an arbitrary curve γ.*

Note that any classical solution of equation (2.13) is also a weak solution. With this in mind, we now investigate what other type of functions $u(x,t)$ are allowed under this new definition of solution.

Discontinuities in $\partial u/\partial x$ and/or $\partial u/\partial t$: suppose that $u(x,t)$ is a function which solves equation (2.13) on either side of a curve $x = \sigma(t)$ across which u is continuous, but not differentiable. Then u is a weak solution, since (non-) differentiability of u does not enter into equation (2.15). Moreover, it can be shown that $x = \sigma(t)$ must be a characteristic projection, i.e. $d\sigma/dt = a/b$. This yields an alternative definition of a characteristic as a curve along which $\partial u/\partial x$ and $\partial u/\partial t$ may be discontinuous. Any "edges" in the solution surface can only propagate along characteristics. This way of viewing a characteristic is very useful, because it does not rely on a geometrical idea and carries over to systems of PDEs (see Section 2.5).

Discontinuities in u: suppose that $u(x,t)$ is a function satisfying equation (2.13) on either side of a curve $x = \sigma(t)$ across which u itself is discontinuous. This *does* have a bearing on equation (2.15) and it needs to be examined which discontinuities are compatible with the notion of weak solution. Using Green's theorem on the portions of D separated by $x = \sigma(t)$ (see Figure 2.3) yields an ordinary differential equation relating the speed of the discontinuity to the limiting values u^+ and u^-

obtained as the discontinuity is approached from either side:

$$\frac{d\sigma}{dt} = \frac{P^+ - P^-}{Q^+ - Q^-} \tag{2.16}$$

where $P^{\pm} = \lim_{x \to \sigma^{\pm}(t)}\{P(x,t,u(x,t))\}$ and $Q^{\pm} = \lim_{x \to \sigma^{\pm}(t)}\{Q(x,t,u(x,t))\}$. Note that the discontinuity is independent of the source term R. For linear and semi-linear equations, we have $P = a(x,t)u$, $Q = b(x,t)u$ and equation (2.16) becomes $d\sigma/dt = a/b$, which shows that $x = \sigma(t)$ is a characteristic projection. For quasi-linear equations, a and/or b are dependent on u and a curve of discontinuity $x = \sigma(t)$ corresponds to a characteristic projection only if the vectors (a^+, b^+) and (a^-, b^-) at each point $(\sigma(t), t)$ are in the same direction. Such a discontinuity is called a *contact discontinuity*. In general, (a^+, b^+) and (a^-, b^-) are linearly independent and the curve $x = \sigma(t)$ is not a characteristic.

The problem with the situation as it stands is that it allows for the construction of discontinuities that do not make sense physically. This has to do with the *characteristic speed* $\lambda = a/b$ of a solution value. If $\lambda^+ > d\sigma/dt > \lambda^-$, then the value immediately ahead of the discontinuity (u^+) travels faster than the value immediately behind the discontinuity (u^-). This type of weak solution is thought to be physically incorrect and will therefore be excluded by the following definition.

Definition: An *admissible discontinuity* in $u(x,t)$ along a curve $x = \sigma(t)$ satisfies equation (2.16) and is such that $\lambda^+ \leq d\sigma/dt \leq \lambda^-$. It is called a *contact discontinuity* if $\lambda^+ = d\sigma/dt = \lambda^-$, a *shock* if $\lambda^+ < d\sigma/dt < \lambda^-$ and a *semi-shock* if either $\lambda^+ = d\sigma/dt$ or $\lambda^- = d\sigma/dt$.

The shock condition (strict inequality) expresses *causality*, which says that the characteristics must run into the shock path from either side. This is also called the *Lax entropy condition*, based on the idea that a certain "entropy function" (in terms of the physical quantity u) must increase in the discontinuity. Another approach of obtaining an admissibility condition is by the "vanishing viscosity" method, in which a diffusive term $\epsilon \partial^2 u/\partial x^2$ is added to equation (2.13) to make it physically more "realistic". The idea is that a discontinuity of the original first-order equation should be the limit of a smooth solution of this second-order equation as $\epsilon \to 0$.

"Building" a weak solution: In general, a weak solution u of a Cauchy Problem will consists of different analytical components, which are joined together according to the rules laid out above. Discontinuities in the partial derivatives of u, i.e. edges at which two classical solution components meet, must travel along characteristics. In regions where the characteristic projections intersect, a discontinuity of u is introduced, which must satisfy equation (2.16) as well as a suitable entropy condition.

The ideas presented thus far are illustrated in Appendix A, where the weak solution to the *Riemann Problem* for the Buckley-Leverett equation is constructed. This is an example of a scalar *conservation law*, obtained when $R(x,t,u) = 0$, $Q(x,t,u) = u$ and $P(x,t,u) = P(u)$ in equation (2.13). Such equations have straight line characteristic projections along which the solution stays constant. The slopes are determined by the Cauchy data and the derivative of the *flux function* $P(u)$. In a Riemann Problem, the Cauchy data are piecewise constant. This setup admits the construction of a weak solution consisting of rarefaction waves, contact discontinuities and shocks.

2.5 Systems of quasi-linear PDE

Let $\mathbf{u}(x,t) = (u_1(x,t), u_2(x,t), ..., u_n(x,t))^T \in \mathbb{R}^n$ be a column vector of n dependent variables in terms of x and t, related to each other as follows:

$$\mathbf{A}\left(x,t,\mathbf{u}\right)\frac{\partial \mathbf{u}}{\partial x} + \mathbf{B}\left(x,t,\mathbf{u}\right)\frac{\partial \mathbf{u}}{\partial t} = \mathbf{c}\left(x,t,\mathbf{u}\right) \tag{2.17}$$

The coefficients $\mathbf{A}$, $\mathbf{B}$ are C^1-functions $\mathbb{R}^{n+2} \to \mathbb{R}^{n\times n}$ and $\mathbf{c}$ is a C^1-function $\mathbb{R}^{n+2} \to \mathbb{R}^n$, so that equation (2.17) represents a system of n scalar PDEs with coefficients dependent on x, t, as well as the unknowns u_1, ..., u_n. The classification into linear, semi-linear and quasi-linear systems is exactly the same as for scalar equations. The notion of weak solution and the Rankine-Hugoniot relation for the propagation of discontinuities also carry over naturally. However, there is no straightforward generalisation of the method of characteristics explained in section 2.2, because the coefficients of the scalar PDE for u_i in general depend on $u_1, ..., u_{i-1}, u_{i+1}, ..u_n$ as well. This prevents the geometrical definition of a characteristic as an integral

curve of a vector field tangent to the solution surface $z = u_i(x,t)$. However, we saw in section 2.4 that a characteristic projection could also be described as a plane curve across which the partial derivatives of the scalar $u(x,t)$ may be discontinuous. The generalisation of this interpretation to the vector $\mathbf{u}(x,t)$ is the *definition* of a characteristic projection of equation (2.17) and it can be shown that a parametrised plane curve $(x(s),t(s)) \subset \mathbb{R}^2$ is a characteristic projection if and only if

$$\det\left(\frac{dx}{ds}\mathbf{B} - \frac{dt}{ds}\mathbf{A}\right) = 0 \tag{2.18}$$

where the matrices $\mathbf{A}$, $\mathbf{B}$ are evaluated on the curve. Assuming $\mathbf{B}^{-1}$ exists, we can re-write equation (2.18) as $\det\left(\mathbf{B}^{-1}\mathbf{A} - \lambda\mathbf{I}\right) = 0$ with $\lambda = dx/dt$. Hence, the slope of a characteristic projection is given by an eigenvalue of the matrix $\mathbf{B}^{-1}\mathbf{A}$. At a given point in the domain, the system of equations is said to be *strictly hyperbolic* if all n eigenvalues of $\mathbf{B}^{-1}\mathbf{A}$ are real and distinct at that point. This implies the (local) existence of n distinct families characteristic projections. Analogous to the scalar case, equation (2.17) reduces to a system of ODEs along these curves. To see this, let λ_i be the i-th eigenvalue of $\mathbf{B}^{-1}\mathbf{A}$ and $\boldsymbol{l}_i^T$ the corresponding left eigenvector. Then, *along* the curve $(x(s_i),t(s_i))$ defined by $dx/dt = \lambda_i$, equation (2.17) becomes

$$\boldsymbol{l}_i^T \frac{d\mathbf{u}}{ds_i} = \boldsymbol{l}_i^T \mathbf{B}^{-1}\mathbf{c} \tag{2.19}$$

Example 2.3: Consider the system of equations (1.6)-(1.8) with $D = 0$ (no dispersion) and $\Pi > 0$, $C < C_s$ in the dissolution rate equation. The resulting system of two equations for C and Γ can be written in the form of equation (2.17):

$$\begin{pmatrix} 1 & 0 \\ 0 & 1 \end{pmatrix}\begin{pmatrix} C_t \\ \Gamma_t \end{pmatrix} + \begin{pmatrix} v & 0 \\ 0 & 0 \end{pmatrix}\begin{pmatrix} C_x \\ \Gamma_x \end{pmatrix} = \begin{pmatrix} \kappa\left(C_s - C\right) - r_a\left[\Gamma_{eq}\left(C\right) - \Gamma\right] \\ r_a\left(\Gamma_{eq}\left(C\right) - \Gamma\right) \end{pmatrix} \tag{2.20}$$

Here, $\mathbf{B} = \mathbf{I}$, so $\mathbf{B}^{-1}\mathbf{A} = \mathbf{A}$ and $\mathbf{B}^{-1}\mathbf{c} = \mathbf{c}$. The matrix $\mathbf{A}$ has eigenvalues $\lambda_1 = v$, $\lambda_2 = 0$ and suitable left-eigenvectors are $\boldsymbol{l}_1^T = (1,0)$, $\boldsymbol{l}_2^T = (0,1)$. The characteristic projections corresponding to λ_1 are given by $x(s_1) = vs_1 + \text{constant}$, $t(s_1) = s_1$ and, along these curves, equation (2.20) reduces to

$$\frac{dC}{ds_1} = \kappa(C_s - C) - r_a\left[\Gamma_{eq}(C) - \Gamma\right] \tag{2.21}$$

Similarly, along the λ_2-characteristics $x(s_2) = \text{constant}$, $t(s_2) = s_2$, we have

$$\frac{d\Gamma}{ds_2} = r_a \left[\Gamma_{eq}(C) - \Gamma\right] \tag{2.22}$$

Equations (2.21) is the rate of change of C along the λ_1-characteristics and equations (2.22) is the rate of change of Γ along the λ_2-characteristics. Since dC/ds_2 and $d\Gamma/ds_1$ are not given, the equations are not integrable without assuming a particular functional relationship between C and Γ.

Example 2.3 highlights a practical problem in applying equation (2.19) to find analytical solutions. Although the system of PDEs can be reduced to a single ODE along each characteristic projection, this ODE generally involves more than one unknown and is therefore not integrable. Thus, in contrast to the scalar case, analytical solutions for systems are available only in special cases. For example, if equation (2.19) can be re-written in the form

$$\frac{d}{ds_i} r_i(x, t, \mathbf{u}) = 0 \tag{2.23}$$

then the so-called *Riemann-invariant* $r_i(x, t, \mathbf{u})$ stays constant along characteristics. This equation *is* integrable and may lead to a full analytical solution if a complete set of n Riemann invariants exists. This evidently requires equation (2.17) to be homogenous ($\mathbf{c} = \mathbf{0}$). Homogenous systems have a better chance of being solved analytically, particularly if they are *reducible*, i.e.

$$\mathbf{A}(\mathbf{u}) \frac{\partial \mathbf{u}}{\partial x} + \mathbf{B}(\mathbf{u}) \frac{\partial \mathbf{u}}{\partial t} = \mathbf{0} \tag{2.24}$$

In this case, the *Hodograph transformation* can be used to inter-change the role of the dependent and independent variables, leading to a linear system which is much easier to analyse as the characteristic projections can be calculated *a priori*.
A particular class of reducible systems appearing in many physical context are *systems of conservation laws*, for which $\mathbf{B} = \mathbf{I}$ and $\mathbf{A}(\mathbf{u}) = \partial \mathbf{F}/\partial \mathbf{u}$, the derivative of the generalised flux function $\mathbf{F}(\mathbf{u})$. Somewhat analogous to the scalar case, the Riemann Problem for a system of conservation laws can be solved systematically if the system is strictly hyperbolic. The weak solution $\mathbf{u}(x, t)$ can be constructed as

a sequence of constant states, rarefaction waves, contact discontinuities and shocks or semi-shocks. This procedure is illustrated in Appendix B for the 2×2 system of conservation laws modelling a polymer flood in EOR.

2.6 Numerical solutions

We saw in the previous section that analytical solutions are generally not available for systems of first-order quasilinear PDE, unless the system takes a particularly simple form. This is even more true for fully non-linear PDE. For this reason, PDEs must usually be solved numerically. A huge variety of numerical methods have been developed, the most common ones being finite difference, finite element and finite volume methods. The underlying idea of all these methods is to transform the PDE into a system of algebraic equations which can be solved using iterative schemes. Which methods works best depends largely on the nature of the PDE, the geometry of the domain and the purpose for which a numerical solution is required. By far the easiest to implement is a finite difference scheme, which often involves the discretisation of the domain Ω into a uniform grid. For example, if the system of PDEs given in equation (2.17) is to be solved on the finite domain $\Omega := [0, L] \times [0, T]$, then we may consider a rectangular grid Ω_Δ of $N + 1$ by $M + 1$ points, where $N = L/\Delta x$, $M = T/\Delta t$:

$$\Omega_\Delta := \left\{(x_i, t^j) = (i\Delta x, j\Delta t) \in \Omega, i = 0, .., N, j = 0, .., M\right\} \tag{2.25}$$

A grid-function is a discrete function $\mathbf{w}$ only taking values $\mathbf{w}_i^j = \mathbf{w}(x_i, t^j)$ on the nodes of Ω_Δ. The idea is to approximate the solution $\mathbf{u}(x, t)$ of the PDE by a grid-function. To this end, we need to obtain a discretised version of the PDE by a suitable replacement of the partial derivative operators. The simplest choice are the *forward space* and *forward time* finite-difference operators $\mathcal{L}_x$, $\mathcal{L}_t$:

$$\mathcal{L}_x \mathbf{w}_i^j := \frac{\mathbf{w}_{i+1}^j - \mathbf{w}_i^j}{\Delta x} \ , \ \mathcal{L}_t \mathbf{w}_i^j := \frac{\mathbf{w}_i^{j+1} - \mathbf{w}_i^j}{\Delta t} \tag{2.26}$$

Applied to a smooth function on Ω, these difference operators yield first order approximations of its partial derivatives with respect to x and t. An example of a

finite difference scheme for equation (2.17) is now obtained by replacing $\partial/\partial x$, $\partial/\partial t$ with $\mathcal{L}_x$, $\mathcal{L}_t$ and the unknown function $\mathbf{u}(x,t)$ with the grid-function $\mathbf{w}$. Assuming invertibility of the matrix $\mathbf{B}$, this yields the following explicit iterative procedure:

$$\mathbf{w}_i^{j+1} = \mathbf{w}_i^j - \frac{\Delta t}{\Delta x}\left(\mathbf{B}^{-1}\right)_i^j \mathbf{A}_i^j \left(\mathbf{w}_{i+1}^j - \mathbf{w}_i^j\right) + \Delta t \left(\mathbf{B}^{-1}\right)_i^j \mathbf{c}_i^j \tag{2.27}$$

where $\mathbf{A}_i^j = \mathbf{A}\left(x_i, t^j, \mathbf{w}_i^j\right)$, $(\mathbf{B}^{-1})_i^j = \mathbf{B}^{-1}\left(x_i, t^j, \mathbf{w}_i^j\right)$, $\mathbf{c}_i^j = \mathbf{c}\left(x_i, t^j, \mathbf{w}_i^j\right)$. Computation of the $(j+1)$-th time-level vector $\mathbf{w}_i^{j+1}$ involves the vectors $\mathbf{w}_i^j$ and $\mathbf{w}_{i+1}^j$ in a three-point stencil. Therefore, given $\mathbf{w}_i^0$, $\mathbf{w}_0^j$ for $i = 0, .., N$, $j = 0, .., M$, all values of $\mathbf{w}$ on Ω_Δ can be calculated. We hope that, if $\mathbf{w}_i^0 = \mathbf{u}(x_i, 0)$ and $\mathbf{w}_0^j = \mathbf{u}(0, t^j)$, the solution $\mathbf{w}$ of equation (2.27) is "close" to the exact solution $\mathbf{u}(x,t)$ of equation (2.17) if Δx and Δt are small. The quantification of this notion is based on the concepts of *consistency*, *convergence* and *stability*.

Consistency: a finite difference scheme is called *consistent* if it is at least first-order *accurate*. The order of accuracy is the order of the *truncation error*, which is the amount by which a smooth solution $\mathbf{u}(x,t)$ of the PDE deviates if it is substituted in a finite difference scheme and only one iteration is performed. For example, if $\mathbf{w}$ is replaced by $\mathbf{u}(x,t)$ in equation (2.26), a Taylor expansion yields a truncation error (remainder) of order $O(\Delta x) + O(\Delta t)$. This scheme is first-order accurate and therefore consistent, which means that it is a good approximation of equation (2.17) if Δx and Δt are sufficiently small.

Convergence: roughly speaking, a finite difference is said to be *convergent* if its solution $\mathbf{w}$ get closer to the exact solution $\mathbf{u}(x,t)$ upon successive refinements of the grid. More precisely, the *discretisation error* $\|\mathbf{w} - \mathbf{u}\|$ vanishes as $\Delta x, \Delta t \to 0$. Note that, in general, consistency does not imply convergence. Consistency only says that the finite difference scheme is a good model of the PDE, not that its solution is also solution is close to the solution of the PDE. Progress in this direction can be made by considering the *stability* of the method.

Stability: essentially, this criterion is the analog of well-posedness for exact solutions: a small change in the initial/boundary data can only effect a small change

in the numerical solution. Another way of saying this is that errors (e.g. due to round-off) are bounded even upon repeated iterations. In an unstable scheme, the error grows unboundedly, typically leading to large oscillations in the numerical solution. For linear PDE, stability can be established by Von Neumann analysis. This usually leads to a constraint on Δx, Δt, such as the Courant-Friedrich-Lax (CFL) condition $v\Delta t/\Delta x < 1$.

The numerical analysis for linear PDEs is well-developed, culminating in the *Lax-Richtmeyer Equivalence Theorem*, which says that "stability + consistency $\Leftrightarrow$ convergence". This is an extremely useful result, because it shifts the burden from a (difficult) convergence proof to a (relatively simple) stability proof. The "$\Rightarrow$" also holds for non-linear PDE, but the stability proof is generally much harder.

Another problem associated with numerical solutions is the issue of convergence to solutions which are not regular, such as the weak solutions discussed in sections 2.1-2.5. A "naive" explicit first-order finite difference scheme like equation (2.27) will definitely not converge uniformly in the presence of discontinuities, due to the effects of "numerical viscosity". Even worse, these schemes may converge to the wrong weak solution if no entropy condition is embedded in the numerical formulation. Various "shock-capturing" and "conservative" schemes exists to prevent this from happening, which usually are finite volume methods based on the weak formulation of the system of PDEs. Although the analytical solutions developed in this PhD are weak solutions, we will not use these more sophisticated numerical methods. Instead, we will show that the explicit scheme in equation (2.27) converges well to the analytical solutions. The disadvantage of this method is that small time-steps Δt in relation to Δx are required to ensure stability. This involves very long computation times as the grid is refined.

Chapter 3

Exact solution of the scale inhibitor model with constant fluid velocity and no adsorption

3.1 Introduction

With no adsorption and diffusion, the model equations (1.6)-(1.8) simplify to

$$\frac{\partial C}{\partial t} + v\frac{\partial C}{\partial x} = -\frac{\partial \Pi}{\partial t} \tag{3.1}$$

$$\frac{\partial \Pi}{\partial t} = -\kappa\left[C_s - C\right] \cdot \left[H\left(\Pi\right) + H\left(C - C_s\right) - H\left(\Pi\right) H\left(C - C_s\right)\right] \tag{3.2}$$

In this chapter, we solve the Cauchy Problem for this system in $\Omega = [0, L] \times [0, \infty)$ with data on $\partial\Omega$ given by the *constant* initial profiles

$$C\left(x, 0\right) = C_s \ , \ \Pi\left(x, 0\right) = \Pi_0 \ \text{ for } \ 0 \leq x \leq L \tag{3.3}$$

and the feed/boundary condition

$$C\left(0, t\right) = 0 \ \text{ for } \ t > 0 \tag{3.4}$$

Equation (3.3) corresponds to the conditions in the rock core at $t = 0$, when the scale inhibitor solution (concentration $C_i > C_s$) has reached equilibrium and a uniform layer of precipitate has formed (see Figure 1.4). Equation (3.4) is needed during a flow stage ($v > 0$) in which fresh water ($C = 0$) is injected. This condition assumes

an immediate response, the concentration at the inlet dropping from $C = C_s$ at $t = 0$ to $C = 0$ at $t = 0^+$. We will see that the model predicts a similar effect at other points in the system as the injected water pushes ahead a bank of constant concentration $C = C_s$. At any point behind this front, there is a balance between dissolution of precipitate and concentration being carried off by the fluid, resulting in a steady-state region where $C < C_s$. Equations (3.2) and (3.4) imply that, as longs as $\Pi > 0$, the rate of dissolution at the inlet boundary is κC_s and therefore $\Pi(0,t) = \Pi_0 - \kappa C_s t$ for $0 \leq t \leq t^*$, where

$$t^* = \frac{\Pi_0}{\kappa C_s} \tag{3.5}$$

It will be shown that $\Pi(x,t) > 0$ on $(0, L]$ for all $0 \leq t \leq t^*$, from which it follows that the precipitate first runs out at the inlet. Since no precipitate can be added if $C < C_s$, we have $\Pi(0,t) = 0$ for all $t \geq t^*$. Gradually, the precipitate at neighbouring points will also be exhausted and a "zero precipitate region" advances through the system. We adopt the following notation to describe this:

Definition: Let $x = \alpha_\Pi(t)$ be a curve in Ω such that $\Pi \equiv 0$ on $\Omega_0 := \{x \leq \alpha_\Pi\} \cap \Omega$ and $\Pi > 0$ on $\Omega_+ := \{x > \alpha_\Pi\} \cap \Omega$. We will call this the *moving boundary curve*.

Note that equation (3.1) is homogenous in Ω_0 and non-homogenous in Ω_+, which means that there are two separate Cauchy problems to be considered, requiring knowledge of C on $x = \alpha_\Pi(t)$. An ordinary differential equation of the form $d\alpha_\Pi/dt = F(C(\alpha_\Pi, t))$ can be derived and it will be shown that $C(\alpha_\Pi, t) = 0$ for all $t \geq t^*$. The boundary curve is then a straight line of slope $F(0) < v$ (see Figure 3.1), which will lead to the emergence of a travelling wave solution region in Ω_+, alongside the solution profile formed while $t < t^*$. The balance between flux and dissolution which maintains the steady-state region is gradually tipped in favour of scale inhibitor being transported out of the system. The different solution regimes of C in Ω_+ can be used to find the corresponding expressions for Π up to arbitrary functions. These will be determined by the assumption that $\Pi(x,t)$ is continuous everywhere. This assumption has a bearing on the differential equation for α_Π and its correctness will be verified by a mass-balance calculation of the resulting weak solution to equation (3.1).

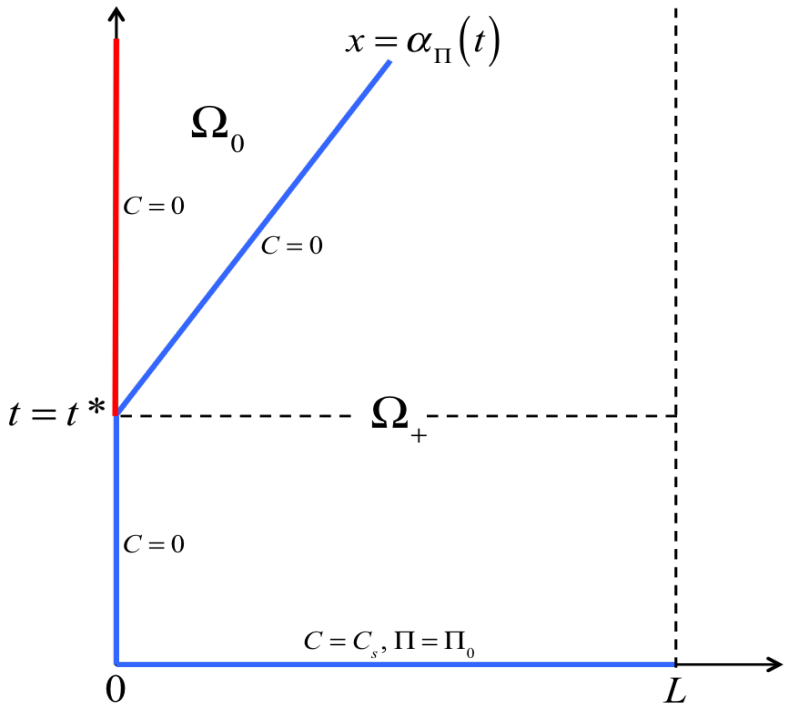

Figure 3.1: *Emergence of a new boundary at $t = t^*$. There are separate Cauchy problems for equation (3.1) on the sub-domains Ω_0 and Ω_+.*

3.2 Solution for $0 \leq t < t^*$

We first consider the period when there is some precipitate at every location in the reservoir. At $t = 0$, we have $\Pi = \Pi_0$ for all $0 \leq x \leq L$. Since $\partial\Pi/\partial t$ is finite, there must be some positive time interval $[0, t')$ such that $\Pi(x, t) > 0$ for all $0 \leq x \leq L$, $t \in [0, t')$. This allows us to substitute $\partial\Pi/\partial t = -\kappa(C_s - C)$ in equation (3.1) to obtain the non-homogenous, quasi-linear PDE

$$\frac{\partial C}{\partial t} + v\frac{\partial C}{\partial x} = \kappa(C_s - C) \tag{3.6}$$

Comparing this with equation (2.1) we have $a(x, t, z) = v$, $b(x, t, z) = 1$ and $c(x, t, z) = \kappa(C_s - z)$. We therefore need to solve the characteristic system

$$\frac{dx}{ds} = v, \quad \frac{dt}{ds} = 1, \quad \frac{dz}{ds} = \kappa(C_s - z) \tag{3.7}$$

Instead of parametrising $\partial\Omega$, we can map $\{x = 0, t > 0\}$ to $\{x < 0, t = 0\}$ and solve equation (3.6) on the upper-half plane, using the initial condition $C(x, 0) = f(x)$, which is to be chosen such that $C(0, t) = 0$. Now, requiring that the solutions

of equation (3.7) pass through the initial data curve $\Sigma_0 = \{(r, 0, f(r)), r \in \mathbb{R}\}$, we obtain the family of characteristics

$$z(r,s) = C_s + f(r)\, e^{-\kappa s} \tag{3.8}$$

$$x(r,s) = vs + r \tag{3.9}$$

$$t(r,s) = s \tag{3.10}$$

The characteristic projections have a global inverse $s = t$, $r = x - vt$ and the general solution to equation (3.6) in these coordinates becomes

$$C(x,t) = C_s + f(x - vt)\, e^{-\kappa t} \tag{3.11}$$

The problem now is to specify the function f for the situation we wish to model. From equation (3.3), $C(x,0) = C_s + f(x)$. In order to satisfy the initial condition $C(x,0) = C_s$ on $[0, L]$, we therefore require $f(x) = 0$ for $x \geq 0$. We also have the boundary condition $C(0,t) = C_s + f(-vt)\, e^{-\kappa t} = 0$ for all $t > 0$. Replacing $-vt$ with x yields $f(x) = -C_s e^{\kappa x/v}$ for $x < 0$, and hence our required function is

$$f(x) = \begin{cases} 0 \ , & x \geq 0 \\ -C_s e^{\kappa x/v}, & x < 0 \end{cases} \tag{3.12}$$

The solution C is obtained by substituting equation (3.12) into (3.11). Thus,

$$C(x,t) = \begin{cases} C_s \ , & x \geq vt \\ C_s - C_s e^{-\kappa x/v}, & x < vt \end{cases} \tag{3.13}$$

This concentration profile is characterised by the propagation of an initial discontinuity, which decreases in height as it moves through the system at velocity v (i.e. along the characteristic through the origin). Behind the front the solution profile is equal to the steady state solution of equation (3.6) obtained when setting $\partial C/\partial t = 0$. The concentration at each point here remains constant as a result of equality between the rate of dissolution of precipitate and the concentration flux that exists due to the fluid carrying off chemical.

In order to find a corresponding precipitate profile, we substitute equation (3.13) in equation (3.2) and obtain $\partial \Pi/\partial t = 0$ for all $x \geq vt$, which means that $\Pi = \Pi_0$ here.

For $x < vt$ we have $\partial\Pi/\partial t = -\kappa C_s e^{-\kappa x/v}$. Integration yields the solution in terms of an arbitrary function:

$$\Pi\left(x,t\right) = g\left(x\right) - \kappa C_s t e^{-\kappa x/v} \tag{3.14}$$

We will choose g in such a way that the profile $\Pi = \Pi(x,t)$ is continuous, which implies that equation (3.14) should take the value Π_0 at $x = vt$. Substituting $t = x/v$, this condition may be expressed as

$$\Pi_0 = \Pi\left(x, \frac{x}{v}\right) = g\left(x\right) - \frac{\kappa C_s x}{v} e^{-\kappa x/v} \tag{3.15}$$

This choice of the function g results in the following precipitate profile:

$$\Pi\left(x,t\right) \;= \begin{cases} \Pi_0 \;\;, \;\; x \geq vt \\ \\ \Pi_0 + \dfrac{\kappa C_s}{v}\left(x - vt\right) e^{-\kappa x/v} \;\;, \;\; x < vt \end{cases} \tag{3.16}$$

Differentiating equation (3.16) with respect to x, we obtain

$$\frac{\partial \Pi}{\partial x} = \frac{\kappa^2 C_s}{v^2}\left(\frac{v}{\kappa} + vt - x\right) e^{-\kappa x/v} > 0 \quad , \quad x < vt \tag{3.17}$$

This shows that the first time the precipitate runs out must be at $x = 0$, when $t = t^* = \Pi_0/\kappa C_s$. Until this time, the concentration and precipitate profiles on $0 \leq x \leq L$ are entirely defined by equations (3.13) and (3.16). Figure 3.2 shows these profiles at some time $t < t^*$. The horizontal line represents a fixed precipitate value $P \in [\Pi_0 - \kappa C_s t\,,\;\; \Pi_0]$. Let x_P denote the point of intersection of $\Pi(x,t)$ with the line $\Pi = P$, so

$$0 = \Pi_0 - P + \frac{\kappa C_s}{v}\left(x_P - vt\right) \exp\left(\frac{-\kappa x_P}{v}\right) \tag{3.18}$$

Using the Lambert W-function ([41]), equation (3.18) can be solved explicitly for x_P as a function of t. However, for reasons that will become clear shortly, we are mainly interested in the rate of change of x_P. By defining $G\left(x_{\mathrm{P}}, t\right) = \Pi\left(x_{\mathrm{P}}, t\right) - P$

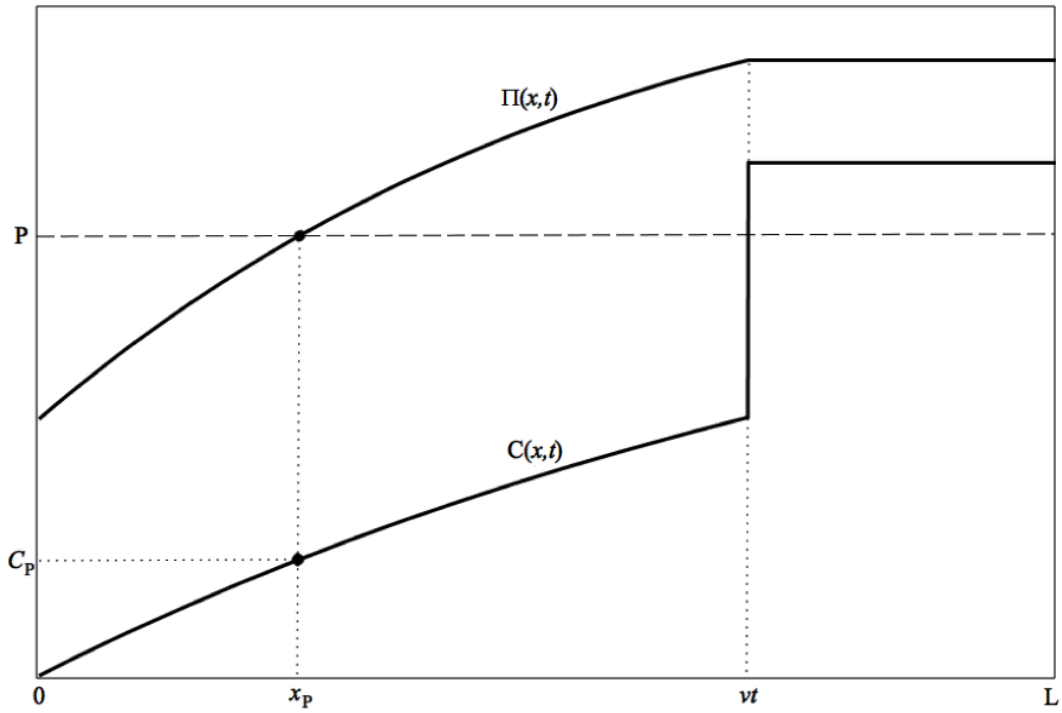

Figure 3.2: *Solution profiles for some $t < t^*$. We want to determine the rate of change of the fixed value P in terms of the corresponding variable concentration C_P.*

and applying the Implicit Function Theorem ([42]) to the equation $G(x_{\mathrm{P}}, t) = 0$, we find

$$\frac{dx_{\mathrm{P}}}{dt} = -\frac{\partial G}{\partial t}\left(\frac{\partial G}{\partial x_{\mathrm{P}}}\right)^{-1} \tag{3.19}$$

Since P is a constant, $\partial G/\partial t = \partial \Pi/\partial t$ and $\partial G/\partial x_P = \partial \Pi/\partial x_P$. Introducing the notation $C_P = C(x_P, t)$ and using equations (3.17) and (3.18), we obtain

$$\frac{\partial \Pi}{\partial t} = -\kappa (C_s - C_P) \tag{3.20}$$

$$\frac{\partial \Pi}{\partial x_P} = \frac{\kappa^2 C_s}{v^2}\left(\frac{v}{\kappa} + vt - x_P\right)\exp\left(\frac{-\kappa x_P}{v}\right) = \frac{\kappa}{v}(\Pi_0 - P + C_s - C_P) \tag{3.21}$$

Substituting these into equation (3.19) yields the rate of change of x_P in terms of the precipitate level P and the corresponding concentration value C_P:

$$\frac{dx_P}{dt} = \frac{v(C_s - C_P)}{\Pi_0 - P + C_s - C_P} \tag{3.22}$$

For instance, at some fixed time $\tau < t^*$ the precipitate level at $x = 0$ is $P = \Pi_0 - \kappa C_s \tau$ with corresponding concentration level $C_P = 0$. Equation (3.22) now implies that the "horizontal" rate of change of the precipitate profile at the inlet is $v/(1 + \kappa\tau)$.

3.3 Solution for $t \geq t^*$

The precipitate profile satisfies $\Pi(0, t^*) = 0$ and $\Pi(x, t^*) > 0$ for $x > 0$. The dissolution rate at the reservoir inlet suddenly drops from κC_s for $t < t^*$ to 0 at $t = t^*$ and the system of equations (3.1) and (3.2) changes to its alternate form $\partial C/\partial t = -v\partial C/\partial x$, $\partial \Pi/\partial t = 0$ here. This simpler system is no longer satisfied by equations (3.13) and (3.16). In order to give an intuitive description of what happens next, we let α_C be the point on the concentration profile such that $C \equiv 0$ if $x \leq \alpha_C$ and $C > 0$ if $x > \alpha_C$. This definition is analogous to the point α_Π on the precipitate profile. Note that we must have $\alpha_C \leq \alpha_\Pi$. Indeed, if $\alpha_C > \alpha_\Pi$, then $C \equiv 0$ and $\Pi > 0$ on the interval $\alpha_\Pi < x \leq \alpha_C$. But since $C \equiv 0$ is not a solution of equation (3.1) when $\Pi > 0$, this is a contradiction.

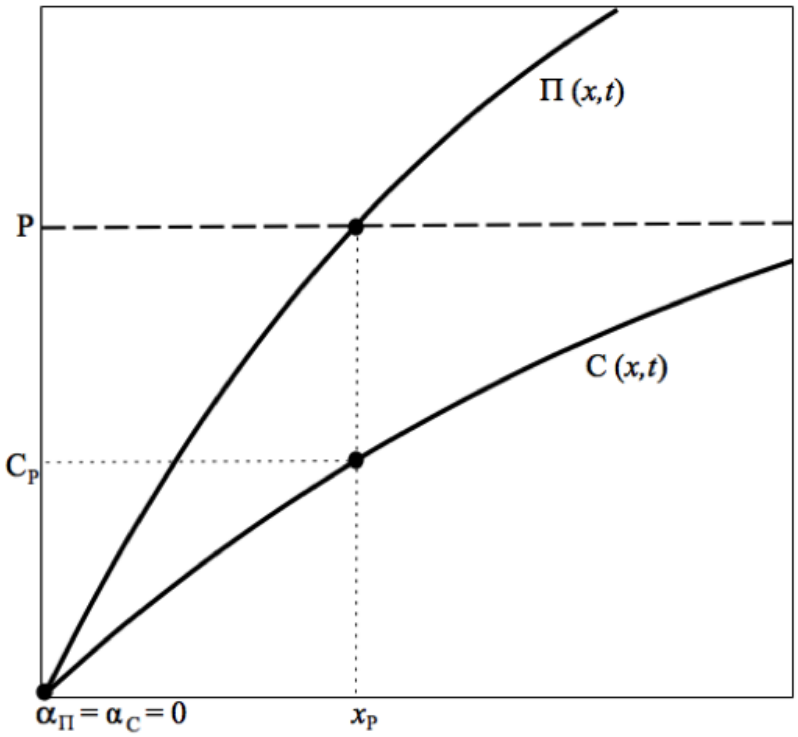

Figure 3.3: *Solution profiles at $t = t^*$.*

Figure 3.3 shows the situation at $t = t^*$, when $\alpha_\Pi = \alpha_C = 0$. On $0 < x \leq L$,

equations (3.13) and (3.16) still define the solution profiles and therefore equation (3.22) still describes the speed $x_P{}'(t)$ of any precipitate value $0 < P \leq \Pi_0$ in terms of the corresponding concentration value $C_P = C(x_P, t)$. Let us now make the assumption that this intrinsic relationship also applies to α_Π, despite the fact that the system of equations takes the form $\partial C/\partial t = -v\partial C/\partial x$, $\partial \Pi/\partial t = 0$ here (the correctness of this assumption will proved in Section 4.8). Then, substituting $P = 0$ and $C_0 = C(\alpha_\Pi, t)$, we obtain the relation

$$\frac{d\alpha_\Pi}{dt} = \frac{v(C_s - C_0)}{\Pi_0 + C_s - C_0} \tag{3.23}$$

Because $0 \leq C_0 \leq C_s$ and $\Pi_0 > 0$, equation (3.23) implies that $\alpha_\Pi{}'(t) < v$. We observe further that any solution of the transport equation $\partial C/\partial t = -v\partial C/\partial x$ must be of the form $C = C(x - vt)$. Since such a solution is propagated forward at velocity v, we deduce that $\alpha_C{}'(t) = v$. Given that $\alpha_\Pi(t^*) = \alpha_C(t^*) = 0$, it would therefore seem that α_C is about to overtake α_Π. However, as noted above, there is the constraint $\alpha_C \leq \alpha_\Pi$. This condition instantaneously "slows down" α_C, forcing it to have the same speed as α_Π, from which it follows that $\alpha_C = \alpha_\Pi$ during some time interval $[t^*, t^* + \delta t]$. Repeating this argument at $t = t^* + \delta t$ and subsequent stages, we deduce that $\alpha_C = \alpha_\Pi$ for all $t \geq t^*$.

In line with the notation used previously, we let $x_0 := \alpha_\Pi$, the root of the precipitate profile. Since $x_0 = \alpha_C$ by the above argument, we find that $C_0 = C(x_0, t) = 0$ in equation (3.23), and hence

$$\frac{dx_0}{dt} = U := \frac{vC_s}{\Pi_0 + C_s} \tag{3.24}$$

Using the initial condition $x_0(t^*) = 0$, we find $x_0(t) = U(t - t^*)$. We now look for a solution C^* of the system of equations (3.1) and (3.2) satisfying the condition $C^*(x_0, t) = 0$ for all $t \geq t^*$. Since $\Pi > 0$ for $x > x_0$, C^* will be of the form of equation (3.11). Substituting $x = x_0(t)$, the "moving boundary condition" is

$$0 = C_s + f(Ut - Ut^* - vt)\, e^{-\kappa t} \tag{3.25}$$

Introducing the variable $z = Ut - Ut^* - vt$ and rearranging terms, we find

$$f(z) \ = -C_s \exp\left(\frac{\kappa z + Ut^* z}{U - v}\right) \tag{3.26}$$

Note that $\kappa(U-v)^{-1} = -\left(C_s + \Pi_0\right) v^{-1}\kappa{\Pi_0}^{-1} = -(Ut^*)^{-1}$. Substituting equation (3.26) back into equation (3.11) then yields

$$C^*\left(x,t\right) = C_s - C_s \exp\left(\frac{Ut - Ut^* - x}{Ut^*}\right) \tag{3.27}$$

Putting C^* into equation (3.2) we obtain

$$\frac{\partial \Pi^*}{\partial t} = -\kappa C_s \exp\left(\frac{Ut - Ut^* - x}{Ut^*}\right) \tag{3.28}$$

As before, integrating with respect to t determines the precipitate up to an arbitrary function $h = h(x)$:

$$\Pi^*\left(x,t\right) = h\left(x\right) - \Pi_0 \exp\left(\frac{Ut - Ut^* - x}{Ut^*}\right) \tag{3.29}$$

We can use the condition $\Pi^*(x_0,t) = 0$ to find $h(x) = \Pi_0$. Comparing this with equation (3.27) we see that Π^* is just a scalar multiple of C^*:

$$\Pi^*\left(x,t\right) = \frac{\Pi_0}{C_s} C^*\left(x,t\right) \tag{3.30}$$

Direct substitution shows that C^* and Π^* coincide with equations (3.13) and (3.16) at $x = v(t-t^*)$. The solution in the "new region" $U\left(t-t^*\right) < x < v\left(t-t^*\right)$ is therefore continuously joined to the solution for all $x \geq v(t-t^*)$, along the characteristic through $(0,t^*)$. Equations (3.13) and (3.27) then constitute a weak solution of equation (3.1) on Ω_+ (i.e. equation (3.6)). We remark that the characteristic projections of equation (3.2) are the lines $x = \textit{constant}$, but that the edges in $\Pi(x,t)$ move along with the edges in $C(x,t)$. This is not a problem, because in *each* solution region of $C(x,t)$, equation (3.2) takes a *different* form, just as equation (3.1) is different in Ω_0 and Ω_+. The theory of weak solutions developed in Chapter 2 only applies if the coefficients of the PDE are differentiable.

We note that C^*, Π^* satisfy $\partial C/\partial t = -U\partial C/\partial x$, $\partial \Pi/\partial t = -U\partial \Pi/\partial x$ respectively and that they are consistent with equation (3.22): substituting $P = \Pi^*\left(x_P,t\right)$ and

$C_P = C^*(x_P, t) = C_s P/\Pi_0$ yields $dx_P/dt = U$. We also observe that the of velocity of a precipitate value P changes in a continuous way as it enters the new region. To see this, note that the front end of this region reaches P at time $\tau = t^* + x_P/v$. Using equation (3.18), we then have $P = \Pi_0 - \kappa C_s t^* \exp(\kappa t^* - \kappa\tau)$ and $C_P = C_s - C_s \exp(\kappa t^* - \kappa\tau)$. Substituting these values in equation (3.22) yields $dx_P/dt = U$, which shows that P already has velocity U when it falls into the new solution region. On the other hand, the velocity of the corresponding concentration value C_P "jumps" from 0 to U at $t = \tau$.

The existence of the travelling wave solution region has the following physical explanation: from the instant ($t = t^*$) the precipitate runs out at $x = 0$, *no* scale inhibitor is carried by the flux to the neighbouring point. The dissolution mechanism at that point can not react quickly enough to provide the sudden demand for "extra" scale inhibitor to maintain the steady-state concentration level. This again has the effect of *less* material being transported to the next point, and so on. Since the flux has velocity v, the disturbance away from the steady-state propagates at this velocity too. Of course, in the meantime, the precipitate has run out some distance away from the inlet and the process repeats itself. This causes a gradual overall reduction of concentration levels in the region $x < v(t - t^*)$. The distribution of scale inhibitor along the system in this case dictates that the concentration at any point decreases according to $\partial C/\partial t = -U\partial C/\partial x$, where U is the rate of "complete disappearance" of precipitate from the system. We stress that this physical interpretation works only if $U < v$, because the flux is then able to transfer "information" to the next point *before* the precipitate runs out there. In Chapter 4, we will see that this is not necessarily the case.

Dropping the notation involving C^* and Π^*, the solutions for $t \geq 0$, $0 \leq x \leq L$ are concisely written as follows:

$$C(x,t) = \begin{cases} C_s\ ,\ vt \leq x \leq L \\ C_s - C_s e^{-\kappa x/v}\ ,\ v(t - t^*) \leq x < vt \\ C_s - C_s \exp\left(\dfrac{Ut - Ut^* - x}{Ut^*}\right),\ U(t - t^*) \leq x < v(t - t^*) \\ 0\ ,\ 0 \leq x \leq U(t - t^*) \end{cases} \tag{3.31}$$

and

$$\Pi(x,t) = \begin{cases} \Pi_0 \ , \ vt \leq x \leq L \\ \Pi_0 + \dfrac{\kappa C_s}{v}(x - vt)\, e^{-\kappa x/v} \ , \ v(t - t^*) \leq x < vt \\ \dfrac{\Pi_0}{C_s} C(x,t) \ , \ U(t - t^*) \leq x < v(t - t^*) \\ 0 \ , \ 0 \leq x \leq U(t - t^*) \end{cases} \tag{3.32}$$

Although equation (3.31) is clearly a weak solution of equation (3.1) for $x > U(t - t^*)$ and as such will conserve scale inhibitor, the conserved *amount* clearly depends on Π. It should be remembered that, mathematically, these solutions were constructed using the assumption that the precipitate profile must be continuous, which uniquely determined the solution of equation (3.2) in each interval. The correctness of this assumption can be checked by verifying that the total amount of scale inhibitor initially present in the system, $L(C_s + \Pi_0)$, is preserved. The amount of chemical that is added to the mobile phase after some time $t > 0$ is found by evaluation of the definite integral of $C(x,t)$ between $x = 0$ and $x = vt$. In order for the solution to be physically correct, this must be equal to the total amount of precipitate used up. In other words, we need

$$\int_0^{vt} [\Pi_0 - \Pi(x,t)]\, dx = \int_0^{vt} C(x,t)\, dx \tag{3.33}$$

It is straightforward to show that equations (3.31) and (3.32) indeed satisfy equation (3.33). An alternative way to prove the conservation of mass is to consider the effluent concentration flux $vC_{eff}(t) := vC(L,t)$, which is the amount of chemical passing the reservoir outlet $x = L$ per unit time. Using equation (3.31) we have

$$vC_{eff}(t) = \begin{cases} vC_s \ , \ 0 \leq t \leq L/v \\ vC_s - vC_s e^{-\kappa L/v} \ , \ L/v \leq t < t^* + L/v \\ vC_s - vC_s \exp\left(\dfrac{Ut - Ut^* - L}{Ut*}\right) \ , \ t^* + L/v \leq t < \ t^* + L/U \end{cases} \tag{3.34}$$

Evaluation of the definite integral of $vC_{eff}(t)$ between 0 and $t^* + L/U$ yields

$$\begin{aligned}
\int_0^{t^*+L/U} vC_{eff}\,(t)\,dt &= [vC_s t]_0^{L/v} + \left[vC_s t - vC_s t \exp\left(\frac{-\kappa L}{v}\right)\right]_{L/v}^{L/v+t^*} \\
&\quad + \left[vC_s t - vC_s t^* \exp\left(\frac{Ut - Ut^* - L}{Ut^*}\right)\right]_{L/v+t^*}^{L/U+t^*} \\
&= vC_s\left(\frac{L}{U} + t^*\right) - vC_s t^* \exp\left(\frac{-\kappa L}{v}\right) - vC_s t^* \\
&\quad + vC_s t^* \exp\left(\frac{UL - vL}{vUt^*}\right) \\
&= L\,(C_s + \Pi_0) \qquad (3.35)
\end{aligned}$$

The question that arises is whether the argument can be reversed and if we can arrive at equation (3.31) and (3.32) by imposing the mass balance requirement in the first place. This amounts to proving that the correct amount of scale inhibitor is conserved if $\Pi(x,t)$ is chosen to be continuous.

Example 3.1: We consider the case with full solubility level $C_s = 1$ and initial precipitate level $\Pi_0 = 0.5$ on a reservoir of unit length ($L = 1$). Let the dissolution rate parameter and fluid velocity be $\kappa = 1$ and $v = 0.5$ respectively, so that the Damkohler number is $\kappa L/v = 2$. With these parameters, we find $t^* = 0.5$ and $U = 1/3$. Figure 3.4 shows the concentration and precipitate in-situ profiles for this case at time $t = 1.5$. The exact solutions given by equations (3.31) and (3.32) are plotted together with two numerical solutions obtained using the explicit first order finite difference scheme discussed in section 2.6. While the coarse calculation ($\Delta x = 0.01$) clearly shows the effects of "numerical viscosity" near irregular (non-smooth) points, the finer calculation ($\Delta x = 0.001$) achieves very good agreement with the exact solution. Figure 3.5 shows the effluent concentration flux curve for this example. The point x_0 reaches the outlet at $t = t^* + L/U = 3.5$ and $C \equiv 0$ afterwards. We note that increasing or decreasing the Damkohler number $\kappa L/v$ in these plots would lead to a higher or lower concentration profile respectively. Analogous to this "vertical" effect of the Damkohler number, the ratio Π_0/C_s affects the profiles "horizontally". Very low values of Π_0/C_s result in $U \approx v$, so that the

new region is very narrow and could be confused with a shock discontinuity. On the other hand, very high values of Π_0/C_s stretch this region considerably (since then $U << v$).

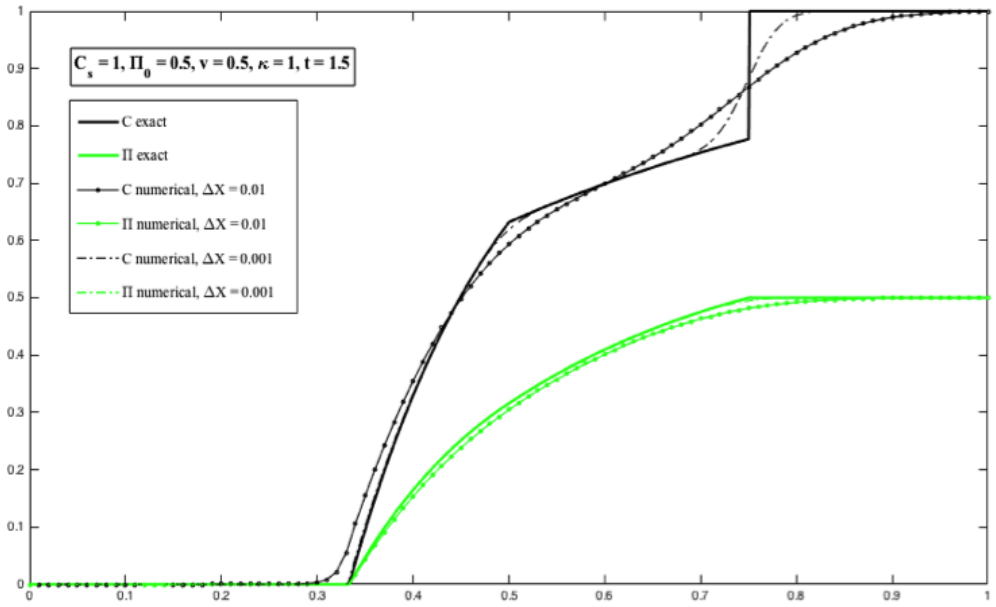

Figure 3.4: *Analytical and numerical* C *and* Π *profiles for example 3.1 at* $t = 1.5$

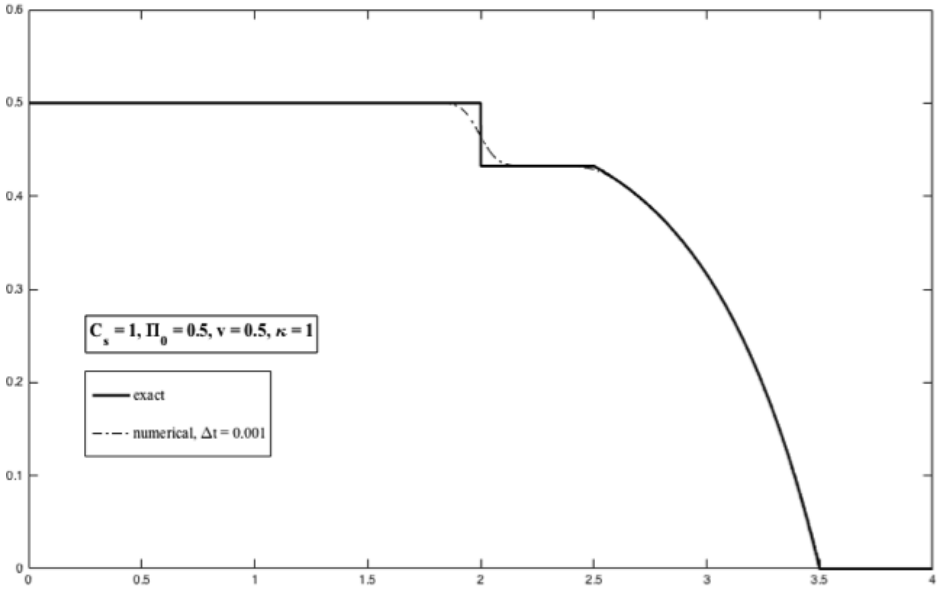

Figure 3.5: *Effluent concentration flux for example 3.1*

3.4 Interpretation in terms of characteristics

We will now describe equation (3.31) in terms of characteristics. Consider $x_0(t) = U(t - t^*)$ for $t \geq t^*$, where $U := v\Pi_0/(\Pi_0 + C_s) < v$ is the *known* constant speed found in section 3.2. This line separates the domains Ω_0 and Ω_+, as shown again

in Figure 3.6. In Ω_0, equation (3.1) is the homogenous transport equation and the solution is a travelling wave of speed v. In Ω_+, equation (3.1) is non-homogenous with general solution given by equation (3.11). Note that $C = C(x, t^*)$ is given by equation (3.13), as a result of the initial condition $C(x, 0) = C_s$ and the boundary condition $C(0, t) = 0$ for $t > 0$. In order to find the solution on Ω_+ for $t > t^*$, we need to have knowledge of C on the boundary curve $x_0 = x_0(t)$. The characteristics of equation (3.36) are the lines $x - vt = \beta$ in both domains. Since the equation is homogenous in Ω_0, the solution here is constant along characteristics. With $C(0, t) = 0$, this implies that $C \equiv 0$ in Ω_0, which also determines the required boundary condition $C(x_0, t) = 0$. Equation (3.11) can now be specified to obtain equation (3.27) and the solution profile at some $\tau \geq t^*$ consists of four regions.

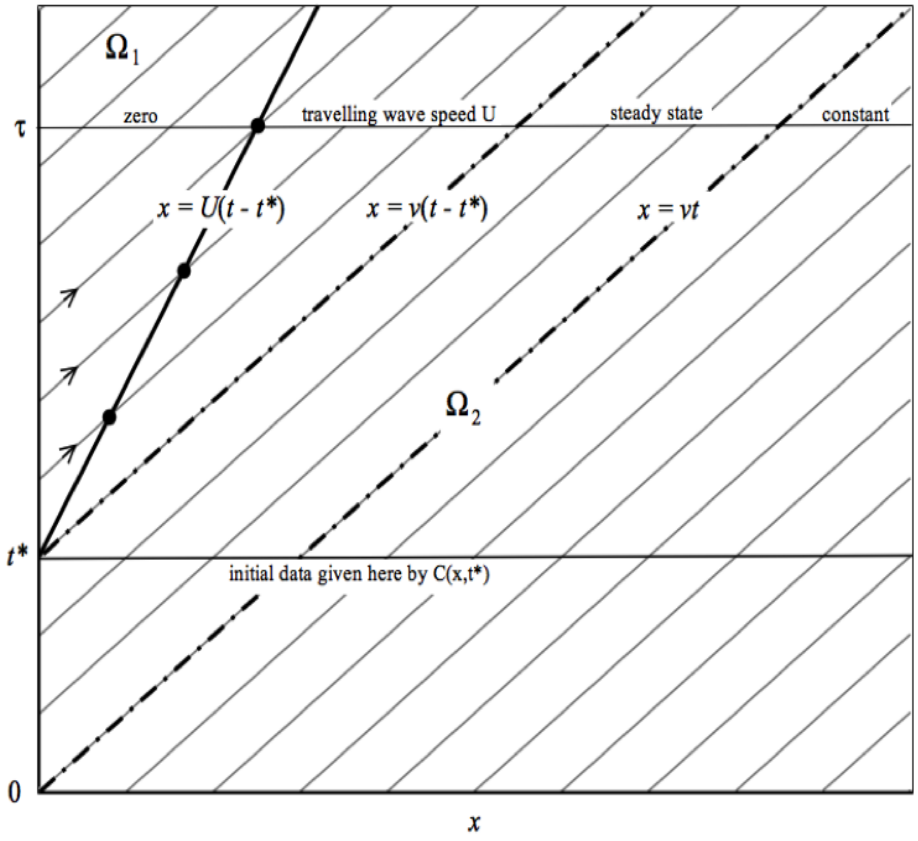

Figure 3.6: *The solution regions of the Cauchy problem when the constant $U < v$ is the slope of the moving boundary.*

The boundary data on $\partial\Omega$ are "sent" along characteristics to the boundary curve $x_0 = U(t - t^*)$, thus providing the information needed to solve equation (3.1) on Ω_+. This is only possible because $U < v$ here. Since this will not be the case in general (see Chapter 4) it is worthwhile examining what would happen if $U > v$.

For simplicity, we will assume that U is a constant, although we could equally well carry out the analysis in this section for a more general velocity, $U = U(x, t, C)$ say.

Suppose that the solution is known at some time τ (see Figure 3.7). Let $D = (x_0, \tau) \in \Omega_0$ be a point on the boundary, where the solution takes the value $\xi(D)$. Since $D \in \Omega_0$, the value $\xi(D)$ will be transported along characteristic L_1 and, some time $\delta\tau$ later, arrive at $F = (x_0 + v\delta\tau, \tau + \delta\tau) \in \Omega_0$. Now consider the point $E = (x_0 + (U - v)\delta\tau, \tau)$ in Ω_+, with solution value $\xi(E)$. In time $\delta\tau$ this will travel along characteristic L_2 through $G = (x_0 + U\delta\tau, \tau + \delta\tau)$ on the boundary and in doing so changes its value to $\xi(G)$. Since $G \in \Omega_0$, the value $\xi = \xi(G)$ will remain constant on L_2 from $\tau + \delta\tau$ on. In this way the moving boundary "builds" a travelling wave solution in Ω_0 from the solution in Ω_+ . As a consequence, C no longer vanishes at x_0. Indeed, the process described in Figure 3.7 results in a (non-zero) travelling wave being "left behind" the moving boundary.

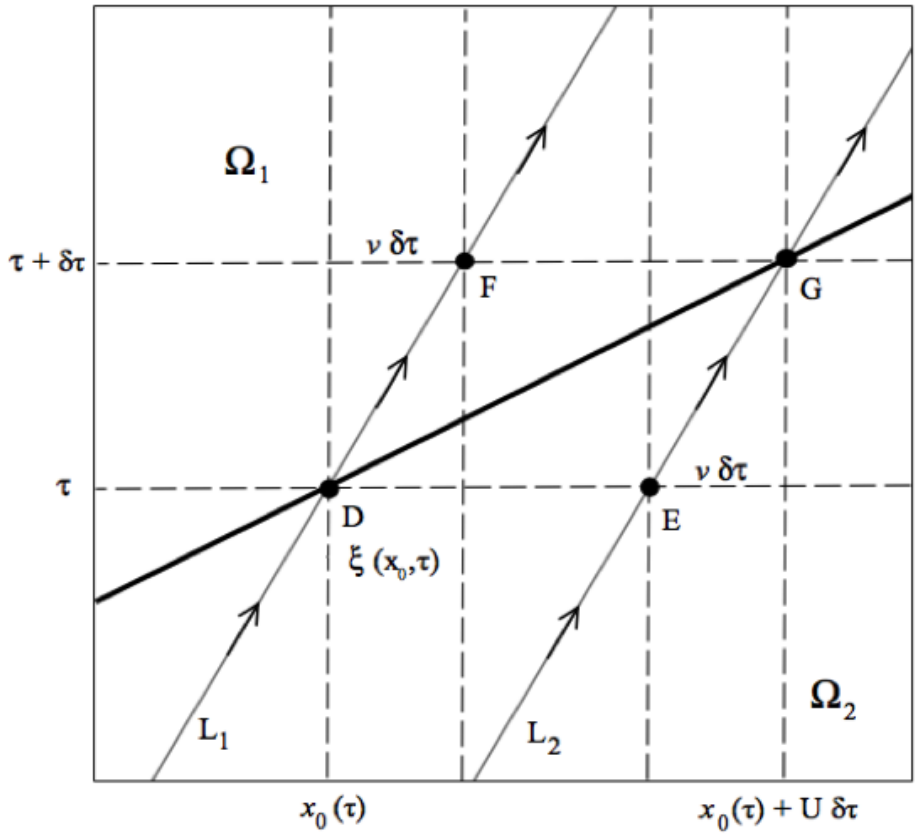

Figure 3.7: *Formation of a travelling wave solution in* Ω_0 *if* $U > v$.

3.5 Summary

In this chapter, we have examined the scale inhibitor model with no adsorption and dispersion, when the system of equations (1.6)-(1.8) reduces to equations (3.1)-(3.2). We solved the Cauchy Problem on Ω with piecewise constant data $C(x,0) = C_s$, $\Pi(x,0) = \Pi_0$ on $0 \leq x \leq L$ and $C(0,t) = 0$ for $t > 0$. These conditions implied that the precipitate at the reservoir inlet ran out at $t = t^* = \Pi_0/\kappa C_s$, which was the first time that the Heaviside function in equation (3.2) played a role on Ω. The solution for $t < t^*$ was constructed in section 3.2 (equations (3.13) and (3.16)) and we used it to find a relationship for the rate of change of an arbitrary precipitate value P in terms of the corresponding concentration value C_P (equation (3.22)). This relationship was then *assumed* to apply also to the "root" α_Π of the precipitate profile, even though equations (3.13) and equations (3.16) did not solve the system at $x = \alpha_\Pi$. As a result of this assumption, the concentration and precipitate profiles for $t > t^*$ were seen to have a joint root x_0 moving along the x-axis with constant velocity $U = vC_s/(\Pi_0 + C_s)$. This implied the emergence of a travelling wave solution component. Explicit integration showed that the resulting weak solution (equation (3.31)) of equation (3.1) conserves the total amount of injected chemical, thus confirming that our assumption of a continuous precipitate profile is physically correct. The question arose as to whether this process could be reversed and if we could prove that mass conservation implies the continuity requirement in the first place. This is simple if we know a priori that $d\alpha_\Pi/dt$ is constant, but far from obvious if this information is not given. There is bound to be some deeper connection between the conservation of mass and the "invariance" of equation (3.22), but it is as yet unresolved.

With a view towards Chapter 4, we looked at how the point $\alpha_\Pi(t)$ traces out a boundary curve dividing Ω into the regions Ω_0 (where $\Pi \leq 0$) and Ω_+ (where $\Pi > 0$). Knowledge of C on this boundary allows the construction of the solution everywhere in Ω. For the Cauchy problem discussed in this chapter, we had a straight line boundary of slope $U < v$. The condition $C(0,t) = 0$ for $t > 0$ could then be transported along characteristics to the new boundary condition $C(\alpha_\Pi, t) = 0$, which then determined the solution in Ω_2. However, in general, the velocity U depends on x, t and C and it can happen that $U > v$. We explained how the solution in Ω_+ then defines a solution in Ω_0.

Chapter 4

Exact solutions of the scale inhibitor model with variable fluid velocity and no adsorption

4.1 Introduction

We now extend the discussion given in Chapter 3 and consider what happens when the flow at constant velocity $v = v_1$ is stopped (i.e. $v = 0$) during a "shut-in" period $t_1 \leq t < t_2$, and is then restarted at a different constant velocity, $v = v_2$. This process is described by the equations

$$\frac{\partial C}{\partial t} + v(t)\frac{\partial C}{\partial x} = -\frac{\partial \Pi}{\partial t} \tag{4.1}$$

$$\frac{\partial \Pi}{\partial t} = -\kappa\left(C_s - C\right) \cdot \left[H\left(\Pi\right) + H\left(C - C_s\right) - H\left(\Pi\right) H\left(C - C_s\right)\right] \tag{4.2}$$

where the time-dependent velocity term in equation (4.1) is

$$v\left(t\right) = \begin{cases} v_1 \ , \ 0 \leq t < t_1 \\ 0 \ , \ t_1 \leq t < t_2 \\ v_2 \ , \ t_2 \leq t \end{cases} \tag{4.3}$$

Figure 4.1 shows how this sub-divides $\Omega = [0, L] \times [0, \infty)$. With Cauchy data $C\left(x, 0\right) = C_s$, $\Pi\left(x, 0\right) = \Pi_0$ and $C\left(0, t\right) = 0$, the solution during the first flow

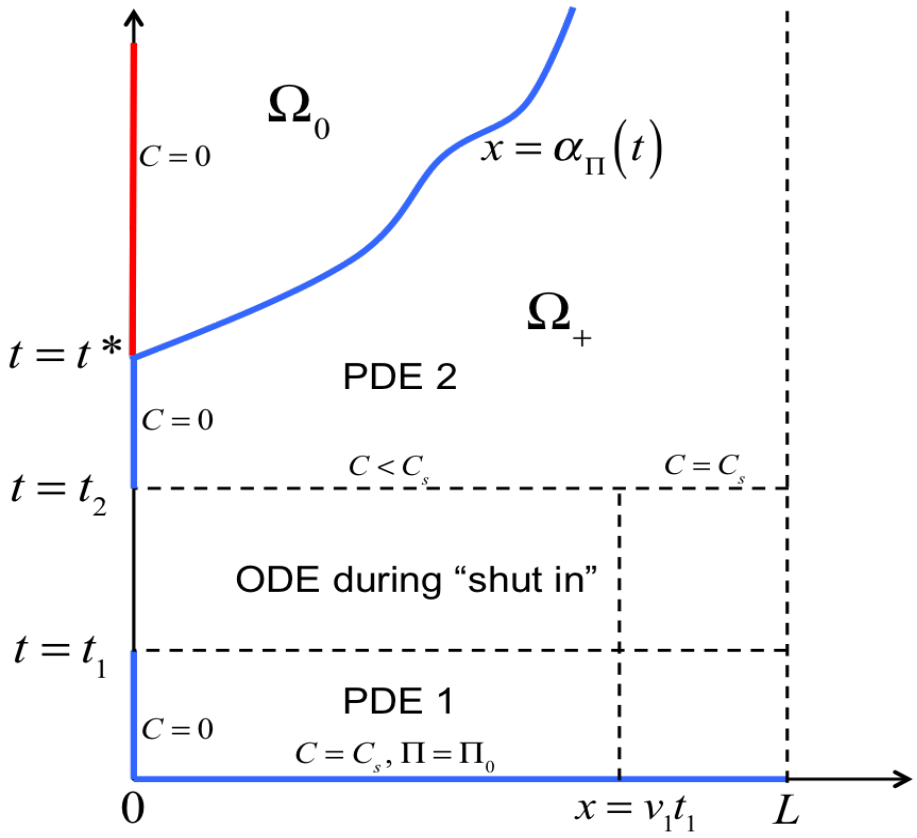

Figure 4.1: *Schematic of the regions of* Ω *in Case 1:* $t^* > t_2$.

phase $0 < t < t_1$ (when $v = v_1$) is given by equations (3.31) and (3.32). This defines initial conditions for the ODEs which govern the shut-in phase $[t_1, t_2)$ (when $v = 0$). In this static dissolution process, the concentration increases everywhere and approaches C_s if $t_2 >> t_1$ (provided there is enough precipitate). If $v_1 t_1 < L$, a discontinuity in $\Pi(x,t)$ forms at $x = v_1 t_1$, since $C = C_s$ for $v_1 t_1 \leq x \leq L$. The profiles at $t = t_2$ are initial conditions for the second flow phase ($v = v_2$), when the boundary condition $C(0,t) = 0$ is needed again.

As in Chapter 3, we consider the time t^* such that $\Pi(0,t^*) = 0$. It will be shown that this is the first time the precipitate runs out on $[0, L]$. Depending on the parameters $C_s, \Pi_0, \kappa, t_1, t_2$, several scenarios are possible. During the first flow phase, we have $\Pi(0,t) = \Pi_0 - \kappa C_s t$. Clearly, if $\Pi_0 < \kappa C_s t_1$, this reaches zero at $t^* = \Pi_0/\kappa C_s < t_1$ (we refer to this as **Case 3**). On the other hand, if $\Pi_0 \geq \kappa C_s t_1$, then $\Pi(0,t_1) > 0$ and we determine $C(0,t) = C_s - C_s e^{\kappa t_1 - \kappa t}$ and $\Pi(0,t) = \Pi_0 - \kappa C_s t_1 - C_s + C_s e^{\kappa t_1 - \kappa t}$ for some $t > t_1$. It follows that if $\Pi_0 < C_s(1 + \kappa t_1 - e^{\kappa t_1 - \kappa t_2})$, the precipitate at the inlet runs out during the shut-in phase (**Case 2**), at time

$$t^* = t_1 - \frac{1}{\kappa} \ln \left[1 + \kappa t_1 - \frac{\Pi_0}{C_s} \right] \tag{4.4}$$

Finally, if $\Pi_0 \geq C_s \left(1 + \kappa t_1 - e^{\kappa t_1 - \kappa t_2}\right)$, we have $\Pi\left(0, t_2\right) > 0$ (**Case 1**). During the second flow phase, we have $\Pi\left(0, t\right) = \Pi_0 - \kappa C_s t_1 - C_s + C_s e^{\kappa t_1 - \kappa t_2} - \kappa C_s t$ for some $t > t_2$ and then

$$t^* = t_2 - t_1 + \frac{1}{\kappa} \left[\frac{\Pi_0}{C_s} + e^{\kappa t_1 - \kappa t_2} - 1 \right] \tag{4.5}$$

We will focus primarily on the solution of Case 1, when Π_0 is high enough to ensure that $t^* > t_2$ (this case is shown in Figure 4.1). For $t \geq t^*$, the boundary curve $x = \alpha_\Pi(t)$ defines the region Ω_0 in which $\Pi(x, t) = 0$. The initial conditions (at $t = t_2$) for the PDE in the second flow phase are *not* constant and this will lead to an ODE of the form $d\alpha_\Pi/dt = F\left(C(\alpha_\Pi, t), \alpha_\Pi\right)$. It will emerge that, depending on the values of Π_0 and the ratio v_1/v_2, we can have $d\alpha_\Pi/dt < v_2$ for all $t \geq t^*$ (**Case 1a**). Full analytical solutions may then be derived (sections 4.4 and 4.5). Explicit formulae are available if $v_1 = v_2$ and an implicit description must be used when $v_1 \neq v_2$. However, another case (**Case 1b**) can occur, where there is a time $\tau > t^*$ such that $d\alpha_\Pi/dt > v_2$ for $t^* < t < \tau$ and $d\alpha_\Pi/dt > v_2$ for $t > \tau$. In this scenario, the rate at which the "zero precipitate zone" advances is initially greater than the fluid velocity. The precipitate at $x = \alpha_\Pi$ then disappears before the flux can carry off the dissolved scale inhibitor, resulting in a non-zero concentration region in Ω_0, as was discussed in section 3.4. This concentration is carried back into Ω_+ when $d\alpha_\Pi/dt > v_2$. We will see that there is no full analytical solution for this case. Similarly, Case 2 and Case 3 split into *a*-cases, admitting a full analytical solution, and *b*-cases, in which such a solution can not be obtained. The only difference here is that the boundary curve emerges already during the shut-in or first flow phase.

4.2 First flow phase and shut-in phase (Case 1)

The concentration and precipitate profiles during the first flow phase are the same as in Chapter 3, with $v = v_1$. That is,

$$C\left(x, t\right) = \begin{cases} C_s \ , & v_1 t \leq x \leq L \\ C_s - C_s e^{-\kappa x / v_1}, & 0 \leq x < v_1 t \end{cases} \tag{4.6}$$

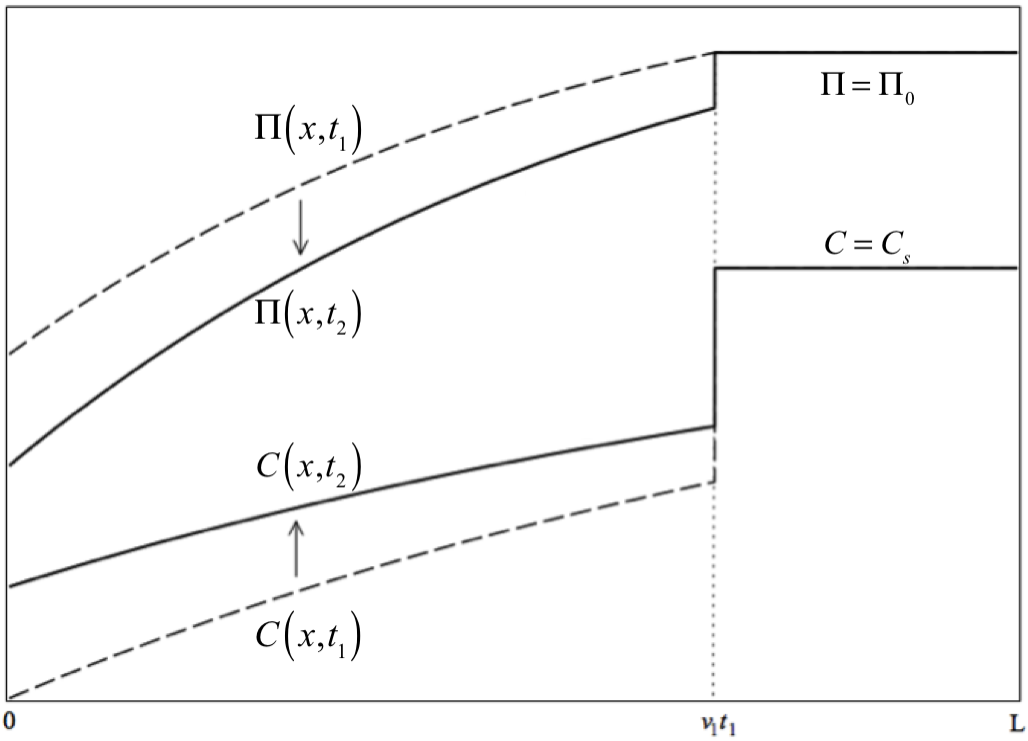

Figure 4.2: *Solution profiles at $t = t_1$ correspond to the dashed line plots and those at $t = t_2$ to the solid line plots.*

and

$$\Pi(x,t) = \begin{cases} \Pi_0 \ , & v_1 t \le x \le L \\ \Pi_0 + \dfrac{\kappa C_s}{v_1}(x - v_1 t)\, e^{-\kappa x / v_1} , & 0 \le x < v_1 t \end{cases} \tag{4.7}$$

With $v(t) = 0$ for $t \in [t_1, t_2)$ and $\Pi > 0$, equations (4.1) and (4.2) reduce to

$$\frac{\partial C}{\partial t} = -\frac{\partial \Pi}{\partial t} = \kappa (C_s - C) \tag{4.8}$$

This gives $C(x,t) = C_s + A(x)\, e^{-\kappa t}$, where the coefficient $A(x)$ is determined by evaluating equation (4.6) at $t = t_1$. Thus, for $x < v_1 t_1$, we need $C(x,t_1) = C_s + A(x)\, e^{-\kappa t_1} = C_s - C_s e^{-\kappa x / v_1}$, from which we find $A(x) = -C_s e^{\kappa t_1 - \kappa x / v_1}$. Similarly, $A(x) = 0$ for $x \ge v_1 t_1$, and hence

$$C(x,t) = \begin{cases} C_s \ , & v_1 t_1 \le x \le L \\ C_s - C_s e^{\kappa t_1 - \kappa t - \kappa x / v_1} \ , & 0 \le x < v_1 t_1 \end{cases} \tag{4.9}$$

The corresponding precipitate profile is now found by substituting equation (4.9) into equation (4.8) and evaluating equation (4.7) at $t = t_1$. This yields

$$\Pi(x,t) = \begin{cases} \Pi_0 \ , \ \ v_1 t_1 \leq x \leq L \\ \\ \Pi_0 + C_s \left(\dfrac{\kappa x}{v_1} - \kappa t_1 + e^{\kappa t_1 - \kappa t} - 1 \right) e^{\kappa x / v_1}, \quad 0 \leq x < v_1 t_1 \end{cases} \tag{4.10}$$

Since $\Pi_0 \geq C_s \left(1 + \kappa t_1 - e^{\kappa t_1 - \kappa t_2}\right)$, we have $\Pi(x,t) > 0$ for all $t \in [t_1, t_2)$, $x \in [0, L]$. Figure 4.2 shows the solution profiles given by equation (4.9) and equation (4.10) at the end of the shut-in phase. A discontinuity has appeared in the precipitate profile at $x = v_1 t_1$, which we will refer to as the "Π-discontinuity". For cases with a very long shut-in period, the concentration can be seen to approach full solubility level C_s everywhere.

4.3 Second flow phase (Case 1)

4.3.1 Concentration profile

We now consider what happens during the second flow phase, when $v(t) = v_2$. With $\Pi > 0$, the general solution of equation (4.1) is given in terms of some arbitrary function f as

$$C(x,t) = C_s + f(x - v_2 t)\, e^{-\kappa t} \tag{4.11}$$

The initial solution profiles $C(x, t_2)$ and $\Pi(x, t_2)$ are given by equations (4.9) and (4.10) respectively (see Figure 4.2). Since $\Pi(x, t_2) > 0$ for all $x \in [0, L]$, there must be a time interval at the beginning of the second flow phase during which the concentration profile is of the form of equation (4.11) everywhere on $[0, L]$. The arbitrary function f in that case is determined using two conditions. First of all, equation (4.11) should reduce to equation (4.9) if $t = t_2$. For $0 \leq x < v_1 t_1$ this implies that

$$C_s + f(x - v_2 t_2)\, e^{-\kappa t_2} = C_s - C_s e^{\kappa t_1 - \kappa t_2 - \kappa x / v_1} \tag{4.12}$$

Re-writing this using the substitution $z = x - v_2 t_2$, we find $f = f(z)$ and hence

$$C_1(x,t) = C_s - C_s \exp\left[\frac{-\kappa}{v_1} \left(x + v_1 t - v_2 t + v_2 t_2 - v_1 t_1 \right) \right] \tag{4.13}$$

for $v_2\,(t-t_2) \le x < v_1 t_1 + v_2\,(t-t_2)$. Similarly, for $x > v_1 t_1$ we need $C_s + f\,(x - v_2 t_2)\,e^{-\kappa t_2} = C_s$, from which it follows that the concentration is $C_0\,(x,t) = C_s$ for $x \ge v_1 t_1 + v_2\,(t-t_2)$. In order to determine the function f (and hence C) completely, we must also use the boundary condition $C\,(0,t) = 0$ for all $t > t_2$. Analogous to equation (4.6), this results in

$$C_2\,(x,t) = C_s - C_s e^{-\kappa x/v_2}\ , \quad 0 \le x < v_2(t-t_2) \tag{4.14}$$

The notation C_0, C_1, C_2 is used here to distinguish the different solution components. They are separated by two contact discontinuities (see Figure 4.3).

4.3.2 Precipitate profile

At some time $t > t_2$ the solution profile of Π will consist of four different regions. In Figure 4.3 below the case $v_2(t-t_2) < v_1 t_1$ is considered, when the concentration front connecting C_1 and C_2 has not yet reached the Π - discontinuity at $x = v_1 t_1$. The four regions of the precipitate profile are labeled by A, B, C and D.

Region (A): this is the right-most interval, $v_1 t_1 + v_2\,(t-t_2) \le x \le L$. Here we have $\Pi_A = \Pi_0$. The first concentration discontinuity has not yet reached this region and therefore no precipitate has dissolved.

Region (B): the interval $v_1 t_1 \le x \le v_1 t_1 + v_2\,(t-t_2)$. This is the region between the Π - discontinuity and the first C - discontinuity. We know that $C = C_1$ (equation (4.13)) here. Substitution into equation (4.2) and integration with respect to t yields

$$\Pi_B\,(x,t) = g_B\,(x) + \frac{v_1}{v_1 - v_2} C_s \exp\left[\frac{-\kappa}{v_1}\,(x + v_1(t-t_1) + v_2(t_2 - t))\right] \tag{4.15}$$

The arbitrary function g_B is found by joining this expression to the one describing the precipitate in neighbouring region (A). So at $x = v_1 t_1 + v_2\,(t-t_2)$, we require that $\Pi_B(x,t) = \Pi_0$. Writing $t = t_2 + (x - v_1 t_1)/v_2$ this condition simplifies to

$$g_B\,(x) = \Pi_0 - \frac{v_1}{v_2 - v_1} C_s \exp\left[\frac{-\kappa}{v_2}\,(x + v_2 t_2 - v_1 t_1)\right] \tag{4.16}$$

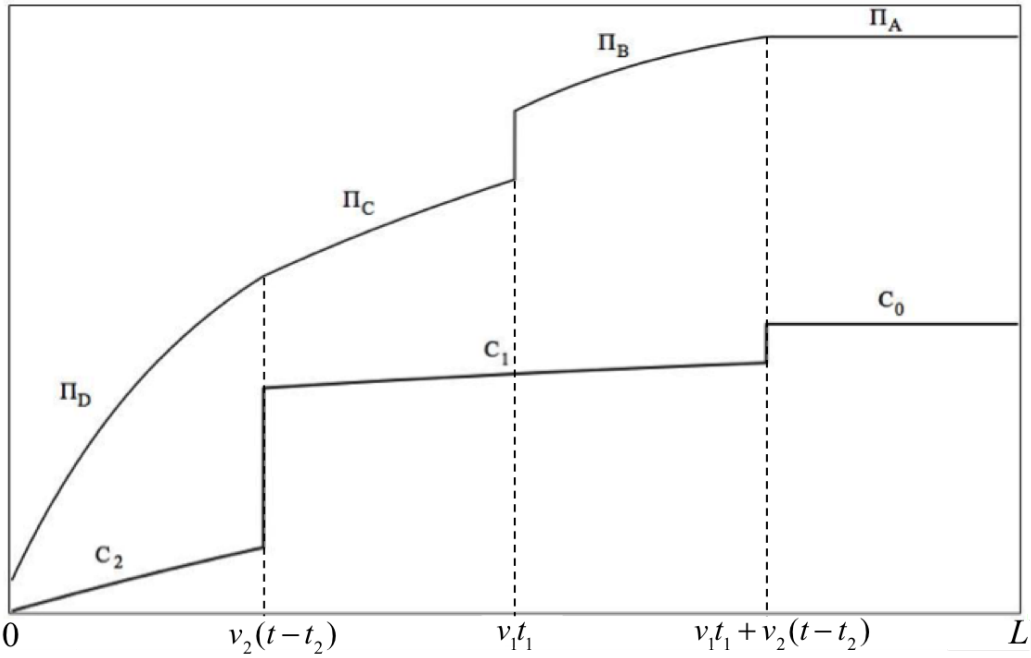

Figure 4.3: *Solution profiles before the second C-discontinuity reaches the* Π-*discontinuity.*

Substituting into equation (4.15), we find

$$\Pi_B(x,t) = \Pi_0 - \frac{v_1}{v_1 - v_2} C_s \exp\left[\frac{-\kappa}{v_2}(x + v_2 t_2 - v_1 t_1)\right] + \frac{v_1}{v_1 - v_2} C_s \exp\left[\frac{-\kappa}{v_1}(x + v_1(t - t_1) + v_2(t_2 - t))\right] \tag{4.17}$$

Region (C): this is the interval $v_2(t - t_2) \leq x \leq v_1 t_1$ between the second C - discontinuity and the Π - discontinuity. Also here the concentration is $C = C_1$ and hence

$$\Pi_C(x,t) = g_C(x) - \frac{v_1}{v_2 - v_1} C_s \exp\left[\frac{-\kappa}{v_1}(x + v_1(t - t_1) + v_2(t_2 - t))\right] \tag{4.18}$$

The function g_C is now found by demanding that equation (4.10) is recovered if $t = t_2$ in equation (4.18). This yields

$$\Pi_C(x,t) = \Pi_0 + \exp\left(\frac{-\kappa x}{v_1}\right) \cdot \left(\frac{\kappa}{v_1}(x - v_1 t_1) + \exp(\kappa t_1 - \kappa t_2) - 1\right) - \frac{v_1}{v_1 - v_2} C_s \exp\left[\frac{-\kappa}{v_1}(x + v_1(t_2 - t_1))\right] + \frac{v_1}{v_1 - v_2} C_s \exp\left[\frac{-\kappa}{v}(x + v_1(t - t_1) + v_2(t_2 - t))\right] \tag{4.19}$$

Region (D): this is the interval $0 \leq x \leq v_2\,(t - t_2)$ between the inlet and the second C - discontinuity; see Figure 4.3. Now $C = C_2$ (equation (4.14)), from which we find

$$\Pi_D\,(x,t) = g_D\,(x) - \kappa C_s t \cdot e^{-\kappa x/v_2} \tag{4.20}$$

The arbitrary function g_D is found as in region (B), by joining the solution at the right-hand boundary to $\Pi = \Pi_C$. So at $x = v_2\,(t - t_2)$ we need to match equations (4.19) and (4.20). This results in the following component:

$$\begin{aligned}\Pi_D\,(x,t) = \Pi_0 &+ \left(\frac{\kappa}{v_1}(x - v_1 t_1) + e^{\kappa t_1 - \kappa t_2} - 1\right) C_s e^{-\kappa x/v_1} \\ &+ \frac{\kappa}{v_2}\left[x - v_2(t - t_2)\right] C_s e^{-\kappa x/v_2} \\ &+ \frac{v_1}{v_1 - v_2} C_s e^{\kappa t_1 - \kappa t_2}\left[e^{-\kappa x/v_2} - e^{-\kappa x/v_1}\right]\end{aligned} \tag{4.21}$$

Assume now that $\Pi(x,t) > 0$ on $[0, L]$ at $t = t_2 + v_1 t_1/v_2$ (whether this is possible will depend on the specific choice of parameters). The second C - discontinuity is then at $x = v_1 t_1$ and precipitate profile consists of the three components Π_A , Π_B, Π_D . For $t > t_2 + v_1 t_1/v_2$, region B splits up into two separate intervals, which we will call B1 and B2 respectively.

Region (B1): the interval $v_2\,(t - t_2) \leq x \leq v_1 t_1 + v_2\,(t - t_2)$, between the two C - discontinuities, which are now both behind the Π- discontinuity; see Figure 4.4. Here the solution for region B given by equation (4.17) remains valid.

Region (B2): interval $v_1 t_1 \leq x \leq v_2\,(t - t_2)$ defines a new region between the Π - discontinuity and the C - discontinuity; see Figure 4.4. The concentration here is C_2 (equation (4.14)) and the precipitate profile is of the form of equation (4.20) with a new arbitrary function g_{B2}. This is found by requiring the solution to satisfy equation (4.17) at $x = v_2(t - t_2)$. Then,

$$\begin{aligned}\Pi_{B2}\,(x,t) = \Pi_0 &+ \frac{\kappa}{v_2}\left[x - v_2(t - t_2)\right] C_s e^{-\kappa x/v_2} \\ &+ \frac{v_1}{v_1 - v_2} C_s e^{\kappa t_1 - \kappa t_2}\left[e^{-\kappa x/v_2} - e^{-\kappa x/v_1}\right]\end{aligned} \tag{4.22}$$

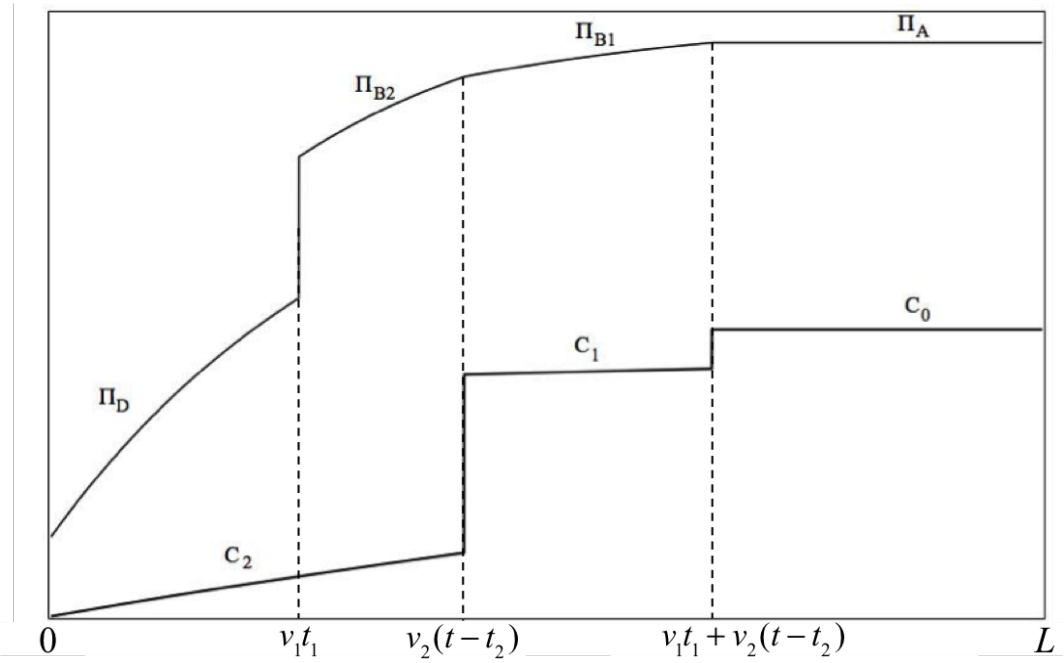

Figure 4.4: *Solution profiles after the second C-discontinuity has passed the* Π-*discontinuity and the new regions B1 and B2 emerge.*

4.4 Solution for $t \geq t^*$ (Case 1)

Setting $x = 0$ in equation (4.21) verifies that $\Pi_D(0, t^*) = 0$, where t^* is the time defined in equation (4.5). Using the formulae for the individual solution components derived in section 4.3, it may be shown that $\Pi(x, t) > 0$ for all $t \in [0, t^*]$, $0 < x \leq L$. The precipitate therefore first runs out at the inlet boundary. For parameter choices satisfying $t^* \leq t_2 + v_1 t_1 / v_2$ there will be the four regions A, B, C, D at (as in Figure 4.3, with $\Pi_D(0, t^*) = 0$ now). On the other hand, if $t^* > t_2 + v_1 t_1 / v_2$ the profiles at $t = t^*$ will consist of the regions A, B1, B2, D (as in Figure 4.4). Either way, the solution in the last region is given by the components C_2 and Π_D.

On the inlet boundary, the dissolution rate of precipitate instantaneously falls from κC_s for $t < t^*$ to 0 at $t = t^*$. With no shut-in phase ($t_1 = t_2$) and a constant fluid velocity ($v = v_1 = v_2$), we saw in Chapter 3 that this discontinuity in $\partial\Pi/\partial t$ led to the emergence of a travelling wave solution of velocity $U = vC_s/(\Pi_0 + C_s)$. This was the consequence of the preservation of a certain relationship between C and Π. In complete analogy with this approach, we will consider a point $(x_P, P) \in \Pi_D$, where P is a fixed precipitate level and $x_P = x_P(t)$ the value such that $\Pi_D(x_P, t) = P$. The horizontal rate of change of x_P is

$$\frac{dx_P}{dt} = -\frac{\partial \Pi_D}{\partial t}\left(\frac{\partial \Pi_D}{\partial x}\right)^{-1} \tag{4.23}$$

Let $C_P = C_2(x_P, t) = C_s - C_s \exp(-\kappa x_P / v_2)$ denote the corresponding concentration value. Note that $\partial \Pi_D / \partial t = -\kappa (C_s - C_P)$. Using equation (4.20), $\Pi_D(x_P, t) = g_D(x_P) - \kappa C_s t \exp(-\kappa x_P / v_2) = P$ and hence

$$\frac{\partial \Pi_D}{\partial x_P} = {g_D}'(x_P) + \frac{\kappa^2 C_s}{v_2} t \exp\left(-\frac{\kappa x_P}{v_2}\right) = {g_D}'(x_P) + \frac{\kappa}{v_2} g_D(x_P) - \frac{\kappa}{v_2} P \tag{4.24}$$

Differentiating g_D and cancelling terms, it can now be shown that

$$\frac{dx_P}{dt} = \frac{v_2 (C_s - C_P)}{\Pi_0 - P + C_s - C_P + \psi(x_P)} \tag{4.25}$$

where $\psi := \psi(x)$ is given by

$$\psi(x) = \frac{v_2}{v_1}\left[1 - e^{\kappa t_1 - \kappa t_2} + \frac{\kappa}{v_1 v_2}(v_1 - v_2)\left(x - v_1 t_1 - \frac{v_1}{\kappa}\right)\right] C_s e^{-\kappa x / v_1} \tag{4.26}$$

Equation (4.25) expresses the "horizontal speed" of the point (x_P, P) on the curve Π_D in terms of itself and the corresponding concentration value C_P on the curve C_2. Note that if $t_1 = t_2$ and $v_1 = v_2$, then $\psi \equiv 0$ and we recover the expression for dx_P/dt found in Chapter 3. In more general cases where either $t_1 \neq t_2$ or $v_1 \neq v_2$, or both, the function ψ is non-zero and can be thought of as containing the information about the shut-in period and change in flow rate. We observe that equation (4.25) is also satisfied by a point (x_P, P) on Π_C, with $C_P = C_1(x_P, t)$. This relationship is therefore invariant between the solution regions C and D. We will treat this idea of invariance more rigorously in section 4.8.

As in Chapter 3, we define the "root" $\alpha_C \geq 0$ for $t \geq t^*$ such that $C \equiv 0$ for $x \leq \alpha_C$, $C > 0$ for $x > \alpha_C$. Note that $\alpha_C(t^*) = \alpha_\Pi(t^*) = 0$ and that the constraint $\alpha_C \leq \alpha_\Pi$ must be obeyed. The system of equations (4.1) and (4.2) takes the simple form $\partial C / \partial t = -v_2 \partial C / \partial x$, $\partial \Pi / \partial = 0$ for all $x \leq \alpha_\Pi$. The components C_2 and Π_D do not solve this system. Nevertheless, we will make the *assumption* (proved in section

4.8) that, for $t \geq t^*$, the point $(\alpha_\Pi, 0)$ *does* satisfies equation (4.25), with $P = 0$ and $C_P = C(\alpha_\Pi, t)$. In particular, at $t = t^*$, the rate of change of α_Π is

$$\left.\frac{d\alpha_\Pi}{dt}\right|_{t=t*} = \frac{v_2 C_s}{\Pi_0 + C_s + \psi(0)} \tag{4.27}$$

We also note that ${\alpha_C}'(t^*) = v_2$ by virtue of equation (4.1) taking the form $\partial C/\partial t = -v_2 \partial C/\partial x$. From equation (3.27) it then follows that

$${\alpha_\Pi}'(t^*) \leq v_2 = {\alpha_C}'(t^*) \quad \Leftrightarrow \quad \psi(0) \geq -\Pi_0 \tag{4.28}$$

This condition is equivalent to the fluid velocities satisfying

$$\frac{v_2}{v_1} \geq R_1 := \frac{1 + \kappa t_1 - \Pi_0/C_s}{2 + \kappa t_1 - \exp(\kappa t_1 - \kappa t_2)} \tag{4.29}$$

We use this inequality to distinguish two sub-cases, **Case 1a**: $v_2/v_1 \geq R_1$ and **Case 1b**: $v_2/v_1 < R_1$. Recall that Case 1 occurs if $\Pi_0 \geq C_s(1 + \kappa t_1) - C_s e^{\kappa t_1 - \kappa t_2}$. If $\Pi_0 \geq C_s(1 + \kappa t_1)$, then we have $R_1 \leq 0$ and the inequality $v_2/v_1 \geq R_1$ holds for all choices $v_1 > 0$, $v_2 > 0$. Thus, Case 1b can only happen if $C_s(1 + \kappa t_1) - C_s e^{\kappa t_1 - \kappa t_2} \leq \Pi_0 < C_s(1 + \kappa t_1)$ *and* $v_2/v_1 < R_1$. Because of this rather limited range of occurrence, our attention will (for now) be restricted to Case 1a. Here, ${\alpha_\Pi}'(t^*) \leq v_2 = {\alpha_C}'(t^*)$ and the argument presented in Chapter 3 can be applied to predict the emergence of a joint root $x_0 = \alpha_\Pi = \alpha_C$ with velocity

$$u(x_0) := \frac{dx_0}{dt} = \frac{v_2 C_s}{\Pi_0 + C_s + \psi(x_0)} \tag{4.30}$$

Consider $u(x_0)$ on the interval $[0, v_1 t_1]$, which is the region to the left of the Π - discontinuity. If $v_2 \geq v_1$, we deduce from equation (4.26) that $\psi(x_0) > 0$ for all $x_0 \in [0, v_1 t_1 + v_1/\kappa]$. Hence $u(x_0) < v_2$ on $[0, v_1 t_1]$. For $v_2 < v_1$, we notice that $\psi(x_0)$ can be expressed in terms of $\psi(0)$:

$$\begin{aligned} \psi(x_0) &= \left[\psi(0) \; + \; \frac{\kappa C_s}{{v_1}^2}(v_1 - v_2)\, x_0\right] \exp\left(\frac{-\kappa x_0}{v_1}\right) \\ &> \psi(0) \exp\left(\frac{-\kappa x_0}{v_1}\right) \end{aligned} \tag{4.31}$$

Since $\psi(0) \geq -\Pi_0$ (Case 1a) it follows that $\psi(x_0) > -\Pi_0$ and hence $u(x_0) < v_2$ for all $x_0 > 0$. The path of x_0 is now found by solving equation (4.30) subject to the initial condition $x_0(t^*) = 0$. In order to simplify the notation, we define constants λ, μ as follows:

$$\lambda = \frac{1 - e^{\kappa t_1 - \kappa t_2}}{\kappa} \tag{4.32}$$

$$\mu = t_2 - \frac{v_1}{v_2} t_1 + \frac{\Pi_0}{\kappa C_s} \tag{4.33}$$

Observe that

$$t^* = \mu - \lambda + \frac{v_1 - v_2}{v_2} t_1 \tag{4.34}$$

We consider the function $\theta : \mathbb{R} \to \mathbb{R}$ given by

$$\theta(x) = -\frac{\Pi_0}{C_s} x + \left[v_2 \lambda + \frac{v_1 - v_2}{v_1} (x - v_1 t_1) \right] e^{-\kappa x / v_1} - v_2 \mu \tag{4.35}$$

It can now be shown that the solution of equation (4.30) satisfies the following implicit relation:

$$x_0 - v_2 t = \theta(x_0) \tag{4.36}$$

4.5 Case 1a with $v_1 = v_2 = v$, $t \geq t^*$

Note that $R_1 < 1$, so that Case 1b cannot occur if the two flow velocities are equal. The formulae for the concentration and precipitate profiles found in section 4.3 simplify considerably if we set $v_1 = v_2 = v$. The concentration components given by equations (4.13) and (4.14) become

$$C_1(x,t) = C_s - C_s e^{\kappa t_1 - \kappa t_2 - \kappa x / v}, \; v(t - t_2) \leq x < v t_1 + v(t - t_2) \tag{4.37}$$

$$C_2(x,t) = C_s - C_s e^{-\kappa x / v}, \; 0 \leq x < v(t - t_2) \tag{4.38}$$

In the regions B, C, D, B1, B2 the formulae for the precipitate components contain terms involving $(v_1 - v_2)^{-1}$. These can be simplified and their limit evaluated as $v_1 - v_2 \to 0$. For reasons that will become apparent shortly, we are particularly interested in the equations describing regions D and B2.
It can be shown that

$$\lim_{v_1 - v_2 \to 0} \left\{ \frac{e^{-\kappa x/v_2} - e^{-\kappa x/v_1}}{v_1 - v_2} \right\} = \frac{-\kappa x}{{v_1}^2} \cdot e^{-\kappa x/v_1} \tag{4.39}$$

Writing $v = v_1 = v_2$ then yields a simplified version in region D:

$$\begin{aligned} \Pi_D(x,t) = \Pi_0 &+ \left(1 - \frac{\kappa x}{v}\right) \cdot C_s e^{\kappa t_1 - \kappa t_2 - \kappa x/v} \\ &+ \left(\frac{2\kappa x}{v} - \kappa(t + t_1 - t_2) - 1\right) \cdot C_s e^{-\kappa x/v} \end{aligned} \tag{4.40}$$

In a similar way we can find the expressions for all other regions mentioned above. For region B2,

$$\Pi_{B2}(x,t) = \Pi_0 \ + \frac{\kappa C_s}{v} \left[x + v\left(t_2 - t - t_1 e^{\kappa t_1 - \kappa t_2}\right)\right] e^{-\kappa x/v} \tag{4.41}$$

4.5.1 New solution region E

We now use the point $x_0 = \alpha_\Pi = \alpha_C$ to construct a new concentration component C_3 for $t \geq t^*$. With $v_1 = v_2 = v$, we have

$$\theta(x) = -\frac{\Pi_0}{C_s} x + v\lambda \exp\left(\frac{-\kappa x}{v}\right) - v\mu, \qquad \mu = t_2 - t_1 + \frac{\Pi_0}{\kappa C_s} \tag{4.42}$$

Since $\Pi > 0$ for $x > x_0$, C_3 must be of the form of equation (4.11) and we need $C_s + f_3(x_0 - vt)\exp(-\kappa t) = 0$ for $t > t^*$. Introducing the variable $z = x_0 - vt$ and solving equation (4.36) for x_0 yields

$$\frac{\kappa x_0}{v} = -\frac{\kappa C_s}{\Pi_0}\left(\mu + \frac{z}{v}\right) + W\left[\frac{\kappa C_s \lambda}{\Pi_0} \exp\left(\frac{\kappa C_s}{\Pi_0}\left(\mu + \frac{z}{v}\right)\right)\right] \tag{4.43}$$

Here, W denotes the Lambert W-function. We then find

$$\begin{aligned} f_3(z) &= -C_s \exp(\kappa t) \\ &= -C_s \exp\left[\frac{\kappa(x_0 - z)}{v}\right] \\ &= -C_s \exp\left\{-\frac{\kappa C_s}{\Pi_0}\left(\mu + \frac{z}{v}\right) - \frac{\kappa}{v} z \right. \\ &\qquad \left. + W\left[\frac{\kappa C_s \lambda}{\Pi_0} \exp\left(\frac{\kappa C_s}{\Pi_0}\left(\mu + \frac{z}{v}\right)\right)\right]\right\} \end{aligned} \tag{4.44}$$

Putting this back into the general solution (equation (4.11)) we obtain the following expression for the component C_3:

$$\begin{aligned} C_3(x,t) = C_s - C_s \exp\left\{-\frac{\kappa x}{v} - \frac{\kappa C_s}{\Pi_0}\left(\mu - t + \frac{x}{v}\right)\right. \\ \left. + W\left[\frac{\kappa C_s \lambda}{\Pi_0} \exp\left(\frac{\kappa C_s}{\Pi_0}\left(\mu - t + \frac{x}{v}\right)\right)\right]\right\} \end{aligned} \tag{4.45}$$

Let $x = v(t - t^*) = v(t - \mu + \lambda)$ in equation (4.45). By definition of the Lambert W-function, $W(\kappa C_s \lambda/\Pi_0 \exp(\kappa C_s \lambda/\Pi_0)) = \kappa C_s \lambda/\Pi_0$ and hence $C_3(v(t-t^*), t) = C_s - C_s \exp(\kappa t^* - \kappa t) = C_2(v(t-t^*), t)$, which shows that C_2 and C_3 intersect at $x = v(t - t^*)$ for all $t > t^*$. Consistent with the notation used in section 4.3, we therefore introduce region E: $x_0(t) \leq x \leq v(t - t^*)$, where the concentration is given by equation (4.45). The corresponding precipitate component Π_E is found by substitution in equation (4.2). We obtain

$$\begin{aligned} \Pi_E(x,t) = g_E(x) - \kappa C_s \lambda e^{-\kappa x/v} W\left[\frac{\kappa C_s \lambda}{\Pi_0} \exp\left(\frac{\kappa C_s}{\Pi_0}\left(\mu - t + \frac{x}{v}\right)\right)\right]^{-1} \\ + \kappa C_s \lambda \ln\left[W\left[\frac{\kappa C_s \lambda}{\Pi_0} \exp\left(\frac{\kappa C_s}{\Pi_0}\left(\mu - t + \frac{x}{v}\right)\right)\right]\right] \end{aligned} \tag{4.46}$$

To determine g_E we use the condition that $\Pi_E = \Pi_D$ at $x = v(t - t^*)$. Writing this as $t = x/v + t^*$ and substituting into equation (4.46) yields

$$\Pi_E\left(x, t^* + \frac{x}{v}\right) = g_E(x) - \Pi_0 e^{-\kappa x/v} + \kappa C_s \lambda \ln\left(\frac{\kappa C_s \lambda}{\Pi_0}\right) \tag{4.47}$$

And, from equation (4.40),

$$\Pi_D\left(x, t^* + \frac{x}{v}\right) = \Pi_0 - \Pi_0 e^{-\kappa x/v} + \frac{\kappa x}{v}\kappa\, C_s \lambda e^{-\kappa x/v} \tag{4.48}$$

Combining equations (4.47) and (4.48), we find

$$\Pi_E(x,t) = \Pi_0 + \kappa C_s \lambda e^{-\kappa x/v}\left\{\frac{\kappa x}{v} - W\left[\frac{\kappa C_s \lambda}{\Pi_0}\exp\left(\frac{\kappa C_s}{\Pi_0}\left(\mu - t + \frac{x}{v}\right)\right)\right]^{-1}\right.$$
$$\left. + \ln\left[W\left[\frac{\kappa\, C_s \lambda}{\Pi_0}\exp\left(\frac{\kappa C_s}{\Pi_0}\left(\mu - t + \frac{x}{v}\right)\right)\right]\right] - \ln\left(\frac{\kappa\, C_s \lambda}{\Pi_0}\right)\right\} \tag{4.49}$$

Equations (4.45) and (4.49) define the solution on the interval $x_0(t) \le x \le v(t - t^*)$. Given an arbitrary precipitate value P on Π_E, we can determine its path $x_P = x_P(t)$ from $P = \Pi_E(x_P, t)$. It may be shown that

$$\frac{dx_P}{dt} = \frac{v_2\left[C_s - C_3(x_P, t)\right]}{\Pi_0 - P + C_s - C_3(x_P, t) + \psi_D(x_P)} \tag{4.50}$$

We note that this is equation (4.25) with $C_P = C_3(x_P, t)$, which confirms that this relationship for the point (x_P, P) is satisfied by both the solution pairs C_2, Π_D and C_3, Π_E. It is "invariant" between the two regions. This is not entirely surprising, as the point x_0 was assumed to obey equation (4.25) in the first place.

4.5.2 Solution profiles on $0 \le x \le vt_1$ and $vt_1 \le x \le L$

At $t = t_1 + t^*$ the front end of the new region E coincides with the Π - discontinuity and the solution profiles on $0 \le x \le vt_1$ are entirely defined by C_3, Π_E. This is illustrated in Figure 4.5. Let $T_{stop} > t_1 + t^*$ be the time such that $x_0(T_{stop}) = vt_1$. Using equation (4.36) for the motion of x_0, we find that

$$T_{stop} = t_1 + \frac{\Pi_0}{C_s}t_1 - \lambda e^{-\kappa t_1} + \mu = \frac{\Pi_0}{\kappa C_s} + \frac{\Pi_0}{C_s}t_1 + t_2 + \frac{e^{-\kappa t_2} - e^{-\kappa t_1}}{\kappa} \tag{4.51}$$

For $t_1 + t^* < t < T_{stop}$ the solution on $0 \le x \le vt_1$ is given by C_3, Π_E. As was the case with C_2 earlier on, the Π - discontinuity has no immediate effect on the

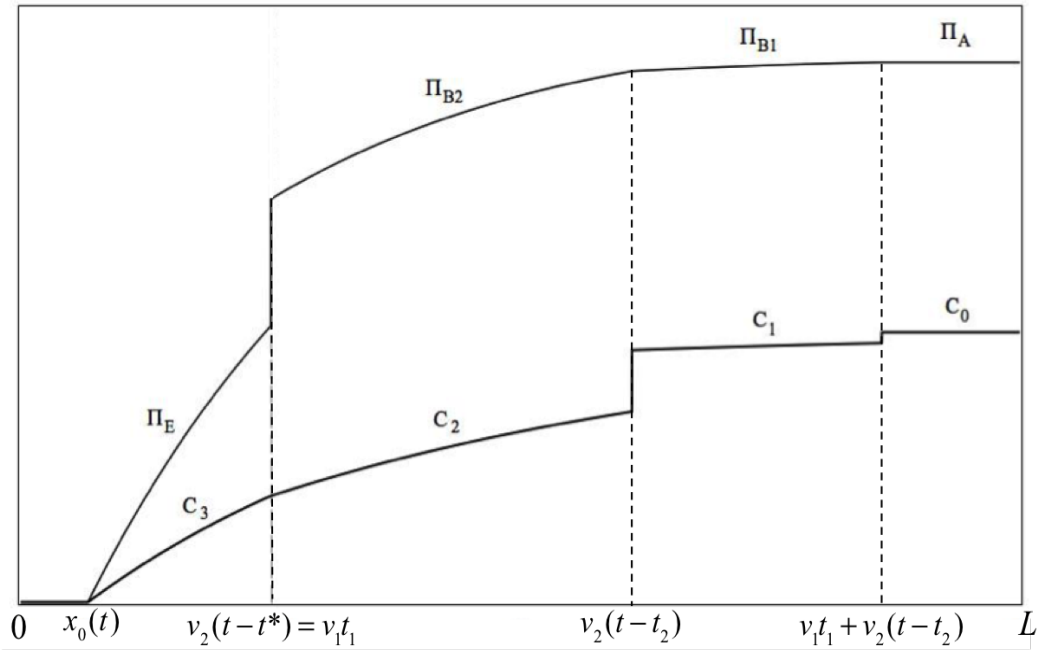

Figure 4.5: *Solution profiles at* $t = t_1 + t^*$

concentration profile and we can therefore expect C_3 to apply also on the interval $vt_1 \leq x \leq v\,(t - t^*)$. This will however affect the precipitate profile here and we must introduce a new component Π_{B3}. This component will be of the form of equation (4.46) with a new arbitrary function g_{B3}, which will be determined as usual by demanding that $\Pi_{B3} = \Pi_{B2}$ at $x = v\,(t - t^*)$. Substituting $t = x/v + t^*$ in equation (4.41), we get

$$\Pi_{B2}\left(x, t^* + \frac{x}{v}\right) = \Pi_0 - \Pi_0 e^{-\kappa x/v} + (1 + \kappa t_1)\,\kappa\, C_s \lambda e^{-\kappa x/v} \tag{4.52}$$

Combining this with equation (4.47), we find

$$g_{B3}\,(x) = \Pi_0 + \kappa\, C_s \lambda \left(1 + \kappa t_1 - \ln\left(\frac{\kappa\, C_s \lambda}{\Pi_0}\right)\right) e^{-\kappa x/v} \tag{4.53}$$

Finally, the precipitate profile on $vt_1 \leq x \leq v\,(t - t^*)$ is

$$\begin{aligned}\Pi_{B3}\,(x,t) = \Pi_0 + \kappa\, C_s \lambda e^{-\kappa x/v} \Bigg\{ 1 + \kappa t_1 - W\left[\frac{\kappa C_s \lambda}{\Pi_0} \exp\left(\frac{\kappa C_s}{\Pi_0}\left(\mu - t + \frac{x}{v}\right)\right)\right]^{-1} \\ + \ln\left[W\left[\frac{\kappa\, C_s \lambda}{\Pi_0} \exp\left(\frac{\kappa\, C_s}{\Pi_0}\left(\mu - t + \frac{x}{v}\right)\right)\right]\right] - \ln\left(\frac{\kappa\, C_s \lambda}{\Pi_0}\right) \Bigg\}\end{aligned} \tag{4.54}$$

Figure 4.6 shows the solution profiles for some $t_1 + t^* < t < T_{stop}$. The interval in which C_3, Π_{B3} apply is indicated by the dashed lines. A relationship similar to equation (4.25) holds for C_2, Π_{B2}, and it can be shown that this relation is also satisfied by C_3, Π_{B3}.

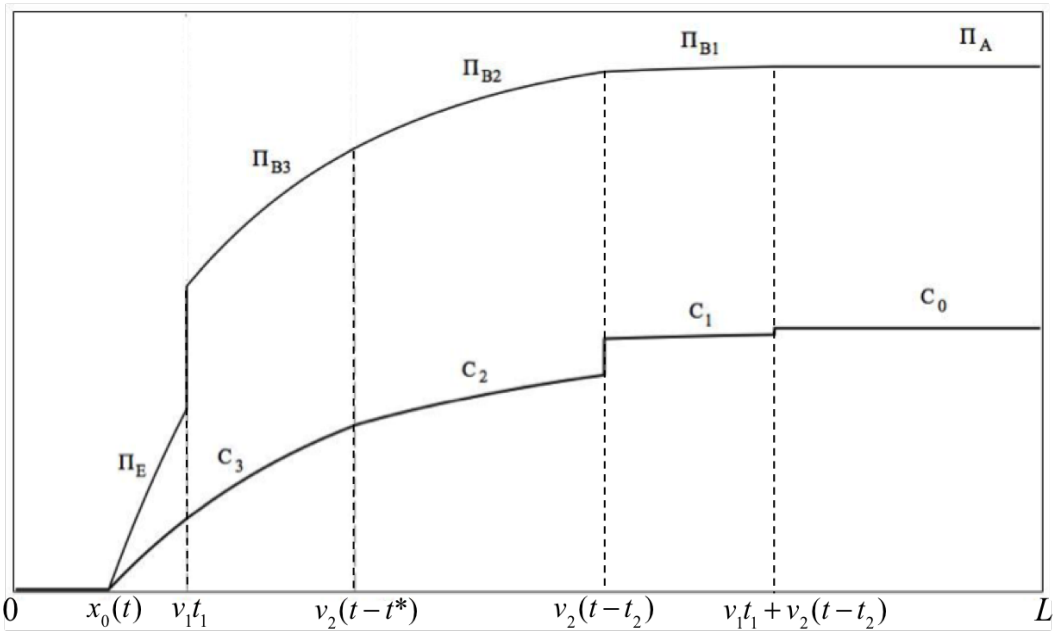

Figure 4.6: *Solution profiles for* $t_1 + t^* < t < T_{stop}$

4.5.3 The Π - discontinuity

At $t = T_{stop}$ we have $C_3\left(vt_1, T_{stop}\right) = \Pi_E\left(vt_1, T_{stop}\right) = 0$ and region E disappears. To see the "height" of the Π - discontinuity at this time, we evaluate equation (4.54) at $x = vt_1$, $t = T_{stop}$. The exponents in this expression then are

$$\begin{aligned} \frac{\kappa C_s}{\Pi_0}\left(\mu - T_{stop} + t_1\right) &= \frac{\kappa C_s}{\Pi_0}\left(\mu - \frac{\Pi_0}{C_s}t_1 + \lambda e^{-\kappa t_1} - \mu\right) \\ &= \frac{\kappa C_s \lambda}{\Pi_0}e^{-\kappa t_1} - \kappa t_1 \end{aligned} \tag{4.55}$$

Noticing that

$$\begin{aligned} W\left[\frac{\kappa C_s \lambda}{\Pi_0}\exp\left(\frac{\kappa C_s \lambda}{\Pi_0}e^{-\kappa t_1} - \kappa t_1\right)\right] &= W\left[\frac{\kappa C_s \lambda}{\Pi_0}e^{-\kappa t_1} \cdot \exp\left(\frac{\kappa C_s \lambda}{\Pi_0}e^{-\kappa t_1}\right)\right] \\ &= \frac{\kappa C_s \lambda}{\Pi_0}e^{-\kappa t_1} \end{aligned} \tag{4.56}$$

and simplifying terms, we derive

$$\Pi_{B3}\left(vt_1, T_{stop}\right) = \kappa C_s \lambda e^{-\kappa t_1} = C_s\left(e^{-\kappa t_1} - e^{-\kappa t_2}\right) > 0 \tag{4.57}$$

We recognize this as the last term in equation (4.51) multiplied by $-\kappa C_s$.

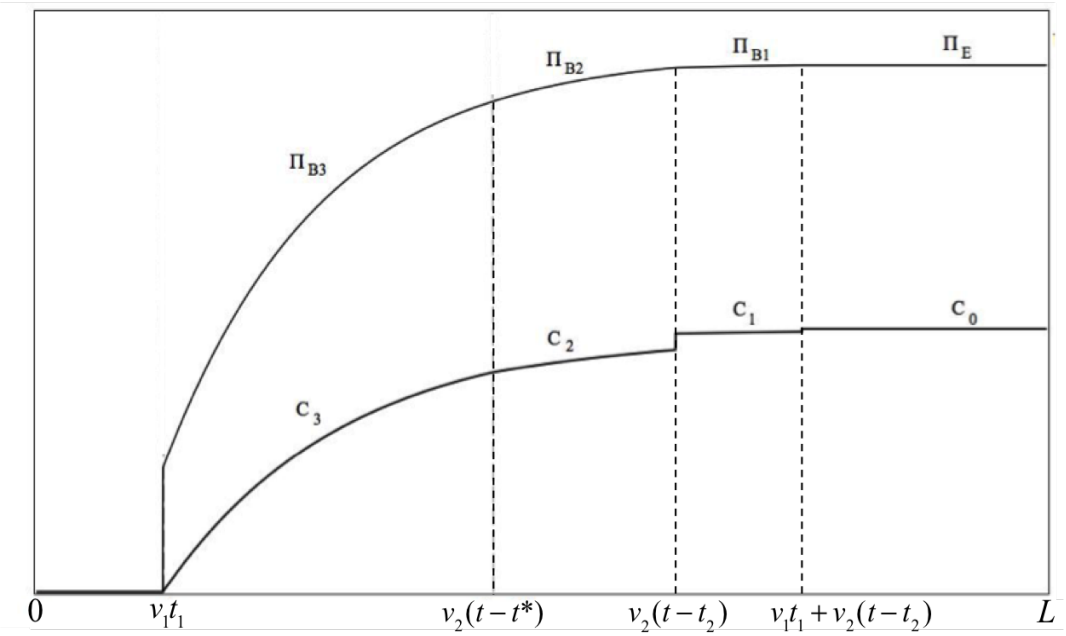

Figure 4.7: *Solution profiles at* $t = T_{stop}$

Figure 4.7 shows the solution profiles at $t = T_{stop}$. The moving boundary point $x_0(t)$ has come to a halt at $x = vt_1$. On the interval $0 \leq x < vt_1$, equation (4.1) takes its simple form $\partial C/\partial t = -v\partial C/\partial x$ and the boundary data $C(0,t) = 0, t > t_2$ are carried along characteristics to $x = vt_1$. This leads to the condition $C(vt_1, t) = 0$ for $t > T_{stop}$. Using equation (4.11) we obtain

$$C_4(x,t) = C_s - C_s e^{\kappa t_1 - \kappa x/v} \tag{4.58}$$

Direct substitution shows that $C_3\left(vt_1 + vt - vT_{stop},\ t\right) = C_4\left(vt_1 + vt - vT_{stop}, t\right)$, so equation (4.58) will describe the solution on the interval $vt_1 \leq x \leq v\left(t_1 + t - T_{stop}\right)$. This is shown in Figure 4.8. The new precipitate component is found by substituting C_4 into equation (4.2), which yields

$$\Pi_{B4}(x,t) = g_{B4}(x) - \kappa C_s t e^{\kappa t_1 - \kappa x/v} \tag{4.59}$$

As usual, the condition $\Pi_{B4} = \Pi_{B3}$ at $x = v\left(t_1 + t - T_{stop}\right)$ is used to determine $g_{B4}(x)$. Substituting $vt = x - v\left(t_1 - T_{stop}\right)$ in equation (4.54), the exponents

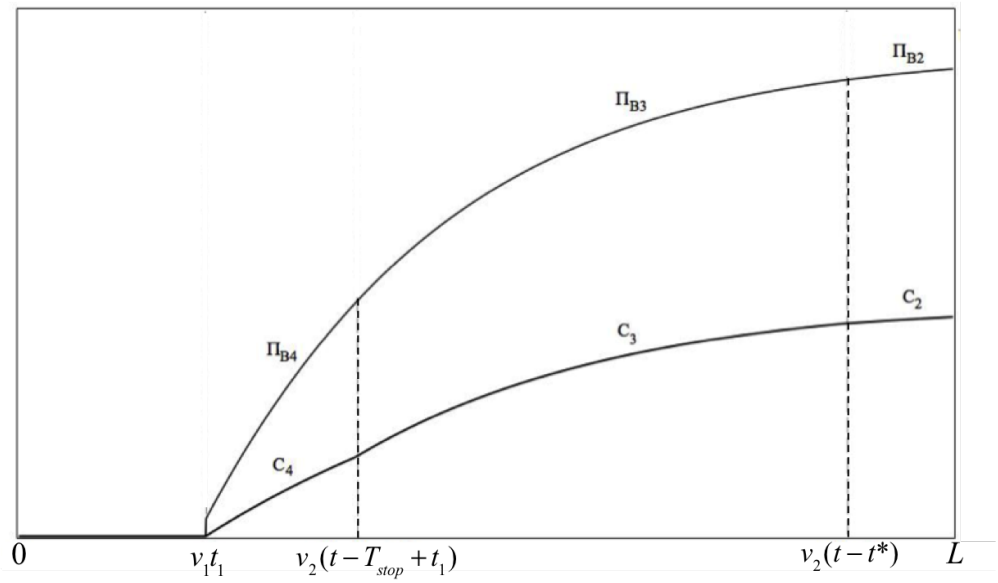

Figure 4.8: *Solution profiles at* $t = T_{stop}$

evaluate as shown in equation (4.55). Then:

$$\begin{aligned}\Pi_{B3}\left(x, T_{stop} - t_1 + \frac{x}{v}\right) &= \Pi_0 + \kappa C_s \lambda e^{-\kappa x/v}\left\{1 + \kappa t_1 - \ln\left(\frac{\kappa\, C_s \lambda}{\Pi_0}\right)\right. \\ &\qquad \left. - \frac{\Pi_0 e^{\kappa t_1}}{\kappa\, C_s \lambda} + \ln\left[\frac{\kappa\, C_s \lambda}{\Pi_0} e^{-\kappa t_1}\right]\right\} \\ &= \Pi_0 + \kappa C_s \lambda e^{-\kappa x/v} - \Pi_0 \exp e^{\kappa t_1 - \kappa x/v} \end{aligned} \tag{4.60}$$

The same is now done for equation (4.59):

$$\begin{aligned}\Pi_{B4}\left(x,\ T_{stop} - t_1 + \frac{x}{v}\right) &= g_{B4}(x) - \kappa C_s\left(T_{stop} - t_1 + \frac{x}{v}\right) e^{\kappa t_1 - \kappa x/v} \\ &= g_{B4}(x) - \kappa C_s\left(\frac{\Pi_0}{C_s} t_1 - \lambda e^{-\kappa t_1} + \mu + \frac{x}{v}\right) e^{\kappa t_1 - \kappa x/v} \\ &= g_{B4}(x) - \left(\Pi_0 t_1 \kappa - \kappa C_s \lambda e^{-\kappa t_1} + \kappa C_s \mu + \frac{\kappa C_s x}{v}\right) e^{\kappa t_1 - \kappa x/v} \end{aligned} \tag{4.61}$$

Equating both expressions and cancelling the terms involving λ, we find $g_{B4}(x)$ and hence

$$\Pi_{B4}(x,t) = \Pi_0 + \frac{C_s \kappa}{v}\left(\frac{\Pi_0 v}{C_s} t_1 + v t_2 - v t_1 + x - v t\right) e^{\kappa t_1 - \kappa x/v} \tag{4.62}$$

We note that $\Pi_{B4}(v t_1, t) = 0$ for $t = T_{start}$ defined by

$$T_{start} := \frac{\Pi_0}{\kappa C_s} + \frac{\Pi_0}{C_s} t_1 + t_2 \tag{4.63}$$

4.5.4 Recovering a familiar solution

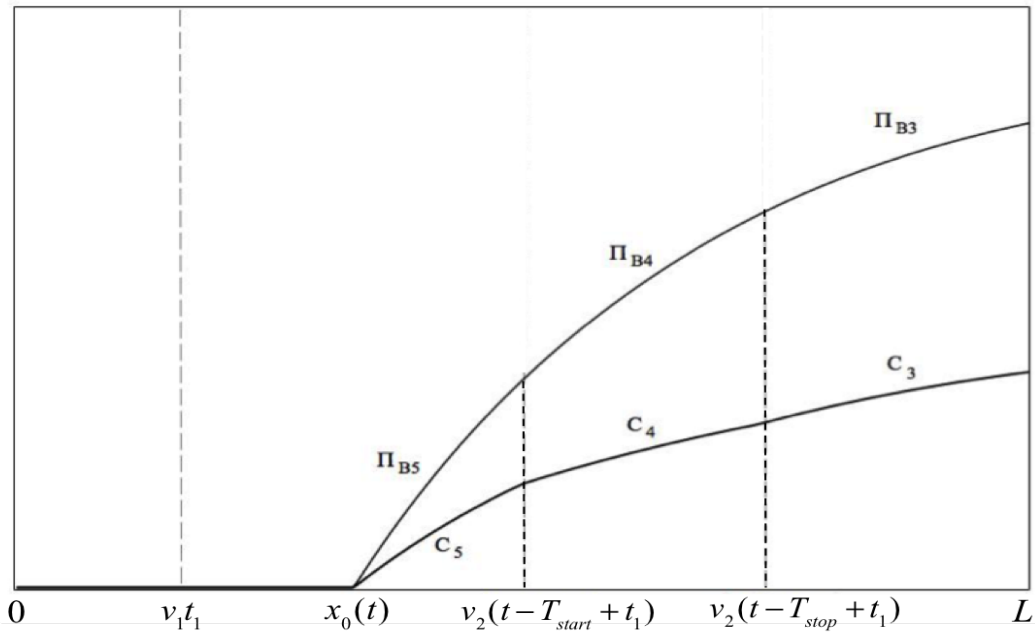

Figure 4.9: *Solution for* $t > T_{start}$

For $T_{stop} \leq t \leq T_{start}$, the concentration and precipitate profiles each consist of five non-zero components, with C_4 and Π_{B4} defining the solution in the interval $vt_1 \leq x \leq v\left(t_1 + t - T_{stop}\right)$ (see Figure 4.8). Notice that C_4 is equation (4.6) translated to the right by vt_1 and that Π_{B4} is equation (4.7) shifted in space by vt_1 and in time by $\Pi_0 t_1/C_s + t_2 = T_{start} - \Pi_0/\kappa C_s$. The situation on $vt_1 \leq x \leq v\left(t_1 + t - T_{stop}\right)$ is now seen to be equivalent to case examined in Chapter 3, where $t_1 = t_2$ and $t^* = \Pi_0/\kappa C_s$. We should therefore expect the emergence of a travelling wave solution component C_5. This will be the consequence of the common point $x_0 = \alpha_\Pi = \alpha_C$ having constant velocity $dx_0/dt = U = vC_s/\left(\Pi_0 + C_s\right)$ for $t \geq T_{start}$. Using the condition $x_0\left(T_{start}\right) = vt_1$, we find

$$C_5\left(x,t\right) = C_s - C_s \exp\left(\frac{\kappa C_s}{\Pi_0}\left(t - T_{start} + \frac{vt_1 - x}{U}\right)\right) \tag{4.64}$$

We recognize this as equation (3.27) shifted in x by vt_1 and in t by $\Pi_0 t_1/C_s + t_2$. This interpretation also makes sense of T_{start}: it is the sum of the shut-in time, $t_2 - t_1$, the run-out time $t^* = \Pi_0/\kappa C_s$ (when $t_1 = t_2$), and vt_1/U, which is the time it takes for the travelling wave solution to go from $x = 0$ to $x = vt_1$. It may be verified that $C_5\left(vt_1 + vt - vT_{start}, t\right) = C_4\left(vt_1 + vt - vT_{start}, t\right)$. On the interval $U\left(t_1 + t - T_{start}\right) \leq x \leq v\left(t_1 + t - T_{start}\right)$, the concentration profile is defined by

C_5 and the precipitate in this region is a scalar multiple,

$$\Pi_{B5}(x,t) = \frac{\Pi_0}{C_s} C_5(x,t) \tag{4.65}$$

4.6 Case 1a with $v_1 \neq v_2$, $t \geq t^*$

The key to constructing the explicit formulae in section 4.5 was that equation (4.36) only involves the terms x_0, $\exp(x_0)$ when $v_1 = v_2$. The Lambert W-function could be used here to find $C_3(x,t)$ (equation (4.45)). More generally, if $v_1 \neq v_2$, equation (4.36) involves the terms x_0, $\exp(x_0)$ and $x_0 \exp(x_0)$. The addition of the latter term now prevents a closed-form solution by application of the Lambert W-function. Consequently, this approach does not lead to an explicit formula for C_3 when $v_1 \neq v_2$. However, the results of section 4.5 can be used as guidance for conjecturing an implicit solution.

4.6.1 Concentration profile for arbitrary v_1, v_2

If we had not set $v_1 = v_2 = v$ from section 4.5.1 on and instead maintained the notational distinction v_1 and v_2 (although $v_1 = v_2$) throughout, then we would see that equation (4.45) is actually

$$C_3(x,t) = C_s - C_s \exp\left\{ -\frac{\kappa x}{v_1} - \frac{\kappa C_s}{\Pi_0}\left(\mu + \frac{v_2 t}{v_1} - \frac{x}{v_1}\right) + W\left[\frac{\kappa C_s \lambda}{\Pi_0} \exp\left(\frac{\kappa C_s}{\Pi_0}\left(\mu + \frac{v_2 t}{v_1} - \frac{x}{v_1}\right)\right)\right] \right\} \tag{4.66}$$

Furthermore, C_3 is connected to C_2 at the point $x = v_2(t - t^*)$. An arbitrary concentration value $0 \leq c < C_s$ lies at $x_c = -v_2 \kappa^{-1} \log(1 - c/C_s)$ until time $t = t^* + x_c/v_2 = t^* - \kappa^{-1} \log(1 - c/C_s)$, when it "falls" into the new solution region (see Figure 4.10).

For $t \geq t^* - \kappa^{-1} \log(1 - c/C_s)$, the path $x_c = x_c(t)$ is determined from $c = C_3(x_c, t)$, where C_3 is given by equation (4.66). This may be solved explicitly to yield the time t at which the solution value c "arrives" at an arbitrarily chosen point x_c. The

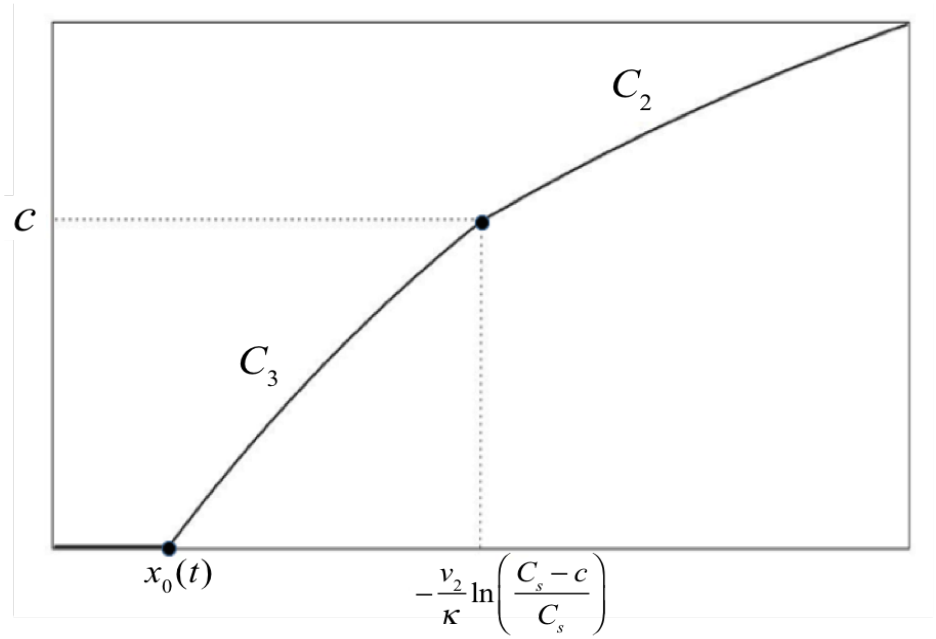

Figure 4.10: *The moment when c "falls" into the new solution region*

velocity $u_{c,\,v_1=v_2}$ of c is then found by differentiation as

$$u_{c\,,\,v_1=v_2}\left(x_c\right)=\frac{dx_c}{dt}=\frac{v_2C_s\left(\dfrac{C_s-c}{C_s}\right)^{\frac{v_2}{v_1}}}{\left(\Pi_0+C_s\right)\left(\dfrac{C_s-c}{C_s}\right)^{\frac{v_2}{v_1}}+\psi_{v_1=v_2}\left(x_c\right)} \tag{4.67}$$

Since $v_1 = v_2$, equation (4.67) would simplify further by cancelling the C_s terms. However, distinguishing between v_1 and v_2 in this way is instructive when seeking a more general velocity term u_c for when $v_1 \neq v_2$. We note that, at $t = t^* - \kappa^{-1}\log\left(1 - c/C_s\right)$, the velocity of the concentration value "jumps" from zero to

$$u_{c,\,v_1=v_2}\left[-\frac{v_2}{\kappa}\ln\left(\frac{C_s-c}{C_s}\right)\right] \;=\; \frac{v_2C_s}{\Pi_0+C_s+\psi_{v_1=v_2}\left(0\right)} \tag{4.68}$$

This shows that each concentration value $0 \leq c < C_s$ has the same "initial" velocity. Assuming that this feature carries over to the case $v_1 \neq v_2$, the requirements for the velocity term u_c for arbitrary v_1, v_2 may be summarised as follows:

Condition 1: Recover equation (4.30) if $c = 0$

Condition 2: Recover equation (4.67) if $v_1 = v_2$

Condition 3: The velocity u_c at $t = t^* - \kappa^{-1}\log\left(1 - c/C_s\right)$ is the same for every $0 \leq c < C_s$

Together, conditions 1 and 3 imply that the velocity of $0 \leq c < C_s$ "jumps" from zero to

$$u_c\left[-\frac{v_2}{\kappa}\ln\left(\frac{C_s-c}{C_s}\right)\right] = u_0(0) = \frac{v_2 C_s}{\Pi_0 + C_s + \psi(0)} \tag{4.69}$$

This is united with condition 2 in the following expression for u_c :

$$u_c(x_c) = v_2 C_s\left(\frac{C_s-c}{C_s}\right)^{\frac{v_2}{v_1}}\left[(\Pi_0+C_s)\left(\frac{C_s-c}{C_s}\right)^{\frac{v_2}{v_1}} + \psi(x_c)\right.$$
$$\left. + \frac{v_2}{v_1}\left(1-\frac{v_2}{v_1}\right)\ln\left(\frac{C_s-c}{C_s}\right)C_s\exp\left(\frac{-\kappa x_c}{v_1}\right)\right]^{-1} \tag{4.70}$$

In order to find a relation between x_c, t and c we solve the initial value problem

$$\frac{dx_c}{dt} = u_c(x_c), \quad x_c\left[t^* - \frac{1}{\kappa}\ln\left(\frac{C_s-c}{C_s}\right)\right] = -\frac{v_2}{\kappa}\ln\left(\frac{C_s-c}{C_s}\right) \tag{4.71}$$

When $c = 0$ the solution of equation (4.71) is given by equation (4.36). For $c \neq 0$, it can be shown that the solution is

$$t = -\frac{v_1-v_2}{v_1 v_2}\left(\frac{C_s-c}{C_s}\right)^{-\frac{v_2}{v_1}}\left[x_c - v_1 t_1 + \frac{v_2}{\kappa}\ln\left(\frac{C_s-c}{C_s}\right) + \frac{v_1 v_2 \lambda}{v_1-v_2}\right]\exp\left(-\frac{\kappa x_c}{v_1}\right)$$
$$+ \frac{\Pi_0+C_s}{v_2 C_s}x_c + \frac{\Pi_0}{\kappa C_s}\ln\left(\frac{C_s-c}{C_s}\right) + \mu \tag{4.72}$$

We remark here that equation (3.72) may be derived in a more straightforward manner by choosing characteristic coordinates s, r of equation (4.1) such that $s = 0$ on the boundary curve $x_0 = x_0(t)$ defined by equation (4.36). Recall that the characteristic system of ODEs has general solution $C(r,s) = C_s + f(r)e^{-\kappa s}$, $x(r,s) = v_2 s + g(r)$, $t(r,s) = s + h(r)$ where f, g and h are arbitrary functions. We would like to choose these functions in such a way that the curve $\{(x,t) \in \mathbb{R}^2 : \ x - v_2 t = \theta(x)\}$ is mapped onto the r-axis ($s = 0$). This is achieved by letting $g \equiv r$ (so that $x = r \Leftrightarrow s = 0$) and

$$h(r) = \frac{r-\theta(r)}{v_2} \tag{4.73}$$

The condition that $C = 0$ on the boundary curve is applied by setting $f \equiv -C_s$, so that

$$s = -\frac{1}{\kappa} \ln \left(\frac{C_s - c}{C_s} \right) \tag{4.74}$$

Equation (4.72) can now be obtained by substituting $r = x - v_2 s$ in the equation for t, so:

$$t = s + h\left(x - v_2 s\right) = \frac{x}{v_2} - \frac{1}{v_2}\theta \left[x - v_2 \ln \left(\frac{C_s - c}{C_s} \right) \right] \tag{4.75}$$

This second derivation of equation (4.72) is much more powerful as it reveals a general solution technique that may be applied in other circumstances. We will see it again in the context of Case 2 (in section 4.7.2). Nevertheless, the first derivation via the construction of the velocity term u_c is interesting in its own right and allows for more insight into the mechanisms of this specific problem.

In order to understand the shape of the concentration component C_3 when $v_1 \neq v_2$, let x be an arbitrary point in $[0, L]$ and consider the arrival times $t_x(c)$ given by equation (4.72). Denoting $c_x := C_2(x) = C_s - C_s \exp(-\kappa x / v_2)$ it may be shown that

$$\begin{aligned} \frac{dt_x}{dc} = \frac{1}{\kappa v_1 \left(C_s - c\right)} \left(\frac{C_s - c}{C_s - c_x} \right)^{-\frac{v_2}{v_1}} \Bigg[& \frac{\kappa}{v_1} \left(v_2 - v_1\right) \left(x + \frac{v_2}{\kappa} \ln \left(\frac{C_s - c}{C_s} \right) \right) \\ & - \frac{v_1 \Pi_0}{C_s} \left(\frac{C_s - c}{C_s - c_x} \right)^{\frac{v_2}{v_1}} + v_1 \left(1 + \kappa t_1\right) - v_2 \left(2 + \kappa t_1 - e^{\kappa t_1 - \kappa t_2}\right) \Bigg] \end{aligned} \tag{4.76}$$

In particular,

$$\frac{dt_x}{dc}\left(c_x\right) = \frac{1}{\kappa v_1 \left(C_s - c_x\right)} \left[v_1 \left(1 + \kappa t_1 - \frac{\Pi_0}{C_s} \right) - v_2 \left(2 + \kappa t_1 - e^{\kappa t_1 - \kappa t_2}\right) \right] \tag{4.77}$$

Here, we recognise the constant R_1 defined in equation (4.29) and see that $v_2 / v_1 = R_1$ if and only if $t_x{}'(c_x) = 0$. In this case, the graph of $t_x = t_x(c)$ has a local maximum or minimum at $c = c_x$ and, for $0 \leq c < c_x$, we have

$$\frac{dt_x}{dc} = \frac{1}{\kappa v_1 (C_s - c)} \left(\frac{C_s - c}{C_s - c_x} \right)^{-\frac{v_2}{v_1}} \left[\frac{\kappa}{v_1} (v_2 - v_1) \left(x + \frac{v_2}{\kappa} \ln \left(\frac{C_s - c}{C_s} \right) \right) \right.$$
$$\left. - \frac{v_1 \Pi_0}{C_s} \left(\frac{C_s - c}{C_s - c_x} \right)^{\frac{v_2}{v_1}} + \frac{v_1 \Pi_0}{C_s} \right] \quad (4.78)$$

Because $0 < R_1 < 1$, it must be that $v_2 < v_1$ and we therefore have the inequality $(v_2 - v_1)(x + v_2 \kappa^{-1} \ln(1 - c/C_s)) < 0$. Also, since $(C_s - c)/(C_s - c_x) > 0$ it follows that ${t_x}'(c) < 0$ for all $0 \leq c < c_x$. If $v_2/v_1 > R_1$, the argument can be modified to show that ${t_x}'(c) < 0$ for all $0 \leq c \leq c_x$. Thus, in Case 1a ($v_2/v_1 \geq R_1$), lower concentration values arrive at x later than higher concentration values. Since this is true for any $x \in [0, L]$, the in-situ concentration profile in these cases must be single-valued. The slope of the profile is infinite at x if $v_2/v_1 = R_1$, indicating that it is about to "fold over" and become multi-valued.

The remaining concentration components C_4 and C_5 can be developed in complete analogy with sections 4.5.3 and 4.5.4. In fact, the only difference is the appearance of v_1/v_2 in the following equations, which would also have been found if the distinction between v_1 and v_2 was maintained throughout section 4.5.

Substituting $c = 0$ and $x_0 = v_1 t_1$ in equation (4.72) yields the time T_{stop} in the following form:

$$T_{stop} := \frac{\Pi_0}{\kappa C_s} + \frac{v_1}{v_2} \frac{\Pi_0}{C_s} t_1 + t_2 + \frac{e^{-\kappa t_2} - e^{-\kappa t_1}}{\kappa} \quad (4.79)$$

The component C_4 (see equation (4.58)) is then found to be

$$C_4(x, t) = C_s - C_s \exp\left(-\frac{\kappa}{v_2} (x - v_1 t_1) \right) \quad (4.80)$$

This describes the concentration profile on the interval $v_1 t_1 \leq x \leq v_1 t_1 + v_2 (t - T_{stop})$ until some time T_{start}. The difference $\Delta T = T_{start} - T_{stop}$ is the time it takes to dissolve the amount of precipitate in the Π - discontinuity. For the case $v_1 = v_2$, the precipitate level at $t = T_{stop}$ is given by equation (4.57). If the same is true for

arbitrary v_1, v_2, we find

$$T_{start} := T_{stop} + \frac{e^{-\kappa t_2} - e^{-\kappa t_1}}{\kappa} = \frac{\Pi_0}{\kappa C_s} + \frac{v_1}{v_2}\frac{\Pi_0}{C_s}t_1 + t_2 \tag{4.81}$$

Finally, assuming that x_0 has constant velocity $U = v_2 C_s/(\Pi_0 + C_s)$ for $t \geq T_{start}$, the last component C_5 is

$$C_5(x,t) = C_s - C_s \exp\left[\frac{\kappa C_s}{\Pi_0}\left(t - T_{start} + \frac{v_1 t_1 - x}{U}\right)\right] \tag{4.82}$$

4.6.2 Mass conservation

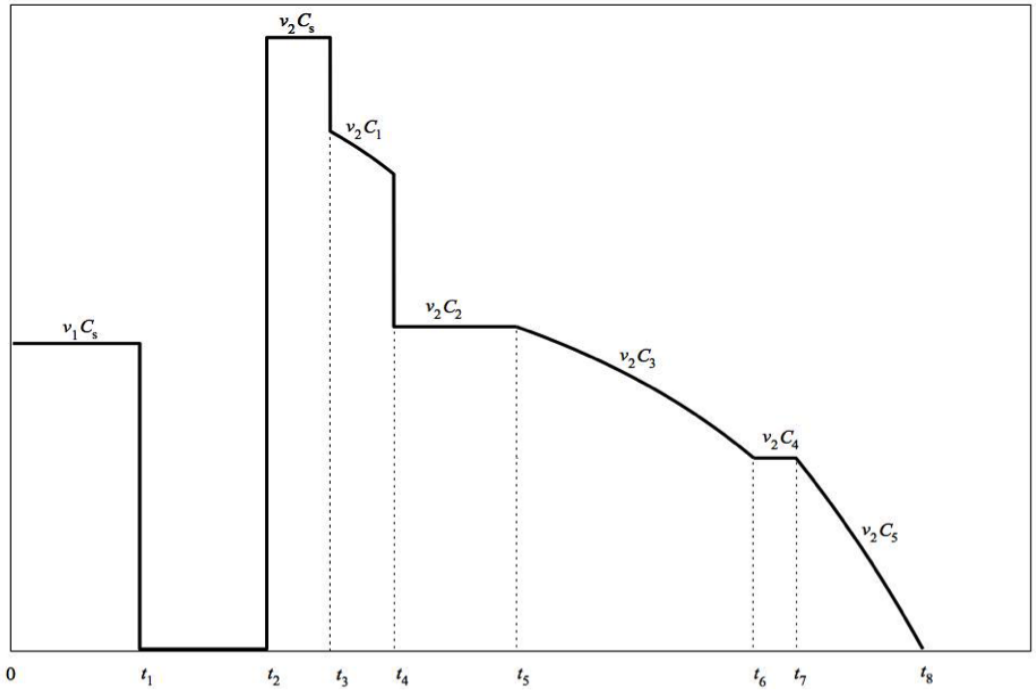

Figure 4.11: *Concentration flux at* $x = L$ *for* $0 \leq t \leq t_8 := T_{start} + (L - v_1 t_1)/U$

Consider the effluent concentration flux defined as $C_F := t \mapsto v(t) C(L,t)$. If $v_1 t_1 < L$ the five components C_n, $n = 1,2,3,4,5$ all feature in the concentration profile and the resulting flux consists of seven separate regions (see Figure 4.11). In addition to the shut-in times t_1, t_2 we introduce $t_3 := t_2 + (L - v_1 t_1)/v_2$, the time at which first concentration front reaches the outlet. We see that $C_F \equiv v_1 C_s$ for $0 \leq t \leq t_1$, $C_F \equiv 0$ for $t_1 \leq t \leq t_2$ and $C_F \equiv v_2 C_s$ for $t_2 \leq t \leq t_3$. The second front comes through at $t_4 := t_2 + L/v_2$, and for $t_3 \leq t \leq t_4$ we have $C_F(t) = v_2 C_1(L,t)$ (equation (4.13)), which is strictly decreasing if $v_1 < v_2$ (shown in Figure 4.11), strictly increasing if $v_1 > v_2$ and constant if $v_1 = v_2$. After this, $C_F(t) = v_2 C_2(L,t)$

(equation (4.14)) until $t_5 := t^* + L/v_2$, which is when the regions C_3, C_4, C_5 defined by equations (4.72), (4.80) and (4.82) respectively start coming through. Defining $t_6 = T_{stop} + (L - v_1 t_1)/v_2$, $t_7 := T_{start} + (L - v_1 t_1)/v_2$ and $t_8 := T_{start} + (L - v_1 t_1)/U$, we see that $C_F(t) = v_2 C_3(L,t)$ for $t_5 \leq t \leq t_6$, $C_F(t) = v_2 C_4(L,t)$ for $t_6 \leq t \leq t_7$ and $C_F(t) = v_2 C_5(L,t)$ for $t_7 \leq t \leq t_8$. Careful integration shows that the total amount of chemical exiting the system is

$$S := \int_0^\infty C_F(t)dt \;\; = \int_0^{t_8} C_F(t)dt = (\Pi_0 + C_s)\, L \tag{4.83}$$

4.6.3 Precipitate profile

In section 4.5.1 we could use the formula $C_3(x,t)$ to determine the precipitate components Π_E and Π_{B3} by direct integration of $\kappa(C_s - C_3)$ with respect to t. This is not possible in the case $v_1 \neq v_2$, when C_3 is defined implicitly by equation (4.72). It might be that a similar implicit relation exists for the precipitate component, which could (perhaps) be derived using equation (4.72) to substitute for dt in the integral. However, as we are mainly interested in the concentration profile, we shall not pursue this and instead obtain Π_E and Π_{B3} by means of an algorithmic construction. We first consider a point $(x_P, P) \in \Pi_D$ with $C_P = C_2(x_P, t)$ denoting the corresponding concentration level. Then,

$$\frac{dx_P}{dt} = u_P(P, C_P, x_P) \tag{4.84}$$

where u_P is given by equation (4.25). In section 4.4 it was argued that the point $(\alpha_\Pi, 0)$ must also obey this equation. For Case 1a, we were then able to deduce the emergence of the joint root $x_0 = \alpha_\Pi = \alpha_C$ with velocity $u_0(0,0,x_P)$. For the case $v_1 = v_2$, this lead to explicit formulae for C_3 and Π_E and it could be verified (equation (4.50)) that equation (4.84) also applied to a point $(x_P, P) \in \Pi_E$ with $C_P = C_3(x_P, t)$. Thus, the formula for dx_P/dt was invariant between the regions C_2, Π_D and C_3, Π_E. Assuming the same invariance is true when $v_1 \neq v_2$, we can construct the precipitate profile in the following way: let P be a fixed precipitate level such that $(x_P(t), P) \in \Pi_D$ and define the time $T \geq t^*$ by the relation $x_P(T) = v_2(T - t^*)$. That is, T denotes the instant at which the precipitate level P falls into the new solution region E, where C_3 is implicitly described by equation (4.72) and

Π_E is to be determined. Using $C_P(T) = C_2(x_P(T),\ T) = C_s - C_s \exp(\kappa t^* - \kappa T)$, the first point on the path of P in region E is calculated as

$$x_P(T+\delta t) = v_2(T-t^*) + u_P[P, C_s - C_s \exp(\kappa t^* - \kappa T), v_2(T-t^*)] \cdot \delta t \quad (4.85)$$

The corresponding concentration level $C_P(T+\delta t)$ now has to be determined using the implicit concentration profile given by equation (4.72). Given x_P, C_P at $T+\delta t$, we can use equation (4.84) to compute the next point on the path of P as

$$x_P(T+2\delta t) = x_P(T+\delta t) + u_P[P,\ C_P(T+\delta t),\ x_P(T+\delta t)] \cdot \delta t \quad (4.86)$$

We then find $C_P(T+2\delta t)$ and use it to compute $x_P(T+3\delta t)$, and so forth. Repeating this procedure for all relevant P, the solution component Π_E is computed.

A similar procedure may be established for Π_{B3}. The components C_2, Π_{B2} satisfy equation (4.25) with $\psi \equiv 0$ (the relation found also in Chapter 3). Assuming this relation holds for C_3, Π_{B3} too, the paths of the individual precipitate values on Π_{B3} can be obtained as shown above.

Finally, we note that explicit formulae are available again for the components Π_{B4} and Π_{B5}. As in section 4.5.4, we have $\Pi_{B5} = \Pi_0 C_5/C_s$, where C_5 is given by equation (4.82). The component Π_{B4} can then be determined using equation (4.80) and the condition that $\Pi_{B4} = \Pi_{B5}$ at $x = v_1 t_1 + v_2(t - T_{start})$.

4.6.4 Examples

Example 4.1: $L = 1, \Pi_0 = 1, C_s = 1,\ \kappa = 1, t_1 = 0.2, t_2 = 1, v_1 = 1, v_2 = 0.5$. We compute $t^* = 1.249, T_{stop} = 1.949, T_{start} = 2.4$. From equation (4.29) we obtain $R_1 = 0.114$, so that $v_2/v_1 > R_1$ and Case 1a occurs. Figures 4.12 and 4.13 show the solution at $t^* + 0.3$ and $t^* + 0.6$ respectively, when the concentration profile has components C_s, C_1, C_2, C_3. In Figure 4.12, $v_2(t-t^*) = 0.15 < v_1 t_1$ and the precipitate profile has components $\Pi_0, \Pi_{B1}, \Pi_{B2}, \Pi_D, \Pi_E$. In Figure 4.13, where $v_2(t - t*) =$

$0.3 > v_1 t_1$, the precipitate profile has components $\Pi_0, \Pi_{B1}, \Pi_{B2}, \Pi_{B3}, \Pi_E$. The markers on Π_E and Π_{B3} indicate the individual values for which the paths are computed using the algorithm described in section 4.6.3. Figure 4.14 shows the solution at $T_{stop} + 0.3 < T_{start}$, when the components C_4 and Π_4 have emerged. Notice how the values on Π_{B3} are still determined algorithmically, as explained above. In Figure 4.15, at $t = T_{start} + 0.1 = 2.5$, all solution components have emerged. We observe that $\Pi_{B5} = C_5$ since $\Pi_0 = C_s$ here. Figure 4.16 shows the effluent concentration flux C_F for this example case. The trailing edge of the solution reaches the outlet at time $T_{start} + U^{-1}(L - v_1 t_1) = 5.6$.

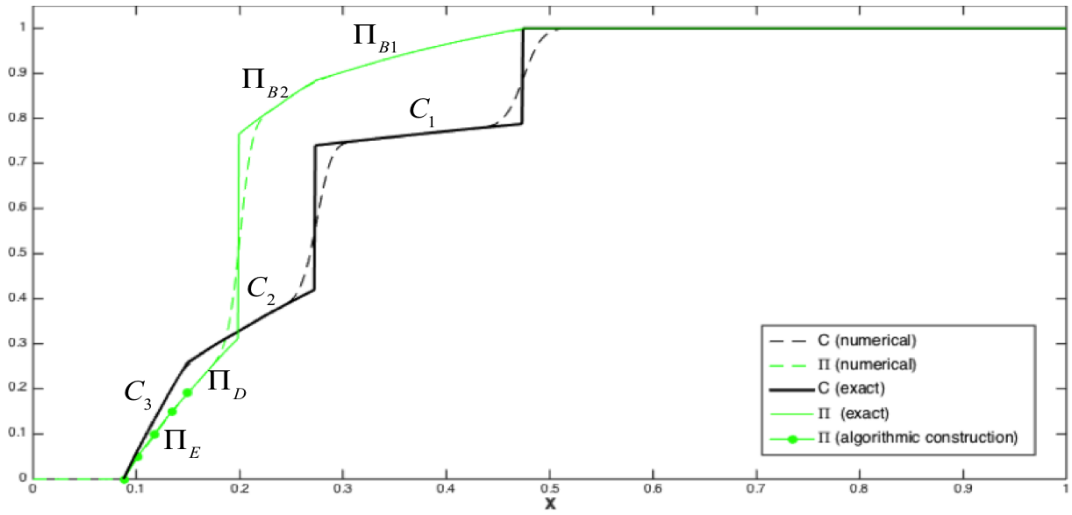

Figure 4.12: *Example 4.1 at* $t = t^* + 0.3$

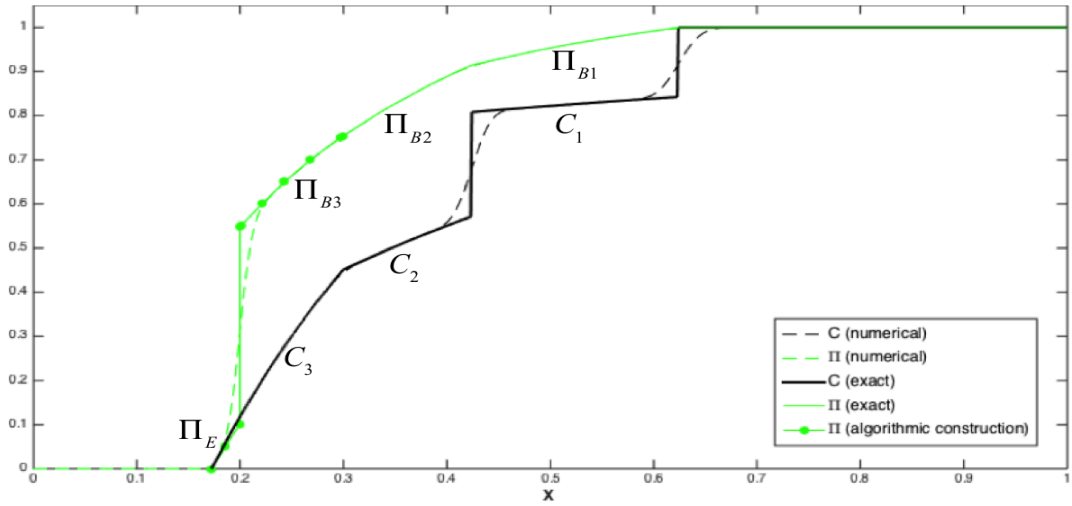

Figure 4.13: *Example 4.1 at* $t = t^* + 0.6$

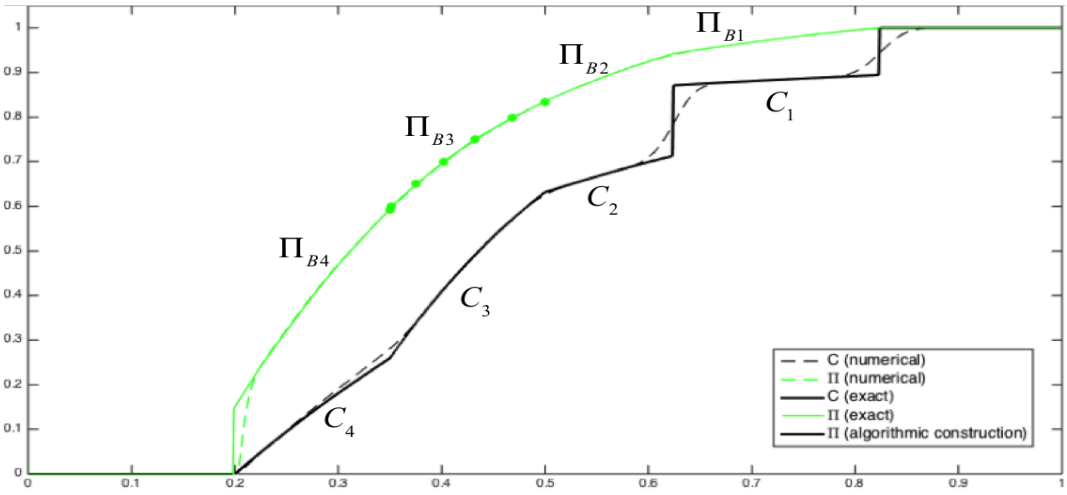

Figure 4.14: *Example 4.1 at* $t = T_{stop} + 0.3$

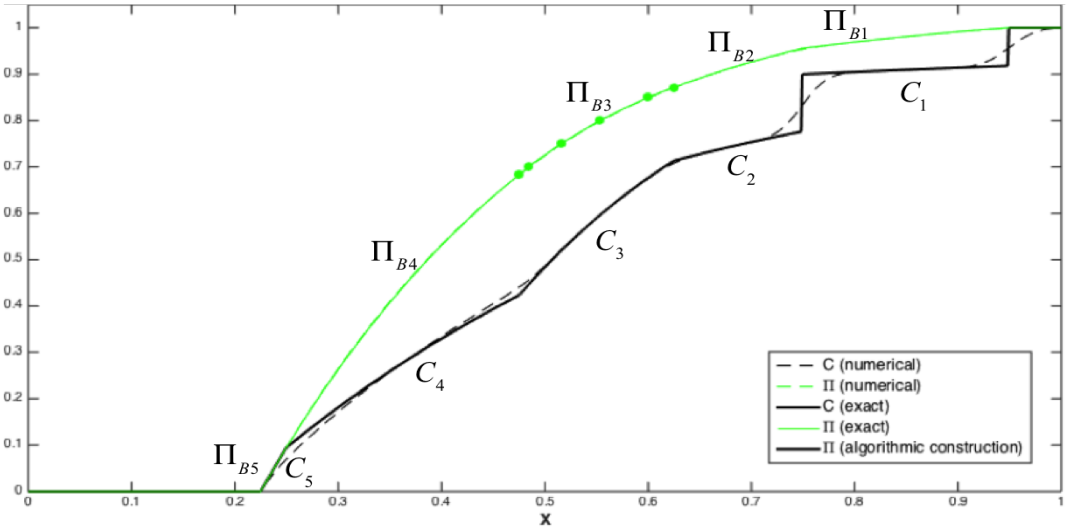

Figure 4.15: *Example 4.1 at* $t = T_{start} + 0.1$

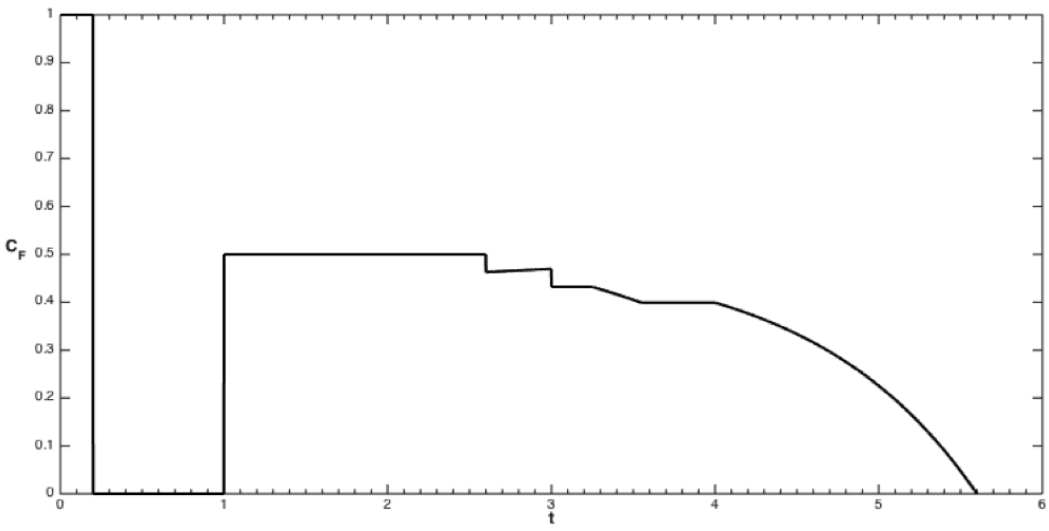

Figure 4.16: *Effluent concentration flux for Example 4.1*

Example 4.2: $L = 1, \Pi_0 = 1, C_s = 1, \kappa = 1, t_1 = 0.4, t_2 = 0.6, v_1 = 1, v_2 = 0.3$. We compute $t^* = 1.019, T_{stop} = 2.812, T_{start} = 2.933$ and $R_1 = 0.253$. Note that $v_2/v_1 > R_1$ (Case 1a), but that the ratio of velocities is much closer to the critical value R_1 than was the case in example 4.1. This results in a steeper C_3 component, which has a region near $x = v_2(t - t^*)$ where the second derivative is positive (see Figure 4.17 for a plot at $t = t^* + 1$). In fact, if we lower the velocity v_2 so that $v_2/v_1 = R_1$, then equation (4.77) implies that C_3 has infinite slope at $x = v_2(t - t^*)$! This point at which $\partial C/\partial x$ blows up is related to the fact that $\alpha_\Pi'(t^*) = v_2$ if $v_2/v_1 = R_1$, i.e. the boundary curve is tangent to the characteristic at $(0, t^*)$.

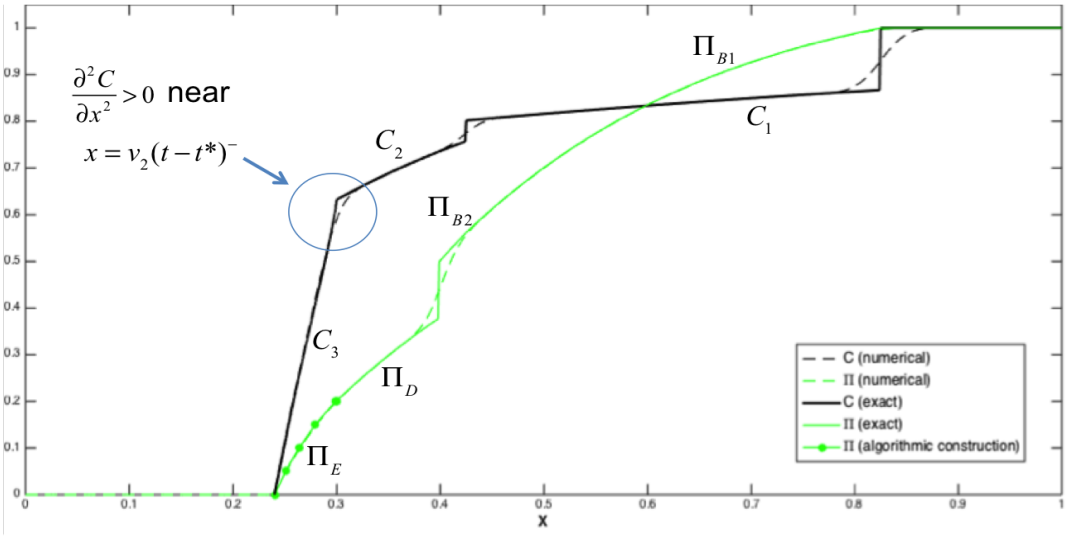

Figure 4.17: *Example 4.2 at* $t = t^* + 1$

4.7 Remaining Cases

4.7.1 Case 1b: $v_2/v_1 < R_1$

Suppose that the solution at $t = t^*$ is as shown in Figure 4.2, with C_1, Π_C and C_2, Π_D defining the solution on $[0, v_1 t_1]$. In sections 4.5 and 4.6, we made the assumption that $v_2/v_1 \geq R_1$ (Case 1a). If $\Pi_0 < C_s(1 + \kappa t_1)$, then we have $0 < R_1 < 1$ and there exists $v_2 < v_1$ such that $v_2/v_1 < R_1$ (Case 1b), which is equivalent to $\alpha_\Pi{}'(t^*) > v_2$. In contrast to Case 1a, a joint root $x_0 = \alpha_\Pi = \alpha_C$ with corresponding new solution regions does *not* form at $t = t^*$. Instead, α_Π satisfies $\Pi_D(\alpha_\Pi, t) = 0$ during some time interval and, consequently, its rate of change is given by equa-

tion (4.25) with $P = 0$ and $C_P = C_2(\alpha_\Pi, t)$. Depending on the specific choice of parameters, several scenarios are possible, but let us assume here that there exists $T_1 > t^*$ such that $\alpha_\Pi(T_1) = v_2(T_1 - t_2) < v_1 t_1$. In other words, α_Π "overtakes" the concentration discontinuity separating C_1 and C_2 before this reaches the Π - discontinuity. The solution region C_2, Π_D then disappears and α_Π satisfies $\Pi_C(\alpha_\Pi, t) = 0$ for $t \geq T_1$, which means that $d\alpha_\Pi/dt$ is given by equation (4.25) with $P = 0$ and $C_P = C_1(\alpha_\Pi, t)$. By assumption, the velocity of α_Π at $t = T_1$ is greater than v_2, which is equivalent to $\psi(\alpha_\Pi) < -\Pi_0$. Since C increases in the discontinuity, the velocity of α_Π also increases instantaneously. We shall assume here that $d\alpha_\Pi/dt > v_2$ until $T_2 > T_1$ such that $\alpha_\Pi(T_2) = v_1 t_1$. Thus, α_Π satisfies $\Pi_D(\alpha_\Pi, t) = 0$ for $t \in [0, T_1]$ and $\Pi_C(\alpha_\Pi, t) = 0$ for $t \in [T_1, T_2]$. During this entire time, α_Π determines a non-zero travelling wave solution on Ω_0: given a concentration value $c \in [0,\ C_1(v_1 t_1,\ T_2)]$, its path $x_c = x_c(t)$ is determined by the components C_1 and C_2 until $\tau \geq t^*$ such that $\alpha_\Pi(\tau) = x_c(\tau)$. The value c then "falls" into the region Ω_0 and travels at velocity v_2 for $t \geq \tau$. This is illustrated in example 4.3.

Example 4.3: let $C_s = 1$, $\Pi_0 = 1/2$, $\kappa = 1/3$, $t_1 = 0.6$, $t_2 = 1$, $v_1 = 1$, $v_2 = 0.2$. Figure 4.18 shows the solution at $t^* = 1.526$. The precipitate profile here has components $\Pi_0, \Pi_B, \Pi_C, \Pi_D$. We compute $R_1 = 0.528$, so $v_2/v_1 < R_1$ and Case 1b occurs. Here, $\alpha_\Pi{}'(t^*) = 0.354 > v_2$. The equation $\Pi_D(v_2(T_1 - t_2), T_1) = 0$ yields $T_1 = 2.175$ and hence $\alpha_\Pi(T_1) = v_2(T_1 - t_2) = 0.235 < v_1 t_1$, as required in the discussion above. Figure 4.19 shows the solution at $t = t^* + 0.3 < T_1$, when $v_2(t - t^*) = 0.06$. Note the travelling wave solution (blue curve) in Ω_0.
At $t = T_1$, we compute $\alpha_\Pi{}'(T_1) = 0.366$ using equation (4.25) with C_2 and $\alpha_\Pi{}'(T_1) = 0.415$ using equation (4.25) with C_1, which indicates that the velocity of α_Π increases abruptly as it overtakes the concentration front. For $t \geq T_1$, it may be verified that $d\alpha_\Pi/dt > v_2$ until $T_2 = 3.202$ (see Figure 4.20). The velocity then drops from $\alpha_\Pi{}'(T_2) = 0.302$ to 0, as the progress of α_Π is halted by the Π - discontinuity. For $t \geq T_2$, the travelling wave solution determines the concentration level at $x = v_1 t_1$, which leads to the emergence of a new solution region. This problem will be discussed in the context of Case 2 in section 4.7.2.

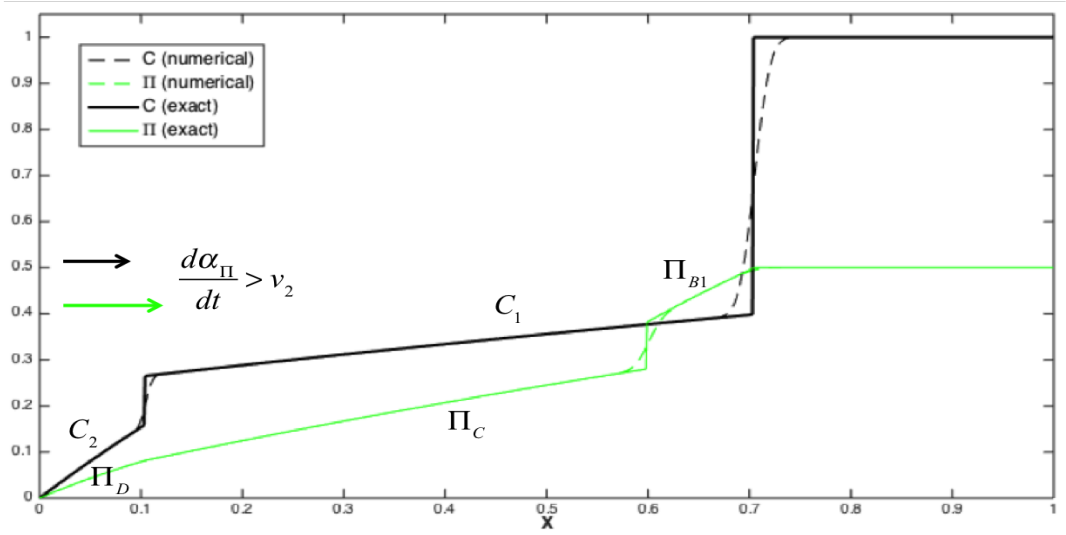

Figure 4.18: *Example 4.3 at* $t = t^*$

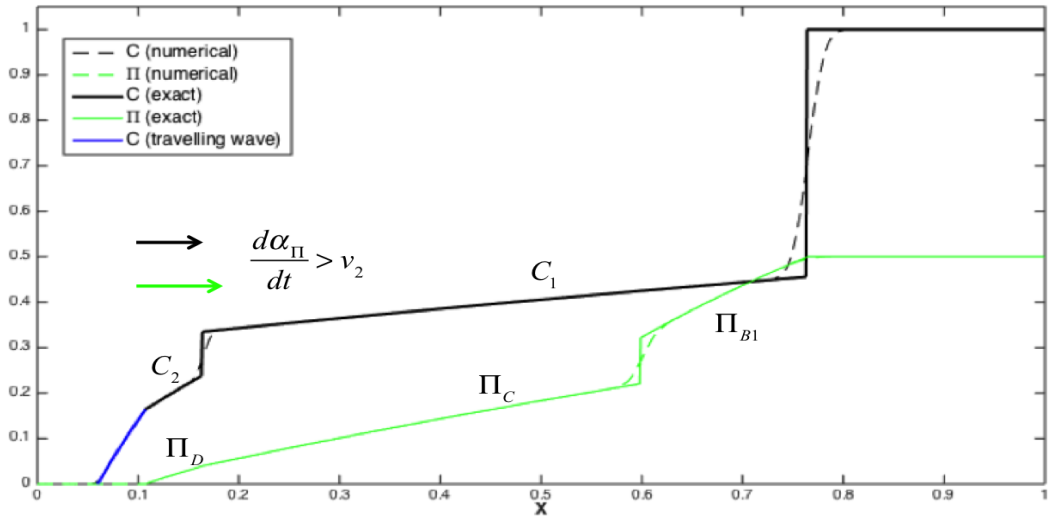

Figure 4.19: *Example 4.3 at* $t = t^* + 0.3$

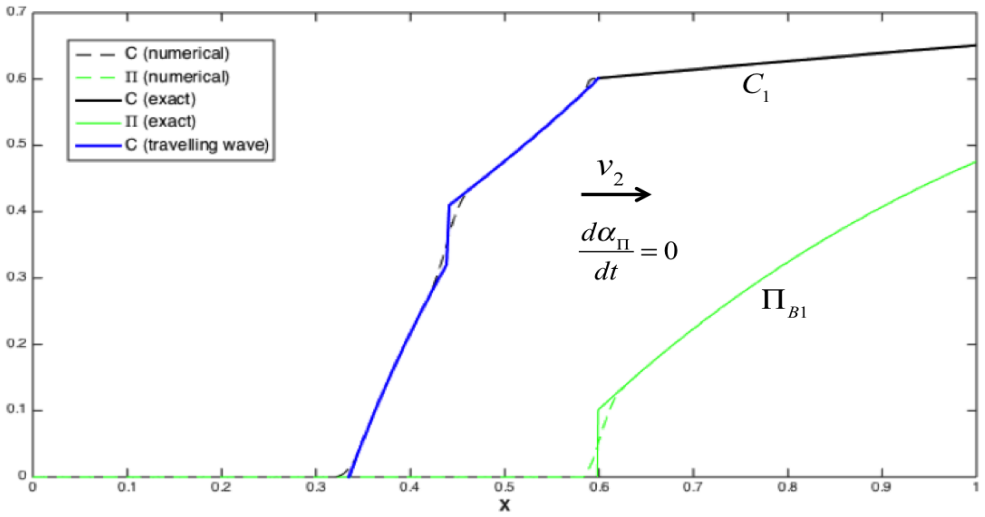

Figure 4.20: *Example 4.3 at* $t = T_2$, *when* $\alpha_\Pi = v_1 t_1$.

4.7.2 Case 2: precipitate runs during the shut-in phase

Motivated by example 4.3, we will now consider what happens if a non-zero travelling wave solution to the left of α_Π is moving faster than this point. As a prototype for this type of problem, we study Case 2, where $C_s\kappa t_1 < \Pi_0 < C_s\left(1 + \kappa t_1 - e^{\kappa t_1 - \kappa t_2}\right)$, so that the precipitate runs out during the shut-in phase ($t_1 < t^* < t_2$). Figure 4.21 shows a typical solution profile for this case at $t = t_2$.

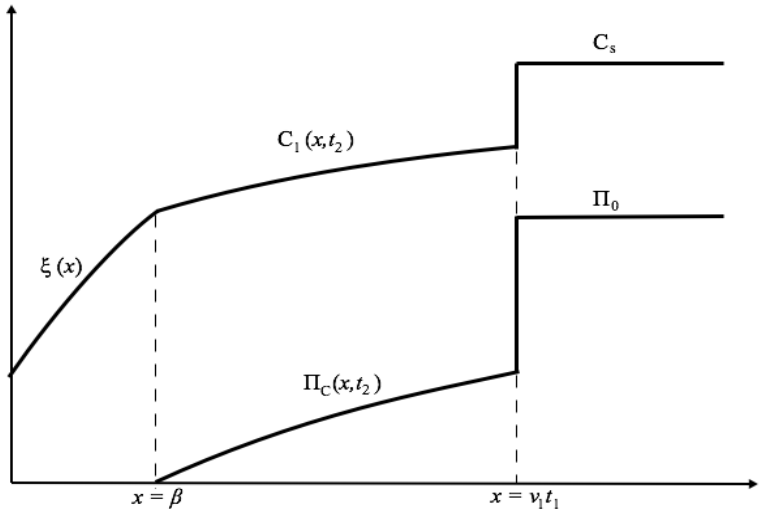

Figure 4.21: *Typical solution profiles in Case 2, at* $t = t_2 > t^*$

Let $\beta := \alpha_\Pi(t_2)$. For $x \geq \beta$, equations (4.13) and (4.19) define $C_1(x, t_2)$ and $\Pi_C(x, t_2)$ respectively. Between the run-out time t^* and the end of the shut-in, $\alpha_\Pi(t)$ is given by the root of equation (4.10). That is, we have

$$-C_s e^{\kappa t_1 - \kappa t} = \Pi_0 \exp\left(\frac{\kappa\,\alpha_\Pi}{v_1}\right) + C_s\left(\frac{\kappa\alpha_\Pi}{v_1} - \kappa t_1 - 1\right)\ ,\ t \in [t^*, t_2] \tag{4.87}$$

The curve $\xi = \xi(x)$ describes the concentration profile on $[0, \beta]$ and is found by considering an arbitrary point $x \in [0, v_1 t_1]$. The concentration level at x during the shut-in phase is determined by equation (4.9), until $t = {\alpha_\Pi}^{-1}(x)$. We then define $\xi := \mathbb{R} \to \mathbb{R}$ by $x \mapsto C\left(x, \alpha_\Pi^{-1}(x)\right)$. Substituting $t = {\alpha_\Pi}^{-1}(x)$ in equation (4.9) and using equation (4.87), we obtain

$$\xi(x) = \Pi_0 + C_s + C_s \exp\left(\frac{-\kappa x}{v_1}\right) \cdot \left(\frac{\kappa x}{v_1} - \kappa t_1 - 1\right) \tag{4.88}$$

We now investigate the evolution of α_Π during the second flow phase $[t_2, \infty)$. Noting that $C_1(\beta, t_2) = \xi(\beta)$ and that C_1 and Π_C obey equation (4.25), it follows that

$$\left.\frac{d\alpha_\Pi}{dt}\right|_{t=t_2} = \frac{v_2 C_s - v_2 \xi(\beta)}{\Pi_0 + C_s - \xi(\beta) + \psi(\beta)} \tag{4.89}$$

Using the fact that $\beta = \alpha_\Pi(t_2)$ satisfies equation (4.87), it can be shown that

$$\left.\frac{d\alpha_\Pi}{dt}\right|_{t=t_2} \leq v_2 \quad \Leftrightarrow \quad \frac{v_2}{v_1} \geq R_2 := \frac{C_s e^{\kappa t_1 - \kappa t_2 - \kappa\beta/v_1}}{\Pi_0 + C_s e^{-\kappa\beta/v_1}} \tag{4.90}$$

Let us assume that $v_2/v_1 \geq R_2$ (**Case 2a**). This implies that the travelling wave solution $\xi[x - v_2(t - t_2)]$ moves faster than α_Π and it therefore determines the concentration level at this point. The invariance of equation (4.25) then implies that the velocity of α_Π for $t \geq t_2$ is given by the ODE

$$\frac{d\alpha_\Pi}{dt} = \frac{v_2 C_s - v_2 \xi[\alpha_\Pi - v_2(t - t_2)]}{\Pi_0 + C_s - \xi[\alpha_\Pi - v_2(t - t_2)] + \psi(\alpha_\Pi)} \tag{4.91}$$

With ξ given by equation (4.88), this has the solution

$$\alpha_\Pi(t) = \eta(t) := \frac{v_1}{\kappa}\left\{\frac{\kappa t_1}{C_s} + \frac{q_1(t)}{q_2(t)} - W\left[\frac{q_3(t)}{q_2(t)}\exp\left(\frac{\kappa t_1}{C_s} + \frac{q_1(t)}{q_2(t)}\right)\right]\right\} \tag{4.92}$$

where the functions q_1, q_2 and q_3 are

$$q_1(t) = v_2\Pi_0\left(1 + \kappa(t - t_2)\right) \tag{4.93}$$

$$q_2(t) = v_1 C_s\left[\frac{v_2}{v_1} - 1 + \exp\left(\frac{\kappa v_2(t - t_2)}{v_1}\right)\right] \tag{4.94}$$

$$q_3(t) = v_2\left[1 - e^{\kappa t_1 - \kappa t_2} + \kappa(t - t_2)\exp\left(\frac{\kappa v_2(t - t_2)}{v_1}\right)\right] \tag{4.95}$$

Equation (4.92) is now used to find the new concentration component on the interval $\alpha_\Pi(t) < x < \beta + v_2(t - t_2)$, which satisfies $C(\alpha_\Pi, t) = \xi[\alpha_\Pi - v_2(t - t_2)]$ on the moving boundary. This is illustrated in Figure 4.22.

Recall that, during the second flow phase, the general solution of equation (4.1) is $x = v_2 s + g(r)$, $t = s + h(r)$, $C = C_s + f(r)e^{-\kappa s}$ for arbitrary functions f, g, h. We now choose these functions in such a way that $s = 0$ on the boundary curve

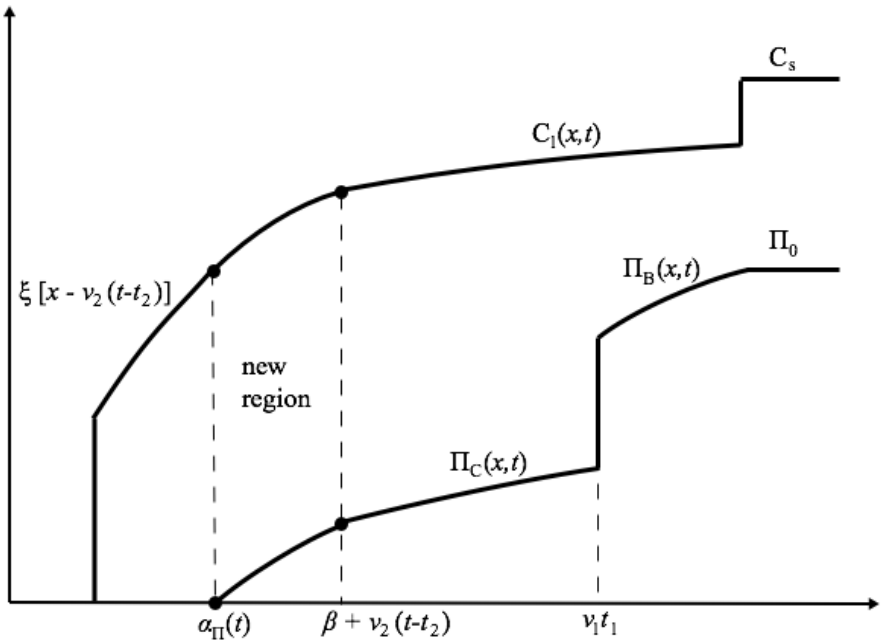

Figure 4.22: *New solution region, which can be described parametrically.*

$x = \eta(t)$. This is achieved by letting $h(r) = r$ and $g(r) = \eta(r)$. Finally, we impose the condition that $C = \xi[x - v_2(t - t_2)]$ when $s = 0$, which implies that $f(r) = \xi[\eta(r) - v_2(r - t_2)] - C_s$. Writing $r = t - s$, we then obtain a pair of equations related by the parameter s:

$$x = \eta(t - s) \tag{4.96}$$

$$C = C_s + [\xi(\eta(t - s) - v_2(t - s - t_2)) - C_s]\, e^{-\kappa s} \tag{4.97}$$

Equations (4.96) and (4.97) are a parametric description of the concentration profile on the interval $\eta(t) < x < \beta + v_2(t - t_2)$. Given x and t, we can find the corresponding value of s using equation (4.96) and then substitute into equation (4.97) to determine the concentration level at (x, t). If η were invertible, this procedure would yield an explicit formula for C. This is not the case and we have to content ourselves with the parametric solution description.

Suppose that there exists $T \geq t_2$ such that $\eta(T) = v_2(T - t_2) < v_1 t_1$. In this scenario, the point α_C catches α_Π before it reaches the Π-discontinuity, resulting in the existence of a joint root $x_0 = \alpha_\Pi = \alpha_C$ for $t \geq T$, the velocity of which is given by equation (4.91) with $\xi = 0$. This leads to new solution component which is similar to equation (4.72). In fact, the only difference comes from the initial condition: instead of $x_0(t^*) = 0$, we must now use $x_0(T) = v_2(T - t_2)$. These ideas are illustrated in example 4.4.

Example 4.4: $C_s = 1$, $\Pi_0 = 0.7$, $\kappa = 0.5$, $t_1 = 0.7$, $t_2 = 3$, $v_1 = 1$, $v_2 = 3/2$. We find $t^* = 2.333$ $(t_1 < t^* < t_2)$, $\beta = \alpha_\Pi(t_2) = 0.377$ and $R_2 = 0.218$. Since $v_2/v_1 > R_2$, Case 2a occurs. Figure 4.24 shows the parametric solution given by equations (4.96) and (4.97) at $t = 3.2$, on the interval between $x = \alpha_\Pi(t) = 0.422$ and $x = \beta + v_2(t - t_2) = 0.677$. The path of α_Π is plotted in Figure 4.25. Note that $\alpha_\Pi(T) = v_2(T - t_2)$ at $T = 3.306$. For $t_2 \le t \le T$, $\xi(\alpha_\Pi) \neq 0$ and α_Π is given by equation (4.92) (plotted in red). For $t \ge T$, we have $x_0 = \alpha_\Pi = \alpha_C$, $\xi(x_0) = 0$ and the path is given by the blue curve.

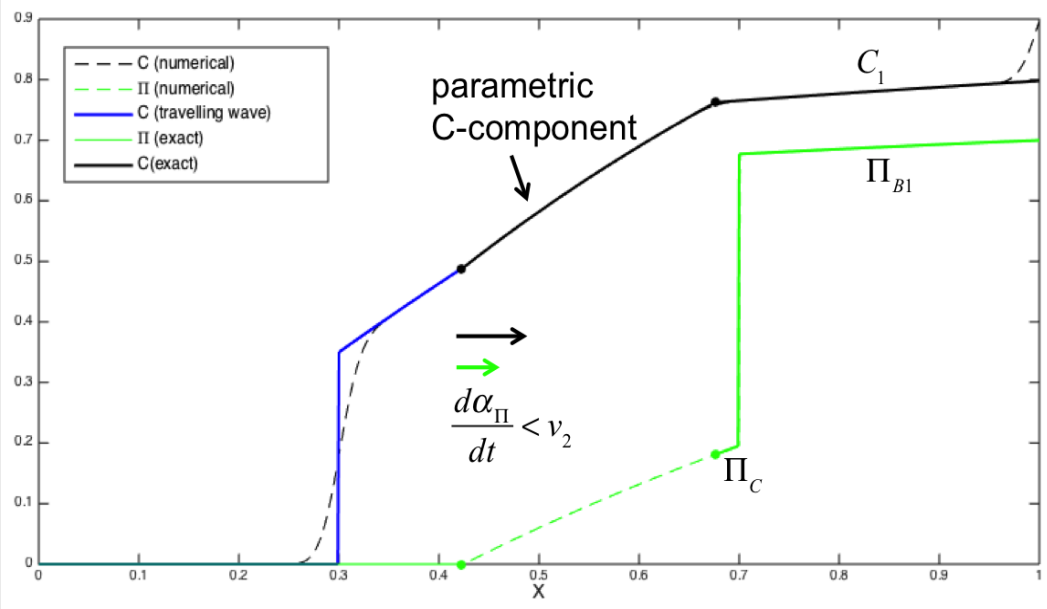

Figure 4.23: *Example 4.4 at* $t = t_2 + 0.2 < T$

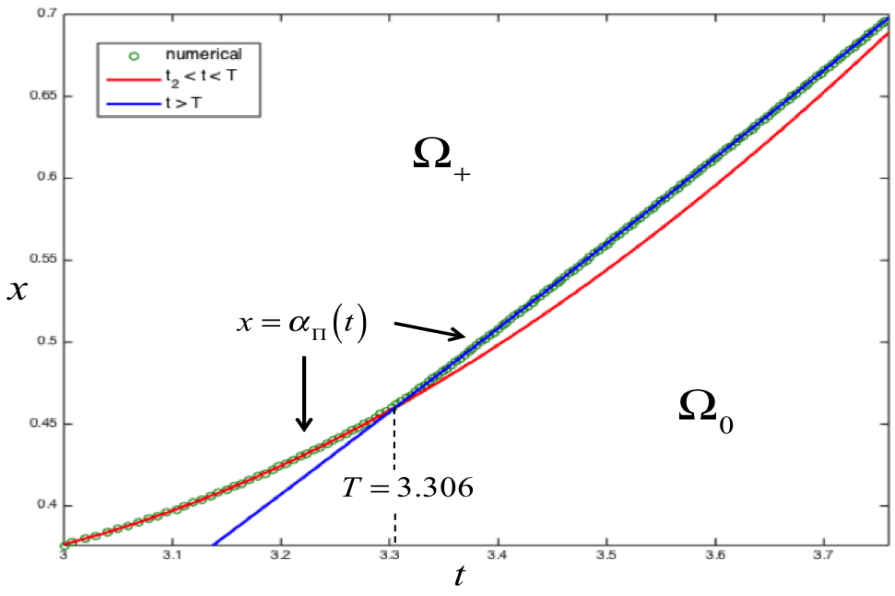

Figure 4.24: *The boundary curve* $x = \alpha_\Pi(t)$ *for* $t > t_2 > t^*$

4.7.3 Case 3: precipitate runs out during the first flow phase

This case can be treated in the same way as Case 2. The run-out time is now $t^* = \Pi_0/\kappa C_s < t_1$ and the solution discussed in Chapter 2 determines the concentration and precipitate profiles until $t = t_1$. We have $\alpha_\Pi(t_1) = \alpha_C(t_1) = U(t_1 - t^*)$, where $U = v_1 C_s/(\Pi_0 + C_s)$. The shape of the solution profiles is altered by the shut-in phase and, at $t = t_2$, the concentration on $\alpha_\Pi(t_1) \leq x \leq \alpha_\Pi(t_2)$ will be given by some non-zero function ξ (analogous to equation (4.89)). We then determine the rate of change of α_Π at $t = t_2$ and identify a constant R_3 such that $\alpha_\Pi{}'(t_2) \leq v_2$ if and only if $v_2/v_1 \geq R_3$ (**Case 3a**). In this case, the motion of α_Π for $t > t_2$ is governed by an ODE involving the travelling wave solution $\xi(x - v_2(t - t_2))$ evaluated at $x = \alpha_\Pi$. The solution of this ODE (if it exists) can then be used to determine a (parametric) solution description by choosing suitable characteristic coordinates.

In the cases 1b, 2b and 3b, we have $\alpha_\Pi{}'(t^*) > v_2$ or $\alpha_\Pi{}'(t_2) > v_2$ and a travelling wave solution ξ is "built" by the motion of the point α_Π, as was illustrated in example 4.3. The description of these travelling waves is implicit, which presents a problem once the velocity of α_Π falls below v_2. This is when α_Π starts to be governed by the incoming travelling wave. Without an explicit formula for ξ, it is impossible to establish the ODE describing the subsequent motion of α_Π. It is at best possible to describe the solution algorithmically in these cases.

4.8 Chapter 2 revisited: arbitrary initial data

We conclude this chapter by considering the problem with constant flow rate and arbitrary initial conditions. This is inspired by the discussion of the preceding sections, where the "initial conditions" for the second flow phase with constant velocity v_2 were determined by the first flow phase and shut-in phase. Let us now revisit the problem with a single, constant fluid velocity v, as in Chapter 3, but with Cauchy data $C(x,0) = C_0(x)$, $\Pi(x,0) = \Pi_0(x)$ and $C(0,t) = 0$. We will approach this in the most general way, which will reveal exactly why the relationship expressed in equation (4.25) is invariant between solution regions. Assuming that $\Pi_0(x) > 0$ for all x, the solutions for some $t > 0$ are as sketched in Figure 4.25. In the region $x > vt$, the solution components are denoted by $C_1(x,t)$ and $\Pi_1(x,t)$. The

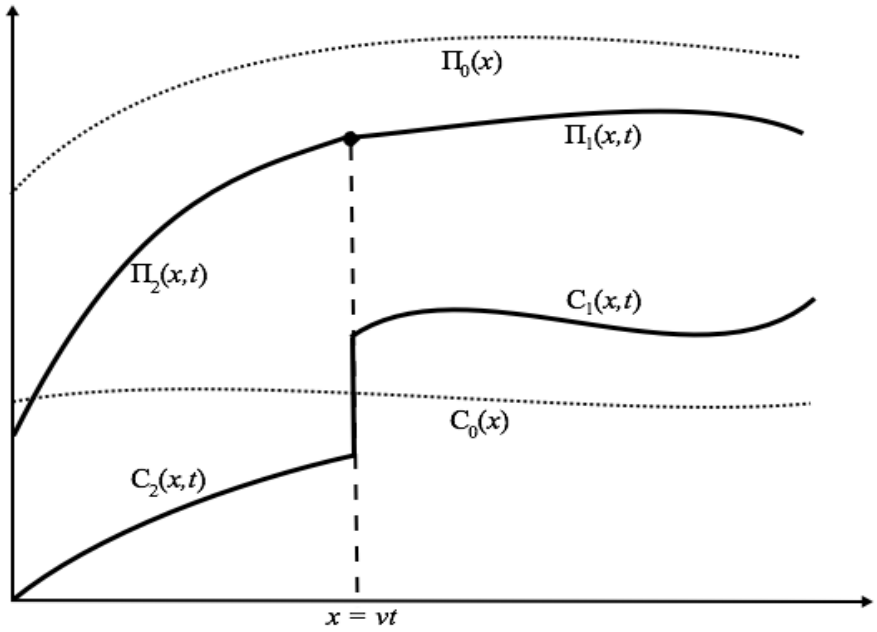

Figure 4.25: *Sketch of solution profiles for some $t > 0$ in the case of arbitrary initial conditions $C_0(x)$, $\Pi_0(x) > 0$.*

general form of the concentration component is $C_1(x,t) = C_s + f_1(x - vt)e^{-\kappa t}$ and the arbitrary function f_1 is determined by applying the initial condition $C(x,0) = C_0(x)$. This yields

$$C_1(x,t) = C_s + [C_0(x - vt) - C_s]e^{-\kappa t} \tag{4.98}$$

The precipitate component $\Pi_1(x,t)$ is found by integration of $-\kappa(C_s - C_1)$ with respect to t. Assuming that the anti-derivative is of the form $\varphi_1(x - vt)e^{-\kappa t}$ and using the initial condition $\Pi(x,0) = \Pi_0(x)$, we find

$$\Pi_1(x,t) = \Pi_0(x) - \varphi_1(x) + \varphi_1(x - vt)e^{-\kappa t} \tag{4.99}$$

Observe that

$$-\kappa(C_s - C_1) = \frac{d}{dt}[\varphi_1(x - vt)e^{-\kappa t}] = -v\varphi_1'(x - vt)e^{-\kappa t} - \kappa\varphi_1(x - vt)e^{-\kappa t} \tag{4.100}$$

Then, using equations (4.99) and (4.100), we have

$$\begin{aligned}
\frac{\partial \Pi_1}{\partial x} &= \Pi_0'(x) - \varphi_1'(x) + \varphi_1'(x - vt)e^{-\kappa t} \\
&= \Pi_0'(x) - \varphi_1'(x) + \frac{\kappa}{v}\left[C_s - C_1 - \varphi_1(x - vt)e^{-\kappa t}\right] \\
&= \Pi_0'(x) - \varphi_1'(x) + \frac{\kappa}{v}\left[C_s - C_1 + \Pi_0(x) - \varphi_1(x) - \Pi_1\right]
\end{aligned} \tag{4.101}$$

We define the function

$$F(x) := \Pi_0(x) - \varphi_1(x) + \frac{v}{\kappa}\left[\Pi_0'(x) - \varphi_1'(x)\right] \tag{4.102}$$

Now consider the equation $\Pi_1(x_P, t) = P$ for some fixed precipitate level P and denote the corresponding concentration level $C_P = C_1(x_P, t)$. By application of the Inverse Function Theorem, we obtain the relation

$$\frac{dx_P}{dt} = -\frac{\partial\Pi_1/\partial t}{\partial\Pi_1/\partial x} = \frac{v(C_s - C_P)}{F(x_P) - P + C_s - C_P} \tag{4.103}$$

Let us assume that we don't know the specific form of the concentration component C_2 yet. The general solution is $C_2(x,t) = C_s + f_2(x - vt)e^{-\kappa t}$ for some arbitrary function f_2. Suppose that integration of $-\kappa(C_s - C_2)$ with respect to t leads to the anti-derivative $\varphi_2(x - vt)e^{-\kappa t}$ and hence the precipitate component $\Pi_2(x,t) = g_2(x) + \varphi_2(x - vt)e^{-\kappa t}$. If the arbitrary function g_2 is determined by the condition that $\Pi_2(x,t) = \Pi_1(x,t)$ at $x = vt$ (see Figure 4.25), we obtain

$$\Pi_2(x,t) = \Pi_0(x) - \varphi_1(x) + \varphi_1(0)e^{-\kappa x/v} - \varphi_2(0)e^{-\kappa x/v} + \varphi_2(x - vt)e^{-\kappa t} \tag{4.104}$$

Differentiating this with respect to x and using equation (4.100) with C_1, φ_1 replaced by C_2, φ_2, it can be deduced that

$$\frac{\partial\Pi_2}{\partial x} = \Pi_0'(x) - \varphi_1'(x) + \frac{\kappa}{v}\left[C_s - C_2 + \Pi_0(x) - \varphi_1(x) - \Pi_2\right] \tag{4.105}$$

This shows that the equation for $\partial\Pi/\partial x$ is invariant between the two solution regions. Since $\partial\Pi/\partial t$ is invariant by definition, it follows that the rate of change of an arbitrary precipitate value P is also invariant and is given by equation (4.103) with $C_P = C_2(x_P, t)$. Since C_2 is completely general (no conditions are applied yet), the argument can be repeated to any further solution regions. As long as we demand that the precipitate profile is continuous, we will always obtain equation (4.103).

We now go about describing in general how the solution can be obtained using the

invariance of equation (4.103). By assumption, $\Pi_0(x) > 0$ for all x, as shown in the sketch in Figure 4.25. The boundary condition $C(0,t) = 0$ can be applied to find the usual steady-state component $C_2(x,t) = C_s - C_s e^{-\kappa x/v}$ and then $\varphi_2(x - vt) = \kappa C_s v^{-1}(x - vt)e^{-\kappa(x-vt)/v}$ in equation (4.104) for the precipitate component. We deduce that $\Pi_2(0,t) = 0$ at $t^* = \Pi_0(0)/\kappa C_s$ and make the assumption that $\Pi_1(x,t^*) > 0$ and $\Pi_2(x,t^*) > 0$ for $x > 0$, so that t^* is the first time the precipitate runs out, as is true for the cases we have encountered thus far in Chapter 3 and the preceding sections of this chapter. In treatment of these problems it became clear how the solution depends on the moving boundary point α_Π. It follows from the invariance of equation (4.103) that

$$\frac{d\alpha_\Pi}{dt} = \frac{v(C_s - C(\alpha_\Pi, t))}{F(\alpha_\Pi) + C_s - C(\alpha_\Pi, t)} \tag{4.106}$$

where $C(\alpha_\Pi, t)$ is the concentration level at $x = \alpha_\Pi$ and depends on the applicable solution region. Suppose now that there is a time $\tau \geq t^*$ such that $F(\alpha_\Pi(\tau)) = 0$, $F'(\alpha_\Pi(\tau)) \neq 0$ and $C(\alpha_\Pi, t) - C_s < F(\alpha_\Pi(t)) < 0$ for all $t^* \leq t < \tau$. Equation (4.106) then implies that $d\alpha_\Pi/dt > v$ for all $t^* \leq t < \tau$ and $\alpha_\Pi'(\tau) = v$. During this time interval, $C(\alpha_\Pi, t) = C_2(\alpha_\Pi, t)$ at first. If τ is large enough, then the region with solution components C_2, Π_2 will disappear and we have $C(\alpha_\Pi, t) = C_1(\alpha_\Pi, t)$ afterwards. We saw this in example 4.3 and it is also assumed in the sketch in Figure 4.26, which shows the solution profiles at $t = \tau$. Here, we let $\beta = \alpha_\Pi(\tau)$ for

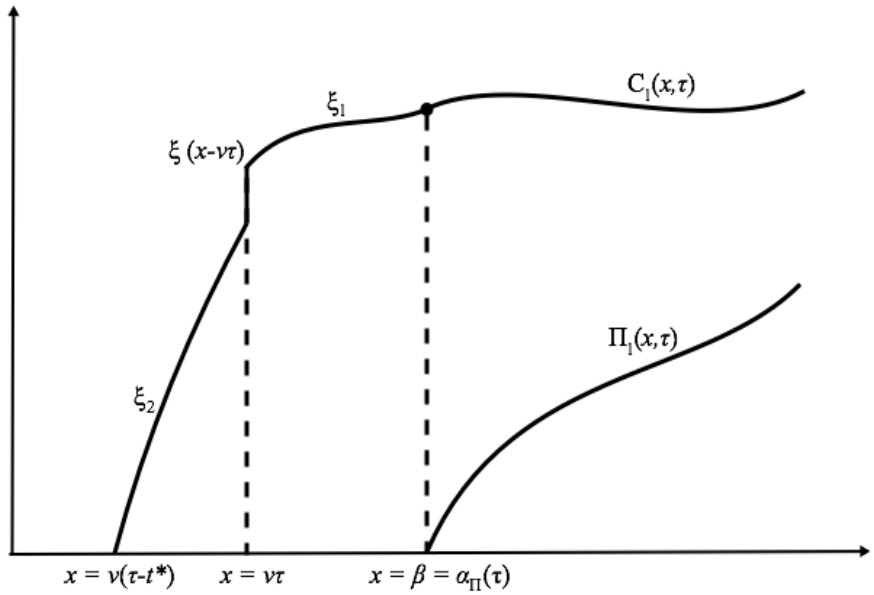

Figure 4.26: *Sketch of solution profiles at $\tau > t^*$, when $d\alpha_\Pi/dt = v$.*

ease of notation. Observe that the motion of α_Π during $t^* \leq t < \tau$ determines a travelling wave solution $\xi(x-vt)$ on the interval $v(t-t^*) < x < \alpha_\Pi(t)$. It does so as it by-passes points on the concentration components C_2, C_1, thus forming the two travelling wave components ξ_2, ξ_1. This is shown schematically in Figure 4.27. For $t^* \leq t < \tau$, the plane characteristics run into the boundary curve $x = \alpha_\Pi(t)$ from Ω_+. This defines the concentration level on the boundary, which in turn determines the travelling wave on the left hand side.

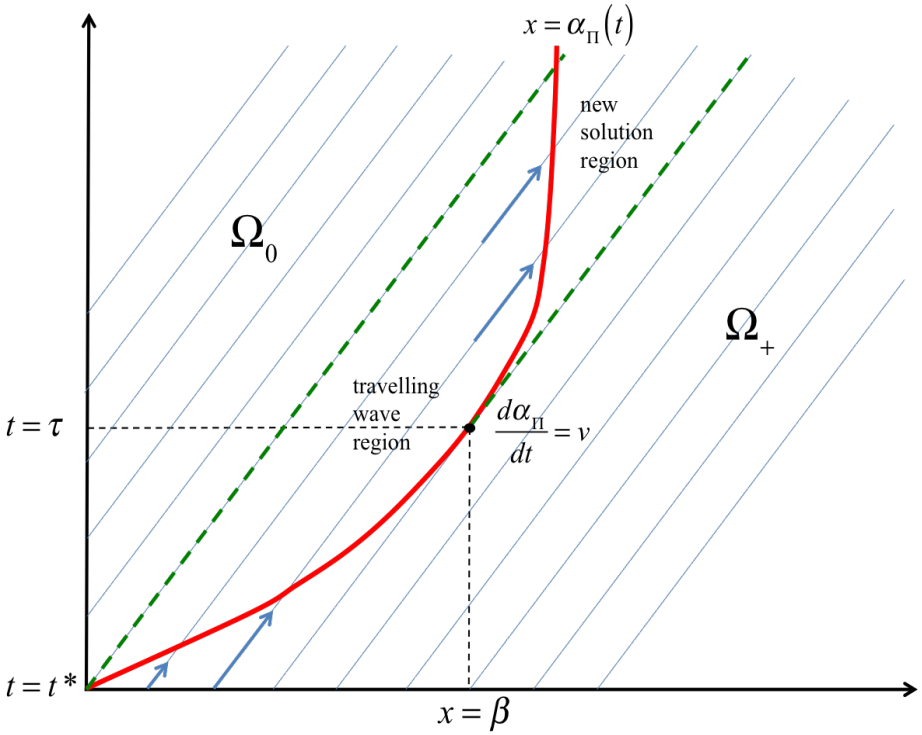

Figure 4.27: *Boundary curve $x = \alpha_\Pi(t)$ and characteristics.*

Since $F'(\beta) \neq 0$ by assumption, there is a time interval $\tau < t < T$ during which $F(\alpha_\Pi(t)) > 0$ and hence $d\alpha_\Pi/dt < v$. The characteristics now run into the boundary curve from Ω_0 and the travelling wave solution $\xi(x-vt)$ determines the concentration on the boundary. This leads to the emergence of new solution components $C_3(x,t) = C_s + f_3(x-vt)e^{-\kappa t}$ and $\Pi_3(x,t) = g_3(x) + \varphi_3(x-vt)e^{-\kappa t}$ on the interval $\alpha_\Pi(t) < x < \beta + v(t-\tau)$ (see Figure 4.28). If the arbitrary function $g_3(x)$ is determined by setting $\Pi_3(x,t) = \Pi_1(x,t)$ at $x = \beta + v(t-\tau)$, then we recover equation (4.103) with $C_P(x_P,t) = C_3(x_P,t)$ using the same argument as before. This is also true if the components C_2, Π_2 still existed at $t = \tau$. We would then connect Π_3 to Π_2 at $x = \beta + v(t-\tau)$.

The arbitrary function f_3 is found using the concentration level on the boundary curve. Since this is determined by the travelling wave, the motion of α_Π for $t \geq \tau$

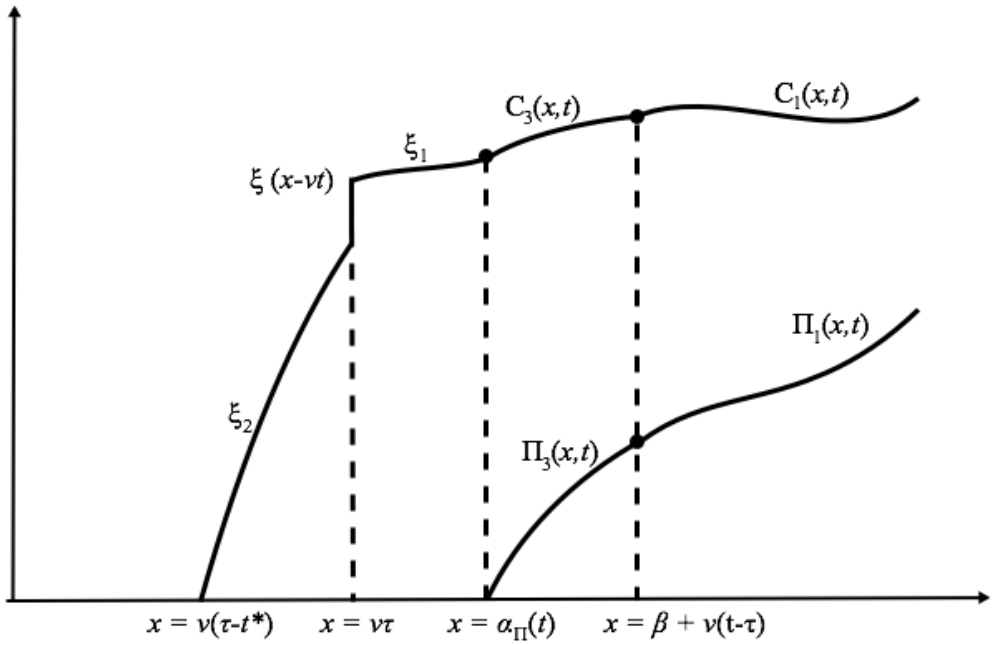

Figure 4.28: *Sketch of solution profiles at $t > \tau$, when $d\alpha_\Pi/dt < v$ and new solution components C_3, Π_3 have emerged.*

is described by

$$\frac{d\alpha_\Pi}{dt} = \frac{v(C_s - \xi(\alpha_\Pi - vt))}{F(\alpha_\Pi) + C_s - \xi(\alpha_\Pi - vt)} \ , \quad \alpha_\Pi(\tau) = \beta \tag{4.107}$$

Let us assume that this initial value problem has a solution $\alpha_\Pi = \eta(t)$. Then, f_3 is determined by the equation $f_3(\eta(t)-vt)e^{-\kappa t} = \xi(\eta(t)-vt)$. Introducing the variable $z = \eta(t) - vt$, the question is if we can invert to find $t^{-1}(z)$. If this is possible, we have $f_3(z) = \xi(z)\exp(\kappa t^{-1}(z))$ and therefore an explicit analytical expression for C_3. The function φ_3 could then be found by direct integration. If the inverse $t^{-1}(z)$ can not be found explicitly, we have to choose characteristic coordinates s, r such that $s = 0$ on the boundary curve $x = \eta(t)$. This procedure leads to either an implicit description of C_3 (as in section 4.6.1) or a parametric description of C_3 (as in section 4.7.2). However, unfortunately invertibility is not the only issue here. The question is also if equation (4.107) admits a closed-form solution. To make matters worse, the travelling wave that formed while $t^* < t < \tau$ can be given as an explicit formula $\xi = \xi(x-vt)$ only in the simplest of cases. In general, ξ can only be defined implicitly, which poses an obvious problem in equation (4.107). Of course, the path of α_Π for $t \geq \tau$ could still be computed, but it would be an algorithmic construction which would not lend itself to the construction of C_3 as described

above. Nevertheless, the present discussion still sheds light on the mechanism of the problem. It also highlights the complete dependence of the motion of α_Π on the initial conditions $C_0(x)$ and $\Pi_0(x)$, through the function F. Earlier in this discussion, it was assumed that the initial profiles were such that the precipitate first runs out at $x = 0$, $t = t^*$, but this is not necessarily the case. The precipitate could of course reach zero in several locations. Moreover, the function F could change sign multiple times and the points α_Π could have negative velocity. Although these factors complicate the construction of the solution, the general approach remains the same. Equation (4.103) is always invariant between solution regions and the concentration at α_Π is always known.

4.9 Summary

In this chapter we have begun to find and categorise the solutions of the Cauchy problem for equations (4.1) and (4.2) on Ω, with Cauchy data $C(x,0) = C_s$, $\Pi(x,0) = \Pi_0$ on $0 \leq x \leq L$, and $C(0,t) = 0$ for $0 < t < t_1$ and $t \geq t_2$. This described the scale inhibitor model with no adsorption or dispersion, using two different constant flow velocities v_1 and v_2 on either side of a shut-in period $t_1 \leq t < t_2$ during which flow is halted ($v = 0$). Using the run-out time t^* of the precipitate level at the inlet, the problem was initially divided into the three scenarios $t^* \geq t_2$ (Case 1), $t_1 \leq t^* < t_2$ (Case 2) and $t^* < t_1$ (Case 3). A further sub-division was made into *a*-cases and *b*-cases using the ratio of the fluid velocities v_2/v_1 in relation to constants R_1 (equation (4.29)), R_2 (equation (4.90)) and R_3 (to be determined). In the *a*-cases, the velocity of the boundary point, $d\alpha_\Pi/dt$, is always *less* than the prevailing fluid velocity and this leads to a clear definition of an ODE for the motion of α_Π, analogous to the "base case" discussed in Chapter 3. The entire process was shown for Case 1a (see equation (4.30)) and Case 2a (see equation (4.91)). The solution of these ODEs defined boundary curves in Ω on which C could be specified using the solution in Ω_0. A suitable choice of characteristic coordinates was then used to find the new solution components in Ω_+. In Case 1a, these components were explicit formulae when $v_1 = v_2$ (section 4.5) and given by implicit relations when $v_1 \neq v_2$ (section 4.6). In Case 2a, the best we could do was give a parametric solution description (see equations (4.96) and (4.97)). It was explained how Case 3a may be approached similarly. All analytical solutions were derived based on the

assumption that the precipitate profile cannot develop discontinuities when the fluid is moving, but only during a shut-in phase (the "Π-discontinuity" is formed). This assumption can be validated by integration of the effluent concentration flux, which was done explicitly in Case 1a in order to demonstrate that the analytical solution preserves the total amount of chemical. The question remains as to how mass conservation can be guaranteed *a priori* by the continuity property of the precipitate profile, which would remove the need to check by integration.

A new problem presented itself in the treatment of the *b*-cases. Here, the velocity of α_Π is initially *greater* than the prevailing fluid velocity. This leads to the formation of a travelling wave solution in Ω_0, which was illustrated in example 4.3 for Case 1b. The trouble is that this travelling wave is implicitly defined. It then becomes unclear how to specify the ODE for α_Π once its velocity drops below the fluid velocity, so that the travelling wave tends to move back into Ω_+.

Finally, the results of section 4.1-4.7 inspired a discussion about the analytical solution of the constant flow rate problem presented in Chapter 3, but with arbitrary initial distributions of concentration and precipitate. The precise nature of the "invariant" relationship between C and Π emerged. It was proved rigorously using the *general form* of $\Pi(x,t)$, which was found from the general solution of $C(x,t)$. We will see in Chapter 5 that this is not always possible.

Chapter 5

Exact solutions of the scale inhibitor model with equilibrium adsorption

5.1 Introduction

In this chapter, we study the sub-case of equations (1.6)-(1.8) in which adsorption occurs at equilibrium. In this idealised process, the adsorption level Γ instantaneously reaches the level predicted by the adsorption isotherm $\Gamma_{eq}(C)$. We already saw that equations (1.6)-(1.8) then reduce to equations (1.11)-(1.12). With no diffusion ($D = 0$), these are

$$\left[1 + \frac{d\Gamma_{eq}}{dC}\right] \frac{\partial C}{\partial t} + v \frac{\partial C}{\partial x} = -\frac{\partial \Pi}{\partial t} \tag{5.1}$$

$$\frac{\partial \Pi}{\partial t} = -\kappa \left[C_s - C\right] \cdot \left[H\left(\Pi\right) + H\left(C - C_s\right) - H\left(\Pi\right) H\left(C - C_s\right)\right] \tag{5.2}$$

This is to be solved on the domain $\Omega = [0, L] \times [0, \infty)$ with constant initial data $C\left(x, 0\right) = C_s$, $\Pi\left(x, 0\right) = \Pi_0$ and $\Gamma\left(x, 0\right) = \Gamma_0 = \Gamma_{eq}(C_s)$, which represent the uniform equilibrium levels of these quantities achieved in the rock-core before the flow is started. For $t > 0$, fresh water ($C = 0$) is injected and an immediate response at the inlet boundary is assumed, expressed by the condition $C\left(0, t\right) = 0$. If there is no precipitate present (i.e. $\Pi_0 = 0$), then $\partial \Pi / \partial t = 0$ and equation (5.1) can be written as $\partial C / \partial t + V_L\left(C\right) \partial C / \partial x = 0$, where the term $V_L(C)$ defines the *Langmuir*

speed (see Figure 5.1) of a concentration value C and is given by

$$V_L(C) := v\left(1+\frac{d\Gamma_{eq}}{dC}\right)^{-1} = \frac{v\,(1+BC)^2}{A+(1+BC)^2} \tag{5.3}$$

The positive constants A, B are the parameters of the Langmuir isotherm discussed in Chapter 1, $\Gamma_{eq}(C) = AC/(1+BC)$.

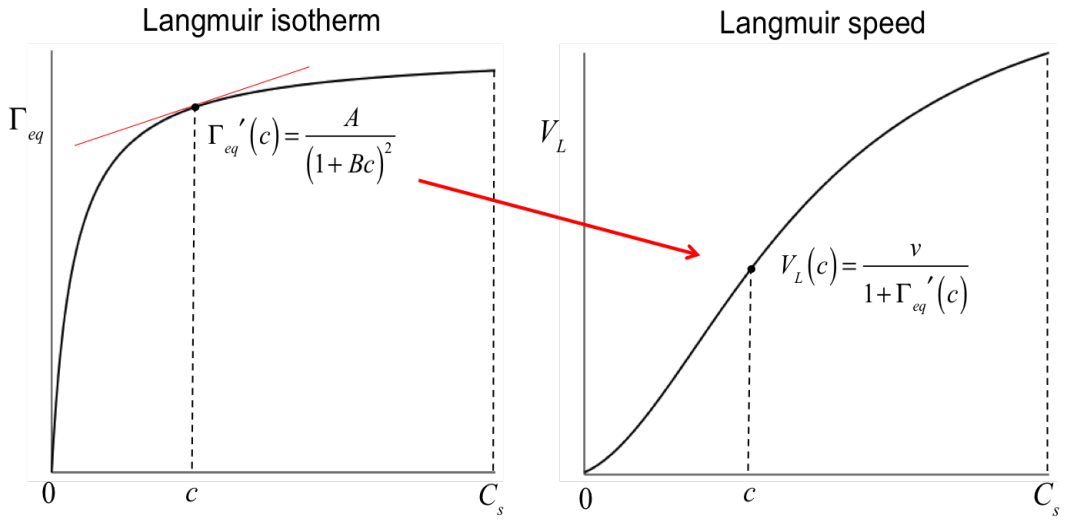

Figure 5.1: *Construction of the Langmuir speed from the Langmuir isotherm.*

Since $V_L'(C) > 0$, the PDE $\partial C/\partial t + V_L(C)\,\partial C/\partial x = 0$ implies that the discontinuity in the data at $x = 0$ develops into a centered rarefaction wave (see Chapter 2), with each concentration value $c \in [0, C_s]$ travelling at constant velocity $V_L(c)$. This is illustrated in Figure 5.2 and contrasted with the "pure dissolution" (i.e. $\Gamma_0 = 0$) solution obtained in Chapter 3. Equilibrium desorption causes a retardation of concentration values with respect to the water front moving through the system at velocity v. In the region $V_L(C_s)\,t \le x \le vt$, a bank of $C = C_s$ is sustained. At points behind this bank, the injected water has succeeded in bringing down the concentration level to some $c < C_s$, triggering instantaneous desorption to $\Gamma = \Gamma_{eq}(c)$, which in turn slows down the horizontal transport of the concentration. In contrast to adsorption/desorption, a precipitation/dissolution process aims to restore concentration to full solubility level C_s. We saw that this leads to a discontinuity at the water front, followed by a steady-state region in which dissolution balances the horizontal transport of concentration (see Figure 5.2). The question addressed in this chapter is how the two mechanisms combine (i.e. $\Pi_0 \neq 0$, $\Gamma_0 \neq 0$). We will see that the bank of $C = C_s$ due to desorption behind the front remains, so

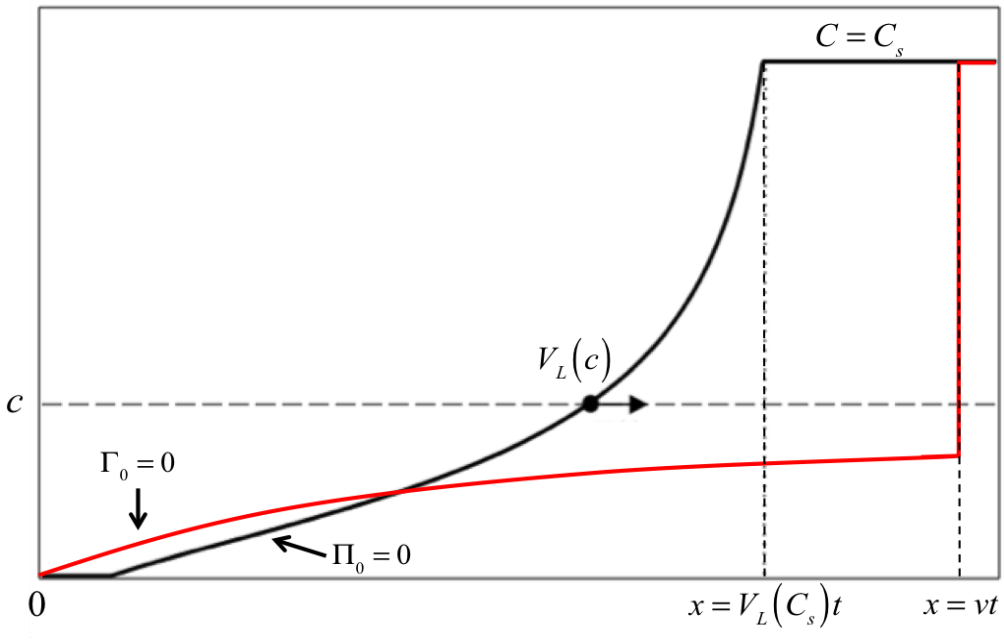

Figure 5.2: *Rarefaction wave for pure equilibrium desorption (* $\Pi_0 = 0$*, black curve) compared with the pure dissolution case (* $\Gamma_0 = 0$*, red curve).*

that no precipitation occurs in this zone. There will also be a growing steady-state region extending from the inlet boundary in which no desorption occurs (since $\partial c/\partial t = 0$). Between these two "extremities" in which only one mechanism is active, there is a zone of mixed behaviour. The interaction of transport, dissolution and desorption described by equation (5.1) has a parametric solution here, which can be used in conjunction with the solution in the other regions to construct a continuous precipitate profile on $[0, L]$. Note that $\Pi(0,t) = \Pi_0 - \kappa C_s t$ and, as in Chapter 3, it will be shown that $\Pi(x,t) > 0$ on $[0,L] \times [0,t^*] \setminus \{(0,t^*)\}$, where $t^* = \Pi_0/\kappa C_s$. From this time on, there is a boundary curve $x = \alpha_\Pi(t)$ separating the domains Ω_0 ($\Pi = 0$) and Ω_+ ($\Pi > 0$). This curve satisfies an ODE of the form $d\alpha_\Pi/dt = F(C(\alpha_\Pi, t))$ and is therefore entirely determined by the concentration level on it, which is "supplied" by the solution in Ω_0 or Ω_+ (see Figure 5.3). We will see that if $\alpha_\Pi'(t^*) > V_L(0)$ there is a time $\tau > t^*$ at which $x = \alpha_\Pi(t)$ becomes a straight line of slope $V_L(C(\alpha_\Pi, t)) > V_L(0)$, i.e. a characteristic projection of equation (5.1) in Ω_0. For $t^* \leq t < \tau$, the concentration on the boundary curve is given by the solution in Ω_+, which then defines a solution in Ω_0. Once the boundary is equal to the characteristic in Ω_0, the concentration on it remains constant and this will lead to a travelling wave solution region in Ω_+.

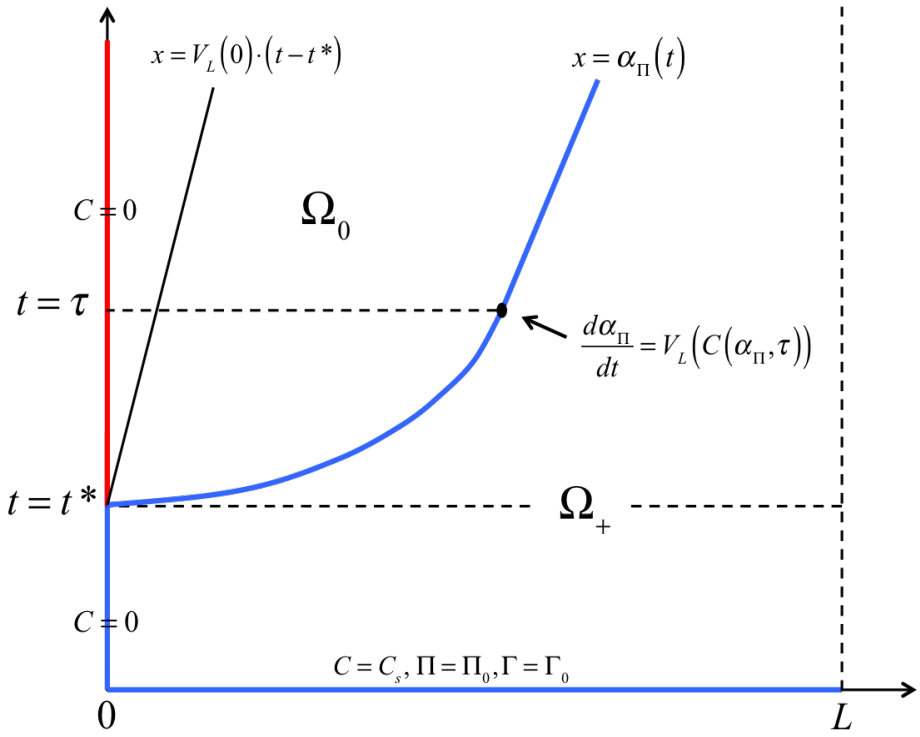

Figure 5.3: *Schematic of the solution procedure of equations (5.1) and (5.2) with constant initial data and constant boundary/feed condition.*

5.2 Solution for $t < t^*$

5.2.1 Concentration profile

To solve equations (5.1) and (5.2) with $\Pi > 0$ by the method of characteristics, it is convenient to use the initial data curve $\Sigma_0 := \{(r, 0, f(r)),\ r \in \mathbb{R}\}$ and solve the problem on the upper half plane, choosing $f(r)$ to satisfy the feed condition. The characteristic system of ODEs corresponding to equation (5.1) is

$$\frac{dZ}{ds} = \kappa\left(C_s - Z\right) \tag{5.4}$$

$$\frac{dx}{ds} = v \tag{5.5}$$

$$\frac{dt}{ds} = 1 + \Gamma_{eq}{}'\left(Z\right) = \frac{A + (1 + BZ)^2}{(1 + BZ)^2} \tag{5.6}$$

From equation (5.4) and Σ_0, we obtain the general solution

$$Z\left(r, s\right) = C_s + f\left(r\right) e^{-\kappa s} \tag{5.7}$$

Moreover, equation (5.5) yields $x(r,s) = vs + r$. Introducing the notation $\Gamma_0 := \Gamma_{eq}(C_s)$, ${\Gamma_0}' := {\Gamma_{eq}}'(C_s)$, we substitute equation (5.7) into equation (5.6) and integrate to find

$$t(r,s) = \frac{{\Gamma_0}'}{\kappa}\ln\left(1 + BZ(r,s)\right) - \frac{\Gamma_0}{\kappa C_s\left(1 + BZ(r,s)\right)} + \frac{v\,s}{V_L(C_s)} + g(r) \tag{5.8}$$

We now choose $g(r)$ such that $t(r,0) = 0$, so

$$g(r) = -\frac{{\Gamma_0}'}{\kappa}\ln\left(1 + BZ(r,0)\right) + \frac{\Gamma_0}{\kappa C_s\left(1 + BZ(r,0)\right)} \tag{5.9}$$

From equation (5.6), we see that $\partial t/\partial s > 0$ and hence

$$t = 0 \Leftrightarrow s = 0 \Leftrightarrow x = r \quad \text{and} \quad t > 0 \Leftrightarrow s > 0 \Leftrightarrow x > r \tag{5.10}$$

We now express the Cauchy data in the r,s-coordinates in order to determine the function $f(r)$. Using equation (5.10), we find that the initial condition $C(x,0) = C_s$, $0 \le x \le L$ is equivalent to $Z(r,0) = C_s + f(r) = C_s$, $0 \le r \le L$. Moreover, since $x = 0$ if and only if $r = -vs$, it follows that the boundary condition $C(0,t) = 0$, $t > 0$ is equivalent to $Z(r,-r/v) = C_s + f(r)\exp(\kappa r/v)$, $r < 0$. Thus, the required function is

$$f(r) = \begin{cases} 0\ , & r \ge 0 \\ -C_s e^{-\kappa r/v}, & r < 0 \end{cases} \tag{5.11}$$

In order to single out a point on the discontinuity at $r = 0$ we introduce an auxiliary parameter $\lambda \in [0,1]$ and let $f(0) = (\lambda - 1)C_s$. This will allow us to distinguish between the characteristic projections emanating from the origin.

At $t = 0$, we have $r = x$ and therefore $Z(r,0) = C(x,0) = C_s + f(x)$. This is shown in Figure 5.4. The feed condition $C(0,t) = 0, t > 0$ is accommodated by an initial condition $C(x,0) = C_s - C_s e^{-\kappa x/v}$ on $-\infty < x < 0$. We will proceed to consider what is happening on the larger domain $(-\infty, L] \times [0,\infty)$ and subsequently restrict attention to Ω.

Using $x = vs + r$ we can eliminate s from equations (5.7) and (5.8) by defining

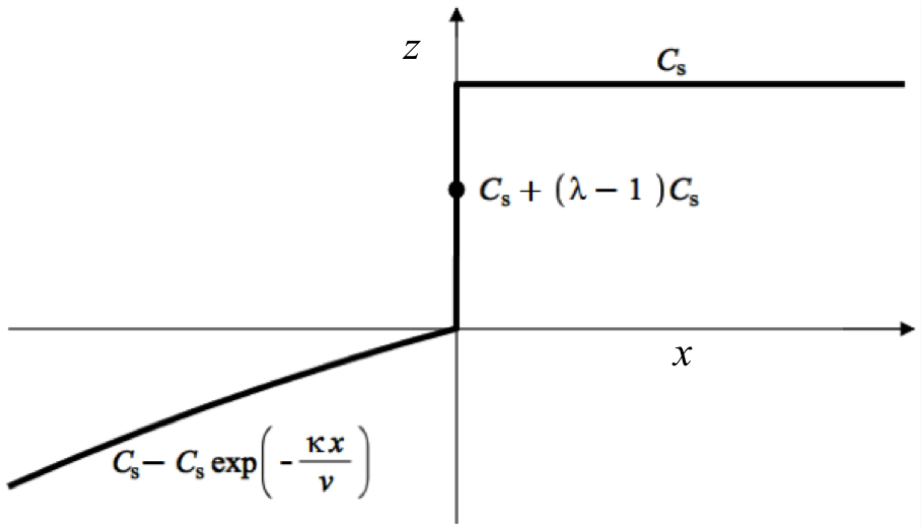

Figure 5.4: *Initial conditions for equation (5.1) on* $-\infty \leq x \leq L$ *are chosen to satisfy* $C(x,0) = C_s$ *on* $[0,L]$ *and* $C(0,t) = 0$ *for* $t > 0$.

$\tilde{C}(x,r)$ and $\tilde{t}(x,r)$ as follows:

$$\tilde{C}(x,r) := Z\left(r, \frac{x-r}{v}\right) = C_s + f(r)\, e^{\kappa(r-x)/v}, \quad \tilde{t}(x,r) := t\left(r, \frac{x-r}{v}\right) \tag{5.12}$$

We note that $\tilde{t}(x,r) \in [0,\infty)$ if and only if $x \geq r > r_{\min}$, where

$$r_{\min} := -\frac{v}{\kappa} \ln\left(\frac{1+BC_s}{BC_s}\right) \tag{5.13}$$

According to the different components of the piecewise function $f(r)$, we distinguish solutions regions I, II and III (see Figures 5.5 and 5.6).

Region I: here, $r > 0$ and hence $\tilde{C}_1(x,r) = C_s$. The characteristics $t = \tilde{t}_1(x,r) = (x-r)/V_L(C_s)$ are straight lines. We can invert to find $r = x - V_L(C_s)\, t$ and therefore the explicit solution $C_1(x,t) = C_s$. There is a widening bank of constant concentration $C = C_s$ behind the advancing water front. This is purely due to equilibrium desorption.

Region II: here, $r = 0$ and hence $\tilde{C}_2(x,0) = C_s + f(0)e^{-\kappa x/v}$. The auxiliary parameter $\lambda \in [0,1]$ is now used to pick a value of $f(0)$ and we may write

$$\tilde{C}_2(x,\lambda) = C_s + (\lambda - 1)\, C_s e^{-\kappa x/v} \tag{5.14}$$

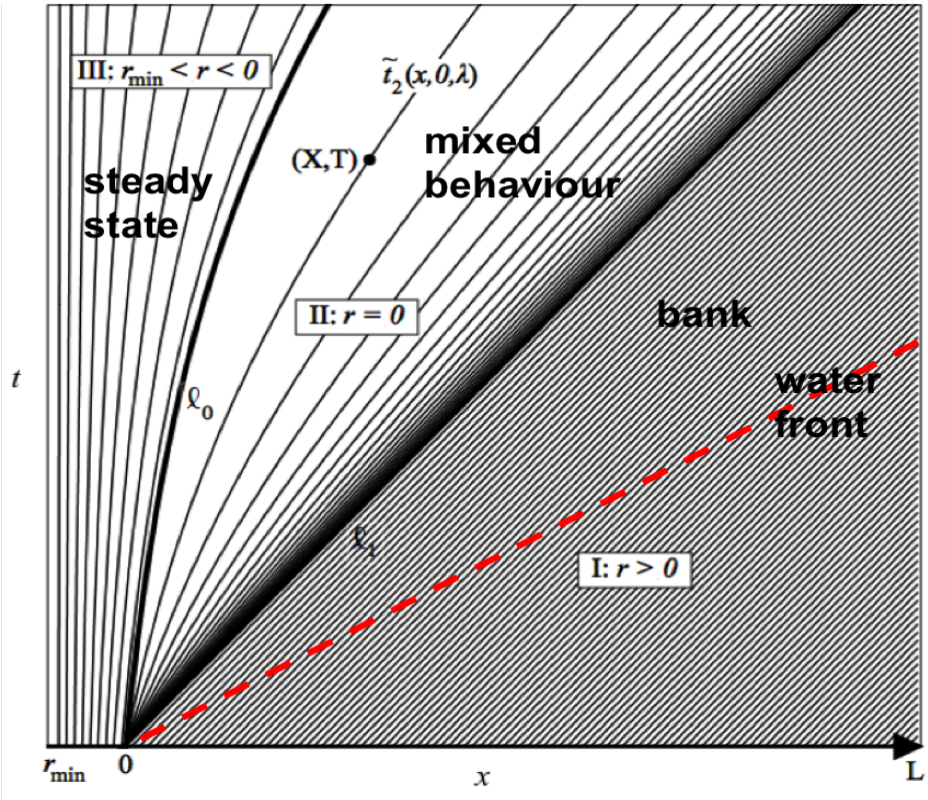

Figure 5.5: *Characteristic projections of equation (5.1) with initial conditions given by equation (5.11), which are shown in Figure 5.4.*

and

$$\tilde{t}_2(x,\lambda) = \frac{x}{V_L(C_s)} + \frac{\Gamma_0'}{\kappa}\ln\left(\frac{1+B\tilde{C}_2(x,\lambda)}{1+\lambda BC_s}\right) + \frac{\Gamma_0}{\kappa C_s}\left[\frac{1}{1+\lambda BC_s} - \frac{1}{1+B\tilde{C}_2(x,\lambda)}\right] \tag{5.15}$$

The characteristics are the curves $t = \tilde{t}_2(x,\lambda)$, with $\ell_0 := \{t = \tilde{t}_2(x,0)\}$ and the line $\ell_1 := \{t = \tilde{t}_2(x,1)\}$ bounding region II. It will sometimes be convenient to write $\tilde{t}_2(x,0,\lambda)$ and $\tilde{C}_2(x,0,\lambda)$ to emphasise the correspondence with $r = 0$.
Given a point (X,T) in region II, we can use equation (5.15) to find the unique value of λ such that $\tilde{t}_2(X,\lambda) = T$. The concentration level $\tilde{C}_2(X,\lambda)$ at (X,T) is then found using equation (5.14). This parametric description is the closest we get to an explicit solution of equation (5.1) in region II. As indicated on Figure 5.5, dissolution and desorption occur simultaneously in this zone.

Region III: here, $r_{\min} < r < 0$, and hence $\tilde{C}_3(x,r) = C_s - C_s e^{-\kappa x/v}$. Thus, for a fixed value of x, the concentration remains constant, while $\tilde{t}(x,r)$ varies with r. In

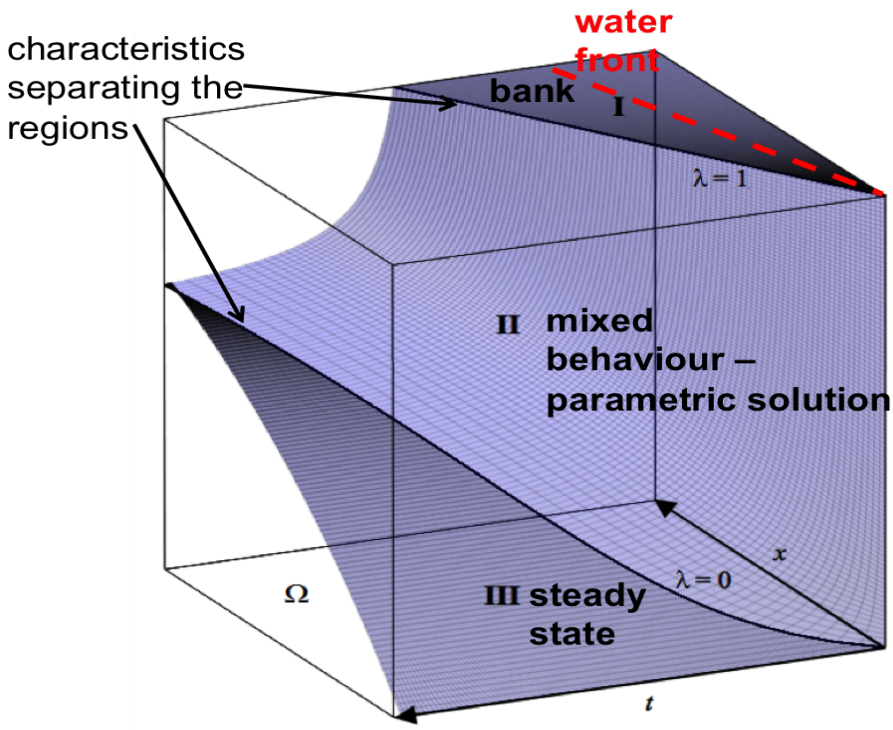

Figure 5.6: *Solution surface consisting of the characteristics of equation (5.1).*

other words, the concentration in this region is independent of t and we can write

$$C_3(x) = C_s - C_s e^{-\kappa x/v} \tag{5.16}$$

We recognise this as the steady-state solution of equation (5.1). Since $\partial C_3/\partial t = 0$, no (equilibrium) desorption occurs in this region. The characteristic projections are the curves

$$\begin{aligned} t = \tilde{t}_3(x,r) = \frac{x}{V_L(C_s)} + \frac{\Gamma_0'}{\kappa}\ln\left(\frac{1+BC_3(x)}{1+BC_3(r)}\right) \\ + \frac{\Gamma_0}{\kappa C_s}\left[\frac{1}{1+BC_3(r)} - \frac{1}{1+BC_3(x)}\right] \end{aligned} \tag{5.17}$$

5.2.2 Precipitate profile

We now construct an expression for Π on Ω. If $\Pi > 0$, equation (5.2) yields

$$\Pi(x,t) = \kappa \int [C(x,t) - C_s]dt \tag{5.18}$$

This integral is straightforward in regions I and III. With $C_1(x,t) = C_s$ it follows that $\Pi_1(x,t) = \Pi_0$, since the initial condition $\Pi(x,0) = \Pi_0$, $0 \leq x \leq L$ must be satisfied. In region III, where the concentration is given by equation (5.16), we find

$$\Pi_3(x,t) = y(x) - \kappa C_s\, t e^{-\kappa x/v} \tag{5.19}$$

for some unknown function $y(x)$. This will be determined using the expression for the precipitate in the adjoining region II. An explicit formula $C_2(x,t)$ is not available here, but we can make the substitution $t = \tilde{t}_2(x,\lambda)$ in equation (5.18) and let $C_2\left(x, \tilde{t}_2(x,\lambda)\right) = \tilde{C}_2(x,\lambda)$, given by equation (5.14). Denoting the precipitate in these coordinates by $\tilde{\Pi}_2(x,\lambda)$, it may be shown that

$$\tilde{\Pi}_2(x,\lambda) = \kappa \int \left[\tilde{C}_2(x,\lambda) - C_s\right] \frac{d\tilde{t}_2}{d\lambda} d\lambda = p(x,\lambda) + q(x) \tag{5.20}$$

where the anti-derivative $p(x,\lambda)$ is

$$p(x,\lambda) = \frac{A}{B}\left[\frac{1}{1+B\tilde{C}_2(x,\lambda)} - \frac{e^{-\kappa x/v}}{1+\lambda B C_s}\right] \tag{5.21}$$

We now choose the arbitrary functions $y(x)$ and $q(x)$ in equations (5.19) and (5.20) in such a way that the precipitate profile is always continuous. Thus, we need $\tilde{\Pi}_2(x,1) = \Pi_0$, which determines $q(x) = \Pi_0 - p(x,1)$ and hence

$$\tilde{\Pi}_2(x,\lambda) = \Pi_0 + \frac{A}{B}\left[\frac{1}{1+B\tilde{C}_2(x,\lambda)} - \frac{1+\lambda BC_s + BC_s - B\tilde{C}_2(x,\lambda)}{(1+\lambda BC_s)(1+BC_s)}\right] \tag{5.22}$$

Finally, by equating $\tilde{\Pi}_2(x,\lambda)$ and $\Pi_3(x,t)$ on the curve ℓ_0 separating regions II and III (see Figure 5.5) we find

$$y(x) = \tilde{\Pi}_2(x,0) + \tilde{t}_2(x,0)\,\kappa C_s e^{-\kappa x/v} \tag{5.23}$$

Substituting this into equation (5.19) and cancelling terms then yields the following expression for the precipitate profile in region III:

$$\Pi_3(x,t) = \Pi_0 + C_s e^{-\kappa x/v}\left[\frac{\kappa\, x}{V_L(C_s)} - \kappa\, t + {\Gamma_0}' \ln\left(1 + BC_s - BC_s e^{-\kappa x/v}\right)\right] \tag{5.24}$$

Figure 5.7 visualises the surface described by Π_0 , $\tilde{\Pi}_2(x,\lambda)$ and $\Pi_3(x,t)$ on the

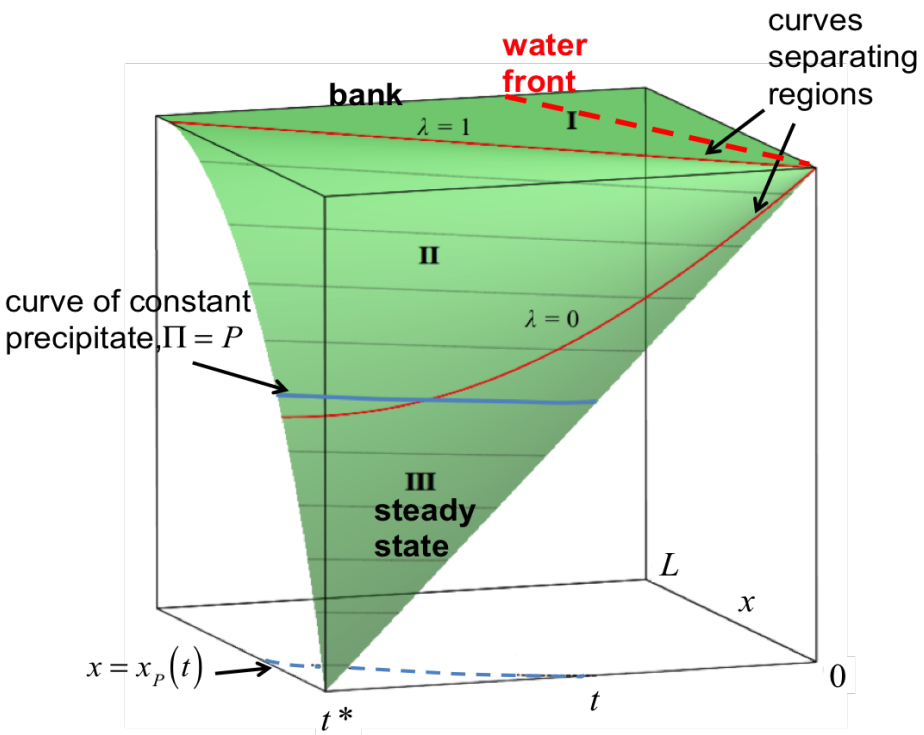

Figure 5.7: *Continuous precipitate surface corresponding to Figure 5.6.*

domain $\{0 \leq x \leq L,\ t \leq t^*\} \subseteq \Omega$. It may be verified that $\tilde{\Pi}_2 > 0$ and $\Pi_3 \geq 0$ here, with $\Pi_3(x,t) = 0$ if and only if $x = 0$, $t = t^*$. For a fixed value P, consider the level curve $(t, x_P(t), P)$ on the surface. In region III, x_P satisfies $\Pi_3(x_P, t) = P$ and, denoting the corresponding concentration value $C_3(x_P)$ by C_P, the Inverse Function Theorem can be used to show that

$$\frac{dx_P}{dt} = \frac{v(C_s - C_P)}{\Pi_0 - P + \dfrac{C_s - C_P}{C_s}\left[C_s + \dfrac{\Gamma_0}{1 + BC_P}\right]} \tag{5.25}$$

In the absence of adsorption (i.e. $\Gamma_0 = 0$), this reduces to equation (3.22). As was the case there, equation (5.25) holds the key to the construction of the entire solution. It describes the velocity of a precipitate value P in terms of the corresponding concentration level C_P. It can be verified (see the discussion in section 5.3.2) that this relationship also holds in region II, with $C_P = C_2(x,t)$. A clear proof of this fact is still at large, but it would probably involve the use of the chain rule in conjunction with the parametric solution components $\tilde{C}_2(x,\lambda)$, $\tilde{\Pi}_2(x,\lambda)$. Ideally, we would like to prove rigorously that equation (5.25) must apply to *any* new solution region which emerges, as long as the precipitate profile is required to be continuous. Recall that in the easier case of pure precipitation, we proved the

invariance of equation (4.103) between all solution regions in the problem with arbitrary initial data $C(x,0) = C_0(x)$, $\Pi(x,0) = \Pi_0(x)$. This was facilitated because we could make an assumption about the general form of the precipitate profile. This is not possible in the present case. With $C(x,0) = C_0(x) \neq C_s$, the concentration in region I would be parametric too (similar to region II). The integral used to find the corresponding precipitate component (see equation (5.20)) would then involve the arbitrary function $C_0(x)$, making it impossible to predict the general form of the anti-derivative. Moreover, if $C_0(x)$ is not monotone increasing, we will have to deal with the emergence of shock solutions too.

An arbitrary initial precipitate profile is much less of a problem. In fact, the above analysis is easily extended to the problem with initial conditions $C(x,0) = C_s$ and $\Pi(x,0) = \Pi_0(x)$. Equation (5.25) then generalises to

$$\frac{dx_P}{dt} = \frac{v(C_s - C_P)}{\Pi_0(x_P) + \dfrac{v}{\kappa}\Pi_0'(x_P) - P + \dfrac{C_s - C_P}{C_s}\left[C_s + \dfrac{\Gamma_0}{1 + BC_P}\right]} \tag{5.26}$$

Note the similarity with equation (4.103). As was the case with that expression, we also expect that equation (5.26) is invariant between all solution regions if the precipitate profile is continuous. In principle, this allows for the construction of the entire solution beyond $t = t^*$. However, the simplest equations are obtained with a constant initial profile $\Pi(x,0) = \Pi_0$ and we will focus on this case in the next few sections.

5.3 Solution for $t \geq t^*$; Case 1: $\Pi_0 \geq BC_s\Gamma_0$

With $\Pi_3(0,t^*) = 0$, equation (5.2) implies that $\partial\Pi/\partial t = 0$, which causes equation (5.1) to change its form to $\partial C/\partial t + V_L(C)\,\partial C/\partial x = 0$. Analogous to the argument given in Chapter 3, it will be useful to introduce the point $\alpha_C = \alpha_C(t)$ such that $C \equiv 0$ for $x \leq \alpha_C$ and $C > 0$ for $x > \alpha_C$. Since $C \equiv 0$ is not a solution of equation (5.1) in Ω_+, we must always have $\alpha_C \leq \alpha_\Pi$, which will effectively "slow down" the movement of α_C.

Note that $\alpha_\Pi(t^*) = \alpha_C(t^*) = 0$ and we consider the velocities of α_Π and α_C to decide what is happening for $t > t^*$. In the case of α_C, we observe that $\Pi(\alpha_C, t) = 0$ since $\alpha_C \leq \alpha_\Pi$. The PDE $\partial C/\partial t + V_L(C)\,\partial C/\partial x = 0$ then implies that

$$\frac{d\alpha_C}{dt} = V_L(0) = \frac{v}{1+A} \tag{5.27}$$

For the motion of α_Π, we use the assumed invariance of equation (5.25) between solution regions. Thus, for $t \geq t^*$, we suppose that

$$\frac{d\alpha_\Pi}{dt} = \frac{vC_s - vC(\alpha_\Pi, t)}{\Pi_0 + \dfrac{C_s - C(\alpha_\Pi, t)}{C_s}\left[1 + \dfrac{\Gamma_0}{1 + BC(\alpha_\Pi, t)}\right]} \ , \ t \geq t^* \tag{5.28}$$

In particular, $C(\alpha_\Pi, t^*) = C(\alpha_C, t^*) = 0$ and hence

$$\left.\frac{d\alpha_\Pi}{dt}\right|_{t=t^*} = \frac{vC_s}{\Pi_0 + C_s + \Gamma_0} \tag{5.29}$$

Comparing equation (5.27) and equation (5.29), we see that

$$\alpha_\Pi{}'(t^*) \leq \alpha_C{}'(t^*) \quad \Leftrightarrow \quad \Pi_0 \geq BC_s\Gamma_0 \tag{5.30}$$

Let us now suppose that $\Pi_0 \geq BC_s\Gamma_0$ (**Case 1**). Together with the constraint $\alpha_C \leq \alpha_\Pi$, this implies the emergence of a joint root $x_0 = \alpha_\Pi = \alpha_C$ for all $t \geq t^*$ moving at constant velocity $U_1 := vC_s(\Pi_0 + C_s + \Gamma_0)^{-1}$ (let $C(\alpha_\Pi, t) = 0$ in equation (5.28)). This suggests there is some new region in Ω, next to region III, in which the concentration and precipitate components are given by travelling wave solutions. To identify these, let $z = x - U_1 t$ and $C = c(z)$ in equation (5.1). This yields the ODE

$$\frac{dc}{dz} = \frac{\kappa(C_s - c)}{v - U_1 - \Gamma_{eq}{}'(c)} \tag{5.31}$$

Equation (5.31) may be solved for z as a function of c to get

$$z = \frac{U_1 - v}{\kappa}\ln(C_s - c) + \frac{U_1\Gamma_0}{\kappa C_s}\frac{1}{1+Bc} + \frac{U_1\Gamma_0{}'}{\kappa}\ln\left(\frac{C_s - c}{1+Bc}\right) + \eta_1 \tag{5.32}$$

Putting back $z = x - U_1 t$ and using the condition that $c = 0$ at $x_0 = U_1(t - t^*)$, we

determine the constant

$$\eta_1 = -U_1 t^* - \frac{U_1 - v}{\kappa} \ln\left(C_s\right) - \frac{U_1 \Gamma_0}{\kappa C_s} - \frac{U_1 {\Gamma_0}'}{\kappa} \ln\left(C_s\right) \tag{5.33}$$

Then, the new solution component, C_4 say, is implicitly defined as follows:

$$\begin{aligned} x + \frac{v}{\kappa} \ln\left(\frac{C_s - c}{C_s}\right) = U_1 \left(t - t^*\right) + \frac{v U_1}{\kappa V_L\left(C_s\right)} \ln\left(\frac{C_s - c}{C_s}\right) \\ - \frac{U_1 {\Gamma_0}'}{\kappa} \ln\left(1 + Bc\right) + \frac{U_1 \Gamma_0}{\kappa C_s} \left[\frac{1}{1 + Bc} - 1\right] \end{aligned} \tag{5.34}$$

To determine region IV in which equation (5.34) applies, we consider its intersection with equation (5.16). Substituting $c = C_3\left(x\right)$ into equation (5.34) and dividing by U_1, we obtain

$$t = t^* + \frac{x}{V_L\left(C_s\right)} + \frac{{\Gamma_0}'}{\kappa} \ln\left(1 + BC_3\left(x\right)\right) + \frac{\Gamma_0}{\kappa C_s} \left[1 - \frac{1}{1 + BC_3\left(x\right)}\right] \tag{5.35}$$

We recognise equation (5.35) as the characteristic $t = \tilde{t}_3\left(x, r_{TW}\right)$ with parameter value r_{TW} defined by the relation

$$\begin{aligned} t^* = \tilde{t}_3\left(0, r_{TW}\right) = \frac{-r_{TW}}{V_L\left(C_s\right)} - \frac{{\Gamma_0}'}{\kappa} \ln\left(1 + BC_3\left(r_{TW}\right)\right) \\ + \frac{\Gamma_0}{\kappa C_s} \left[\frac{1}{1 + BC_3\left(r_{TW}\right)} - 1\right] \end{aligned} \tag{5.36}$$

Figure 5.8 shows region IV bounded by the (blue) line $x_0 = U_1\left(t - t^*\right)$ and the characteristic projection $t = \tilde{t}_3\left(x, r_{TW}\right)$ emanating from $t = t^*$. The characteristics in region IV are not shown, but it is possible to obtain them by using a different parameterisation of the Cauchy problem in which $s = 0$ on the curve $x_0 = U_1\left(t - t^*\right)$ instead of at $t = 0$. The condition $C\left(x_0\right) = 0$ then translates into an equivalent condition in terms of r, enabling us to determine the (new) function $f\left(r\right)$.

Note that, for a fixed concentration value c, equation (5.36) describes its path in region IV. The initial position of c (in region III) is $X_c := -v\kappa^{-1} \ln\left(1 - c/C_s\right)$ and

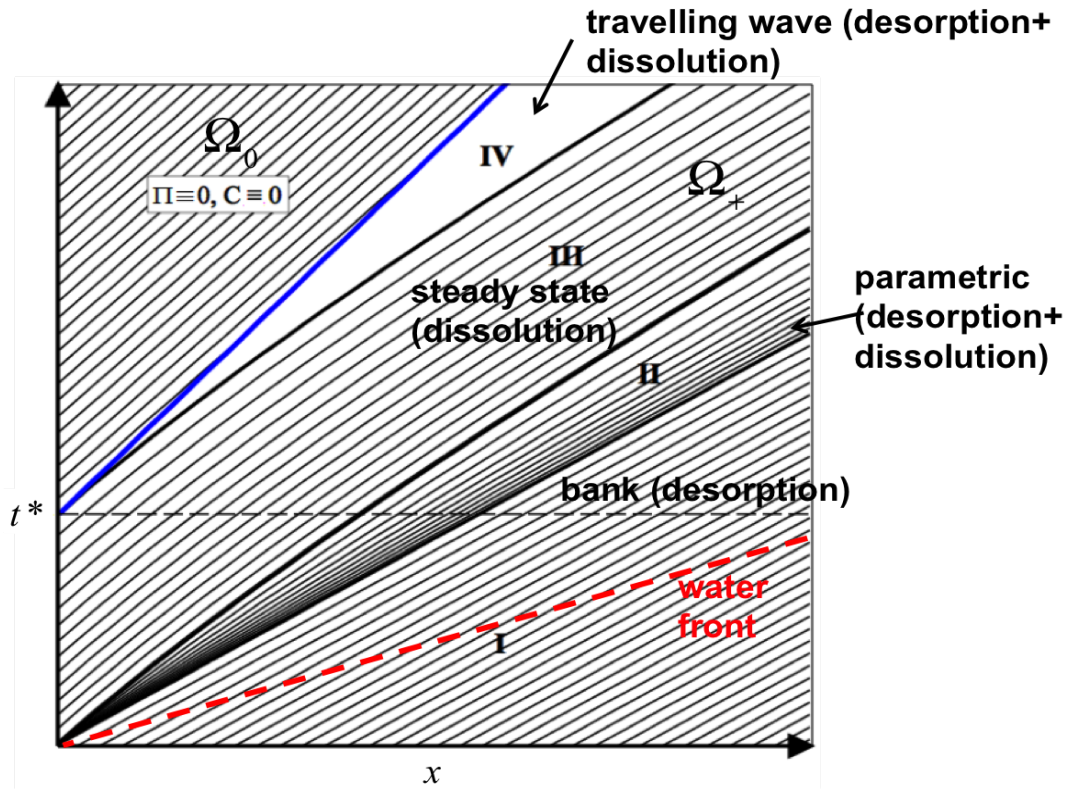

Figure 5.8: *Solution regions and characteristic projections for Case 1 ($\Pi_0 \geq BC_s\Gamma_0$)*

its velocity is U_1 for $t \geq T_c := \tilde{t}_3\left(X_c, r_{TW}\right)$. This observation can also be used to construct Π_4: the precipitate value corresponding to c is $P_c := \Pi_3\left(X_c, T_c\right)$ and the paths traced out by c and P_c in the x,t-plane coincide for $t \geq T_c$.

In summary, if $\Pi_0 \geq BC_s\Gamma_0$, the solution in Ω_+ consists of four regions I, II, III and IV in which the concentration is given by the components C_s, $\tilde{C}_2$, C_3 and C_4 respectively. Region I is due to adsorption and region III due to dissolution, whereas both mechanisms are active in regions II and IV. In Ω_0, equation (5.1) becomes $\partial C/\partial t + V_L\left(C\right)\partial C/\partial x = 0$, describing the case of pure adsorption. The characteristics here are straight lines of slope $V_L\left(0\right) > U_1$, determined by the data $C\left(0,t\right) = 0$, and they run into the moving boundary $x_0 = U_1\left(t - t^*\right)$.

Example 5.1: let $A = 1, B = 10, C_s = 0.1, v = 1, \kappa = 1, L = 1$. We then calculate $\Gamma_0 = \Gamma_{eq}\left(C_s\right) = 0.05$ and the Langmuir velocities $V_L\left(0\right) = 0.5$, $V_L\left(C_s\right) = 0.8$. Note that $BC_s\Gamma_0 = 0.05$, so Case 1 (just) occurs if we choose $\Pi_0 = 0.05$. Figure 5.9 shows the solution profiles consisting of $C_1, \tilde{C}_2, C_3$ and $\Pi_1, \tilde{\Pi}_2, \Pi_3$ at $t = t^* = 0.5$, with the adsorption curve plotted in red. Since $\Pi_0 = BC_s\Gamma_0$, we have $\alpha'_{\Pi}(t^*) = V_L\left(0\right)$ and the travelling wave solution component emerges with this speed (see Figure 5.10).

We observe that $\partial C/\partial x = \infty$ at $x = \alpha_\Pi = V_L(0)\,t$, which is a result of the tangency of the boundary curve and the characteristic $t = \tilde{t}_3(x, r_{TW})$ at $(0, t^*)$. This blow-up is also visible in the effluent concentration plot in Figure 5.11. Note that a larger value of Π_0 would result in a lower travelling wave speed and a more horizontal solution component, the derivative remaining finite everywhere. On the other hand, a lower value of Π_0 leads to qualitatively different solution (see Case 2).

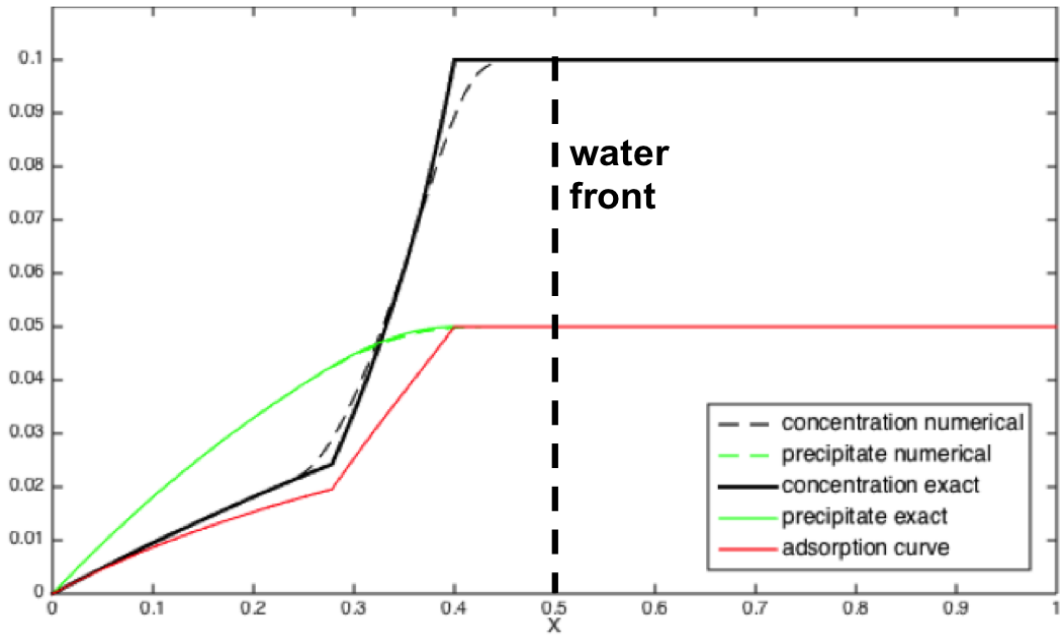

Figure 5.9: *Example 5.1 at* $t = t^* = 0.5$

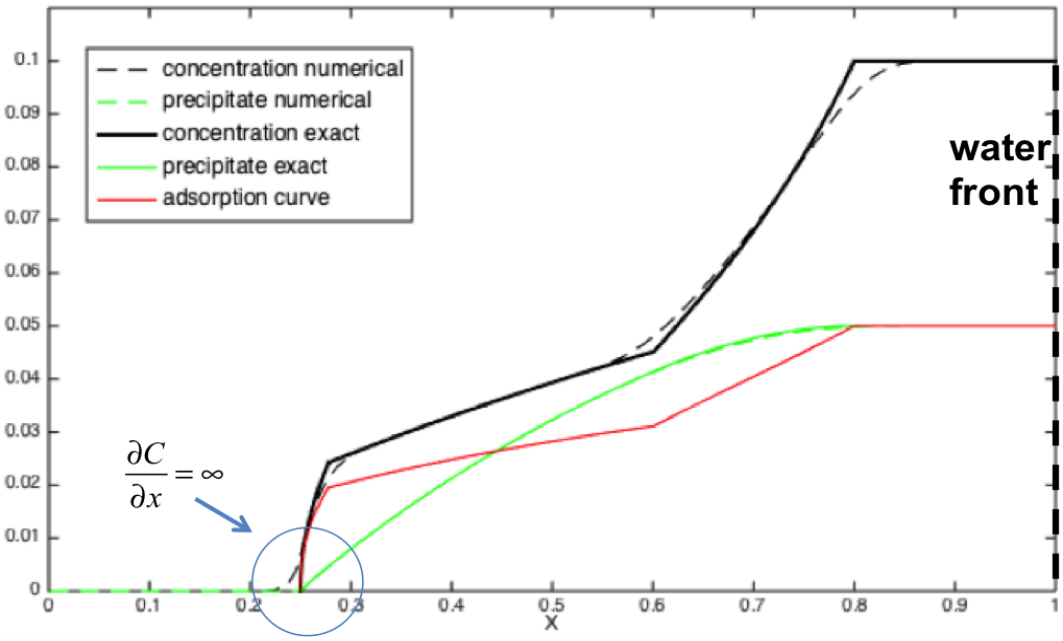

Figure 5.10: *Example 5.1 at* $t = 1$

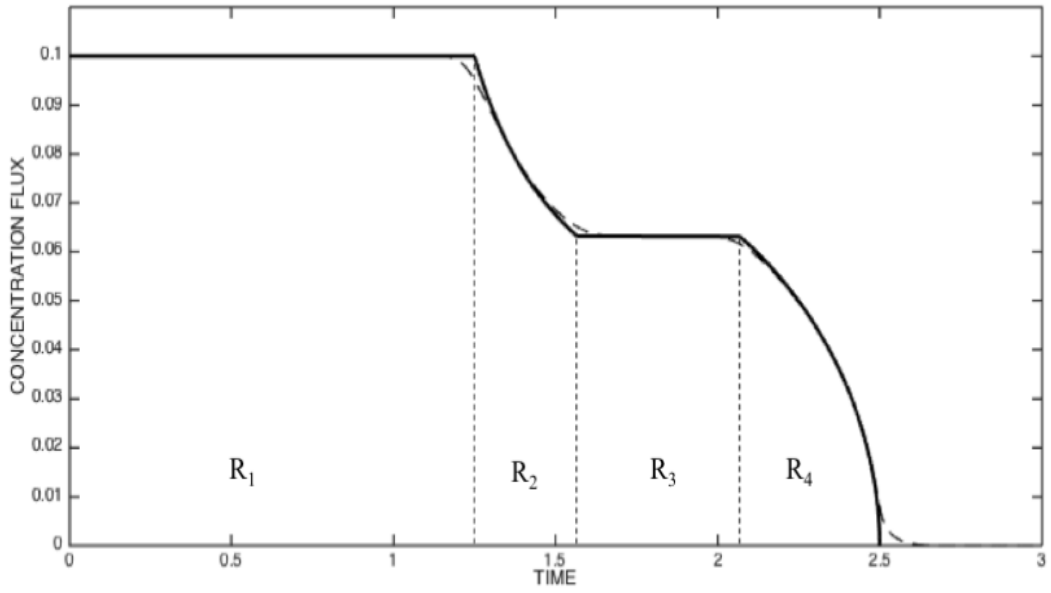

Figure 5.11: *Concentration flux at $x = L$ for example 5.1*

The effluent concentration flux can be used to prove that our solution conserves the total amount of chemical present in the system. The profile can be divided into four parts from left to right, as shown in Figure 5.11. Here, we have

$$R_1 = v\, C_s\, \tilde{t}_2\,(L, 1) = C_s L\,(1 + \Gamma_0{}') \tag{5.37}$$

And, defining the constant $\mu := \tilde{C}_2\,(L, 0) = C_s - C_s e^{-\kappa L/v}$, we compute

$$\begin{aligned} R_2 &= \int_{\lambda=1}^{\lambda=0} v \cdot \tilde{C}_2\,(L, \lambda)\ \cdot \frac{d}{d\lambda}\tilde{t}_2\,(L, \lambda)\ \, d\lambda \\ &= \frac{v}{\kappa}\left[\frac{\Gamma_0 B\mu^2}{C_s\,(1 + B\mu)} + C_s\Gamma_0{}' \ln\,(1 + B\mu)\right] \end{aligned} \tag{5.38}$$

Furthermore, denoting equation (5.34) as $t = t_{TW}(x, c)$, observe that

$$R_3 + R_4 = \int_0^{v\,\mu} t_{TW}\,(L, c)\, dc - v\mu\, \tilde{t}_2\,(L, 0) \tag{5.39}$$

The integral in equation (5.39) evaluates to

$$\begin{aligned} \int_0^{v\,\mu} t_{TW}\,(L, c)\ dC &= \frac{v}{\kappa}\Gamma_0{}'\,(\mu - C_s)\ln\,(1 + B\mu) \\ &\quad + \Gamma_0{}' L\,(\mu - C_s) + L\,(\Pi_0 + \mu + \Gamma_0) \end{aligned} \tag{5.40}$$

and, from equation (5.15),

$$-v\mu\,\tilde{t}_2\,(L,0) = \frac{v}{\kappa}\left[\frac{\Gamma_0\mu}{C_s\,(1+B\mu)} - \frac{\Gamma_0}{C_s}\mu - {\Gamma_0}'\mu\ln\,(1+B\mu)\right] - L\,(1+{\Gamma_0}')\,\mu \quad (5.41)$$

Finally, combining equations (5.37)-(5.41), we find that

$$\sum_{i=1}^{4} R_i = L\,(\Pi_0 + C_s + \Gamma_0) \quad (5.42)$$

This is exactly the amount of scale inhibitor initially present in the system.

5.4 Solution for $t \geq t^*$; Case 2: $\Pi_0 < BC_s\Gamma_0$

With $\Pi_0 < BC_s\Gamma_0$, we have ${\alpha_\Pi}'\,(t^*) > V_L\,(0)$ and, during some time interval after t^*, the boundary curve is defined by $\Pi_3\,(\alpha_\Pi, t) = 0$ (equation (5.24)). Its slope, $V_\Pi = d\alpha_\Pi/dt$, is then given by equation (5.28) with $C\,(\alpha_\Pi, t) = C_3\,(\alpha_\Pi)$. For the purpose of the following discussion, we let $y = C_3\,(\alpha_\Pi)$, so that

$$\alpha_\Pi = {C_3}^{-1}\,(y) = -\frac{v}{\kappa}\ln\left(\frac{C_s - y}{C_s}\right) \quad (5.43)$$

Note that, in terms of y, the equation $\Pi_3\,(\alpha_\Pi, t) = 0$ can be re-written as $t = t_{\Pi 3}\,(y)$, where $t_{\Pi 3} : \mathbb{R} \to \mathbb{R}$ is

$$t_{\Pi 3}\,(y) := \frac{1}{\kappa}\left[\frac{\Pi_0}{C_s - y} + {\Gamma_0}'\ln\,(1+By) - \frac{v}{V_L\,(C_s)}\ln\left(\frac{C_s - y}{C_s}\right)\right] \quad (5.44)$$

Furthermore, we define the function $T_3 : \mathbb{R} \to \mathbb{R}$ by evaluating $\tilde{t}_3\,(x, r = 0)$ (or, equivalently, $\tilde{t}_2\,(x, \lambda = 0)$) at $x = \alpha_\Pi = {C_3}^{-1}\,(y)$, so

$$\begin{aligned} T_3\,(y) &:= \tilde{t}_3\left({C_3}^{-1}\,(y), 0\right) \\ &= \frac{1}{\kappa}\left[-\frac{v}{V_L\,(C_s)}\ln\left(\frac{C_s - y}{C_s}\right) + {\Gamma_0}'\ln\,(1+By) + \frac{\Gamma_0}{C_s}\frac{By}{1+By}\right] \end{aligned} \quad (5.45)$$

Finally, we also consider V_Π in terms of y:

$$V_\Pi(y) = \frac{v(C_s - y)}{\Pi_0 + \frac{C_s - y}{C_s}\left[C_s + \frac{\Gamma_0}{1+By}\right]} \tag{5.46}$$

This will describe $d\alpha_\Pi/dt$ until y is the *minimum* of the following two values:

(a) $\xi_a \in [0, C_s]$ such that $V_\Pi(\xi_a) = V_L(\xi_a)$ and $V_\Pi(y) > V_L(y)$ for all $y \in [0, \xi_a)$

(b) $\xi_b \in [0, C_s]$ such that $t_{\Pi 3}(\xi_b) = T_3(\xi_b)$ and $t_{\Pi 3}(y) > T_3(y)$ for all $y \in [0, \xi_b)$

Note that $V_\Pi(0) > V_L(0)$ and $t_{\Pi 3}(0) = t^* > 0 = T_3(0)$. We will now determine the values ξ_a, ξ_b and establish when $\xi_a \leq \xi_b$ and $\xi_a > \xi_b$. From equations (5.3) and (5.46), it follows that

$$V_\Pi(y) = V_L(y) \qquad \Leftrightarrow \qquad \left(\frac{C_s - y}{1+By}\right)^2 = \frac{\Pi_0 C_s}{B\Gamma_0} \tag{5.47}$$

The quadratic on the right hand side has roots

$${y_a}^\pm = \frac{\Pi_0 + \Gamma_0 \pm (1 + BC_s)\sqrt{\frac{\Pi_0\Gamma_0}{BC_s}}}{\frac{\Gamma_0}{C_s} - B\Pi_0} \tag{5.48}$$

Furthermore, it can be shown that

$$\frac{dV_\Pi}{dy} = \frac{V_\Pi(y) - V_L(y)}{V_L(y)} \tag{5.49}$$

Since $V_\Pi(0) > V_L(0)$, we have ${V_\Pi}'(0) > 0$. From equation (5.46), we deduce that $V_\Pi(0) > V_\Pi(C_s) = 0$ and that V_Π is continuous on $[0, C_s]$. It then follows that V_Π has a maximum on $[0, C_s]$ and, by equation (5.49), $V_L = V_\Pi$ here. In order to determine whether this point is ${y_a}^-$ or ${y_a}^+$, we write $\Pi_0 = (1+\varepsilon)^2 B^{-1} {C_s}^{-1} \Gamma_0$ for some $\varepsilon \in \mathbb{R}$. If $\varepsilon > 0$, the denominator in equation (5.48) is negative and

${y_a}^+ < 0$. The above argument now guarantees that ${y_a}^- \in [0, C_s]$. With $\varepsilon < 0$, the denominator is positive and we need to examine if ${y_a}^- \geq 0$ or ${y_a}^- < 0$. Substituting for Π_0 in the numerator, we find

$$\Gamma_0 \left[\frac{(1+\varepsilon)^2}{BC_s} + 1 - \frac{1+BC_s}{BC_s}(1+\varepsilon) \right] = \frac{\Gamma_0}{BC_s} \left[(1+\varepsilon)^2 + BC_s - (1+BC_s)(1+\varepsilon) \right]$$
$$= \frac{\Gamma_0}{BC_s} \varepsilon (1+\varepsilon - BC_s) \qquad (5.50)$$

By assumption of Case 2, we also have $BC_s\Gamma_0 > \Pi_0 = (1+\varepsilon)^2 B^{-1} {C_s}^{-1} \Gamma_0$. Hence, $1+\varepsilon < BC_s$ and the quantity in equation (4.52) is positive, so that ${y_a}^- > 0$. Moreover, since ${y_a}^- < {y_a}^+$, it must be that ${y_a}^- \in [0, C_s]$. Finally, if the denominator in equation (5.48) is zero (i.e. $\varepsilon = 0$), we can take the limit $\varepsilon \to 0$ to find ${y_a}^- = (BC_s - 1)/2B > 0$, while the other root ${y_a}^+$ is undefined. Thus, for all parameter choices satisfying $\Pi_0 < BC_s\Gamma_0$, ${y_a}^-$ is the lowest value such that $V_\Pi = V_L$ and we write $\xi_a = {y_a}^-$ (see Figure 5.12).

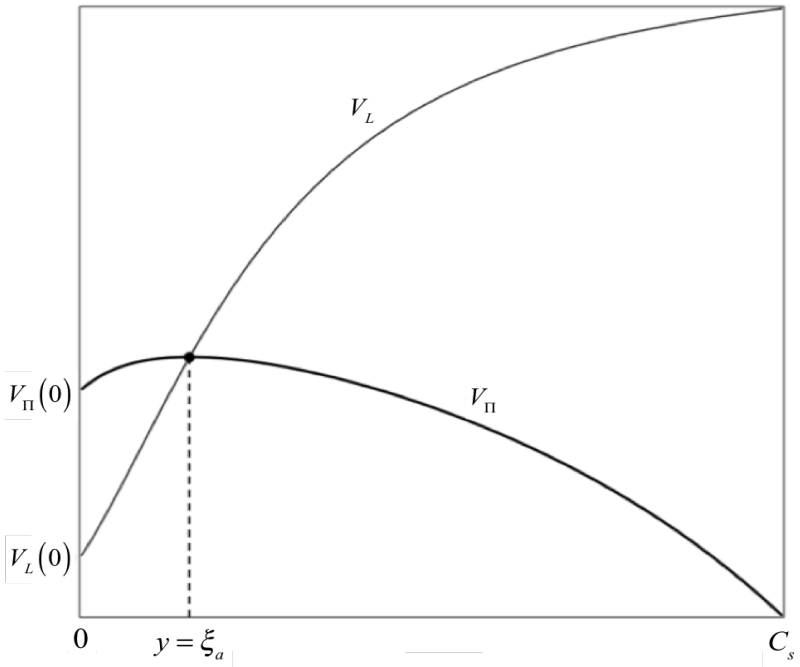

Figure 5.12: *The curves V_Π and V_L meet at $y = \xi_a = {y_a}^-$, given by equation (5.48).*

We need to compare $\xi_a = {y_a}^-$ with the solutions of the equation $t_{\Pi 3}(y) = T_3(y)$. From equations (5.44) and (5.45), it follows that

$$T_3(y) \leq t_{\Pi 3}(y) \quad \Leftrightarrow \quad \frac{y(C_s - y)}{1+By} \leq \frac{\Pi_0 C_s}{B\Gamma_0} \quad \Leftrightarrow \quad y \leq {y_b}^- \ \ or \ \ y \geq {y_b}^+ \quad (5.51)$$

where equality / inequality occur simultaneously and

$$y_b{}^{\pm} = \frac{BC_s\left(\Gamma_0 - \Pi_0\right) \pm \sqrt{D}}{2B\Gamma_0} \tag{5.52}$$

The discriminant is $D = B^2{C_s}^2(\Gamma_0 - \Pi_0)^2 - 4BC_s\Gamma_0\Pi_0$ and we have

$$D = 0 \quad \Leftrightarrow \quad \Pi_0 = \beta^{\pm} = \Gamma_0 + \frac{2\Gamma_0}{BC_s}\left(1 \pm \sqrt{1 + BC_s}\right) \tag{5.53}$$

Moreover, $D > 0$ if and only if $\Pi_0 < \beta^-$ or $\Pi_0 > \beta^+$. But, $\Pi_0 > \beta^+$ implies that $\Pi_0 > \Gamma_0$ and hence $y_b{}^- < y_b{}^+ < 0$. In this case, it follows from equation (5.51) that $t_{\Pi 3}\left(y\right) > T_3\left(y\right)$ for all $y \in [0, C_s]$. The same is true if $D < 0$. Thus, for all parameter choices satisfying $\Pi_0 > \beta^-$, there is *no* ξ_b such that $t_{\Pi 3}\left(\xi_b\right) = T_3\left(\xi_b\right)$.

Now suppose that $\Pi_0 \leq \beta^-$. Then $\Pi_0 < \Gamma_0$ and we have $0 < y_b{}^- < y_b{}^+ < C_s$. It may be verified that

$$\Pi_0 = \beta^- \;\Rightarrow\; y_a{}^- = y_b{}^- = F := \frac{\sqrt{1 + BC_s} - 1}{B} \tag{5.54}$$

For this particular choice of parameters, $V_\Pi = d\alpha_\Pi/dt$ is equal to the Langmuir velocity of $y = C_3\left(\alpha_\Pi\right)$ exactly at the time that solution region III disappears, i.e. when the boundary curve $x = \alpha_\Pi\left(t\right)$ enters region II. Since $D = 0$, the boundary curve is tangent to the characteristic curve $t = \tilde{t}_3\left(x, 0\right)$ at the point $x_a = {C_3}^{-1}\left(y_a{}^-\right),\ \tau_a = t_{\Pi 3}\left(y_a{}^-\right)$ (see Figure 5.13).

If $\Pi_0 < \beta^-$ we have

$$\begin{aligned}
\frac{\Pi_0 C_s}{B\Gamma_0} &< \frac{BC_s + 2\left(1 - \sqrt{1 + BC_s}\right)}{B^2} \\
&= \left(\frac{\sqrt{1 + BC_s} - 1}{B}\right)^2 \\
&= \left(\frac{1 + BC_s - \sqrt{1 + BC_s}}{B\sqrt{1 + BC_s}}\right)^2 \\
&= \left(\frac{C_s - F}{1 + BF}\right)^2
\end{aligned} \tag{5.55}$$

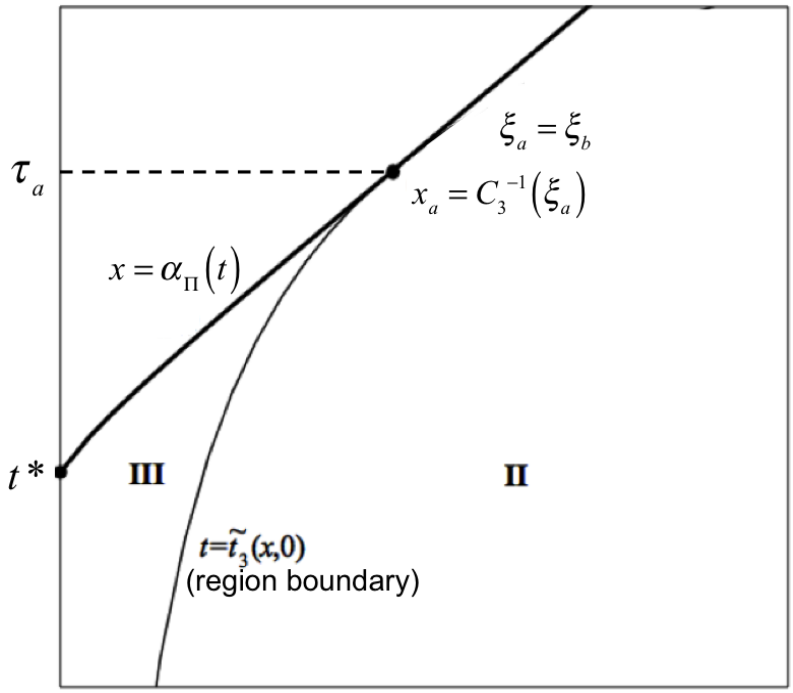

Figure 5.13: *When* $\Pi_0 = \beta^-$ *(equation (5.53)), we have* $\xi_a = \xi_b$.

Since ${y_a}^-$ satisfies equation (5.47), it must be that ${y_a}^- > F$, which is equivalent to

$$ {y_a}^- > \frac{C_s - {y_a}^-}{1 + B\,{y_a}^-} \tag{5.56} $$

Finally, this and equation (4.51) imply that

$$ {y_a}^- \left(\frac{C_s - {y_a}^-}{1 + B\,{y_a}^-} \right) > \left(\frac{C_s - {y_a}^-}{1 + B\,{y_a}^-} \right)^2 = \frac{\Pi_0 C_s}{B\Gamma_0} \quad \Rightarrow \quad T_3\left({y_a}^-\right) > t_{\Pi 3}\left({y_a}^-\right) \tag{5.57} $$

Since $t_{\Pi 3}(0) > T_3(0)$ and $t_{\Pi 3},\ T_3$ are continuous on $[0, C_s]$, the curves $t = t_{\Pi 3}(y)$ and $t = T_3(y)$ intersect on $(0, {y_a}^-)$ and we must have $0 < {y_b}^- < {y_a}^- \leq {y_b}^+$.

In summary, if $\Pi_0 > \beta^-$, then ξ_b does not exist. Region III continues to exist for all time and we have $\xi_a = {y_a}^-$. Define $\tau_a := t_{\Pi 3}(\xi_a)$ and $x_a := {C_3}^{-1}(\xi_a)$. The boundary curve $x = \alpha_\Pi(t)$ now lies above the characteristic $t = \tilde{t}_3(x, 0)$ in the x, t-plane and $V_\Pi = d\alpha_\Pi/dt$ varies according to equation (5.46) with $y = C_3(\alpha_\Pi, t)$ until $t = \tau_a$. We will refer to this scenario as **Case 2a**. It is to be distinguished from **Case 2b**, which occurs if $\Pi_0 \leq \beta^-$. The boundary curve then intersects with the characteristic at the point $x_b := {C_3}^{-1}(\xi_b)$, $\tau_b := t_{\Pi 3}(\xi_b)$, where $\xi_b = {y_b}^- < \xi_a$.

At time $t = \tau_b$, solution region III disappears and for $t \geq \tau_b$, the motion of α_Π is determined by the parametric solution in region II. By assumption of the invariance of equation (5.28), the velocity $V_\Pi = d\alpha_\Pi/dt$ is now given by equation (5.46) with $y = C_2(\alpha_\Pi(\lambda), \lambda)$. We can therefore still expect to have $V_\Pi = V_L$ when $y = \xi_a = y_a^-$. This will be verified in terms of the auxiliary parameter λ in section 5.4.2.

5.4.1 Solution for Case 2a: $\Pi_0 > \beta^-$

For $t > \tau_a$, we have $C(\alpha_\Pi, t) = \xi_a$, which is the concentration level "supplied" by the pure adsorption solution on $0 < x < \alpha_\Pi(t)$. Using the invariance of equation (5.28), we consider the constant velocity $U_2 := V_\Pi(\xi_a) = V_L(\xi_a)$ and look for a travelling wave solution of equation (5.1) in Ω_+. Such a solution is of the form of equation (5.32) with U_1, η_1 replaced by U_2, η_2. The constant of integration, η_2, is now determined by the condition that $c = \xi_a$ at $x = \alpha_\Pi(t) = x_a + U_2(t - \tau_a)$. We then obtain the solution

$$x = U_2(t - \tau_a) + \frac{U_2 x_a}{V_L(C_s)} + \left(\frac{U_2}{V_L(C_s)} - 1\right)\frac{v}{\kappa}\ln\left(\frac{C_s - c}{C_s}\right) - \frac{U_2\Gamma_0{}'}{\kappa}\ln\left(\frac{1 + Bc}{1 + B\xi_a}\right) + \frac{U_2\Gamma_0}{\kappa C_s}\left[\frac{1}{1 + Bc} - \frac{1}{1 + B\xi_a}\right] \tag{5.58}$$

Substituting $c = C_3(x)$ in equation (5.58) and dividing by U_2, it may be verified that, for $t > \tau_a$, the travelling wave solution intersects with component C_3 along the characteristic $t = \tilde{t}_3(x, r_{TW2})$, where the parameter value r_{TW2} is defined by $\tau_a = \tilde{t}_3(x_a, r_{TW2})$. This curve and the line $x = x_a + U_2(t - \tau_a)$ enclose the new solution region IV, as shown in Figure 5.14. The characteristics in this region are not shown, but may be obtained as described for Case 1 in section 5.3. The boundary curve $x = \alpha_\Pi(t)$ is plotted in blue and the characteristic $t = \tilde{t}_3(x, r_{TW2})$ is tangent to this curve at (x_a, τ_a).

As mentioned before, the motion of α_Π for $t^* \leq t \leq \tau_a$ also results in a pure adsorption solution Ω_0:

$$x = -\frac{v}{\kappa}\ln\left(\frac{C_s - c}{C_s}\right) + V_L(c) \cdot (t - t_{\Pi 3}(c)) \tag{5.59}$$

Equation (5.59) describes the path of a concentration value $c \in [0, \xi_a]$. This lies

at $x = -v\kappa^{-1}\ln(1 - c/C_s)$ in region III until $t = t_{\Pi 3}(c)$, when $c = C_3(\alpha_\Pi)$. For $t \geq t_{\Pi 3}(c)$, c moves at its own Langmuir velocity $V_L(c)$. In Figure 5.14, it is illustrated how a characteristic emanates from each point on the boundary curve between $(0, t^*)$ and (x_a, τ_a). The effluent concentration flux for Case 2a consists of five regions (see Figure 5.18 in Example 5.2) and can be used to prove that the solution satisfies mass balance, as was done for Case 1.

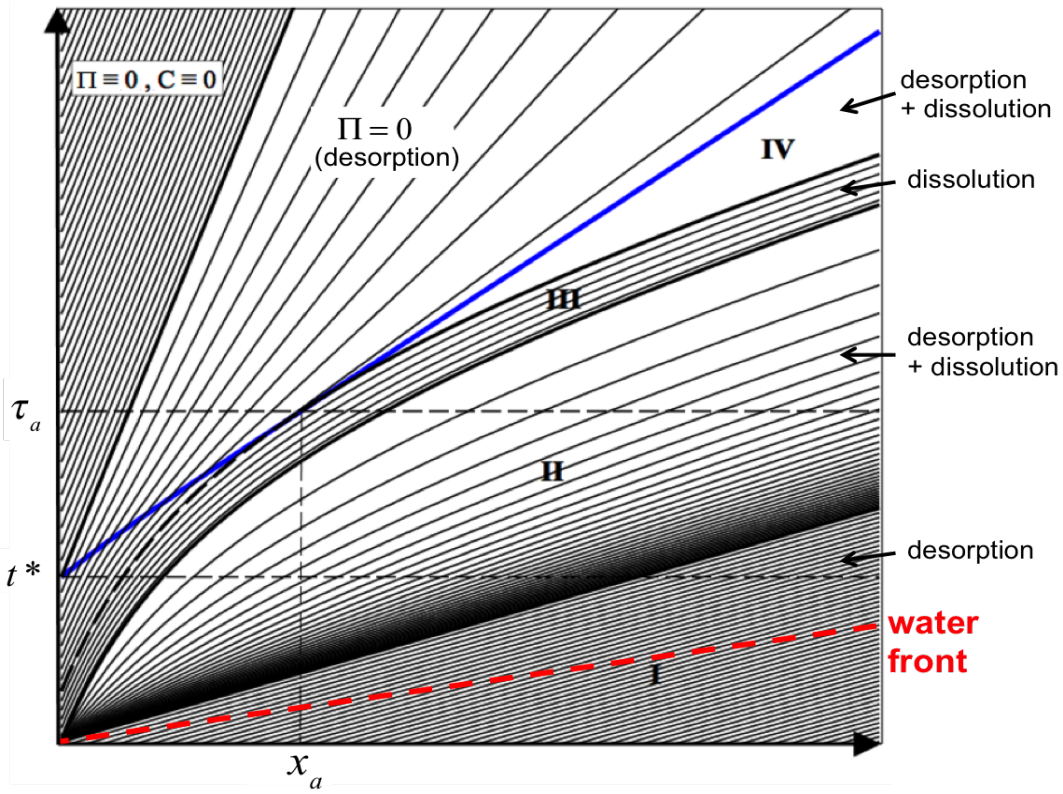

Figure 5.14: *Solution regions in Case 2a ($\Pi_0 > \beta^-$)*

Example 5.2: let $C_s = 0.1, v = 1, \kappa = 1, L = 1$ as before and choose $A = 10, B = 100$. We compute $\Gamma_0 = 0.0909$, $BC_s\Gamma_0 = 0.909$ and $\beta^- = 0.049$, so Case 2a occurs if we let $\Pi_0 = C_s = 0.1$. With $V_L(0) = 0.0909$ and $V_L(C_s) = 0.9237$ now, there is a much greater range of Langmuir velocity than in Example 5.1. This stretches the components $\tilde{C}_2$ and $\tilde{\Pi}_2$, which can be seen in the plot at $t = t^* = 1$ in Figure 5.15 between $x = 0.2535$ and $x = 0.9237$. Equation (5.47) yields $\xi_a = y_a{}^- = 0.01548$ and hence $x_a = C_3{}^{-1}(\xi_a) = 0.1682$, $\tau_a = t_{\Pi 3}(\xi_a) = 1.443$. Figures 5.16 and 5.17 show the solution profiles at $t = \tau_a$ and $t = 2.5 > \tau_a$ respectively. The travelling wave solution component C_4 emerges at $t = \tau_a$ and lies between $x = 0.5845$ and $x = 0.8591$ in Figure 5.17. Its speed is $U_2 = V_L(\xi_a) = 0.3937$. Component C_3 is always present, which is more apparent in the effluent concentration flux plotted Figure 5.18.

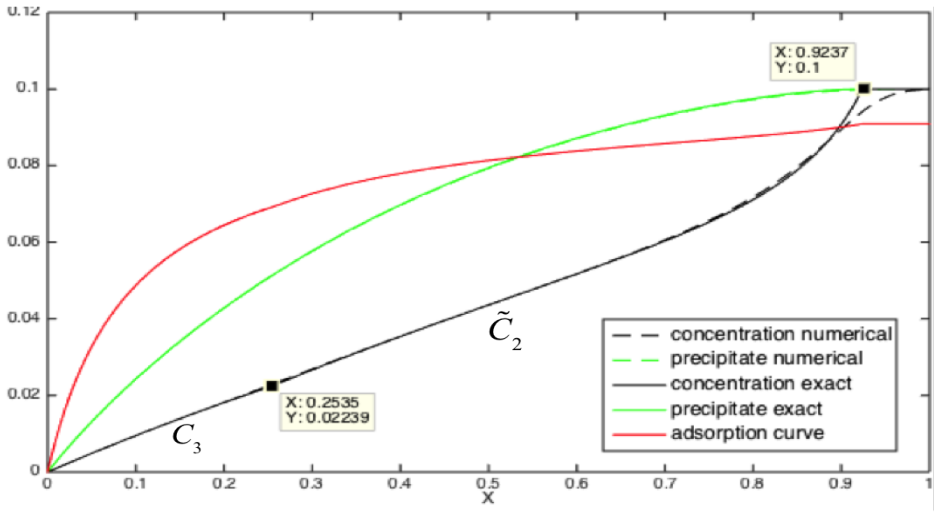

Figure 5.15: *Example 5.2 at* $t = t^* = 1$

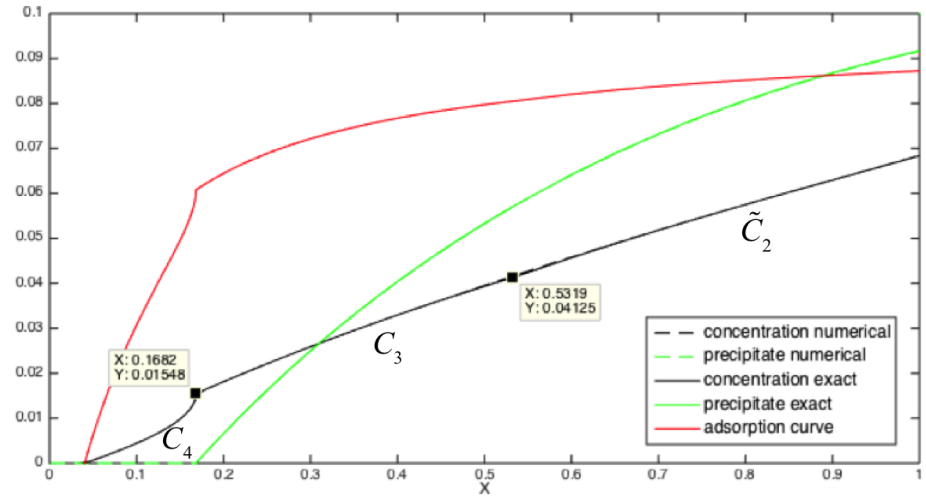

Figure 5.16: *Example 5.2 at* $t = \tau_a = 1.443$

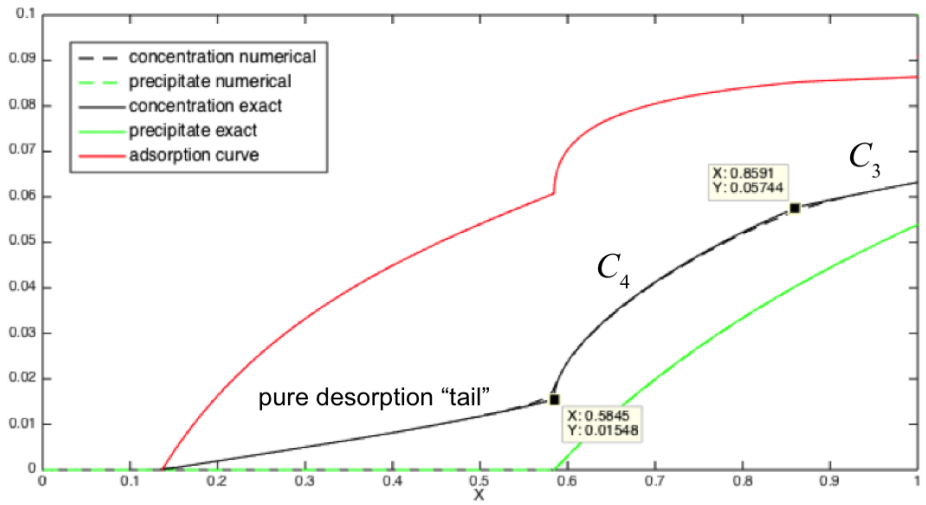

Figure 5.17: *Example 5.2 at* $t = 2.5 > \tau_a$

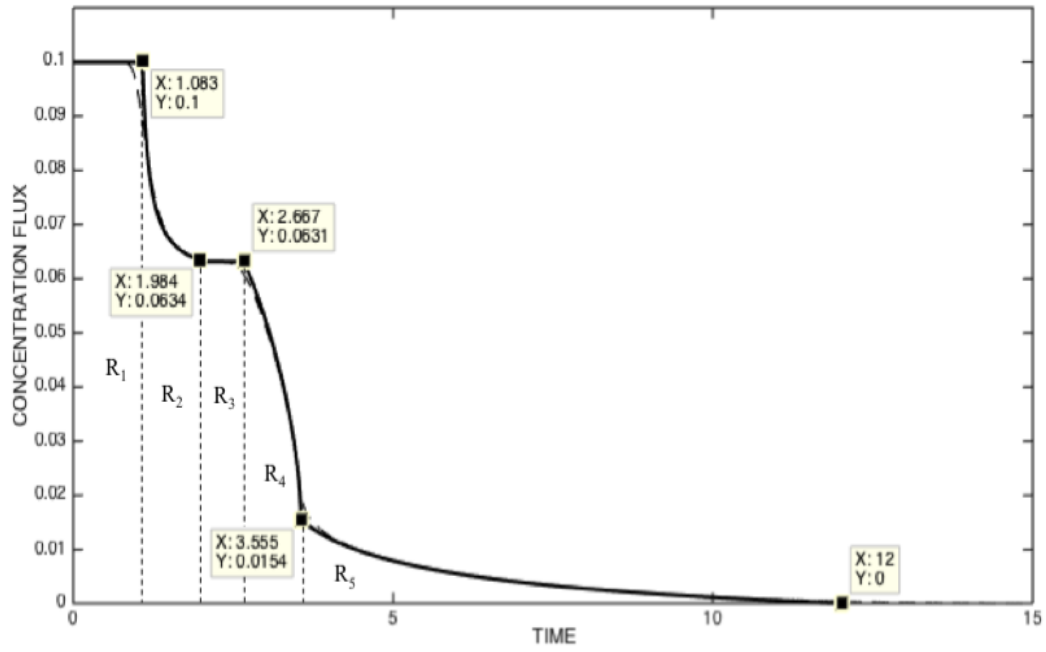

Figure 5.18: *Effluent concentration flux for Example 5.2*

5.4.2 Solution for Case 2b: $\Pi_0 \leq \beta^-$

The characteristic $t = \tilde{t}_3(x,0) = \tilde{t}_2(x,0)$ now intersects the boundary curve $x = \alpha_\Pi(t)$ at (x_b, τ_b) and region III disappears (see Figure 4.19). For $t > \tau_b$, the boundary is determined by the solution in region II and can be found in terms of the auxiliary parameter $\lambda \in [0,1]$, using the equation $\tilde{\Pi}_2(\alpha_\Pi, \lambda) = 0$.

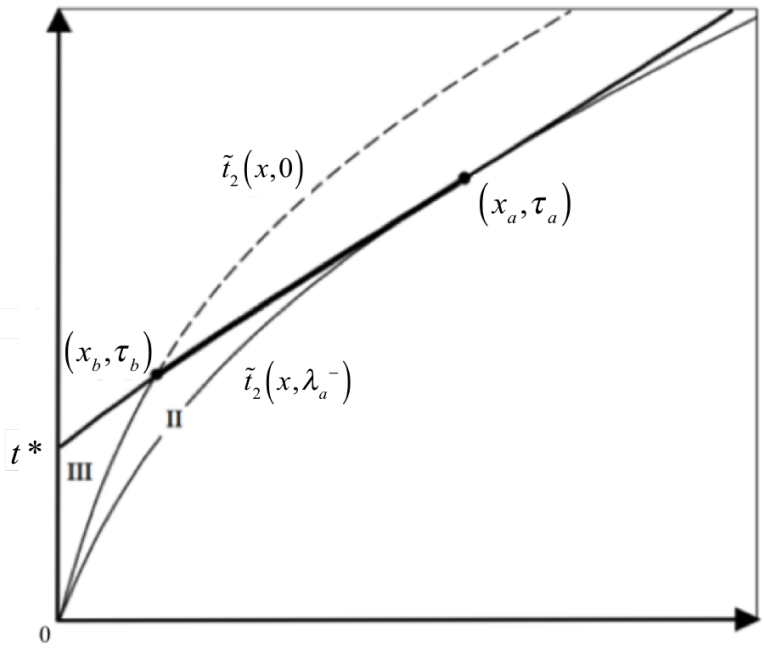

Figure 5.19: *If* $\Pi_0 < \beta^-$, *then* $\xi_b < \xi_a$.

Noticing that $t = \tilde{t}_2(x,\lambda)$ and employing the chain rule, we can determine the

velocity of α_Π in terms of λ as follows:

$$V_\Pi(\lambda) = \frac{d}{dt}\alpha_\Pi(\lambda) = \frac{d\lambda}{dt}\frac{d\alpha_\Pi}{d\lambda} = \left(\frac{d}{d\lambda}\tilde{t}_2\left(\alpha_\Pi(\lambda), \lambda\right)\right)^{-1}\frac{d\alpha_\Pi}{d\lambda} \tag{5.60}$$

The concentration value at $x = \alpha_\Pi(\lambda)$ is $\tilde{C}_2\left(\alpha_\Pi(\lambda), \lambda\right)$ and we want to find out when $V_\Pi(\lambda) = V_L\left(\tilde{C}_2\left(\alpha_\Pi, \lambda\right)\right)$. To simplify this analysis, we introduce

$$F(\lambda) := \frac{BC_s\Pi_0}{\Gamma_0}(1 + \lambda BC_s) - (1 + \lambda)BC_s \tag{5.61}$$

$$G(\lambda) := \frac{4BC_s\Pi_0}{\Gamma_0}(1 + \lambda BC_s) + 4\lambda B^2{C_s}^2 \tag{5.62}$$

In terms of F and G, the solution $\alpha_\Pi(\lambda)$ of $\tilde{\Pi}_2\left(\alpha_\Pi, \lambda\right) = 0$ satisfies

$$\tilde{C}_2\left(\alpha_\Pi, \lambda\right) = \frac{-F(\lambda) \pm \sqrt{F(\lambda)^2 - G(\lambda)}}{2B} \tag{5.63}$$

Clearly, we need to have $0 \leq \tilde{C}_2\left(\alpha_\Pi(\lambda), \lambda\right) \leq C_s$ for $\lambda \in [0, 1]$. Observe that $G(\lambda) > 0$, which implies that both roots in equation (5.63) are negative if $F(\lambda) > 0$ and the equation $\tilde{\Pi}_2\left(\alpha_\Pi, \lambda\right) = 0$ has no meaningful solutions. On the other hand, if $F(\lambda) < 0$, then both roots are positive and we can restrict attention to the smaller root (corresponding to the negative sign), because the solution components $\tilde{C}_2$ and $\tilde{\Pi}_2$ are both decreasing in the x-direction and the t-direction (see Figures 5.6 and 5.7). Using equation (5.14) for $\tilde{C}_2$, we then re-write equation (5.63) to obtain

$$\alpha_\Pi(\lambda) = -\frac{v}{\kappa}\ln\left(\frac{2BC_s + F(\lambda) + \sqrt{F(\lambda)^2 - G(\lambda)}}{2BC_s(1 - \lambda)}\right) \tag{5.64}$$

The roots of the discriminant $D = F(\lambda)^2 - G(\lambda)$ are

$${\lambda_a}^{\pm} = \frac{BC_s\Pi_0(\Gamma_0 - \Pi_0) + 3\Pi_0\Gamma_0 + {\Gamma_0}^2 \pm 2\Gamma_0(1 + BC_s)\sqrt{\frac{\Pi_0\Gamma_0}{BC_s}}}{(\Gamma_0 - BC_s\Pi_0)^2} \tag{5.65}$$

Moreover, $D > 0$ if $\lambda < {\lambda_a}^-$ or $\lambda > {\lambda_a}^+$. Since $\Pi_0 < \beta^- < \Gamma_0$, we always have ${\lambda_a}^+ > 0$ and it may be verified that $\alpha_\Pi(\lambda) < 0$ for all $\lambda \in \left[{\lambda_a}^+, 1\right]$, so that we

can limit our attention to ${\lambda_a}^-$. Using $BC_s + 2 - 2\sqrt{1+BC_s} = \left(1-\sqrt{1+BC_s}\right)^2$, we can show that ${\lambda_a}^- = 0$ if $\Pi_0 = \beta^-$ and ${\lambda_a}^- > 0$ if $\Pi_0 < \beta^-$. Furthermore, it can be shown that $\alpha_\Pi(0) = x_b$ and $\alpha_\Pi(\lambda) > x_b$ for $0 < \lambda \leq {\lambda_a}^-$. This makes perfect sense in terms of the solution in region II: at $t = \tau_b$, the boundary curve hits the characteristic corresponding to $\lambda = 0$. The boundary curve then intersects with subsequent neighbouring characteristics until $\lambda = {\lambda_a}^-$, after which $\alpha_\Pi(\lambda)$ stops being real-valued. Using equations (5.60), (5.64) and (5.65) (and after a lot algebra), it can actually be proved that $\tilde{C}_2\left(\alpha_\Pi\left({\lambda_a}^-\right), {\lambda_a}^-\right) = \xi_a = y_a^-$ (from equation (5.48)) and $V_\Pi\left({\lambda_a}^-\right) = V_L(\xi_a)$. This verifies the invariance of equation (5.28) between solution regions II and III. As before, we now define $x_a := \alpha_\Pi\left({\lambda_a}^-\right)$, $\tau_a := \tilde{t}_2\left(0, {\lambda_a}^-\right)$. The characteristic $t = \tilde{t}_2\left(x, {\lambda_a}^-\right)$ is tangent to the boundary curve at (x_a, τ_a). As in Case 2a (Figure 5.14), a new region IV will exist for $t \geq \tau_a$ in which the solution is a travelling wave of velocity $U_3 := V_L(\xi_a) = V_\Pi\left({\lambda_a}^-\right)$. This region is enclosed by the curve $t = \tilde{t}_2\left(x, {\lambda_a}^-\right)$ and the boundary $x = \alpha_\Pi(t) = x_a + U_3(t - \tau_a)$.

During the time interval $[t^*, \tau_a]$, the motion of α_Π determines a non-zero solution in Ω_0. For $t^* \leq t \leq \tau_b$, this pure adsorption solution is given by equation (5.59). A similar relation applies for $\tau_b \leq t \leq \tau_a$: given an arbitrary concentration value $c \in [\xi_b, \xi_a]$, we solve $c = \tilde{C}_2\left(\alpha_\Pi(\lambda_c), \lambda_c\right)$ for λ_c to obtain the time $\tilde{t}_2\left(\alpha_\Pi(\lambda_c), \lambda_c\right)$. For $t \geq \tilde{t}_2\left(\alpha_\Pi(\lambda_c), \lambda_c\right)$, the velocity of c is $V_L(c)$. This is expressed in the following relation:

$$x = \alpha_\Pi(\lambda_c) + V_L(c) \cdot \left(t - \tilde{t}_2\left(\alpha_\Pi(\lambda_c), \lambda_c\right)\right) \tag{5.66}$$

The effluent concentration flux for this case again consists of five regions (see Figure 5.22 in Example 5.3) and can be used to prove that the solution satisfies the principle of mass conservation.

Example 5.3: let $A = 10, B = 50, C_s = 0.1, v = 1, \kappa = 1, L = 1$. Then $\Gamma_0 = 0.1667$, $BC_s\Gamma_0 = 0.8335$ and $\beta^- = 0.07$, so Case 2b occurs if we choose $\Pi_0 = 0.06$. Equation (5.52) gives $\xi_b = {y_b}^- = 0.0145$ and hence $\tau_b = t_{\Pi 3}(\xi_b) = 0.412$, the time at which the component C_3 disappears. From equations (5.64), (5.65), we find ${\lambda_a}^- = 0.0188$, $\alpha_\Pi\left({\lambda_a}^-\right) = 0.356$. These can be used to determine $\xi_a = \tilde{C}_2\left(\alpha_\Pi\left({\lambda_a}^-\right), {\lambda_a}^-\right) = 0.03124$ and verify that this agrees with $\xi_a = y_a^-$. Then,

we find $\tau_a = \tilde{t}_2\left(\alpha_\Pi\left(\lambda_a{}^-\right), \lambda_a{}^-\right) = 1.563$. Figure 5.20 shows the formation of the desorption tail in terms of characteristic projections. Figure 5.21 is a close-up of the solution profiles at $t = 2 > \tau_a$. The travelling wave component has velocity $U_3 = V_L(\xi_a) = 0.397$ and is between $x = \alpha_\Pi = 0.5284$ and $x = 0.5511$ on this plot.

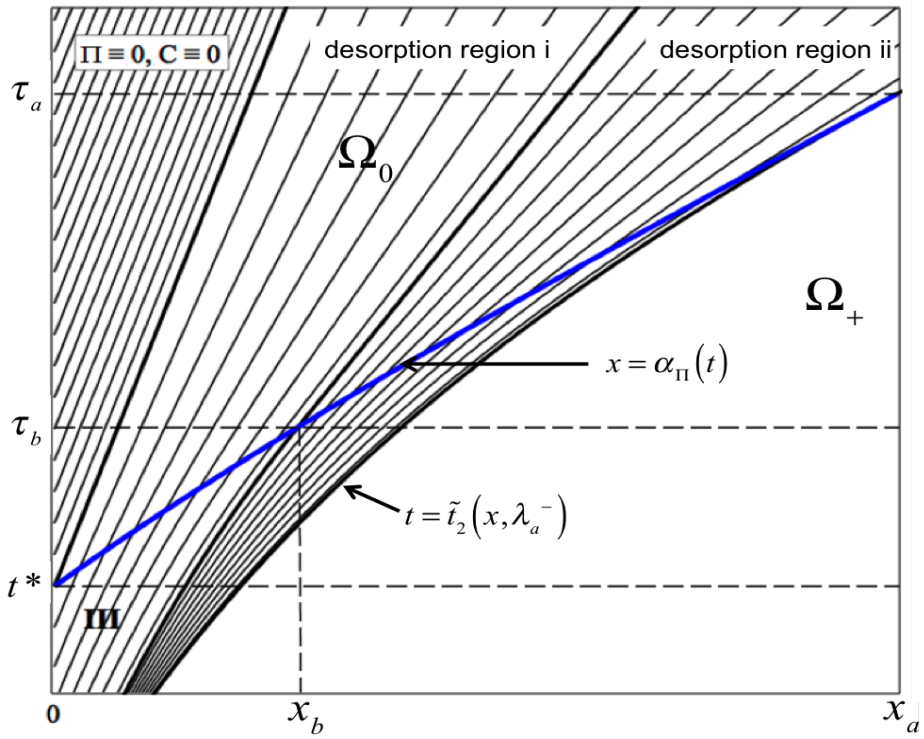

Figure 5.20: *In Case 2b ($\Pi_0 \leq \beta^-$), the boundary curve intersects region II and defines a solution in Ω_0 consisting of two components.*

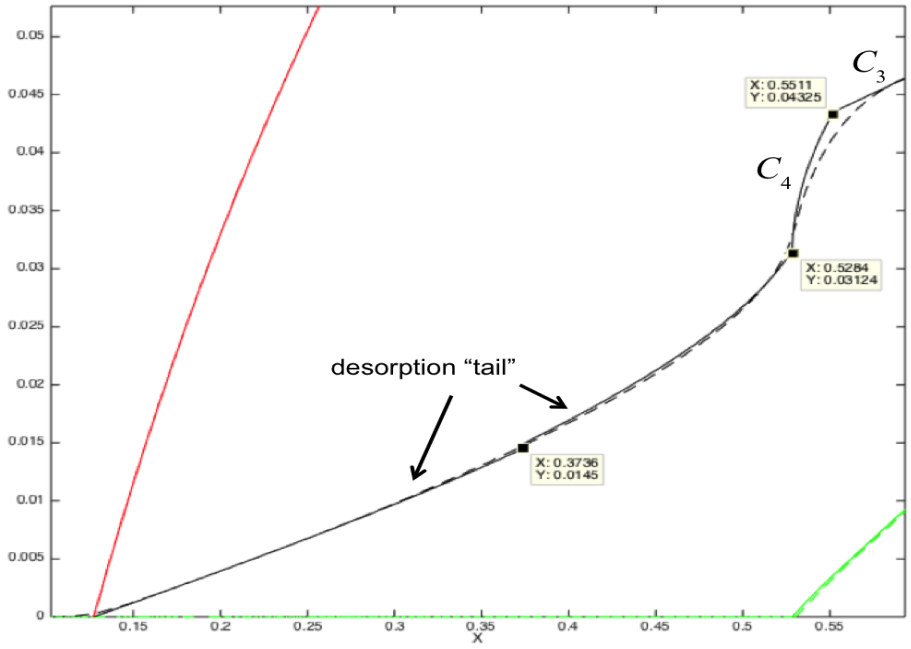

Figure 5.21: *Example 5.3 at $t = 2 > \tau_a$*

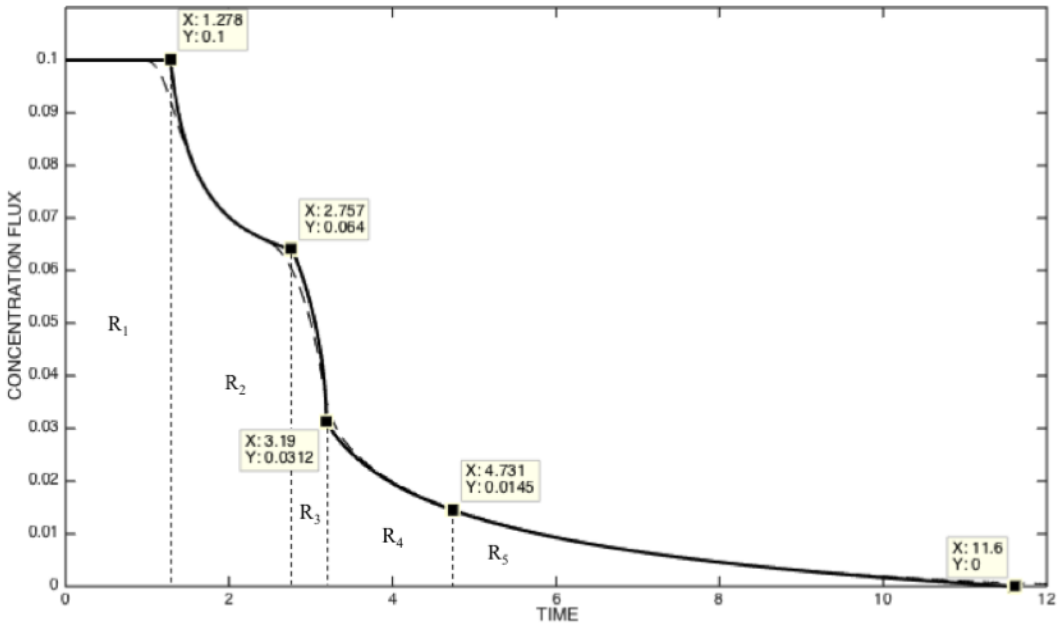

Figure 5.22: *Effluent concentration flux for example 5.3*

5.5 Departing from equilibrium adsorption

In this section we look at the system of equations (1.6)-(1.8) with no dispersion ($D = 0$) and *finite* values of the adsorption rate parameter r_a. This departure from equilibrium adsorption adds a new level of complexity as there are now three coupled PDEs for the three unknown quantities C, Π and Γ. If $\Pi > 0$, this system reduces to two equations for C and Γ. We saw in section 2.5 that this system has eigenvalues v and 0, leading to the characteristic curves $x - vt = constant$ and $t = constant$, along which the solution can be developed according an ODE. Unfortunately, these ODEs are not integrable and we abandon this approach in favour of solving equations (1.6)-(1.8) numerically. The exact solutions for the two limiting cases $r_a = 0$ and $r_a \to \infty$ will serve as useful reference points.

As usual, we are interested in the Cauchy problem on Ω with initial conditions $C(x,0) = C_s$, $\Pi(x,0) = \Pi_0$, $\Gamma(x,0) = \Gamma_0 := \Gamma_{eq}(C_s)$ and boundary condition $C(0,t) = 0$. The latter implies $\Pi(0,t) = \Pi_0 - \kappa C_s t$ and $\Gamma(0,t) = \Gamma_0 \exp(-r_a t)$, from which it follows that the precipitate is exhausted at $t^* = \Pi_0/\kappa C_s$, whereas the level of adsorbed chemical at the inlet vanishes only as $r_a t \to \infty$.

Example 5.4: let $A = 1, B = 10$, $\Pi_0 = 0.1$, $C_s = 0.1$, so that Case 1 (section 5.3) applies, and let $v = 1$, $\kappa = 1$, $L = 1$. With these parameters, the precipitate begins

to run out at $t^* = 1$. Figures 5.23-5.25 show the numerical in-situ concentration, precipitation and adsorption profiles at $t = 0.9$ for $r_a = 0.1, 1, 10, 100$ alongside the exact solutions for the cases $r_a = 0$, $r_a \to \infty$. Figure 5.26 shows the in-situ concentration profiles at $t = 1.7 > t^*$. Figures 5.27 and 5.28 are plots of the corresponding effluent concentration profile.

There is a discontinuity in the concentration profiles at $x = vt$ and we can guess from the numerical solutions that this gets smaller as r_a increases, eventually vanishing when $r_a \to \infty$. At the same time, the concentration between $x = V_L(C_s)t$ and $x = vt$ gradually increases towards $C = C_s$ and has the sharp edge of the equilibrium adsorption solution at $x = V_L(C_s)t$ when $r_a \to \infty$.

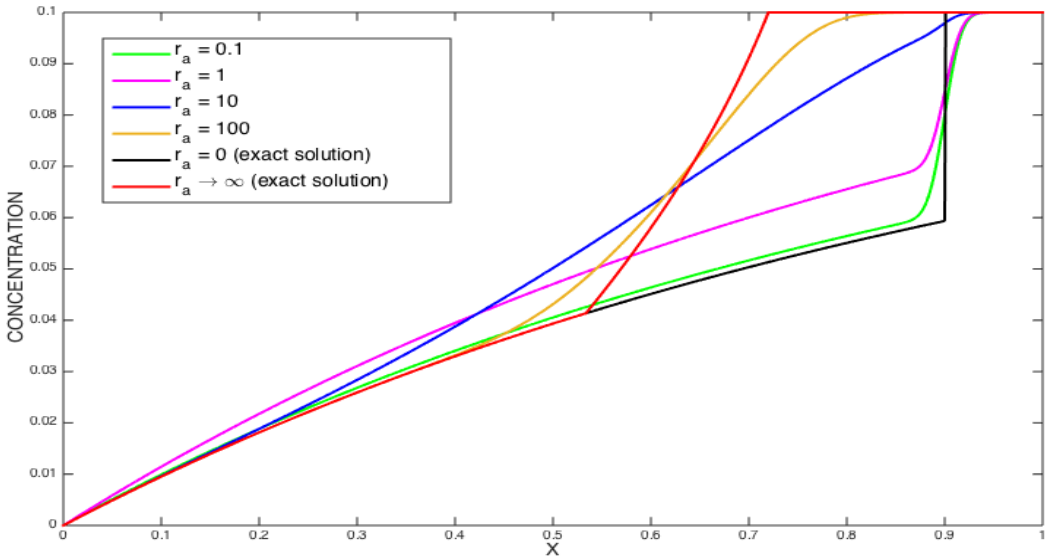

Figure 5.23: *In-situ concentration profiles for Example 5.4 at* $t = 0.9$*, for several values of the desorption rate parameter* r_a.

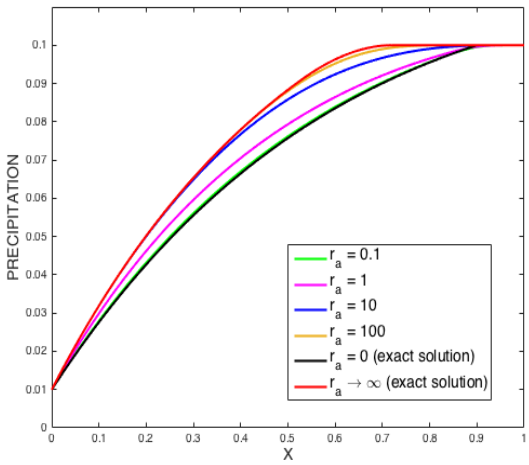

Figure 5.24: *Precipitate profiles for Example 5.4 at* $t = 0.9$.

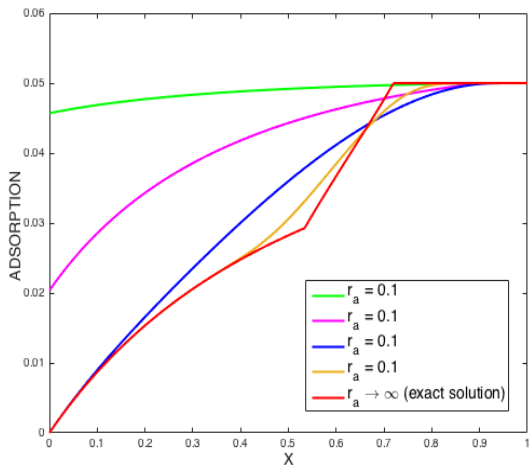

Figure 5.25: *Adsorption profiles for Example 5.4 at* $t = 0.9$

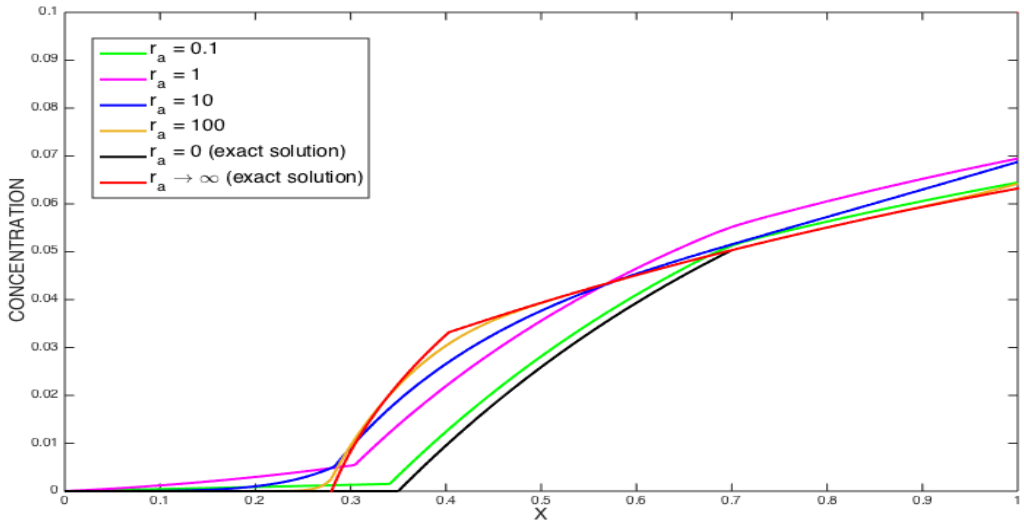

Figure 5.26: *In-situ concentration profiles for Example 5.4 at* $t = 1.7$.

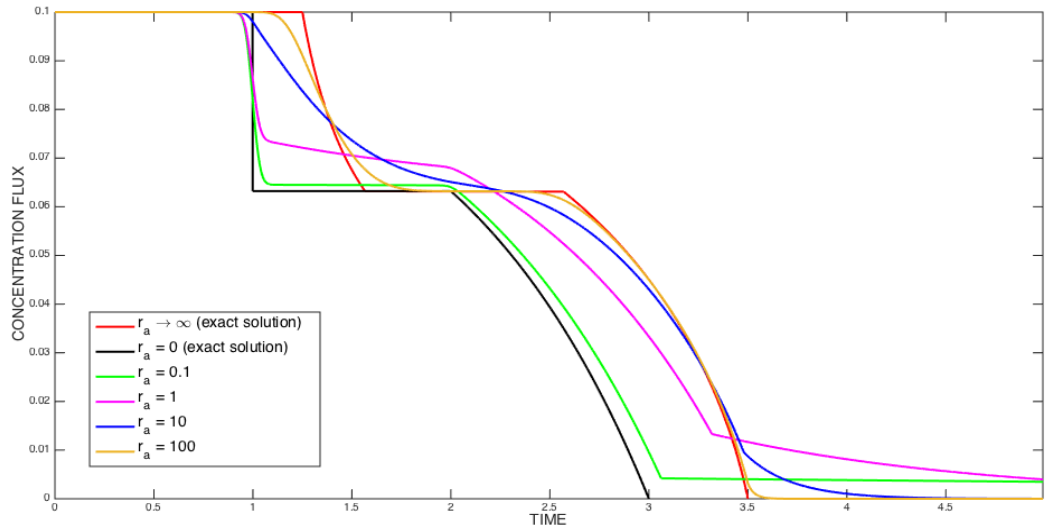

Figure 5.27: *Effluent concentration profiles for Example 5.4*

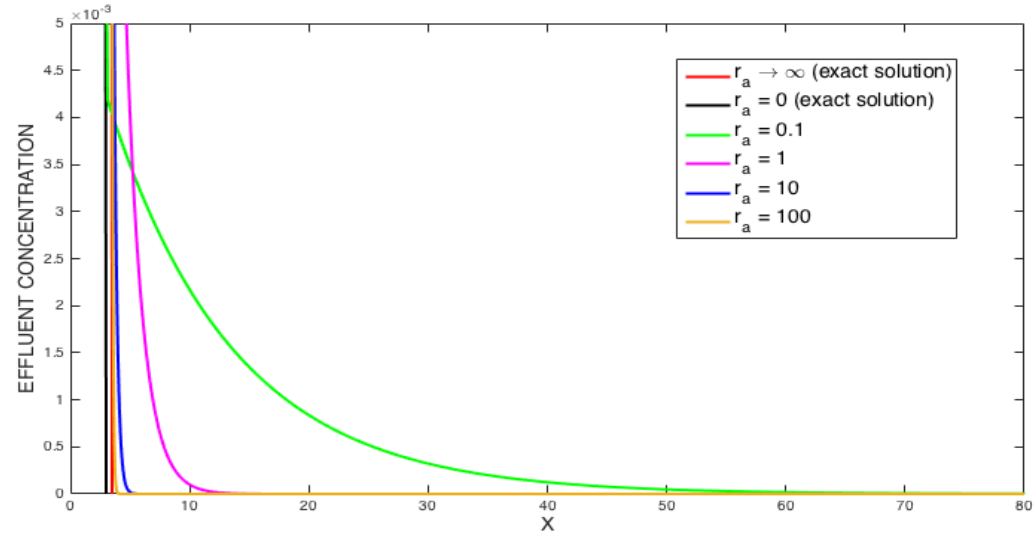

Figure 5.28: *Effluent concentration profiles for Example 5.4 - long term behaviour*

Example 5.5: let $A = 10, B = 100$, $\Pi_0 = 0.1$, $C_s = 0.1$, so that Case 2a (section 5.4.2) applies, and let $v = 1$, $\kappa = 0.25$, $L = 1$. Then, we have $t^* = 4$. The numerical in-situ concentration, precipitation and adsorption profiles at $t = 0.9$ are plotted in Figures 5.29-5.31, for adsorption rate parameters $r_a = 0.1, 1, 10, 100$, alongside the analytical solutions for $r_a = 0$, $r_a \to \infty$. The in-situ concentration profiles for $t = 4.7$ and $t = 6$ are plotted in Figures 5.32-5.33 and effluent concentration profile is shown in Figures 5.34-5.35.

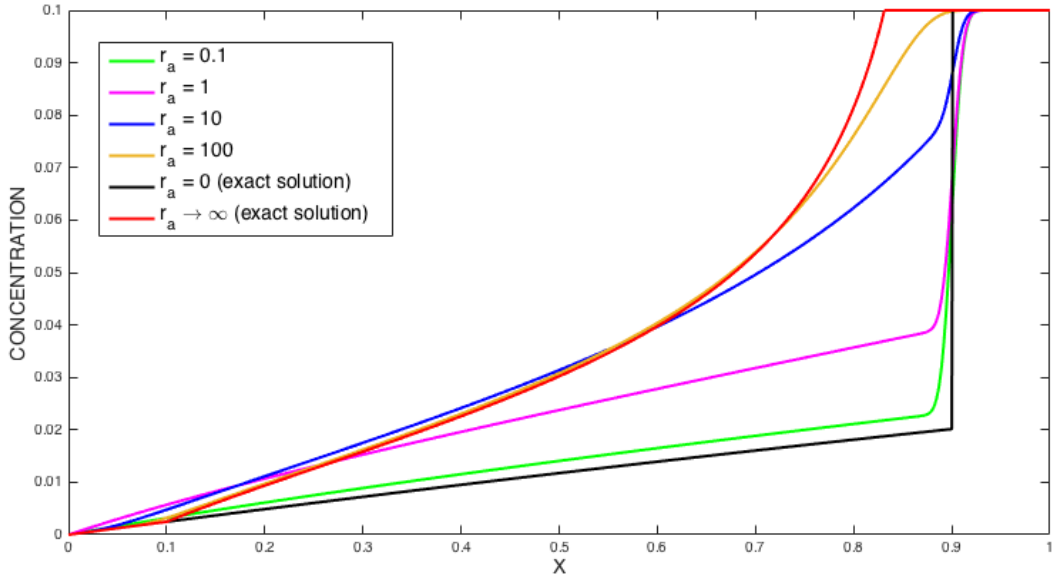

Figure 5.29: *In-situ concentration profiles for Example 5.5 at* $t = 0.9$.

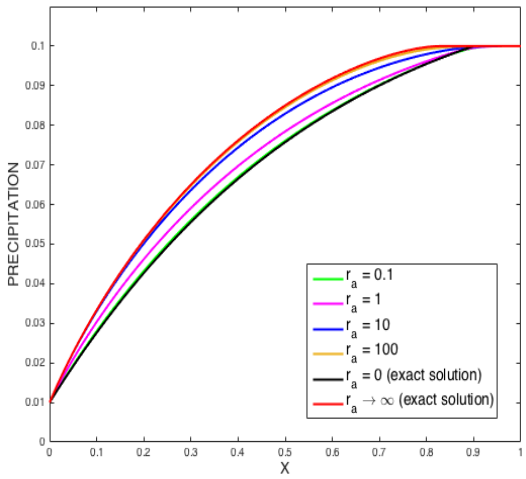

Figure 5.30: *Precipitate profiles for Example 5.5 at* $t = 0.9$

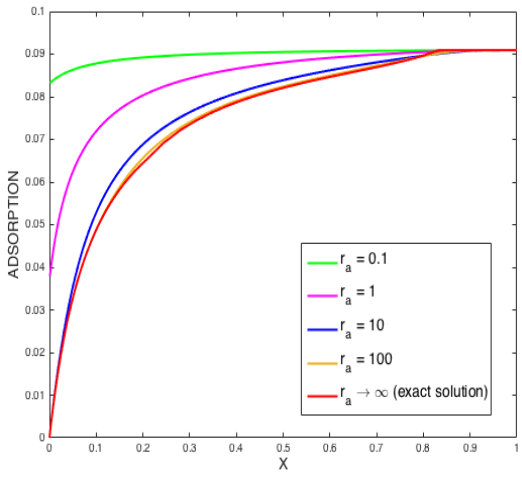

Figure 5.31: *Adsorption profiles for Example 5.5 at* $t = 0.9$

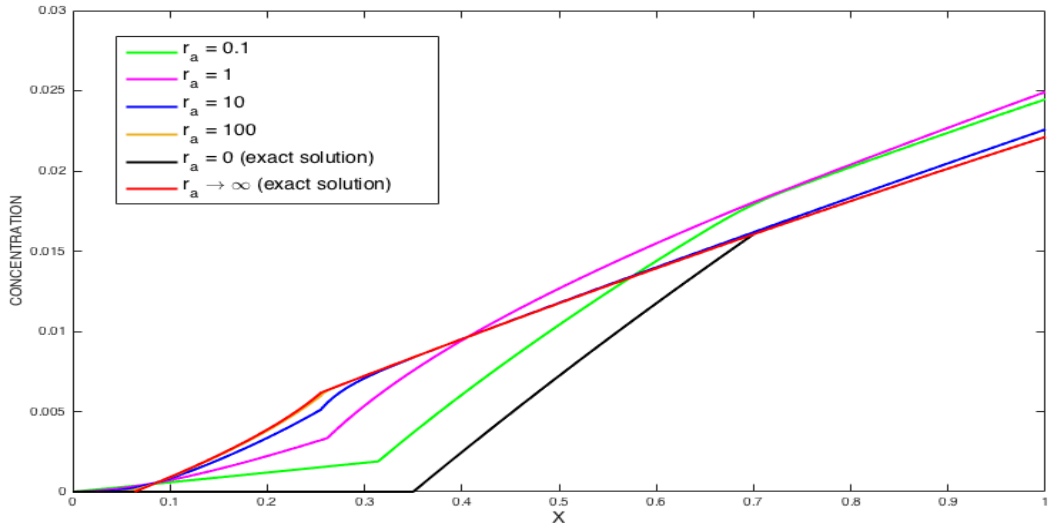

Figure 5.32: *In-situ concentration profiles for Example 5.5 at* $t = 4.7$.

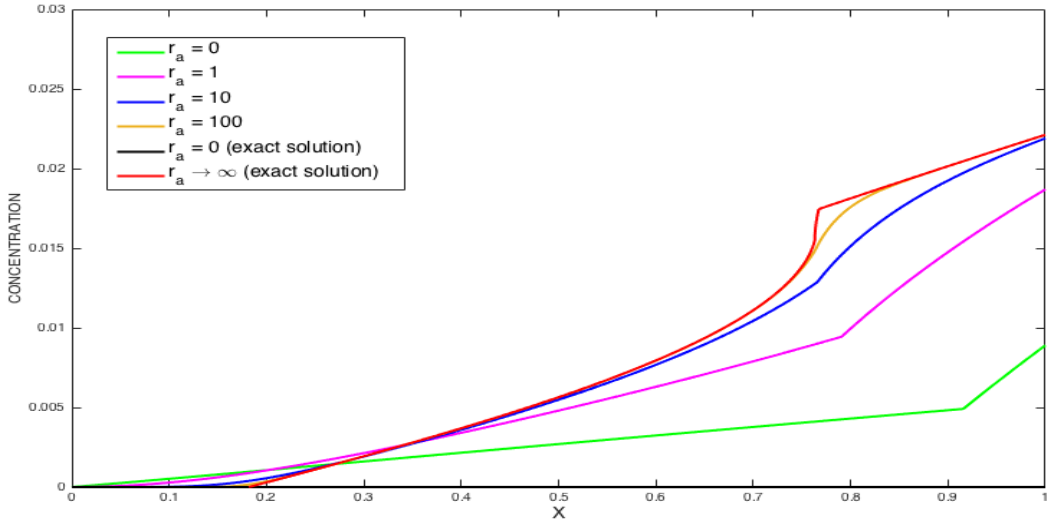

Figure 5.33: *In-situ concentration profiles for Example 5.5 at* $t = 6$.

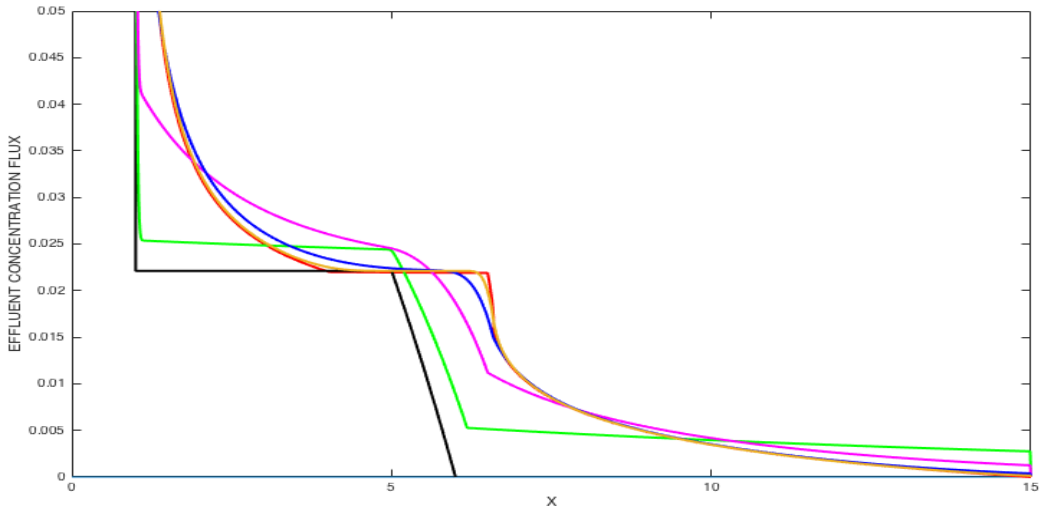

Figure 5.34: *Effluent concentration profiles for Example 5.5*

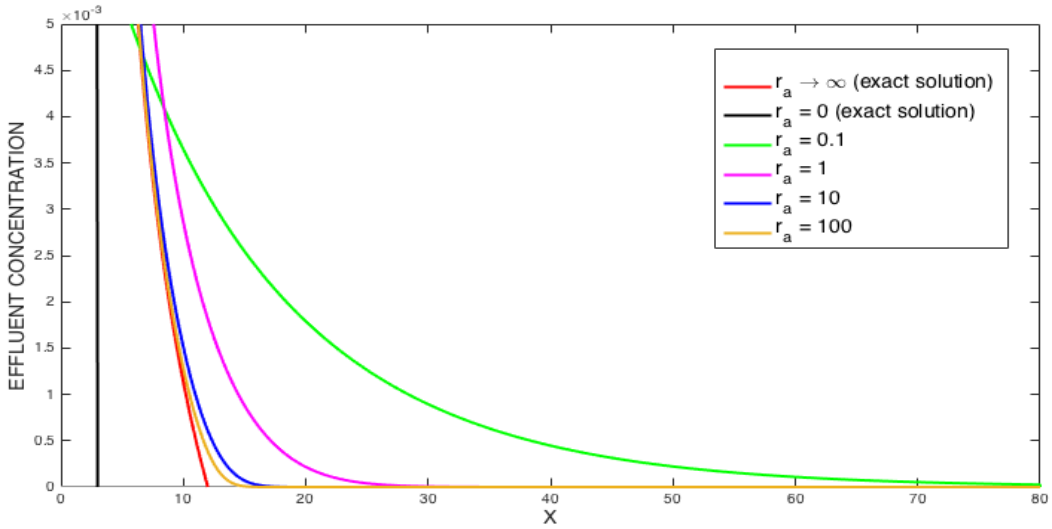

Figure 5.35: *Effluent concentration profiles for Example 5.5 - long term behaviour*

From examples 5.4 and 5.5 we can deduce some qualitative features of the solution of equations (1.6)-(1.8) for finite r_a. In the region where $\Pi > 0$ ($t < t^*$), we identify three (approximate) locations E, F, G on the concentration profile corresponding to some value $0 < r_a < \infty$, as indicated on the sketch in Figure 5.36. The point E is

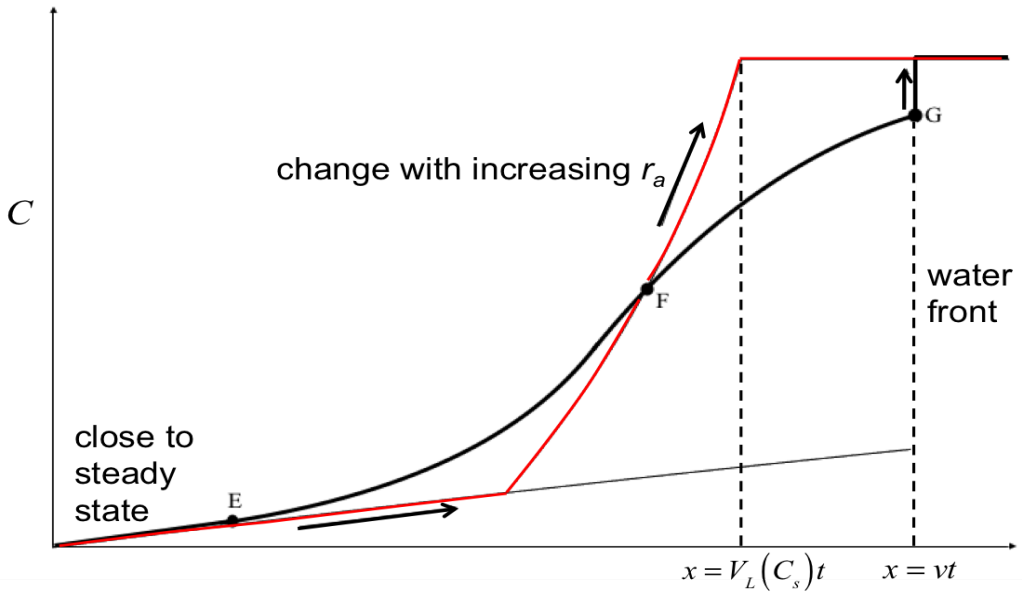

Figure 5.36: *Sketch of the concentration profile for some* $0 < r_a < \infty$*, together with the exact solution for equilibrium desorption (in red).*

where the concentration profile starts to become "visibly close" to the steady-state solution component of the $r_a \to \infty$ solution. Figures 5.25 and 5.31 indicate that the adsorption profile behaves correspondingly. We can most clearly see in Figure 5.23 how E shifts to the right as r_a increases. The concentration and adsorption profiles between the origin and E increasingly align with the steady-state compo-

nent, indicating that this is a solution region dominated by dissolution (almost no desorption takes place here for small r_a). This can also be observed in the effluent concentration profiles (Figures 5.27 and 5.34). The part where the profiles for higher values of r_a intersect the steady-state "plateau" of the equilibrium solution is flatter than for lower values of of r_a.

We see in Figures 5.23 and 5.29 that the concentration profiles intersect the parametric solution component of the equilibrium solution once. This intersection is labelled by F in Figure 5.36. We also marked the point G, which is the lower value of the concentration discontinuity at $x = vt$. Between F and G, the concentration profiles lie below the equilibrium solution. As r_a increases, F tends towards the point $x = V_L(C_s)t$, $C = C_s$, while G moves upwards to $C = C_s$. The shape of the solution between F and G is dependent on r_a in relation to κ. For low values of r_a compared to κ, the profile is concave here (see $r_a = 0.1$, $r_a = 1$ in Figure 5.29). The shape becomes convex for slightly higher values of r_a (see $r_a = 10$ in Figure 5.29) and turns concave again for very high values of r_a. In the limit $r_a \to \infty$, the solution profile between F and G tends towards $C = C_s$ everywhere on the interval $V_L(C_s)t \leq x \leq vt$. This gives physical meaning to the retardation of C_s as implied by the equilibrium solution. Behind the water front, a very high rate of desorption $\partial\Gamma/\partial t$ causes the concentration to be almost fully restored to C_s. This also implies that Γ almost reaches $\Gamma_{eq}(C_s)$. If $r_a \to \infty$, these effects are so extreme that desorption is not "visible". It happens instantaneously, causing $C = C_s$ and $\Gamma = \Gamma_{eq}(C_s)$ in some zone defined by the adsorption isotherm.

For the solutions in the $t > t^*$ region, we can make some observations based on the in-situ concentration profiles in Figures 5.26, 5.32 and 5.33. In example 5.4, the equilibrium solution was of the type seen in Case 1. Here, a travelling wave solution forms immediately at $t = t^*$ and a pure desorption tail is not present. Looking at the in-situ and effluent concentration profiles for different values of r_a in Figures 5.26 and 5.27, it is perhaps more accurate to say that the equilibrium solution *does* have a pure desorption tail, but one in which the concentration (and adsorption) level is identical zero. The situation of Figure 5.26 is sketched in Figure 5.37. The point J on the concentration profile for some $0 < r_a < \infty$ corresponds to $x = \alpha_\Pi$. We remark that the horizontal velocity of J, $d\alpha_\Pi/dt$, is *not* constant, unlike the horizontal velocities of the points M and N. However, it follows from the steep-

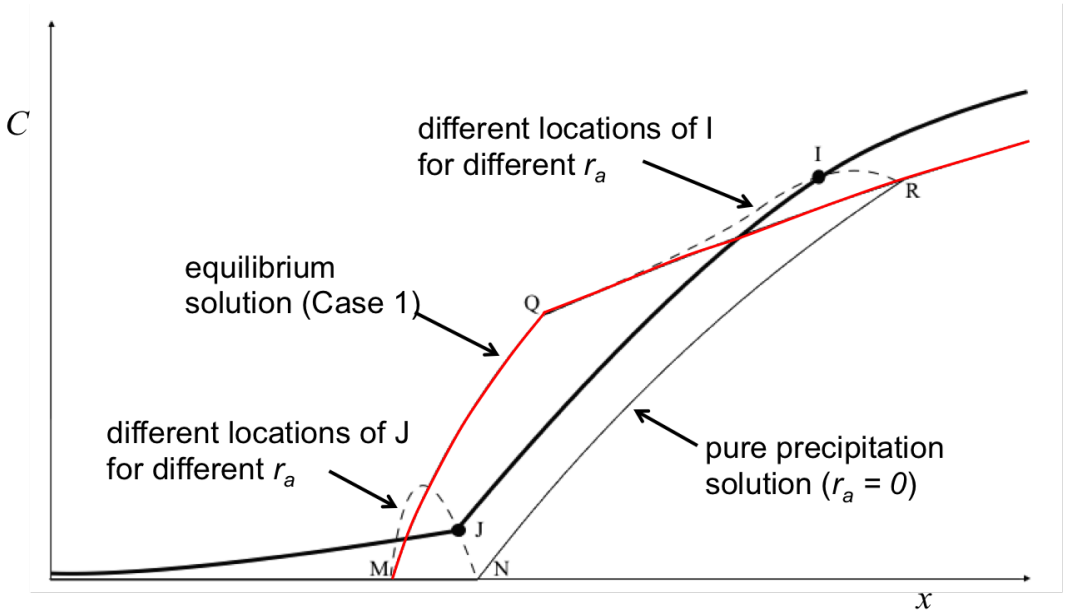

Figure 5.37: *Sketch of the concentration profile for some* $0 < r_a < \infty$*, when* $t > t^*$*, together with the equilibrium solution* ($r_a \to \infty$) *in Case 1 and the pure precipitation solution* ($r_a = 0$).

ness of the precipitation profiles (see Figures 5.24 and 5.30) that $d\alpha_\Pi/dt$ is between $vC_s/(\Pi_0 + C_s + \Gamma_0)$ and $vC_s/(\Pi_0 + C_s)$.

Depending on r_a, the concentration level at J varies. This is illustrated by the dashed line in Figure 5.37. It shows how J increases and then decreases between N and M, which can also be seen in the effluent concentration profile in Figure 5.27. A different situation is observed in Figures 5.32, 5.33 and 5.34. Here, the concentration level at point M is non-zero and J strictly increases between N and M.

We identify a second, approximate point where the concentration profile is noticeably bending. This is labelled "I" in Figure 5.37 and it can be viewed as a "signal" propagating through the solution, carrying the information that the precipitate has run out at J. This signal is the result of a sudden loss of dissolution at the inlet at $t = t^*$, which causes a drop in the concentration level. This effect is propagated through the system due to the convective flux and is most prominent in the $r_a = 0$ and $r_a \to \infty$ solutions, where the sharp edges at Q and R in the profiles travel along characteristics. For $0 < r_a < \infty$, there are no sharp edges, but we do notice a sudden change in direction (in particular in the effluent concentration profiles). This change is smooth and therefore the point I is really an approximate, qualitative, feature of the solution.

5.6 Summary

In this chapter we studied the scale inhibitor model with precipitation and equilibrium adsorption. This is described by equations (5.1)-(5.2) for C and Π, while Γ is determined by the adsorption isotherm $\Gamma_{eq}(C)$. We solved the Cauchy problem for this system with $C(x,0) = C_s$, $\Pi(x,0) = \Pi_0$, $0 \leq x \leq L$ and $C(0,t) = 0$, $t > 0$. If $\Pi > 0$, equation (5.1) is a non-homogenous, quasilinear PDE that incorporates the effects of precipitate dissolution and equilibrium desorption into the mobile phase. We were able to solve this equation using the method of characteristics in combination with the introduction of an auxiliary parameter λ, which enabled us to describe the evolution of the discontinuity in the Cauchy data (see equations (5.14) and (5.15)). This solution exhibits an elegant mixture of the shock discontinuity found in the case of "pure precipitation" ($\Gamma_{eq} = 0$) and the rarefaction wave solution for the case of "pure equilibrium adsorption" ($\kappa = 0$). The introduction of the parameter λ also allowed for the construction of the precipitate profile and we showed that $\Pi > 0$ on Ω for all $t < t^* = \Pi_0/\kappa C_s$. An expression for the velocity of an arbitrary precipitate value P in terms of the corresponding concentration level C_P was found (see equation (5.25)). As in Chapters 3 and 4, the assumption that this relationship is "invariant" between all solution regions lead to the equation of motion of the point α_Π (equation (5.28)). If $\alpha_\Pi'(t^*) \leq V_L(0)$ (Case 1), we saw that a travelling wave solution emerged immediately and the concentration and precipitate profiles behind it were identical zero. On the other hand, if $\alpha_\Pi'(t^*) > V_L(0)$ (Case 2), the solution was characterised by a non-zero pure adsorption tail in the region where the precipitate was used up. This tail continued to form until the velocity of α_Π became equal to the Langmuir velocity of the concentration value at $x = \alpha_\Pi$. It was only at this stage that a travelling wave component began to emerge. The solutions thus constructed were tested for mass conservation by integration of the effluent concentration flux profile and further validated by comparison with numerical solutions in a few example cases. We also looked at what happens when the adsorption rate is finite ($r_a < \infty$). It was seen that the solutions found for the limiting cases $r_a = 0$ and $r_a \to \infty$ serve as good reference points for the appreciation of numerical solutions of the general system with non-equilibrium adsorption.

Chapter 6

Conclusions and future work

6.1 Summary

This PhD constructed analytical solutions for the system of equations describing coupled adsorption/precipitation scale inhibitor transport in porous media. Neglecting dispersion and assuming an equilibrium adsorption/desorption mechanism, the model equations reduced to two first order PDEs for C and Π. The domain $\Omega = [0, L] \times [0, \infty)$ represented a linear rock core of length L and it was assumed that $C(x, 0) = C_s$, $\Pi(x, 0) = \Pi_0$ and $\Gamma(x, 0) = \Gamma_{eq}(C_s)$. Upon the injection of fresh water ($C = 0$) for $t > 0$, the feed condition $C(0, t) = 0$ was adopted as well, assuming an immediate response at the inlet boundary. We first considered the pure precipitation/dissolution case (no adsorption). In Chapter 3, we saw that the precipitate began to run out gradually, starting from inlet boundary at $t = t^* = \Pi_0/\kappa C_s$. The constant initial conditions implied that this depletion occurred at the constant horizontal rate $U = vC_s/(\Pi_0 + C_s)$, leading to a straight-line boundary $x = U(t - t^*)$ dividing Ω into Ω_0 (where $\Pi = 0$) and Ω_+ (where $\Pi > 0$). Since $U < v$, the characteristics on Ω_0 carrying the feed condition ran into this new boundary and determined that $C(\alpha_\Pi, t) = 0$, which defined a travelling wave solution on Ω_+. In Chapter 4, we then examined the effects of having a shut-in period $[t_1, t_2)$ of no flow, with *different* constant flow rates before and after. The first flow phase (studied in Chapter 3) and the shut-in phase determined *non-constant* initial conditions at $t = t_2$ for the problem in the second flow phase, which led to moving boundary curves $x = \alpha_\Pi(t)$ of variable slope. This was made precise in section 4.8, where we proved that, for *arbitrary* initial data $C(x, 0) = C_0(x)$, $\Pi(x, 0) = \Pi_0(x)$, the

moving boundary curve in the pure precipitation/dissolution problem with constant flow rate is defined by a single ODE, $d\alpha_\Pi/dt = F\left[C(\alpha_\Pi, t), \alpha_\Pi\right]$, where the specific form of F is dependent on the initial data. It was shown that a necessary and sufficient condition for the invariance of this ODE is the continuity of the precipitate profile between solution regions, which could be argued physically as long as the initial profile $\Pi_0(x)$ itself is continuous (if $\Pi_0(x)$ has a discontinuity, then a different ODE for α_Π applies on either side of it). The nice thing about this result is that it clearly reveals a two-way mechanism: the boundary curve is *formed* by the solution in Ω_0 and Ω_+, while at the same time it *determines* the solution in these regions. For example, if $d\alpha_\Pi/dt > v$, the characteristics in Ω_+ run into the boundary, thereby determining the concentration level $C(\alpha_\Pi, t)$. This defines the slope of the boundary as well as a solution component in Ω_0, which can often only be described implicitly. We saw that this leads to problems when $d\alpha_\Pi/dt < v$ later on, because the concentration value $C(\alpha_\Pi, t)$ in the ODE is then not explicitly given. Chapter 5 returned to constant initial data, but this time for precipitation/dissolution coupled with equilibrium adsorption/desorption. As in the case of pure precipitation/dissolution, the precipitate began to run out at $t = t^* = \Pi_0/\kappa C_s$. However, it was now possible to have a curved boundary $x = \alpha_\Pi(t)$, defined by an ODE of the form $d\alpha_\Pi/dt = F\left[C(\alpha_\Pi, t)\right]$. When $F(0) > V_L(0)$, the characteristics in Ω_+ initially ran into the boundary, determining $C(\alpha_\Pi, t)$ and the slope $V_L(C(\alpha_\Pi, t))$ of the straight-line characteristics in Ω_0 carrying these concentration values. Once the slope of the moving boundary became equal to the slope of the Ω_0-characteristic emanating from it, the invariance of the ODE for α_Π implied that the boundary thereafter coincided with this Ω_0-characteristic. The constant concentration value on the boundary then led to a travelling wave solution component in Ω_+. An extension of this procedure for arbitrary initial data $C_0(x)$, $\Pi_0(x)$ was also considered. We found that the ODE for α_Π is easily modified to accommodate $\Pi_0(x)$. However, similar to what was described above, this could lead to a reversal of $d\alpha_\Pi/dt$ with respect to the characteristics in Ω_0 and the possibility that $C(\alpha_\Pi, t)$ is only available implicitly. An even greater problem was the inclusion of arbitrary initial concentration profiles $C_0(x)$. In fact, it is only possible to derive the ODE for α_Π if $C_0(x)$ is given by a specific algebraic expression.

6.2 Discussion

6.2.1 Effluent concentration profiles

This work has primarily been concerned with the construction of the in-situ solution profiles, without paying special attention to the finite length L of the rock-core. However, in a laboratory setting, the only measurable quantity is the effluent concentration $C(L,t)$. The variation of this level with time can tell us which regime (desorption or dissolution) is more prominent. It also determines the "lifetime" of a squeeze treatment, the amount of time that the effluent concentration is at least equal to a threshold level C_t below which scale inhibition becomes ineffective. In order to address these matters in terms of the various parameters, we briefly recall the three qualitatively different in-situ profiles found in Chapter 5. They can be distinguished purely in terms of the (uniform) initial levels of precipitation (Π_0) and adsorption ($\Gamma_0 = \Gamma_{eq}(C_s)$). To this end, we write $\Gamma_{eq}(C) = B\Gamma_{max}C/(1+BC)$ and introduce the functions

$$P_1(\Gamma_0) := \frac{\Gamma_0^2}{\Gamma_{max} - \Gamma_0} \tag{6.1}$$

$$P_2(\Gamma_0) := \Gamma_0 + 2(\Gamma_{max} - \Gamma_0) - 2\sqrt{\Gamma_{max}(\Gamma_{max} - \Gamma_0)} \tag{6.2}$$

Here, Γ_{max} is the maximum amount of scale inhibitor that can be retained on the rock surface through adsorption. If $\Pi_0 \geq P_1(\Gamma_0)$, a travelling wave solution emerges at $t = t^*$ (Case 1, section 5.3). On the other hand, if $\Pi_0 < P_1(\Gamma_0)$, then we have $d\alpha_\Pi/dt > V_L(C(\alpha_\Pi, t))$ until $t = \tau_a$ such that $C(\alpha_\Pi, \tau_a) = \xi_a$, where

$$\xi_a = \frac{1}{B}\left[\frac{\Pi_0 + \Gamma_0 - \Gamma_{max}\sqrt{\frac{\Pi_0}{\Gamma_{max}-\Gamma_0}}}{\Gamma_{max} - \Gamma_0 - \Pi_0}\right] \tag{6.3}$$

If $P_2(\Gamma_0) < \Pi_0 < P_1(\Gamma_0)$, then the point $(\alpha_\Pi(\tau_a), \tau_a)$ is in region III, so ξ_a at that time lies on the steady-state component (Case 2a, section 5.4.1). Finally, if $\Pi_0 \leq P_2(\Gamma_0)$, then $(\alpha_\Pi(\tau_a), \tau_a)$ is in region II (Case 2b, section 5.4.2). Prior to this, region III disappears at $t = \tau_b$ such that $C(\alpha_\Pi, \tau_b) = \xi_b$, where

$$\xi_b = \frac{1}{2B}\left[\frac{\Gamma_0 - \Pi_0 - \sqrt{(\Gamma_0 - \Pi_0)^2 - 4\Pi_0(\Gamma_{max} - \Gamma_0)}}{\Gamma_{max} - \Gamma_0}\right] \tag{6.4}$$

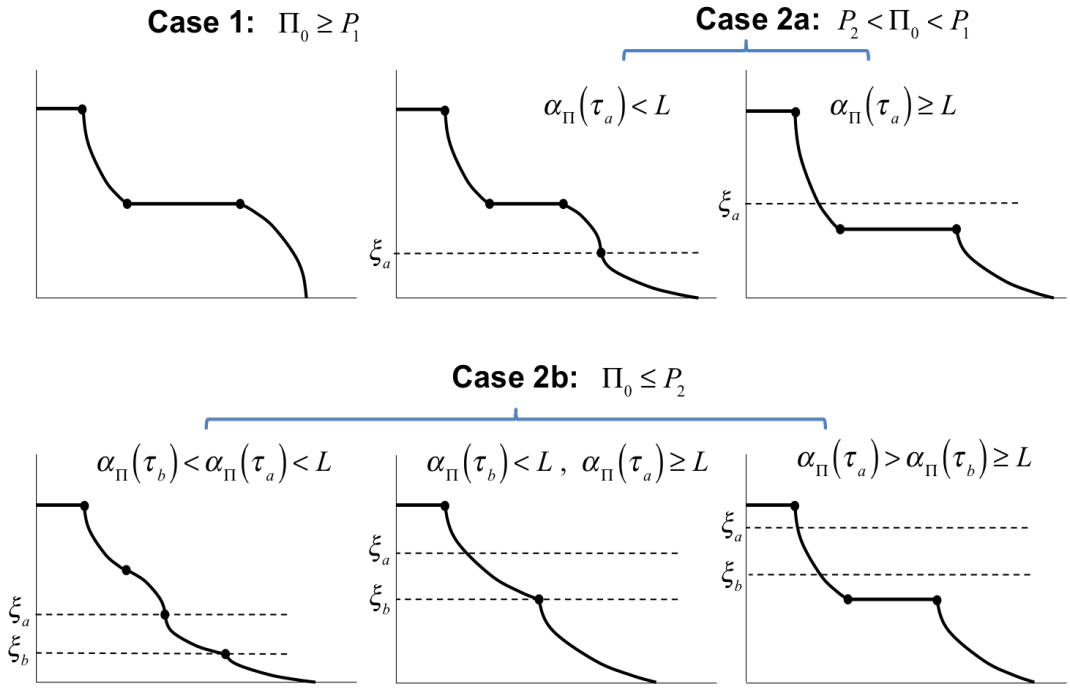

Figure 6.1: *Possible effluent concentration profiles.*

The possible effluent concentration profiles are summarised in Figure 6.1. We note that all cases with initial precipitate level $\Pi_0 > P_2(\Gamma_0)$ have a "plateau" of constant concentration $C_s - C_s e^{-\kappa L/v}$ as a result of the breakthrough of the steady-state component in the in-situ profiles. For $\Pi_0 \leq P_2(\Gamma_0)$, this only occurs if $\alpha_\Pi(\tau_b) = v\kappa^{-1}\ln(1-\xi_b/C_s) > L$. It should be emphasised that Π_0, Γ_0, Γ_{max} determine which qualitative case (1, 2a, 2b) occurs. The values ξ_a, ξ_b only have an additional explicit dependence on B. Once these are fixed, variations in κ, v and L cause the emergence and length of particular solution regions in the effluent profiles. In the next sections, we will identify situations in which a desired threshold concentration C_t is to be maintained for as long as possible, taking into account practical constraints on the variables of the system.

6.2.2 Slow versus fast dissolution

The rate equations in the full scale inhibitor deposition/retention model are governed by the adsorption/desorption rate parameter r_a and the precipitation/dissolution rate parameter κ. There are four limiting behaviours (see Figure 6.2), ranging from the fully kinetic case, when both rate parameters are finite, to the full equilibrium case, when both rate parameters are infinite. In practical applications, the rate parameters need to be considered in relation to the length of the system (reservoir

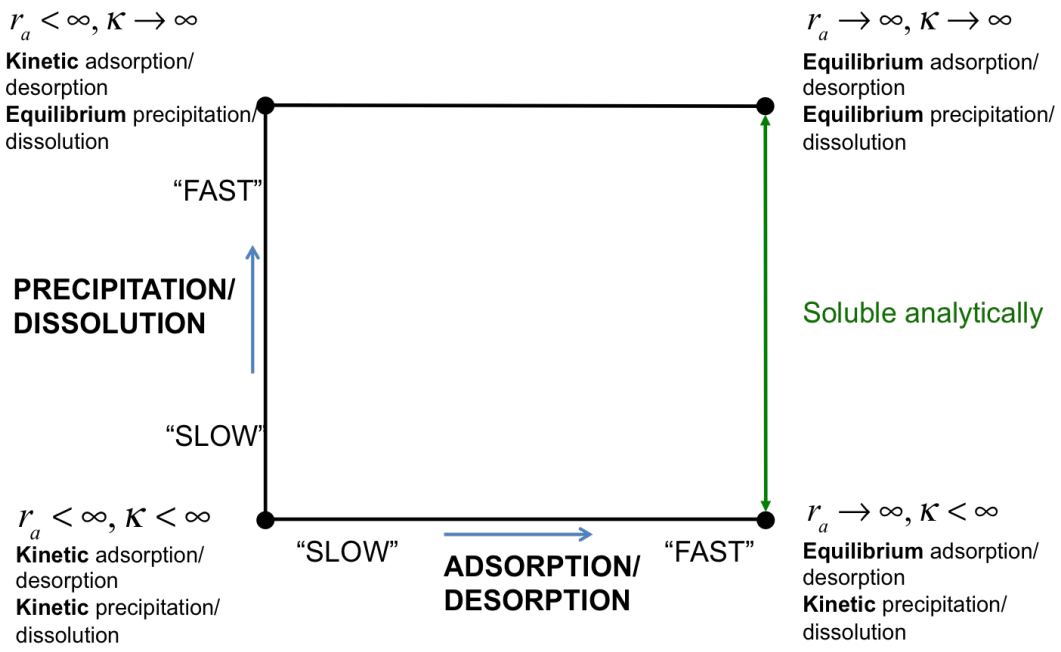

Figure 6.2: *"Phase diagram" illustrating the different combinations of the adsorption and precipitation mechanisms.*

or rock core) and the flow rate, which both determine the impact of the two mechanisms on the mobile phase concentration. For instance, in case of a core-flood experiment on rock core of length L, a *low* flow rate Q implies a low fluid velocity $v = Q/A\phi$ ($A =$ cross-sectional area, $\phi =$ porosity), which corresponds to a *long* fluid residence time L/v. A high but finite rate parameter can then lead to behaviour that is very similar to an equilibrium process. This is no longer the case if the flow rate is increased significantly. Thus, the rate parameters must be considered relative to the residence time of the fluid and kinetic/equilibrium type behaviour can always be achieved by increasing/decreasing v sufficiently. For *fixed* L/v, we say that a desorption/dissolution process is "fast" if it is very close to equilibrium behaviour (typically very high values of κ, r_a). On the other hand, the process is called "slow" if it deviates noticeably from equilibrium (low or medium values of κ, r_a). The analytical solutions found in Chapter 5 are for fast adsorption/desorption processes only, but capture both slow and fast precipitation/dissolution. Figure 6.3 illustrates slow versus equilibrium dissolution in Case 2a. Both in-situ profiles are sketched at a time $\tau_a + \Delta t$, when the travelling wave component (IV) is present. Now, as κ is increased, τ_a becomes closer to t^*, which itself decreases due to faster dissolution of the precipitate. Regions II and III become narrower, while IV widens. At the same time, the concentration in these regions gets closer to C_s. In the limit

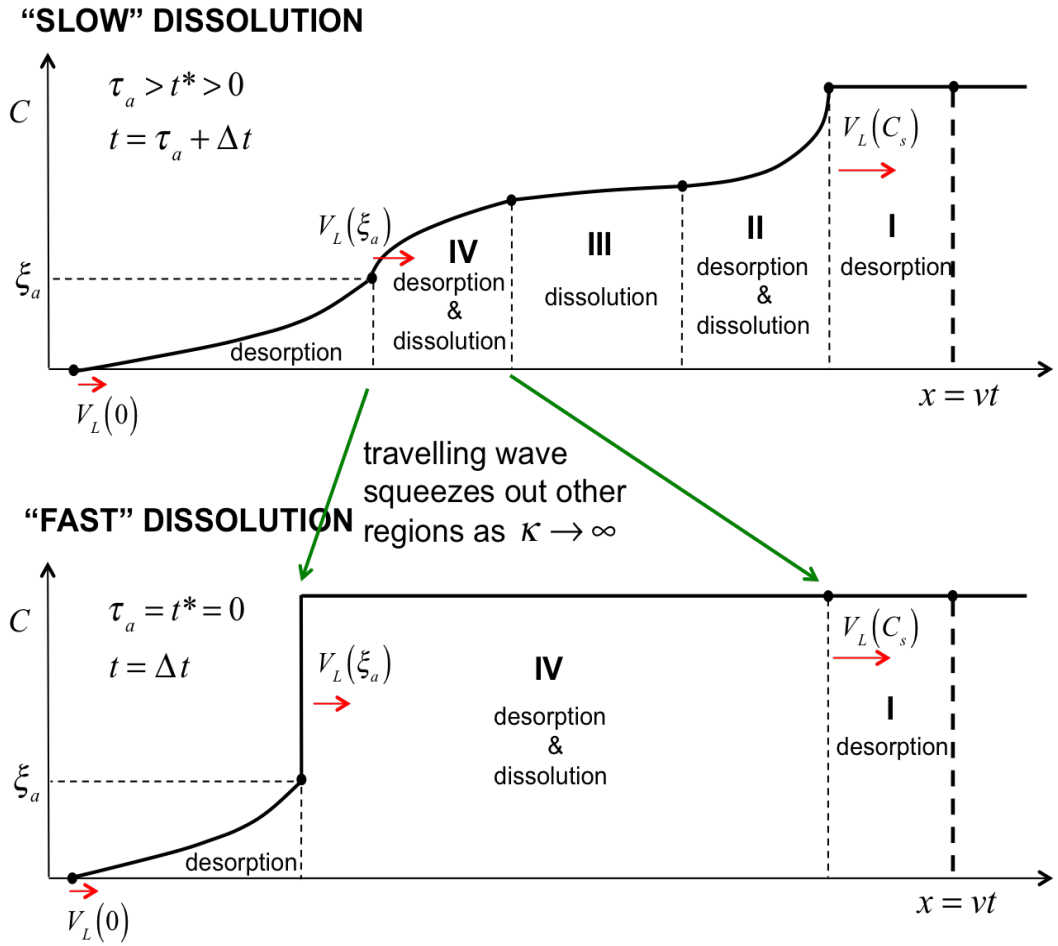

Figure 6.3: *In-situ profiles for $\kappa < \infty$ (top) and $\kappa \to \infty$ (bottom).*

$\kappa \to \infty$, we have $\tau_a = t^* = 0$ and regions II and III disappear completely. The characteristic separating regions III and IV (see Figure 5.14) then collapses onto the characteristic $x = V_L(C_s)\,t$ and the travelling wave develops a discontinuity at $x = V_L(\xi_a)\,t$. In order to emphasise the importance of the time τ_a for the effectiveness of a squeeze treatment, we compare the effluent concentration profiles for "slow" versus "fast" dissolution. In the sketch in Figure 6.3, it is assumed that the threshold concentration is $C_t < \xi_a$ and that $\alpha_\Pi(\tau_a) = v\kappa^{-1}\ln(1 - \xi_a/C_s) < L$, so that the travelling wave can be seen in the effluent profile. We observe that fast (equilibrium) dissolution sustains the concentration level $C = C_s$ before dropping off sharply to ξ_a and decreasing further down to the threshold concentration. The lifetime of the squeeze treatment now depends solely on the Langmuir speed $V_L(C_t)$, as indicated by the red dashed line. If scale inhibitor is just as effective at threshold concentration as it is for higher concentrations, then the fast dissolution process is not economic at all in this case, because a pure adsorption/desorption squeeze treatment would achieve exactly the same lifetime. The initial mobile phase con-

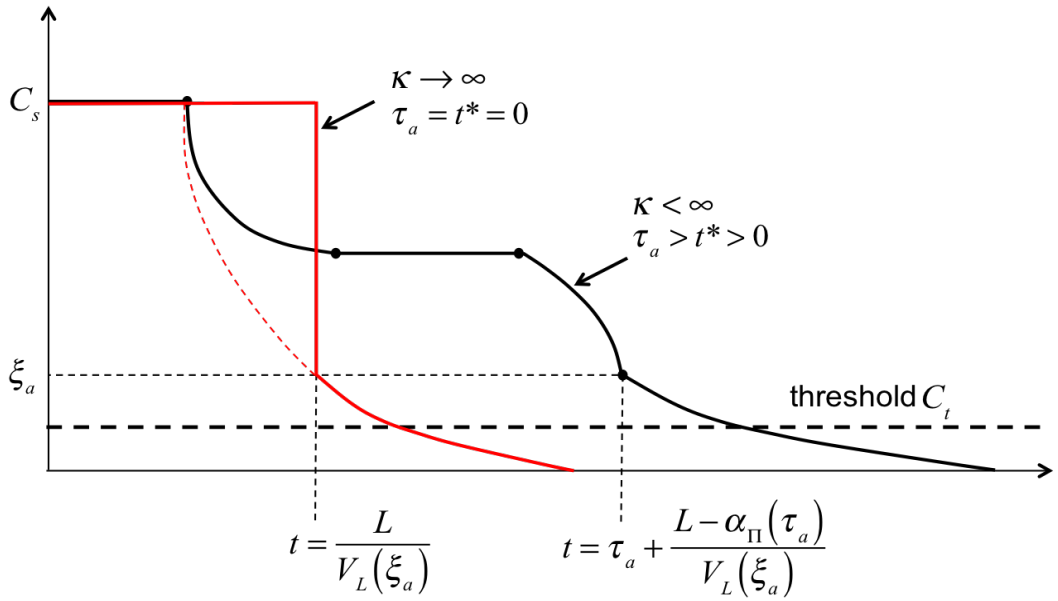

Figure 6.4: *In-situ profiles for $\kappa < \infty$ (top) and $\kappa \to \infty$ (bottom).*

centration for such a treatment just needs to be equal to C_t, far below the solubility level C_s. This evidently requires much less scale inhibitor than the coupled process, in which the injected concentration needs to be greater than C_s in order for the precipitate to form. All this extra scale inhibitor is "wasted" if it just results in a higher return curve rather than delaying the breakthrough time of C_t. The latter is achieved by the slow (kinetic) dissolution mechanism, mainly because of the resulting increase in t^*. In order to optimise usage of the available precipitate, the plateau of concentration $C_s - C_s e^{-\kappa L/v}$ needs to be as close to the threshold level C_t as possible. For a given rate parameter κ, such a low return curve can be obtained by increasing the flow rate. In terms of produced pore volumes, this results in the same lifetime while ensuring optimal usage of the scale inhibitor in the system. A possible drawback to this approach is that the higher flow rate can lead to inefficient oil displacement, with phenomena such a viscous fingering becoming more problematic. Moreover, we should bear in mind that the model with constant fluid velocity only applies to core-flooding experiments. In case of a producing well in the field, the fluid velocity is inversely proportional to the radial distance from the well (see the discussion in Chapter 1). In order to predict the return curves accurately, we would of course need to derive an analytical solution for this radial model. However, qualitative predictions can already be made using the solution of the present linear model. Broadly speaking, the same type of solution components will appear in the radial setting, but they will be stretched considerably in the region

close to the producing well, where the fluid velocity is very high. Also, if the same parameters are used as input for both models, the effect of dissolution in the radial case will be *less* than in the linear case, due to the shorter fluid residence time. In order to achieve similar concentration levels in both return curves, the flow rate in the radial case will then need to be lowered. This is even more true if precipitate is formed only at a certain distance from the producing, due to low temperatures in the near-well region and higher temperatures further into the reservoir.

6.2.3 Lifetime increase due to precipitation

We just saw that, if the steady state component appears in the effluent profile, the available precipitate is used in the most efficient way when the flow rate is adjusted to make $C_s - C_s e^{-\kappa L/v} = C_t$. If no adsorption were to occur, this yields a squeeze lifetime (in pore volumes) of exactly

$$T_{pptn} = \frac{v}{L}\left(1 + \frac{\Pi_0}{\kappa C_s}\right) \tag{6.5}$$

This lifetime is increased due to adsorption. For example, in Case 1 ($\Pi_0 \geq P_1(\Gamma_0)$), the lifetime of the adsorption/precipitation squeeze treatment is found by calculating when the characteristic separating the steady-state and travelling wave components intersects with the line $x = L$. The characteristic is given by equation (5.35), from which it follows that

$$T_{ads/pptn} = T_{pptn} + \frac{v}{\kappa L}\left[\kappa\Gamma_0' + \Gamma_0' \ln\left(1 + BC_t\right) + \frac{\Gamma_0}{C_s}\frac{BC_t}{1 + BC_t}\right] \tag{6.6}$$

where $\Gamma_0 = \Gamma_{eq}(C_s)$, $\Gamma_0' = \Gamma_{eq}'(C_s)$ and $C_t = C_s - C_s e^{-\kappa L/v}$. The last term shows the addition in lifetime due to adsorption. The percentage increase with respect to T_{pptn} is actually limited due to the inter-dependence of the parameters involved. For instance, an increase in the adsorption capacity Γ_{max} will cause both Γ_0 and Γ_0' to increase. However, for larger increases, we will have to increase Π_0 accordingly in order to stay in Case 1. This evidently caps the proportional increase in lifetime, since it increases T_{pptn}. Similarly, changes in B or C_s might increase Γ_0, but simultaneously decrease Γ_0'. Although only a rigorous analysis will reveal what combinations of parameters maximise the "extra lifetime term" in equation (6.6),

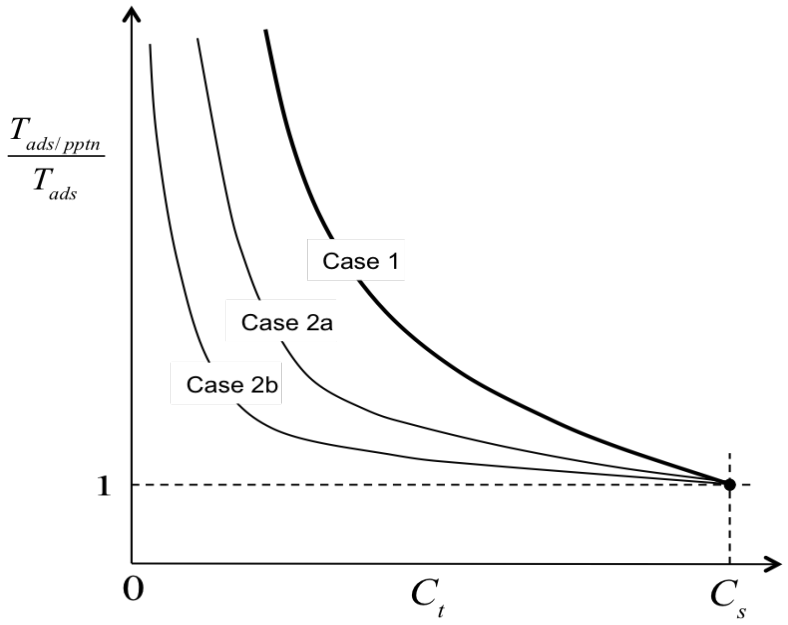

Figure 6.5: *Illustration of the beneficial effect of inducing precipitation.*

we can make some general observations regarding this issue. Notice that, on the one hand, the lifetime tends to $v/L\,(1+\Gamma_0')$ pore volumes as $\kappa \to \infty$ ($C_t \to C_s$), corresponding to the retardation of the value C_s due to desorption. On the other hand, it can be shown that, as $\kappa \to 0$, the last term in equation (6.6) becomes $v/\Gamma_0' L + BC_s\Gamma_0' + B\Gamma_0$. Thus, for small κ, we have $T_{ads/pptn} \approx T_{pptn} \approx \Pi_0/\kappa C_s$. In order to appreciate the benefits of inducing precipitation, we have to compare $T_{ads/pptn}$ with $T_{ads} = v/L\left(1+\Gamma_{eq}'(C_t)\right)$, the lifetime achieved by a pure adsorption treatment. Figure 6.5 illustrates the variation of the ratio of $T_{ads/pptn}$ and T_{ads} with the threshold concentration C_t. Large increases in lifetime are observed particularly if the threshold concentration is much lower than the solubility. A similar benefit-analysis can be carried out in Cases 2a and 2b (also sketched in Figure 6.5). Here, the advantage of inducing precipitation is less prominent for higher threshold values. This is already obvious from the effluent profiles in Figure 6.1. In Case 2b for instance, the effects of desorption can outweigh dissolution so much that the steady-state component is never able to break through. This is because either the amount of precipitate is very low or the isotherm is initially very steep and then levels off, causing Γ_0 to be close to Γ_{max}. Compared to pure adsorption, the squeeze lifetime is still improved, but less so than in Case 1 or 2a. Eventually, when κ is decreased or v is increased (and hence C_t lowered) to such an extent that $\alpha_\Pi(\tau_b) < L$, the steady-state will appear in the effluent profile, resulting in larger percentage improvements.

6.2.4 Lifetime dependence on desorption

In the previous sections considered how dissolution improves squeeze lifetime. In that discussion, it was assumed that the flow rate can always be adjusted to make $C_t = C_s - C_s e^{-\kappa L/v}$, so that the lifetime is defined by the length of the steady-state plateau in the effluent concentration profiles (except possibly in Case 2b). However, in practice, it might not be possible to increase the flow rate to this extent. We could have a situation in which, at the fastest possible flow rate, the effluent concentration level $C_s - C_s e^{-\kappa L/v}$ is still much higher than C_t (as was shown in Figure 6.4). The lifetime then depends significantly on the nature of the desorption mechanism, which is governed by the Langmuir isotherm. A steep rising isotherm with a high adsorption capacity Γ_{max} will cause the lower concentration values in the pure desorption tail (present in Cases 2a and 2b) to propagate slowly. Dissolution improves this further, by delaying the advance of C_t. However, as we saw previously, for very steep isotherms, the improvement on the lifetime achieved by a pure adsorption treatment is limited. In such circumstances, inducing precipitation is only worthwhile if a lot of scale inhibitor can be injected. This will increase Π_0, making the improvement due to dissolution more significant. We then benefit from the "delay" caused by dissolution as well as the slow Langmuir velocity of C_t.

There is another aspect involved with flow rate changes. In the discussion thus far the adsorption/desorption process was always fast (at equilibrium), whereas precipitation/dissolution could be fast or slow (kinetic). This applies if the desorption rate parameter r_a is very high in relation to the fluid residence time L/v. Thus, large increases in the flow rate could lead to adsorption/desorption becoming kinetic too, so that the bottom left corner of the "phase diagram" in Figure 6.2 applies. In this case, the system can only be solved numerically, which was done for some example-problems in section 5.5. These plots emphasised the importance of the ratio κ/r_a. For instance, if precipitation is slow with $\kappa = 10$ and adsorption is fast with $r_a = 100$, then making the flow rate ten times faster effectively decreases the rate parameters to $\kappa = 1$ and $r_a = 10$. Some solution profiles for this particular ratio were plotted in Examples 5.4 and 5.5 (the blue line plots). Both processes are now slow in the sense that the solution profiles clearly show some deviation compared to the $r_a \to \infty$ case. The effluent profiles in Figures 5.27 and 5.34 reveal that the

effect on squeeze lifetime will be rather limited. This may change for high values of κ/r_a, when desorption is slow compared to dissolution. Then, if the threshold concentration is sufficiently low, the squeeze lifetime is increased hugely due to very long pure adsorption tails (see green-line plots in examples 5.4 and 5.5).

6.2.5 Experimental data

We conclude this discussion by presenting some real data obtained in core-flood experiments. Figure 6.6 shows a plot of the measured effluent scale inhibitor concentration in ppm versus time in pore volumes (PV), at three different flow rates $Q = 1, 5, 30$ ml/h. The vertical axis is a log-scale, which means that the discontinuity observed between 0 and 5 PV is very large. It can be seen that the core-flood with $Q = 1$ ml/h clearly shows the features predicted by the analytical solution for kinetic precipitation / equilibrium adsorption. Between 5 and 20 PV, there is a region of constant concentration, presumably due to the steady-state component. The profile then decreases quite rapidly between 20 and 30 PV, before flattening again and decreasing more slowly towards 10 ppm at 45 PV. These two regions might be the travelling wave component and pure desorption tail respectively, or it could all be a pure desorption tail. In making such interpretations it should also be remembered that the data will be affected by some degree of physical diffusion and dispersion, which hasn't been taken into account in our treatment of the model.

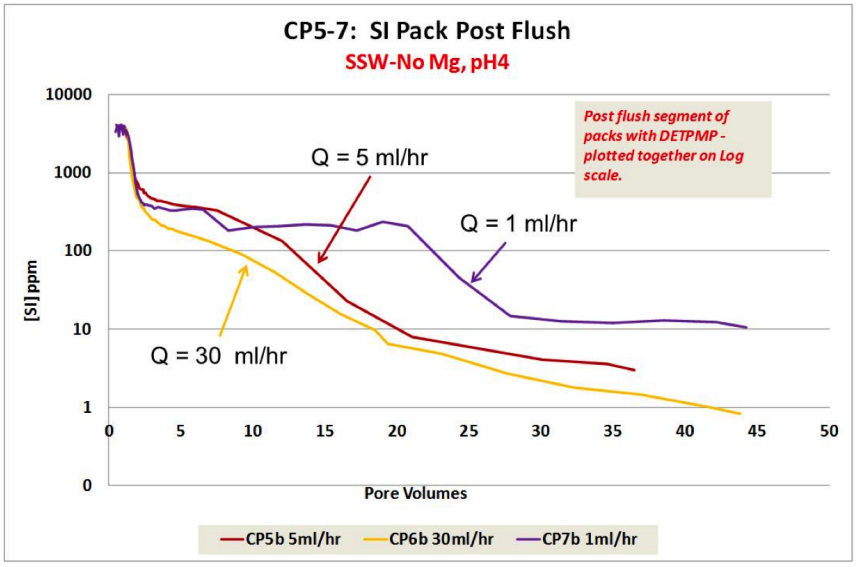

Figure 6.6: *Effluent concentration profiles from core-flood experiments.*

6.3 Future work

In section 4.8 a general solution approach for the problem of pure precipitation with arbitrary initial distributions $C_0(x)$, $\Pi_0(x)$ was developed. In that case, the general functional form of $\Pi(x,t)$ could be inferred from $C(x,t)$. Together with the requirement that the precipitate profile is continuous, this lead to the invariance of the formula for the rate of change dx_P/dt of a precipitate value P between all solution regions. It is worthwhile examining if a similar argument can be developed for the case of coupled precipitation and equilibrium adsorption. Although we were able to derive an analogous expression for dx_P/dt here, it was not rigorously proved to be invariant between all solution regions. Instead, this invariance had to be assumed in order to construct the solution for all $t > t^*$. It was already hinted that such a proof would be far more complicated than in the pure precipitation case, because of the difficulty in deriving a general functional form for $\Pi(x,t)$, which involves integration using the auxiliary parameter λ linking $C(x,\lambda)$ and $t(x,\lambda)$. This is particular difficult (and probably impossible) if $C_0(x)$ is arbitrary.

Future work should also focus on mass conservation and its relation to the continuity of $\Pi(x,t)$. For the problems discussed in Chapters 3-5, we always assumed this continuity in order to uniquely define a precipitate component and then checked mass conservation by explicit integration of the effluent concentration flux profile. The question is if this process can be reversed in the sense that mass conservation can be used as a requirement which enforces continuity of $\Pi(x,t)$. The whole analytical solution can then be constructed in the knowledge that it conserves the total amount of chemical, as is implied by the formulation of the PDEs themselves. Some light might be shed on this issue by the inclusion of a diffusion term $\partial^2 C/\partial x^2$ in the transport equation. This "completes" the PDEs physically by taking into account the tendency of solute molecules to move to areas of lower concentration. Mathematically, the presence of the second term leads to a smoother solution, which does not have the discontinuities and sharp edges that mark the region boundaries of the weak solution to the first-order PDE.

As a next step in the research on these type of problems, it should be investigated what happens for a more general velocity function $v(x,t)$. A spatial velocity de-

pendence is encountered in radial reservoir models and time-dependence could arise as a result of a variable flow rate. In particular the analytical solution of the radial scale inhibitor model would be useful for the purpose of making field predictions about squeeze lifetimes. It is anticipated that the construction of this solution is quite straightforward while $\Pi > 0$, but runs into trouble when the concentration on the boundary curve $x = \alpha_\Pi(t)$ needs to be determined, as this likely to be an implicit process. Ultimately, any future work in this respect should be aimed at exploring to what extent the scope of our solution method applies to a general system of equations of the form

$$a(x,t,C)\frac{\partial C}{\partial t} + v(x,t,C)\frac{\partial C}{\partial x} = -\frac{\partial \Pi}{\partial t} \tag{6.7}$$

$$\frac{\partial \Pi}{\partial t} = b(x,t,C) \cdot H(\Pi) \tag{6.8}$$

with arbitrary initial data $C(x,0) = C_0(x)$, $\Pi(x,0) = \Pi_0$ and an arbitrary boundary condition $C(0,t) = h(t)$. The key aspect of such a solution approach would be to establish an invariant relationship for the rate of change of dx_P/dt. This would lead to an ODE for the motion of the point α_Π in terms of x, t, C. If C is known (explicitly) at $x = \alpha_\Pi$ and we can solve the resulting ODE then we will be able to apply the method of characteristics to construct a solution. This would open up the possibility of solving a whole host of other coupled problems describing physical processes in which one of the unknowns runs out and thereby effects a discontinuous change in the transport equation. We could also explore cases of the scale inhibitor model in which the dissolution rate parameter κ and solubility C_s are dependent on reservoir conditions which may vary with time and space, such as the locally prevailing temperature.

Another idea for future research is to continue the analysis of the full scale inhibitor model with kinetic adsorption/desorption and diffusion. The exact solutions found for the two limiting cases $r_a = 0$ and $r_a \to \infty$ are good reference points for numerical solutions of the full system. More sophisticated methods based on a proper numerical analysis of the equations can be used to analyse the influence of different parameters. This may help to evaluate experimental data such as those shown in

Figure 6.6, which are likely to include kinetic effects as well as diffusion. Finally, it would also be interesting to see if certain behaviours predicted by the analytical solutions found in this work can be reproduced in an experiment. One idea for a laboratory set-up is to use a sand-pack containing a solution of the sparingly soluble compound calcium sulphate ($CaSO_4$). This should be shut in long enough for the chemical to reach full solubility level and for the precipitate to form. Flow with fresh water should then be commenced and we would observe what happens when the $CaSO_4$ precipitate is used up. Perhaps the "adsorption" might be supplied by a clay material in which ion exchange behaves rather like an adsorption process.

Appendices

Appendix A

The solution of the Riemann problem for the Buckley-Leverett equation

The polymer flood model (see Chapter 1) is described by two PDEs:

$$\frac{\partial s}{\partial t} + \frac{\partial}{\partial x} f(s,c) = 0 \tag{A.1}$$

$$\frac{\partial}{\partial t}[s \cdot c + a(c)] + \frac{\partial}{\partial x}[c \cdot f(s,c)] = 0 \tag{A.2}$$

Here, $s \in [0,1]$ is the normalised water saturation, $c \in [0,1]$ is the normalised polymer concentration and $a(c)$ an adsorption isotherm. We take take the fractional flow function $f = f(s,c)$ to be of the form

$$f(s,c) = \frac{1}{1 + \dfrac{(1-s)^{n_o}}{s^{n_w} M(c)}} \tag{A.3}$$

where $M(c) = k^o_{rw}\mu_o / k^o_{ro}\mu_w(c)$ is the end-point mobility ratio ([29], [43]). For the calculations presented in Appendix B we take end-point relative permeabilities $k^o_{rw} = 0.3$, $k^o_{ro} = 0.9$ and oil viscosity $\mu_o = 1$. Because of the polymer treatment, the water viscosity is a function of the polymer concentration $c \in [0,1]$ and is taken to be $\mu_w(c) = 1 + 39c^2$. Finally, we use $n_w = 2$ and $n_o = 3$ in equation (A.3).
The graph of f is S-shaped for all values of c and satisfies the assumptions of the

solution put forward in [31]. Note that, if c is held constant, then $f = f(s)$ and equations (A.1)-(A.2) reduce to the *Buckley-Leverett equation*:

$$\frac{\partial s}{\partial t} + \frac{\partial f(s)}{\partial x} = 0 \tag{A.4}$$

This is an example of a *scalar conservation law* with *flux function* f and *conserved quantity* $s(x,t)$. Using the chain rule, equation (A.4) can be re-written in terms of the *characteristic speed* $f'(s)$:

$$\frac{\partial s}{\partial t} + f'(s)\frac{\partial s}{\partial x} = 0 \tag{A.5}$$

where

$$f'(s) = M^{-1}s^{-n_w-1}(1-s)^{n_0-1}\left[n_0 s + n_w(1-s)\right]f(s)^2 \tag{A.6}$$

Now consider the *Cauchy Problem* for equation (A.5) with initial conditions prescribed along the x-axis:

$$s(0,x) = s_0(x) \tag{A.7}$$

The characteristic projections are the curves defined by the ODE

$$\frac{dx}{dt} = f'(s(x,t)) \tag{A.8}$$

Note that any solution of equation (A.5) is constant along these curves:

$$\frac{d}{dt}[s(x(t),t)] = \frac{\partial s}{\partial t} + \frac{dx}{dt}\frac{\partial s}{\partial x} = \frac{\partial s}{\partial t} + f'(s)\frac{\partial s}{\partial x} = 0 \tag{A.9}$$

This also implies that the characteristic projections on the x-t plane are straight lines with slopes $1/f'(s_0(x))$, determined solely by the characteristic speeds of the initial data. Three different scenarios may be envisaged. If $s_0(x) = s^c$ is constant on some interval $x_l \leq x \leq x_r$, then the characteristic projections emanating from this interval are parallel lines. They span a region of constant state, where the solution is $s(x,t) = s^c$. If $s_0(x)$ is not constant on $x_l \leq x \leq x_r$, but such that $f'(s_0(x))$ is monotone increasing on this interval, then the characteristic projections fan out

clock-wise in what is called an *expansion wave*. This solution region is bounded by the characteristic of slope $1/f'(s^l)$ through $x = x_l$ and the characteristic of slope $1/f'(s^r)$ through $x = x_r$. For the special case that $x_l = x_r$, but $s_l \neq s_r$ and $f'(s)$ is monotone increasing between s^l and s^r, we obtain an expansion wave emanating from $x = x_l = x_r$, also called a *rarefaction wave*. Finally, if $f'(s_0(x))$ is monotone decreasing on $x_l \leq x \leq x_r$, the characteristic projections fan out counter-clockwise in a *contraction wave*. In finite time, this will lead to a shock wave. If $x_l = x_r$, $s_l \neq s_r$ the shock forms immediately. Moreover, if the shock-path $x = \sigma(t)$ divides two regions of constant states s_l, s_r, then we deduce the (constant) speed of the shock from the Rankine-Hugoniot relation (see equation (2.16)):

$$v_\sigma = \frac{d\sigma}{dt} = \frac{f(s_l) - f(s_r)}{s_l - s_r} \tag{A.10}$$

Then, the shock-solution is

$$s(x,t) = \begin{cases} s_l & \text{if } x < v_\sigma t \\ s_r & \text{if } x > v_\sigma t \end{cases} \tag{A.11}$$

An entropy condition is needed to determine if the shock is physically admissible and a common way to to this is by adding a small viscosity term ϵs_{xx} on the right hand side of equation (A.4):

$$s_t + [f(s)]_x = \epsilon s_{xx} \tag{A.12}$$

The idea is that this equation is physically more realistic and thus we will require that any solution of equation (A.4) should be the limit of solutions of equation (A.12) as $\epsilon \to 0$. The *travelling wave entropy condition* consists of demanding that equation (A.11) is the limit as $\epsilon \to 0$ of classical solutions of equation (A.12) having the form $S = S((x - v_\sigma t)/\epsilon)$. Letting $z = (x - v_\sigma t)/\epsilon$, substitution of S into equation (A.12) gives

$$-\frac{v_\sigma}{\epsilon} S'(z) + \frac{1}{\epsilon}[f(S(z))]' = \frac{1}{\epsilon} S''(z) \tag{A.13}$$

Multiplying through by ϵ and integrating, we find

$$-v_\sigma S + f(S) + A = S' \tag{A.14}$$

To determine the constant A, remember that we must recover equation (A.11) in the limit $\epsilon \to 0$. Note that if $x > v_\sigma t$, then $z \to \infty$ as $\epsilon \to 0$. Similarly, $z \to -\infty$ if $x < v_\sigma t$. Thus, we need $S(+\infty) = s_r$, $S(-\infty) = s_l$. Since s_r and s_l are constants, the derivative vanishes, i.e. $S'(\pm\infty) = 0$. Considering separately $z = +\infty$ and $z = -\infty$ we find

$$A = -f(s_r) + v_\sigma s_r = -f(s_l) + v_\sigma s_l \tag{A.15}$$

Rearranging this, we see that the travelling wave entropy condition for a shock solution with constant speed v_σ also incorporates the Rankine-Hugoniot condition (this is not true in general for entropy conditions).

From equation (A.14),

$$\int \frac{dS}{f(S) - v_\sigma S + A} = \int dz = z \tag{A.16}$$

To have a solution $S = S(z)$ the left hand side (a function of S) needs to be invertible on the interval $[s_r, s_l]$. This means that it should be monotone increasing or decreasing on the open interval (s_r, s_l). We deduce that the sign of $f(S) - \sigma S + A$ must be constant and thus $S' > 0$ or $S' < 0$. In particular, if $s_l > s_r$, then $S' < 0$ on (s_r, s_l). So

$$f(S) - f(s_l) < v_\sigma(S - s_l) \tag{A.17}$$

for all $S \in (s_r, s_l)$. On the other hand, if $s_l < s_r$ we obtain

$$f(S) - f(s_l) > v_\sigma(S - s_l) \tag{A.18}$$

We can combine (A.17) and (A.18) to get a single inequality:

$$v_\sigma|S - s_l| < sign(S - s_l)(f(S) - f(s_l)) \tag{A.19}$$

This has to hold for all $S \in (s_r, s_l)$. It expresses the travelling wave entropy condition and is equivalent to the statement that the graph of $f = f(s)$ lies entirely above

or below the straight line segment of slope v_σ connecting the two points $(s_l, f(s_l))$ and $(s_r, f(s_r))$, depending on whether $s_l < s_r$ or $s_l > s_r$ respectively.

The *Riemann problem* for equation (A.5) is the special case in which the Cauchy data are piecewise constant, with a jump discontinuity at the origin:

$$s_0(x) = \begin{cases} s^L & \text{if } x < 0 \\ s^R & \text{if } x > 0 \end{cases} \tag{A.20}$$

In general, the solution to the Riemann problem will not consist of a single (entropy-satisfying) shock wave or rarefaction wave and the strategy is to look for intermediate constant states $s^L = s^0, s^1, ..., s^n, s^{n+1} = s^R$ such that the pairs (s^i, s^{i+1}), $i = 0, ..., n$ can each be connected by a solution of either type. We then obtain a sequence of 'waves'

$$s^L \longrightarrow s^1 \longrightarrow s^2 \longrightarrow .... \longrightarrow s^n \longrightarrow s^R \tag{A.21}$$

To ensure that the individual waves don't overtake each other, we will impose the following rule for such compositions:

Definition (Compatibility Criterion): Given a sequence

$$s^L \longrightarrow s^M \longrightarrow s^R$$

we say the two waves are *compatible* if the right-end speed of the wave $s^L \longrightarrow s^M$ is less than or equal to the left-end speed of the wave $s^M \longrightarrow s^R$. If both waves are shocks, we require strict inequality, otherwise they would form a single shock.

Note that the fractional flow curve satisfies $f'(0) = f'(1) = 0$ and $f'(s) > 0$ for all $s \in (0, 1)$. Thus, f' has a unique maximum at some $s^I \in (0, 1)$, which corresponds to an inflection point on the graph of f (see Figure A.1). This leads to several possible solutions of the Riemann problem with $s^L > s^R$:

Case (i): $s^I \leq s^R < s^L$. Now, the entropy condition for a shock is not satisfied since $s^R < s^L$ and the graph of f lies above the line segment joining $(s^R, f(s^R))$ and $(s^L, f(s^L))$. A solution consisting of a single shock wave is therefore not possible. However, f' is monotone increasing between s^L and s^R (note the direction here!), so

that we can connect these states by a single rarefaction wave.

For the remaining cases, we must have $s^R < s^I$. Consider the line through the point $(s^R, f(s^R))$ which is tangent to the graph of f at some $s^* > s^I$. We will refer to this line as the *Welge tangent with respect to* s^R (see Figure A.1).

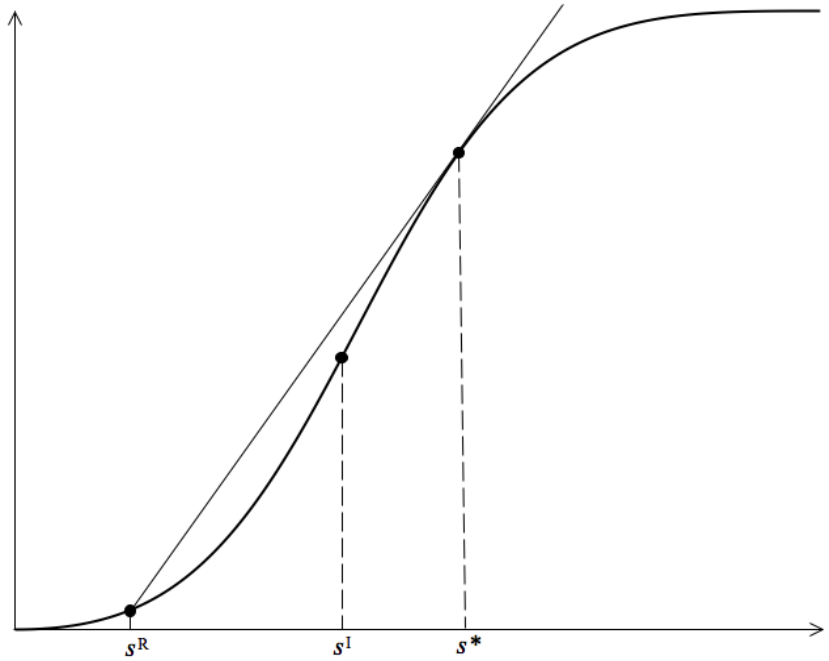

Figure A.1: *Construction of the Welge tangent when* $s^R < s^I$.

Case (ii): $s^R < s^I < s^L \leq s^*$. Since the graph of f now lies entirely below the line segment joining $(s^R, f(s^R))$ and $(s^L, f(s^L))$, it satisfies the entropy condition for a single shock wave of speed

$$\sigma = \frac{f(s^L) - f(s^R)}{s^L - s^R} \tag{A.22}$$

Case (iii): $s^R < s^I$, $s^L > s^*$. Now s^L and s^R cannot be joined directly by a shock wave, because this would violate the entropy condition. A single rarefaction wave is also not possible since f' is not monotone increasing between the states. Thus, we require at least one intermediate state, s^M, such that $s^* \geq s^M$ (otherwise we are back to the original problem). To connect s^M to s^L, we need $s^M \geq s^I$. In particular, the wave $s^L \to s^M$ is a rarefaction (by Case (i)). Since $s^* \geq s^M$, Case (ii) implies that we may connect s^M to s^R by a shock wave of speed

$$v_M = \frac{f(s^M) - f(s^R)}{s^M - s^R} \tag{A.23}$$

The entropy condition demands $f'(s^M) \geq \sigma_M$. Finally, for the sequence $s^L \to s^M \to s^R$ to be compatible, we also need $f'(s^M) \leq \sigma_M$. Putting this together, we find that $f'(s^M) = \sigma_M$, which shows that $s^M = s^*$.

A further three cases are obtained with an analogous argument for $s^L < s^R$. The main difference is that the point $(s^*, f(s^*))$ is now constructed when $s^R > s^I$ and lies on the convex part of the graph (in other words, $s^* < s^I$ now). For simplicity and cataloguing purposes in Appendix B, let us introduce a shorthand notation for these solution sequences. Let s_d^{rf} denote the downward rarefaction wave (Case (i)), s_d^{sk} the downward shock solution (Case (ii)) and $s_d^{rf} s_d^{sk}$ the composition of the downward shock *followed* by the downward rarefaction (Case (iii)). Similarly, we shall write s_u^{rf}, s_u^{sk} and $s_u^{rf} s_u^{sk}$ for the upward solutions (Cases (iv), (v) and (vi)).

Appendix B

The Riemann problem for the system of PDEs describing a polymer flood

B.1 Equivalent matrix versions

Consider equations (A.1) and (A.2) and the fractional flow function (A.3) described at the beginning of Appendix A. The mobility ratio $M = M(c)$ is strictly decreasing. This means that $\partial f/\partial c < 0$ for all $s \in (0,1)$ and $c \in [0,1]$. Furthermore, the adsorption function $a : [0,1] \to \mathbb{R}$ in equation (A.2) is assumed to be smooth and monotone increasing. Consider the map $\psi : [0,1]\times[0,1] \to [0,1]\times[0,\infty)$ which takes (s,c) to $\psi(s,c) = (s,b)$, where $b = sc + a(c)$. Since $a(c)$ is monotone increasing, ψ constitutes an invertible change of coordinates. By defining the functions $G_1(s,b) := f(s,c(s,b))$ and $G_2(s,b) := f(s,c(s,b))\cdot c(s,b)$ we can put equations (A.1) and (A.2) into the canonical form with conserved quantities s and b:

$$\frac{\partial s}{\partial t} + \frac{\partial}{\partial x} G_1(s,b) = 0 \tag{B.1}$$

$$\frac{\partial b}{\partial t} + \frac{\partial}{\partial x} G_2(s,b) = 0 \tag{B.2}$$

The standard way to proceed would be to find the Jacobian matrix $D\mathbf{G}$ of this system and analyse its eigenvalues in the coordinates s and b. Instead, we transform the system back to (s,c) coordinates via the map ψ^{-1}. We have

$$D\psi = \begin{pmatrix} 1 & 0 \\ c & s + a'(c) \end{pmatrix} \quad , \quad (D\psi)^{-1} = \frac{1}{s + a'(c)} \begin{pmatrix} s + a'(c) & 0 \\ -c & 1 \end{pmatrix} \tag{B.3}$$

Now, in matrix form, the system given by (B.1) and (B.2) is written as

$$\begin{pmatrix} s \\ b \end{pmatrix}_t + D\mathbf{G}(s,b) \cdot \begin{pmatrix} s \\ b \end{pmatrix}_x = \begin{pmatrix} 0 \\ 0 \end{pmatrix} \tag{B.4}$$

Note that

$$\begin{pmatrix} s \\ b \end{pmatrix}_t = \frac{\partial}{\partial t}\psi(s,c) = D\psi \cdot \begin{pmatrix} s \\ c \end{pmatrix}_t \quad \text{and} \quad \begin{pmatrix} s \\ b \end{pmatrix}_x = D\psi \cdot \begin{pmatrix} s \\ c \end{pmatrix}_x \tag{B.5}$$

Substituting these into (B.4) and multiplying both sides by $(D\psi)^{-1}$, we obtain

$$\begin{pmatrix} s \\ c \end{pmatrix}_t + \underbrace{(D\psi)^{-1} \cdot D\mathbf{G}(s,b) \cdot D\psi}_{\text{matrix A=A(s,c)}} \begin{pmatrix} s \\ c \end{pmatrix}_x = \begin{pmatrix} 0 \\ 0 \end{pmatrix} \tag{B.6}$$

Consider the matrix $A(s,c) = (D\psi)^{-1} \cdot D\mathbf{G}(s,b) \cdot D\psi$ in equation (B.6). Because A is similar to $D\mathbf{G}$, they have the same eigenvalues. For an analysis of the properties such as the hyperbolicity of the system of conservation laws given by (B.1), (B.2) it thus suffices to study the eigenvalues of A. We note that, in $D\mathbf{G}$, we have

$$\frac{\partial G_2}{\partial s} = \frac{\partial c}{\partial s} G_1 + c\frac{\partial G_1}{\partial s} \quad \text{and} \quad \frac{\partial G_2}{\partial b} = \frac{\partial c}{\partial b} G_1 + c\frac{\partial G_1}{\partial b} \tag{B.7}$$

Then, carrying out the matrix multiplications in (B.6), we find

$$A = \begin{pmatrix} \dfrac{\partial G_1}{\partial s} + c\dfrac{\partial G_1}{\partial b} & (s + a'(c))\dfrac{\partial G_1}{\partial b} \\ (s + a'(c))^{-1}\left(\dfrac{\partial c}{\partial s} + c\dfrac{\partial c}{\partial b}\right) G_1 & \dfrac{\partial c}{\partial b} G_1 \end{pmatrix} \tag{B.8}$$

To simplify the entries of this matrix further, we observe that

$$\frac{\partial G_1}{\partial s} = \frac{\partial f}{\partial s} + \frac{\partial c}{\partial s}\frac{\partial f}{\partial c} \quad \text{and} \quad \frac{\partial G_1}{\partial b} = \frac{\partial c}{\partial b}\frac{\partial f}{\partial c} \tag{B.9}$$

Differentiating $b = sc + a(c)$ with respect to s and b we obtain

$$\frac{\partial c}{\partial s} = \frac{-c}{s + a'(c)} \quad \text{and} \quad \frac{\partial c}{\partial b} = \frac{1}{s + a'(c)} \tag{B.10}$$

Substituting these into equation (5.76) then yields

$$A(s,c) = \begin{pmatrix} \partial f/\partial s & \partial f/\partial c \\ 0 & \dfrac{f(s,c)}{s + a'(c)} \end{pmatrix} \tag{B.11}$$

The eigenvalues of this matrix are $\lambda_1 = \partial f/\partial s$ and $\lambda_2 = f(s,c)/(s + a'(c))$. The λ_1-eigenvector of A is $\mathbf{e}_1 = (1,0)$ and the λ_2-eigenvector is $\mathbf{e}_2 = (\partial f/\partial c, \lambda_2 - \lambda_1)$. Note that for each value $c \in [0,1]$, there is a unique value of s such that $\lambda_1(s,c) = \lambda_2(s,c)$. The set of these points is called the *transition curve* $\mathcal{T}$, which is continuous because $f(s,c)$ and $a(c)$ are smooth. The transition curve divides the state space $[0,1]\times[0,1]$ into regions where $\lambda_1 > \lambda_2$ and $\lambda_1 < \lambda_2$. The system of equations is strictly hyperbolic everywhere except on $\mathcal{T}$.

Definition: In the Riemann problem with left state $\mathbf{u}^\ell$ and right state $\mathbf{u}^r$ a simple j-rarefaction wave is a solution of the form

$$\mathbf{u}(x,t) = \begin{cases} \mathbf{u}^\ell & \text{if } \; x \le \lambda_j(\mathbf{u}^\ell)t \\ \mathbf{v}(x/t) & \text{if } \; \lambda_j(\mathbf{u}^\ell)t \le x \le \lambda_j(\mathbf{u}^r)t \\ \mathbf{u}^r & \text{if } \; x \ge \lambda_j(\mathbf{u}^r)t \end{cases} \tag{B.12}$$

where $\mathbf{v}$ is an integral curve of the eigenvector $\mathbf{e}_j$ which connects $\mathbf{u}^\ell$ and $\mathbf{u}^r$. Moreover, the characteristic speed $\lambda_j = \lambda_j(\mathbf{u})$ is required to be monotone increasing from $\lambda_j(\mathbf{u}^\ell)$ at $\mathbf{u}^\ell$ to $\lambda_j(\mathbf{u}^r)$ at $\mathbf{u}^r$. The integral curve of $\mathbf{e}_j$ is then called the j-rarefaction curve through $\mathbf{u}^\ell$.

We first determine possible rarefaction waves of equation (B.6). Away from the transition curve $\mathcal{T}$, the matrix $A = A(\mathbf{u})$ has two distinct eigenvalues λ_1 and λ_2. Through a state $\mathbf{u}^\ell$, there are therefore two integral curves corresponding to the eigenvectors $\mathbf{e}_1$ and $\mathbf{e}_2$. The integral curve of $\mathbf{e}_1 = (1,0)$ through $\mathbf{u}^\ell$ is the line

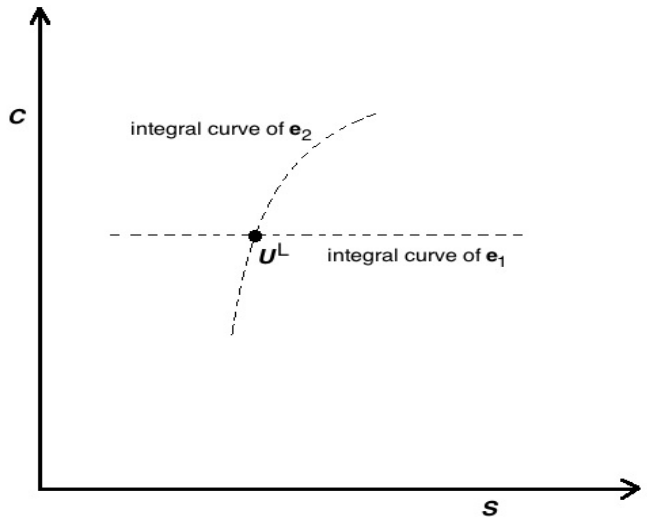

Figure B.1: Integral curves through $\mathbf{u}^L$.

$c = c^\ell$ in the (s, c)-plane (see Figure B.1). Thus, another state $\mathbf{u}^r$ can be connected to $\mathbf{u}^\ell$ by a 1-rarefaction wave only if $c^\ell = c^r$ and $\lambda_1(s, c^\ell) = f_s(s, c^\ell)$ is increasing in the direction *from* $\mathbf{u}^\ell$ *to* $\mathbf{u}^r$. For λ_2, note that an integral curve of $\mathbf{e}_2 = (\partial f/\partial c, \lambda_2 - \lambda_1)$ has a local maximum when it intersects the transition curve $\mathcal{T}$. Moreover, it was shown in [31] that two states $\mathbf{u}^\ell$, $\mathbf{u}^r$ on this integral curve can be joined by a 2-rarefaction wave if c is increasing as we go from $\mathbf{u}^\ell$ to $\mathbf{u}^r$. This implies that the two states must lie on the same side of the transition curve $\mathcal{T}$ and that $c^\ell < c^r$.

Definition: Given a Riemann problem with constant states $\mathbf{u}^\ell$ and $\mathbf{u}^r$, we define a shock wave with shock speed σ to be a solution of the form

$$\mathbf{u}(x,t) = \begin{cases} \mathbf{u}^\ell & \text{if } x < \sigma t \\ \mathbf{u}^r & \text{if } x > \sigma t \end{cases} \tag{B.13}$$

Analogous to the case of a scalar conservation law, a physically relevant shock wave has to satisfy the Rankine-Hugoniot conditions. Since these conditions only involve the conserved quantities across the discontinuity, we have to be careful to use the flux functions of the system in canonical form as given by equations $(B.1)$ and $(B.2)$. The conditions then read

$$f(\mathbf{u}^r) - f(\mathbf{u}^\ell) = \sigma(s^r - s^\ell) \tag{B.14}$$

$$c^r f(\mathbf{u}^r) - c^L f(\mathbf{u}^\ell) = \sigma\left[s^r c^r + a(c^r) - s^\ell - a(c^\ell)\right] \tag{B.15}$$

Given a state $\mathbf{u}^\ell = (s^\ell, c^\ell)$, equations (B.14) and (B.15) determine the set of states $\mathbf{u}^r$ which could be joined to $\mathbf{u}^\ell$ by means of a c-shock wave. This defines a shock curve through the state $\mathbf{u}^\ell$. As was mentioned in Chapter 2, the Rankine-Hugoniot relations turn out not to be restrictive enough and therefore the travelling wave entropy condition was imposed by adding small diffusive terms on the right hand side of the system. It was shown in [31] that this leads to the following additional requirements for a c-shock of speed σ:

1. $c^\ell > c^r$

2. either $f_s(\mathbf{u}^r) < \sigma$ or $f_s(\mathbf{u}^\ell), f_s(\mathbf{u}^r) \geq \sigma$

The Riemann problem was then divided into the two cases $c^L > c^R$ and $c^L < c^R$.

B.2 Solutions with $c^L > c^R$

It can be shown that in a sequence of compatible waves of the form

$$\mathbf{u}^1 \xrightarrow{c1} \mathbf{u}^2 \xrightarrow{s} \mathbf{u}^3 \xrightarrow{c2} \mathbf{u}^4 \tag{B.16}$$

the two c-waves must be rarefaction waves. For the Riemann Problem with $c^L > c^R$, this implies that if there are more than two c-waves in the solution, they must all be c-rarefactions. But we already saw that a necessary condition for the existence of a c-rarefaction is that c increases in it. Since c stays constant in s-waves, the assumption that $c^L > c^R$ now prohibits the existence of any c-rarefaction wave. Therefore, there can only be one c-wave, and this must be a c-shock.
Consider the left state $\mathbf{u}^L = (s^L, c^L)$ and define the quantity

$$h_L(c) = \begin{cases} \dfrac{a(c) - a(c^L)}{c - c^L} & \text{if } \ c \neq c^L \\ a'(c) & \text{if } \ c = c^L \end{cases} \tag{B.17}$$

The single c-shock must connect $\mathbf{u}^L$ to a state $\mathbf{u}^r = (s^r, c^R)$. Using equation (B.17), the Rankine-Hugoniot for the c-shock can now be written in one line as

$$\frac{f(s^r, c^R)}{s^r + h_L(c^R)} = v_\sigma = \frac{f(s^L, c^L)}{s^L + h_L(c^R)} \tag{B.18}$$

In addition to this, we need $f_s(\mathbf{u}^r) < v_\sigma$ *or* $f_s(\mathbf{u}^L), f_s(\mathbf{u}^r) \geq v_\sigma$. Note that, whereas c remains constant in s-waves, s can vary in c-waves. In the following analysis we will say that a c-shock is "downward" if s is decreasing in it and denote this by c_d^{sk}. On the other hand, an "upward" c-shock, in which s increases, will be denoted as c_u^{sk}.

B.2.1 Case 1: $c^L > c^R$, $f_s(\mathbf{u}^L) \geq \frac{f(s^L,c^L)}{s^L+h_L(c^R)}$

Let the state $\mathbf{u}^M = (s^M, c^R)$ and the value $s^K(\mathbf{u}^M)$ be defined by the construction shown in Figure B.2.

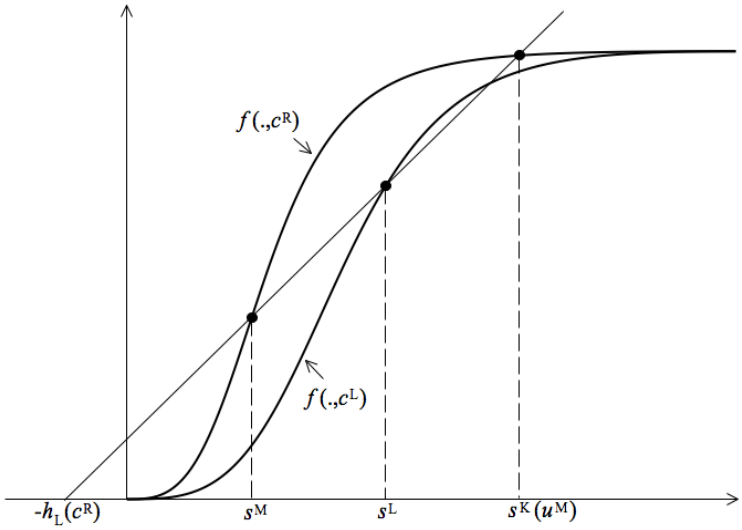

Figure B.2

(A) If $s^R < s^K(\mathbf{u}^M)$ we have the solution sequence

$$u^L \xrightarrow{c-shock} u^M \xrightarrow{s-wave} u^R \tag{B.19}$$

The c-shock is downward ($s^M < s^L$) and the s-wave can take any of the six forms discussed in Appendix A. Examples of these are produced as follows: let $a(c) = c^{0.9}$ and pick initial data $\mathbf{u}^L = (0.7, 1)$, $\mathbf{u}^R = (0.1, 0)$. The left state satisfies the conditions for Case 1. We then compute $s^M = 0.2356$ and $s^K(u^M) = 0.9810$, so that $s^R < s^K(u^M)$ as required. In order to determine the type of the s-wave that connects $\mathbf{u}^M$ to $\mathbf{u}^R$, we note that $s^M > s^R$. The inflection point of the graph of $f(s, 0)$ is at $s^I = 0.1573$ and the Welge tangent with respect to s^R is at $s^* = 0.1886$. Therefore the s-wave consists of a downward shock connecting the states $(s^*, 0)$ and $(s^R, 0)$, followed by a downward rarefaction connecting the states $(s^M, 0)$ and $(s^*, 0)$.

The full solution sequence $c_d^{sk} s_d^{rf} s_d^{sk}$ is plotted in figure B.3.

If we change the right state to $\mathbf{u}^R = (0.3, 0)$ and keep $\mathbf{u}^L = (0.7, 1)$, then $s^R > s^M$ and the Welge tangent with respect to s^R is at $s^* = 0.0656$. Then $s^* < s^M < s^R$ and the s-wave is an upward shock. The solution sequence $c_d^{sk} s_u^{sk}$ is shown in figure B.4. The four remaining variants $c_d^{sk} s_d^{sk}$, $c_d^{sk} s_d^{rf}$, , $c_d^{sk} s_u^{rf} s_u^{sk}$, , $c_d^{sk} s_u^{rf}$, are plotted in figures B.5-B.8.

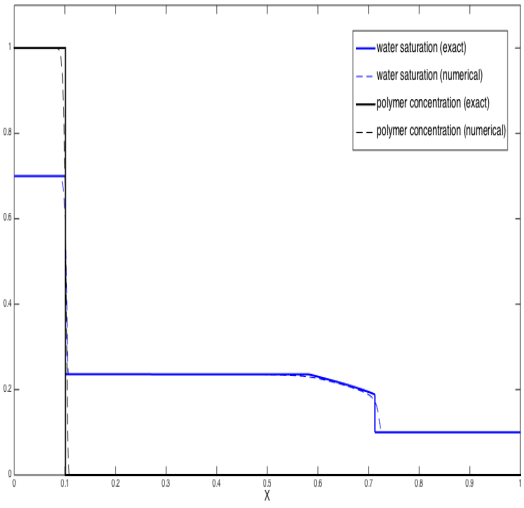

Figure B.3: $c_d^{sk} s_d^{rf} s_d^{sk}$,
$u^L = (0.7, 1)$, $u^R = (0.1, 0)$.

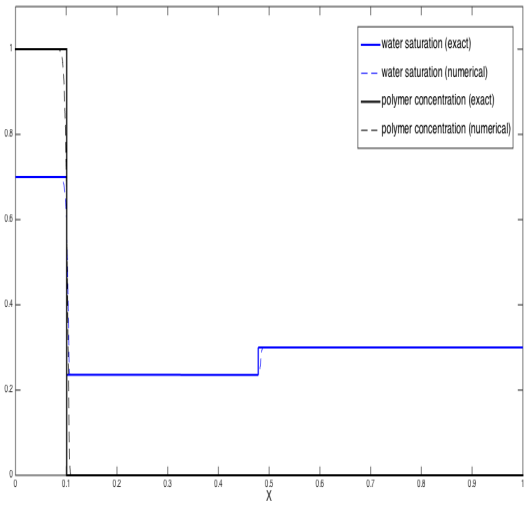

Figure B.4: $c_d^{sk} s_u^{sk}$,
$u^L = (0.7, 1)$, $u^R = (0.3, 0)$.

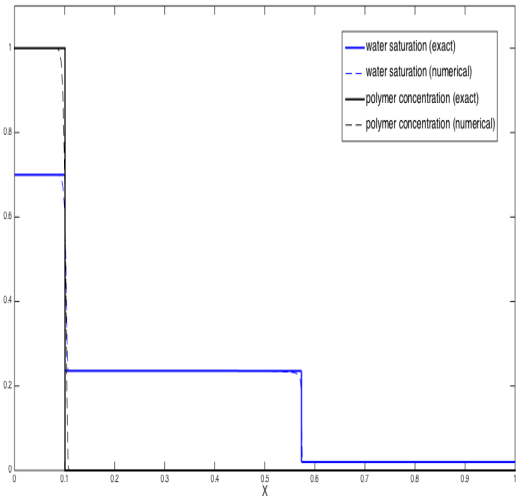

Figure B.5: $c_d^{sk} s_d^{sk}$,
$u^L = (0.7, 1)$, $u^R = (0.02, 0)$

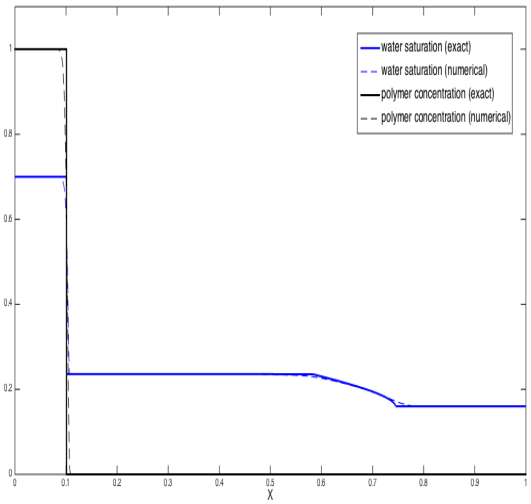

Figure B.6: $c_d^{sk} s_d^{rf}$,
$u^L = (0.7, 1)$, $u^R = (0.16, 0)$.

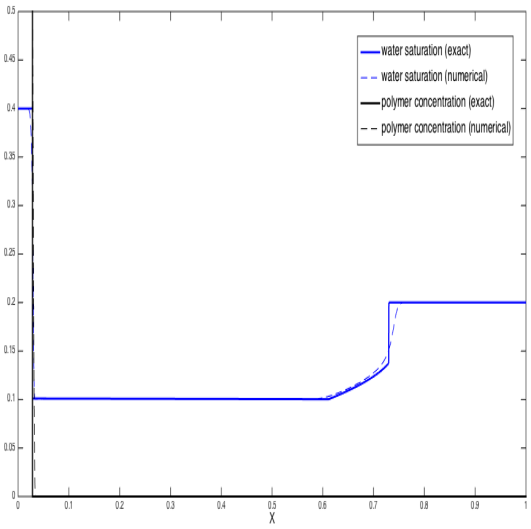

Figure B.7: $c_d^{sk} s_u^{rf} s_u^{sk}$,
$u^L = (0.4, 1)$, $u^R = (0.2, 0)$.

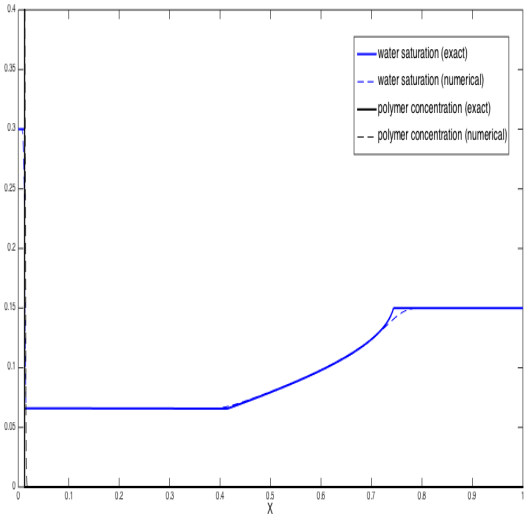

Figure B.8: $c_d^{sk} s_u^{rf}$,
$u^L = (0.3, 1)$, $u^R = (0.15, 0)$.

(B) If $s^R \geq s^K(\mathbf{u}^M)$ in Figure B.2, the sequence given by equation (B.19) does not work. This is because the s-wave could now only be an upward shock with speed less than the c-shock, which means that the sequence is not compatible. This situation is dealt with by defining the state $\mathbf{u}^N = (s^N, c^L)$ as shown in Figure B.9, and then the sequence

$$u^L \xrightarrow{s-wave} u^N \xrightarrow{c-shock} u^R \tag{B.20}$$

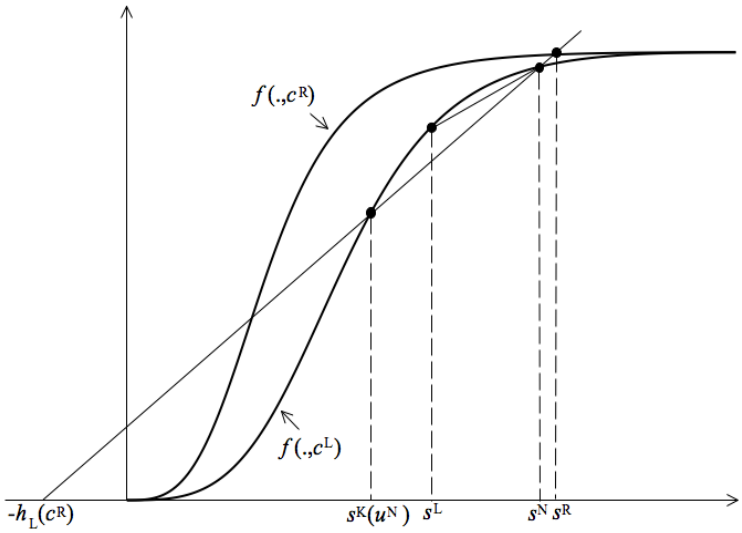

Figure B.9

The c-shock is upward ($s^N < s^R$) and the s-wave connecting $\mathbf{u}^L$ to $\mathbf{u}^N$ can only be an upward shock, since $s^L < s^N$ and they both lie above the Welge tangent point with respect to s^N. To get an example of this solution, we let $a(c) = c^{0.05}$ and choose $u^L = (0.68, 0.8)$ and $u^R = (0.77, 0.6)$. The left state $\mathbf{u}^L$ satisfies the

conditions for Case 1. We find $s^M = 0.5272$ and $s^K(u^M) = 0.7617$. Note that $s^R > s^K(u^M)$ now and we must calculate the new intermediate state $u^N = (s^N, c^L)$. We find $s^N = 0.7367$. The solution sequence $c_u^{sk} s_u^{sk}$ is plotted figure B.10. The numerical solution only captures these two successive upward shocks for increased grid-sizes (20000+ grid-blocks).

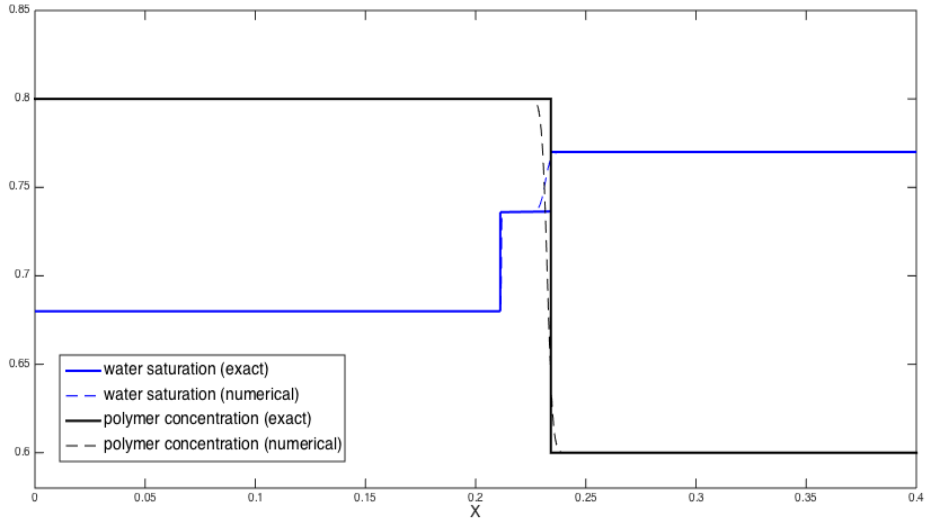

Figure B.10: *Solution* $c_u^{sk} s_u^{sk}$ *with* $u^L = (0.68, 0.8)$ *and* $u^R = (0.77, 0.6)$.

B.2.2 Case 2: $c^L > c^R$, $f_s(\mathbf{u}^L) < \frac{f(s^L, c^L)}{s^L + h_L(c^R)}$

Define the states $\mathbf{u}^* = (s^*, c^L)$, $\mathbf{u}^M = (s^M, c^R)$ and the value $s^K(\mathbf{u}^M)$ by the construction shown in Figure B.11.

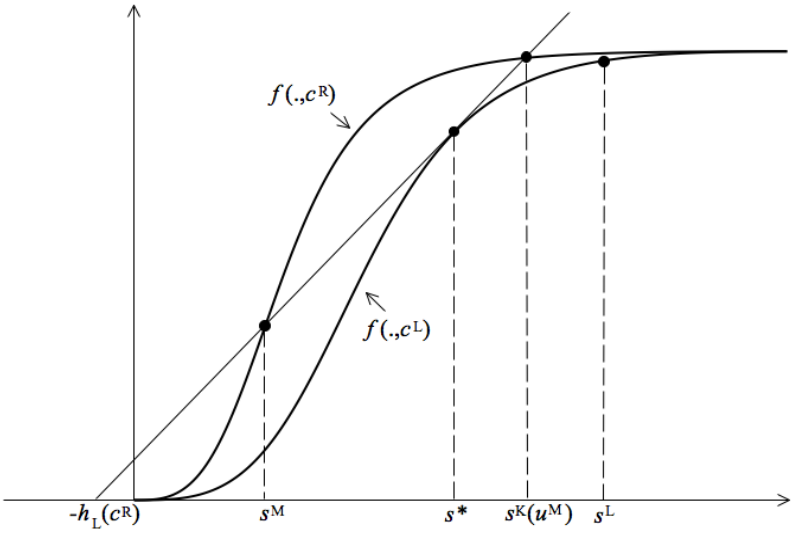

Figure B.11

(A) If $s^R < s^K(\mathbf{u}^M)$ we have the solution sequence

$$u^L \xrightarrow{s-wave} u^* \xrightarrow{c-shock} u^M \xrightarrow{s-wave} u^R \tag{B.21}$$

The c-shock is downward ($s^* > s^M$). The first s-wave $\mathbf{u}^L \to \mathbf{u}^*$ is a downward rarefaction, because $s^L > s^*$ and both lie above the inflection point on the graph of $f(., c^L)$. The second s-wave $\mathbf{u}^M \to \mathbf{u}^R$ can take any of the six forms of Appendix A. For examples of these solutions, choose $a(c) = c^{0.9}$, $\mathbf{u}^L = (0.9, 1)$ and $\mathbf{u}^R = (0.05, 0)$. The left state now satisfies the conditions for Case 2. We compute $s^* = 0.8104$, $s^M = 0.2527$ and $s^K(u^M) = 0.8663$, so that $s^R < s^K(u^M)$. To see what type of s-wave connects $\mathbf{u}^M$ to $\mathbf{u}^R$, we calculate the Welge tangent with respect to s^R. This lies at $s^{**} = 0.2193$. Then $s^M > s^{**} > s^R$ and we have a downward shock connecting $\mathbf{u}^{**}$ to $\mathbf{u}^R$, followed by a downward rarefaction connecting $\mathbf{u}^M$ to $\mathbf{u}^{**}$. The solution sequence $s_d^{rf} c_d^{sk} s_d^{rf} s_d^{sk}$ is plotted in figure B.12. Choosing the right states $\mathbf{u}^R = (0, 0)$ and $\mathbf{u}^R = (0.16, 0)$ produces the other two downward solutions $s_d^{rf} c_d^{sk} s_d^{sk}$ (figure B.13) and $s_d^{rf} c_d^{sk} s_d^{rf}$ (figure B.14) respectively.

If $\mathbf{u}^R = (0.5, 0)$ we find $s^R > s^M$, so that the s-wave connecting u^M and u^R is upward. The Welge tangent is at $s^{**} = 0.0656$. Thus, since $s^{**} < s^M < s^R$, the solution is $s_d^{rf} c_d^{sk} s_u^{sk}$ (see figure B.15). In order to produce the two remaining cases, let the adsorption function be $a(c) = c^{0.001}$. With $u^R = (0.3, 0.2)$ we find $s^* = 0.7313$ and $s^M = 0.1724$. The inflection point of the graph of $f(s, 0.2)$ is at $s^I = 0.2384$ and the Welge tangent at $s^{**} = 0.2094$. So, $s^M < s^{**} < s^R$ and the s-wave is an upward shock connecting s^{**} to s^R followed by an upward rarefaction connecting s^M to s^{**} (see figure B.16).

Finally, with $u^R = (0.23, 0.2)$ there's only a rarefaction (see figure B.17).

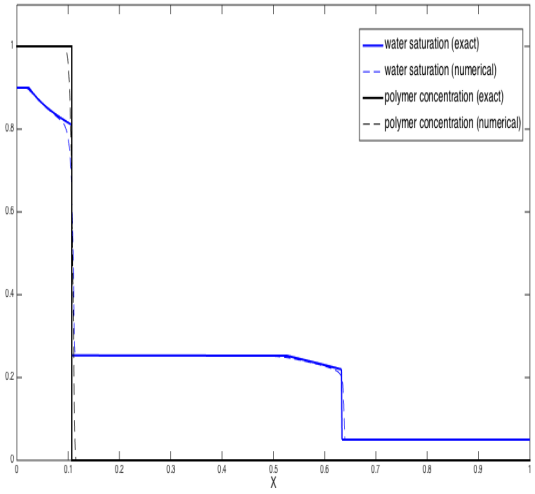

Figure B.12: $s_d^{rf} c_d^{sk} s_d^{rf} s_d^{sk}$, $u^L = (0.9, 1)$ *and* $u^R = (0.05, 0)$.

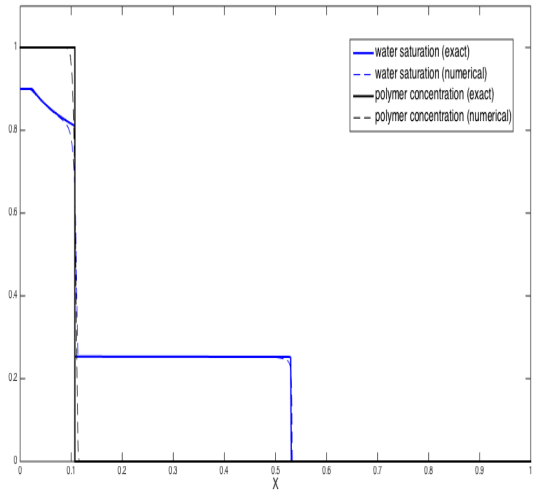

Figure B.13: $s_d^{rf} c_d^{sk} s_d^{sk}$, $u^L = (0.9, 1)$ *and* $u^R = (0, 0)$.

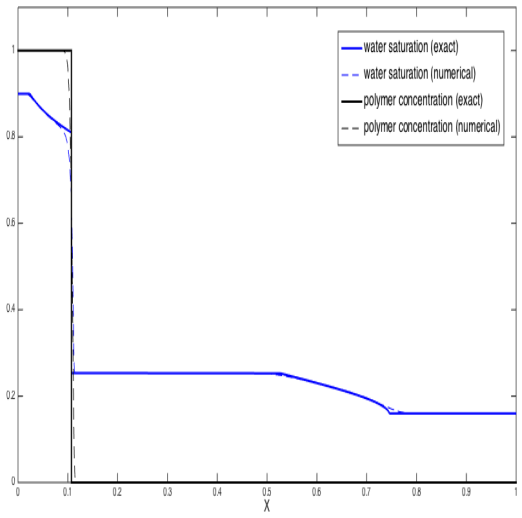

Figure B.14: $s_d^{rf} c_d^{sk} s_d^{rf}$,
$u^L = (0.9, 1)$ *and* $u^R = (0.16, 0)$.

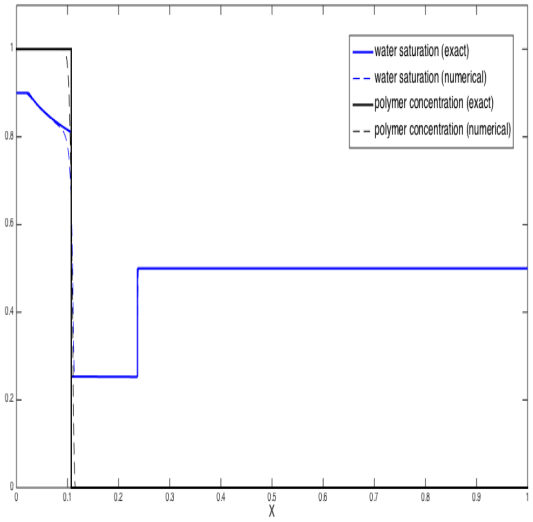

Figure B.15: $s_d^{rf} c_d^{sk} s_u^{sk}$,
$u^L = (0.9, 1)$ *and* $u^R = (0.5, 0)$.

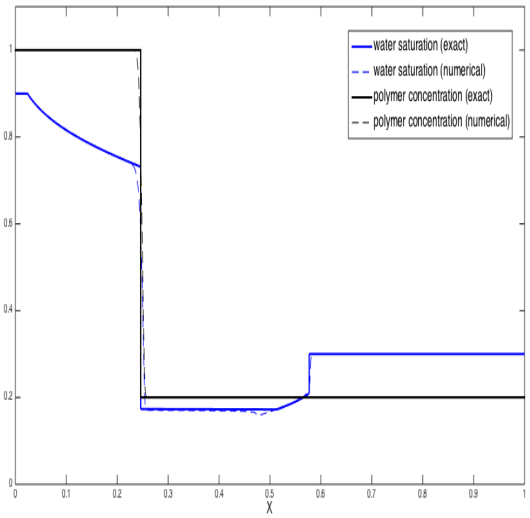

Figure B.16: $s_d^{rf} c_d^{sk} s_u^{rf} s_u^{sk}$,
$u^L = (0.9, 1)$ *and* $u^R = (0.3, 0.2)$.

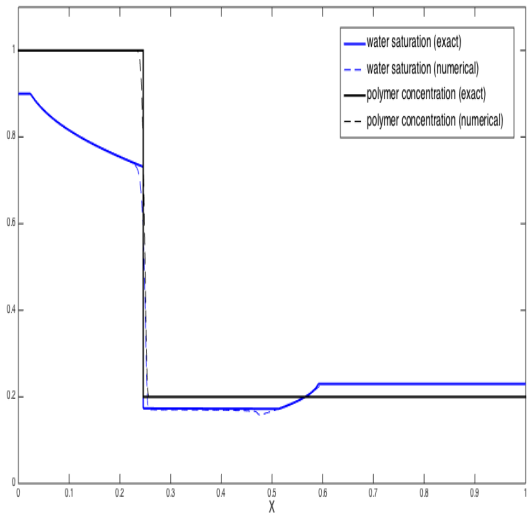

Figure B.17: $s_d^{rf} c_d^{sk} s_u^{rf}$,
$u^L = (0.9, 1)$ *and* $u^R = (0.23, 0.2)$.

(B) If $s^R \geq s^K(\mathbf{u}^M)$, the sequence in equation (B.21) does not work and we look for a state $\mathbf{u}^N = (s^N, c^L)$ as defined by the construction in Figure B.9 for Case 1B. We then have a solution sequence

$$u^L \xrightarrow{s-wave} u^N \xrightarrow{c-shock} u^R \tag{B.22}$$

The c-shock is upward and the s-wave is an upward shock if $s^L < s^N$ (as in Case 1B, Figure B.10) and a downward rarefaction if $s^L > s^N$. For an example of the latter, choose $a(c) = c^{0.9}$, $u^L = (0.95, 1)$ and $u^R = (0.87, 0)$. The critical value is $s^K(u^M) = 0.8663$ and hence $s^R > s^K(u^M)$. We then compute $s^N = 0.8343$. The solution sequence $c_u^{sk} s_d^{rf}$ is plotted in Figure B.18.

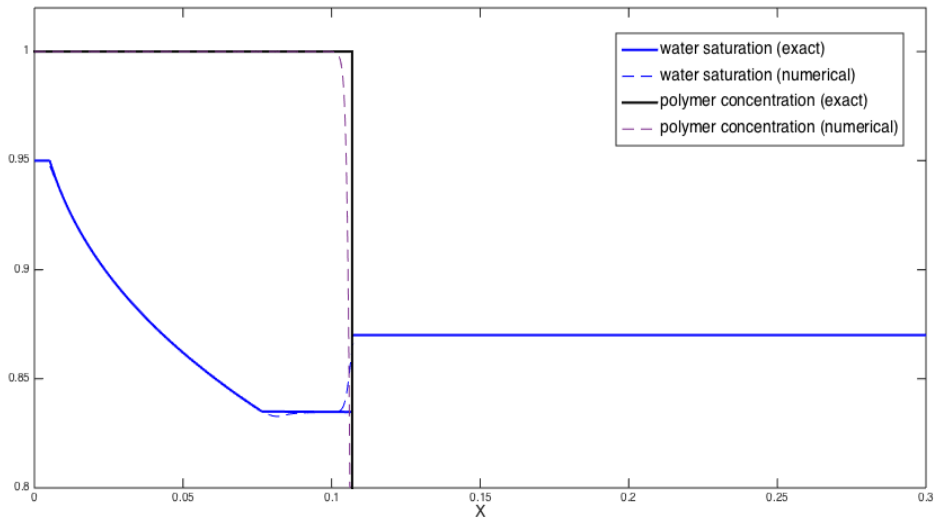

Figure B.18: $c_u^{sk} s_d^{rf}$ *with* $u^L = (0.95, 1)$ *and* $u^R = (0.87, 0)$.

B.3 Solutions with $c^L < c^R$

Recall that the transition curve $\mathcal{T}$ is the set of points at which the eigenvalues $\lambda_1 = f_s$ and $\lambda_2 = f/(s + a'(c))$ are equal. It is continuous and divides $[0,1] \times [0,1]$ into two regions:

$$\mathcal{L} := \{(s,c) \in [0,1] \times [0,1] \ : \ \lambda_1(s,c) > \lambda_2(s,c)\} \tag{B.23}$$

$$\mathcal{R} := \{(s,c) \in [0,1] \times [0,1] \ : \ \lambda_1(s,c) < \lambda_2(s,c)\} \tag{B.24}$$

Suppose that the Riemann problem with $c^L < c^R$ has a solution sequence

$$\mathbf{u}^1 \xrightarrow{c-wave} \mathbf{u}^2 \xrightarrow{s-wave} \mathbf{u}^3 \xrightarrow{c-wave} \mathbf{u}^4 \xrightarrow{s-wave} \mathbf{u}^5 \xrightarrow{c-wave} \mathbf{u}^6 \tag{B.25}$$

We saw earlier that the c-waves in this sequence must all be rarefactions. Johansen/Winther then went on to show that $\mathbf{u}^3 \in \mathcal{R}$ and $\mathbf{u}^4 \in \mathcal{L}$, which means that the c-rarefaction in the middle of this sequence connects two states that lie on different sides of the transition curve $\mathcal{T}$. This is contradiction and therefore, the solution can have at most two c-waves.

B.3.1 Case 3: $c^L < c^R$, $\mathbf{u}^L \in \mathcal{R} \cup \mathcal{T}$

(A) Suppose that $\mathbf{u}^R \in \mathcal{L}$, as in Figure B.19. Let $\mathbf{u}^T = (s^T, c^R) \in \mathcal{T}$ and consider the intermediate state $\mathbf{u}^M = (s^M, c^L) \in \mathcal{R} \cup \mathcal{T}$, which is the intersection point of

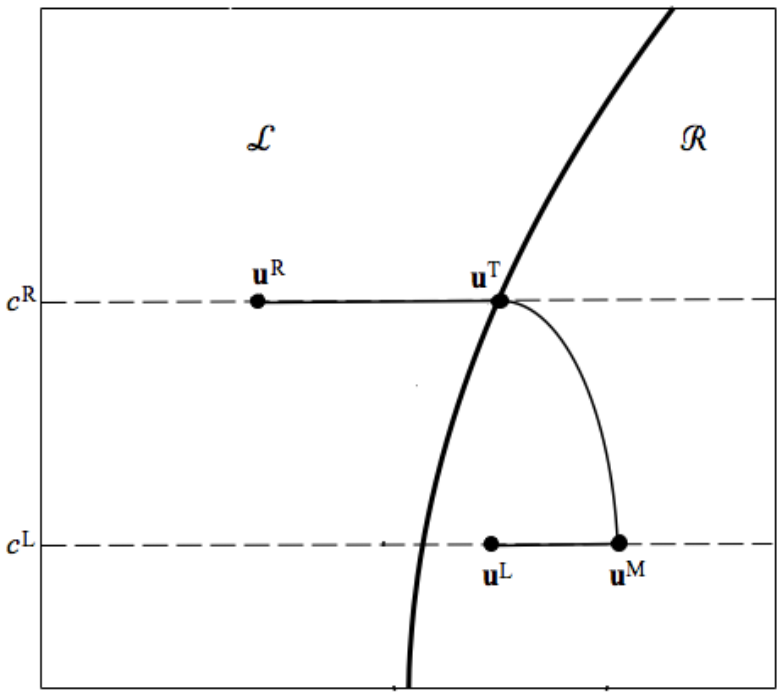

Figure B.19: *Construction of s^K when $\mathbf{u}^M \in \mathcal{L}$ as in Lemma 4(i).*

the line $c = c^L$ and the λ_2-rarefaction curve through $\mathbf{u}^T$. We have the sequence

$$\mathbf{u}^L \xrightarrow{s-wave} \mathbf{u}^M \xrightarrow{c-rarefaction} \mathbf{u}^T \xrightarrow{s-wave} \mathbf{u}^R \tag{B.26}$$

The c-rarefaction is downward ($s^T < s^M$). The form of the first s-wave depends on the saturation values s^L and s^M. Because $\mathbf{u}^M, \mathbf{u}^L \in \mathcal{R} \cup \mathcal{T}$, the corresponding points on the graph of $f(s, c^L)$ lie above the inflection point. This means there are only two choices for this s-wave: a downward rarefaction if $s^L > s^M$ and an upward shock if $s^L < s^M$. The second s-wave is always downward ($s^R < s^T$). Since $a'(c) > 0$, the point $(s^T, f(s^T, c^R))$ on the graph of $f(s, c^R)$ is always above the Welge tangent with respect to s^R, preventing the existence of a single downward shock. Both other s-waves are possible, which leaves a total of four possible solution sequences. To compute examples of these, let $u^L = (0.7, 0.1) \in \mathcal{R}$ and $u^R = (0.3, 0.5) \in \mathcal{L}$ first. We are now in Case 3A and compute $u^T = (0.6901, 0.5)$. The Welge tangent to the graph of $f = f(s, 0.1)$ with respect to s^R is at $s = 0.449872$, so that s-wave will consist of a downward rarefaction wave and a shock wave. The full solution $s_d^{rf} c_d^{rf} s_d^{rf} s_d^{sk}$ is plotted in Figure B.20. The same solution with the downward shock removed is obtained simply by choosing $u^R = (0.5, 0.5) \in \mathcal{L}$, which makes s^R greater than the inflection point on the graph of $f = f(s, 0.5)$ ($s = 0.4002$). See figure B.21. The remaining two cases are similarly constructed (see figures B.22 and B.23).

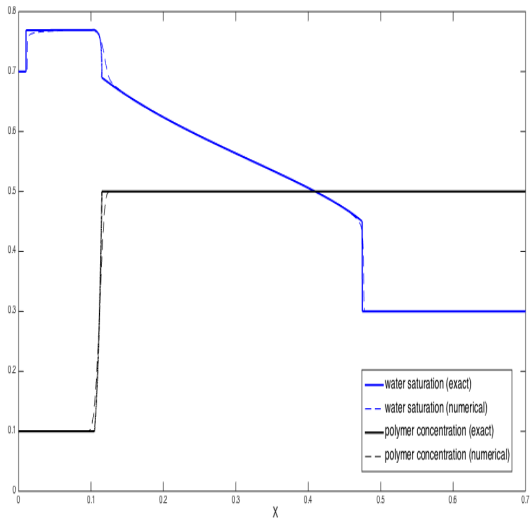

Figure B.20: $s_u^{sk} c_d^{rf} s_d^{rf} s_d^{sk}$,
$u^L = (0.7, 0.1)$, $u^R = (0.3, 0.5)$.

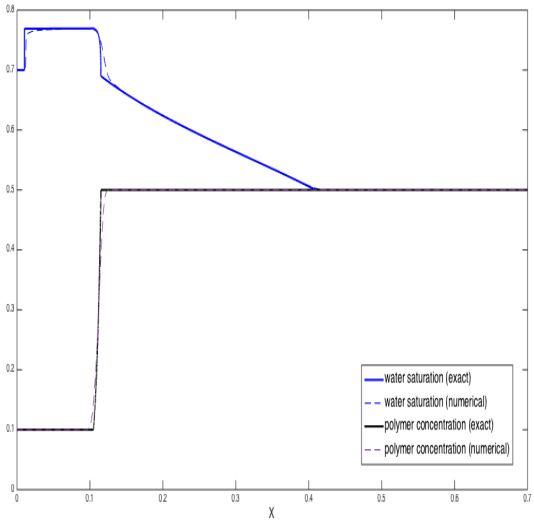

Figure B.21: $s_u^{sk} c_d^{rf} s_d^{rf}$,
$u^L = (0.7, 0.1)$, $u^R = (0.5, 0.5)$.

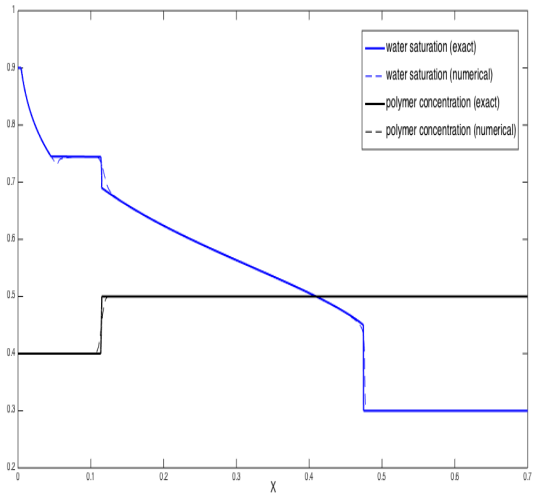

Figure B.22: $s_d^{rf} c_d^{rf} s_d^{rf} s_d^{sk}$,
$u^L = (0.9, 0.4)$, $u^R = (0.3, 0.5)$.

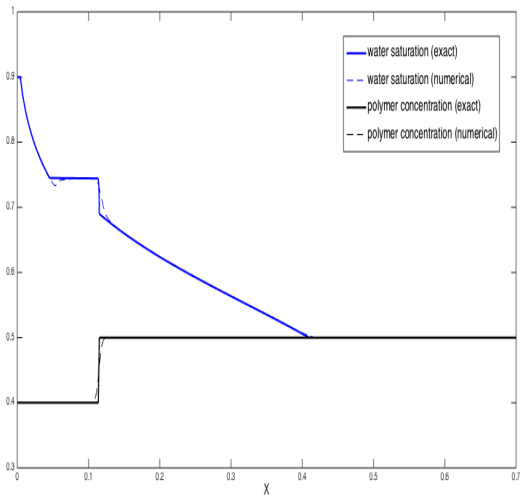

Figure B.23: $s_d^{rf} c_d^{rf} s_d^{rf}$,
$u^L = (0.9, 0.4)$, $u^R = (0.5, 0.5)$.

(B) If $\mathbf{u}^R \in \mathcal{R} \cup \mathcal{T}$, we consider the shorter sequence

$$\mathbf{u}^L \xrightarrow{s-wave} \mathbf{u}^M \xrightarrow{c-rarefaction} \mathbf{u}^R \tag{B.27}$$

where the intermediate state $\mathbf{u}^M = (s^M, c^L) \in \mathcal{R} \cup \mathcal{T}$ is the intersection point of the line $c = c^L$ and the λ_2-rarefaction curve through $\mathbf{u}^R$. This yields two possible solution sequences. For examples of these, we let $\mathbf{u}^L = (0.7, 0.1)$ and $\mathbf{u}^R = (0.7, 0.5)$. Both states are in $\mathcal{R} \cup \mathcal{T}$, so Case 3B occurs. We find $s^M = 0.7714$. The s-wave is now determined by the values s^M, s^L. The Welge tangent with respect to s^M is at $s = 0.0579$ and we therefore obtain a single upward s-shock. The solution $s_u^{sk} c_d^{rf}$

is plotted in Figure B.24. By changing the initial conditions to $u^L = (0.9, 0.4)$ and $u^R = (0.7, 0.5)$, we obtain the other possible solution $s_d^{rf} c_d^{rf}$ (see figure B.25).

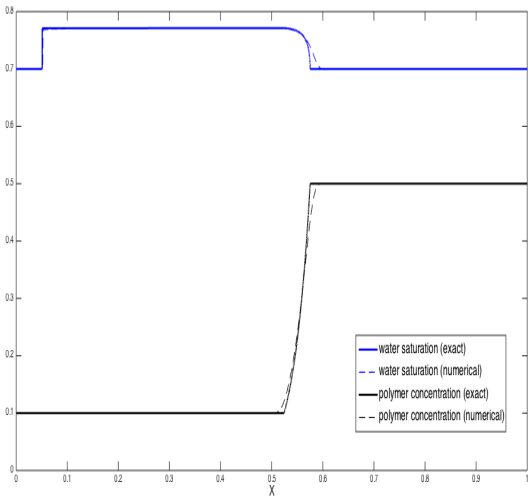

Figure B.24: $s_u^{sk} c_d^{rf}$,
$u^L = (0.7, 0.1)$, $u^R = (0.7, 0.5)$.

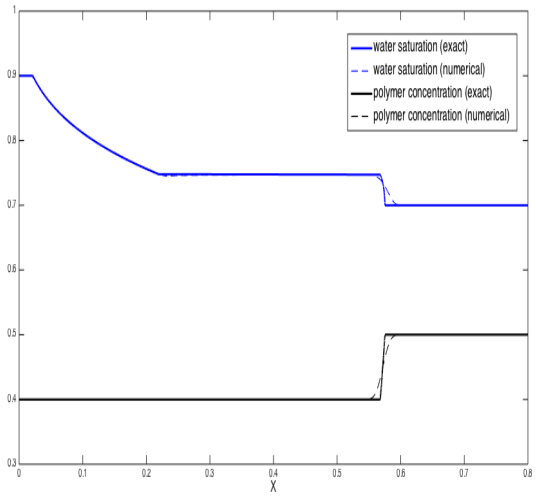

Figure B.25: $s_d^{rf} c_d^{rf}$,
$u^L = (0.9, 0.4)$, $u^R = (0.7, 0.5)$.

B.3.2 Case 4: $c^L < c^R$, $\mathbf{u}^L \in \mathcal{L}$

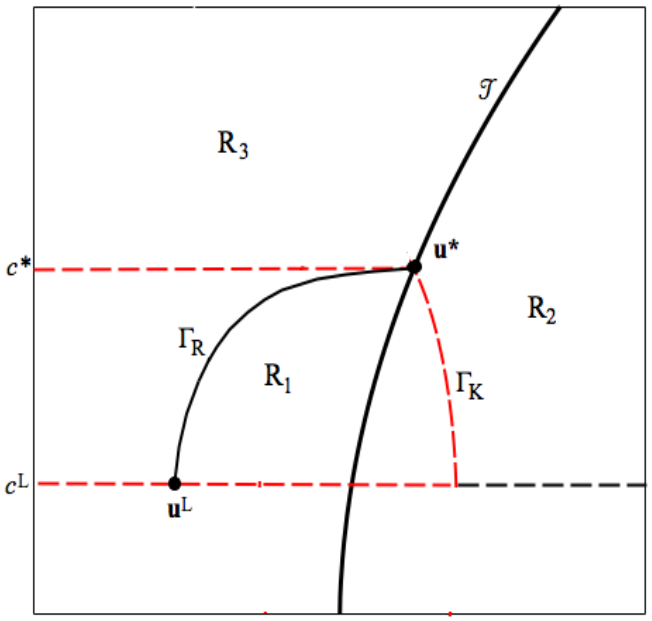

Figure B.26: *The three regions in which u^R might lie.*

Given a state $u = (s, c) \in \mathcal{L}$, we define the critical value $s^K(\mathbf{u})$ such that $(s^K, c) \in \mathcal{R}$ and

$$\frac{f(s,c)}{s + a'(c)} = \frac{f(s^K, c)}{s^K + a'(c)} \tag{B.28}$$

Let Γ_R be the 2-rarefaction curve through $\mathbf{u}^L \in \mathcal{L}$ and let Γ_K be the curve of critical points corresponding to points on Γ_R (see Figure B.26). It was shown in [31] that the curves Γ_R and Γ_K can intersect in at most one point. Let $\mathbf{u}^* = (s^*, c^*)$ be the point where Γ_R and $\mathcal{T}$ intersect. If they don't intersect, we let $\mathbf{u}^* = (s^*, 1)$. Depending on the position of $\mathbf{u}^R$, we consider three sub-cases:

(A) $\mathbf{u}^R \in R_1$, where R_1 is the interior of the region bounded by the lines $c = c^L$, $c = c^*$ and Γ_K (see figure B.26). Let $\mathbf{u}^1 = (s^1, c^R) \in \Gamma_R$ be the intersection of Γ_R with the line $c = c^R$ and consider the sequence

$$\mathbf{u}^L \xrightarrow{c-rarefaction} \mathbf{u}^1 \xrightarrow{s-wave} \mathbf{u}^R \tag{B.29}$$

The s-wave can take any of the six forms of Appendix A. For example, fix the left state $\mathbf{u}^L = (0.365, 0.2) \in \mathcal{L}$. We compute $u^* = (0.7975, 0.9376)$. By choosing the right state $\mathbf{u}^R$ to be in different positions of the region R_1, we can obtain all six possible solutions. Note that, in order to get all downward s-waves, it is necessary to change s^L to a lower value (due to inflection point and Welge tangent). The solution sequences are plotted in Figures B.27-B.32.

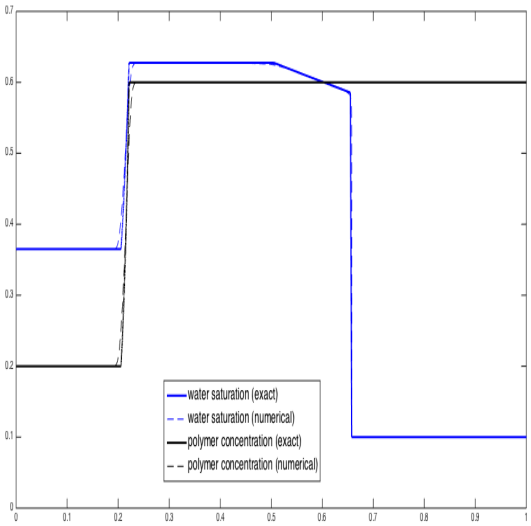

Figure B.27: $c_u^{rf} s_d^{rf} s_d^{sk}$,
$u^L = (0.365, 0.2)$, $u^R = (0.1, 0.6)$

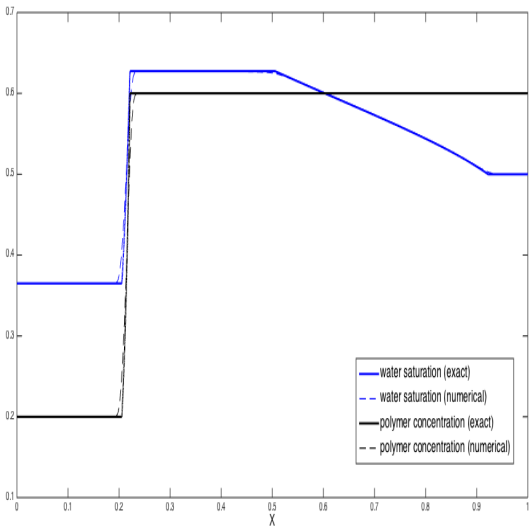

Figure B.28: $c_u^{rf} s_d^{rf}$,
$u^L = (0.365, 0.2)$, $u^R = (0.5, 0.6)$

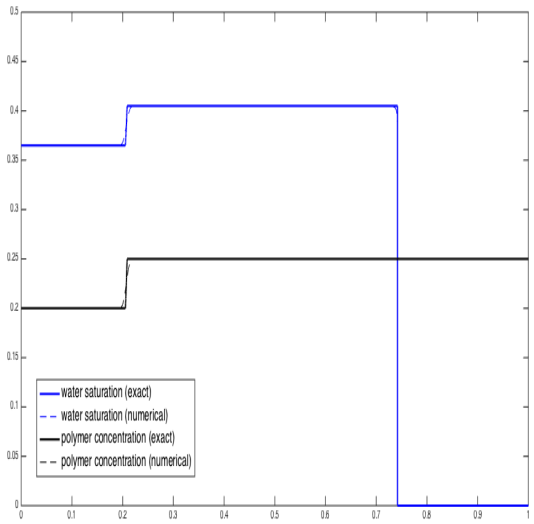

Figure B.29: $c_u^{rf} s_d^{sk}$,
$u^L = (0.365, 0.2)$, $u^R = (0, 0.25)$

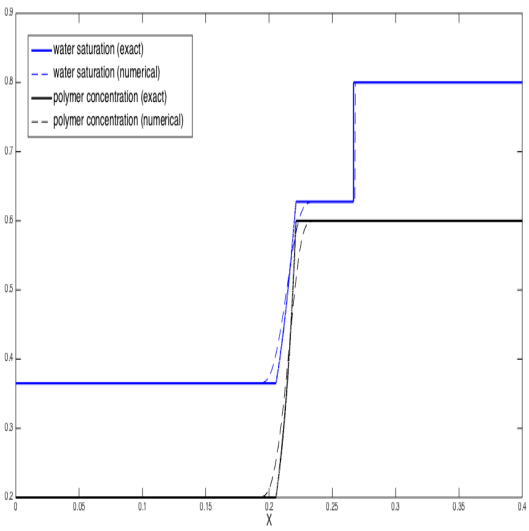

Figure B.30: $c_u^{rf} s_u^{sk}$,
$u^L = (0.365, 0.2)$ and $u^R = (0.8, 0.6)$

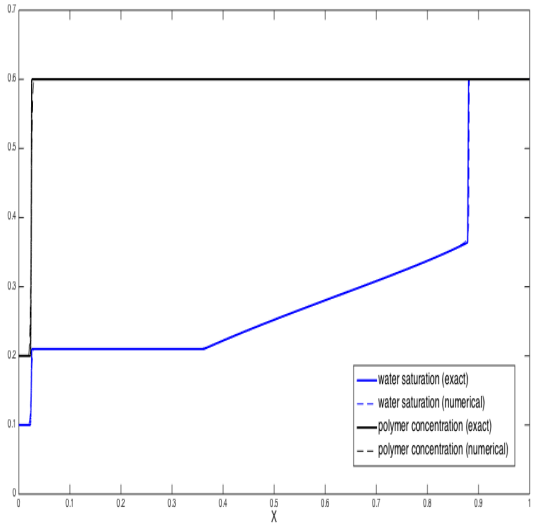

Figure B.31: $c_u^{rf} s_u^{rf} s_u^{sk}$,
$u^L = (0.1, 0.2)$, $u^R = (0.6, 0.6)$

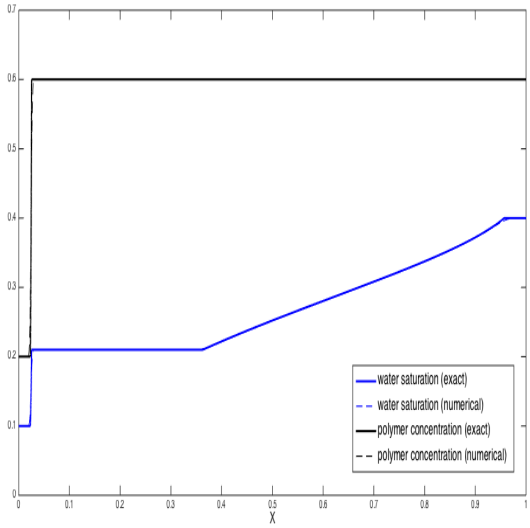

Figure B.32: $c_u^{rf} s_u^{rf}$,
$u^L = (0.1, 0.2)$, $u^R = (0.4, 0.6)$

(B) suppose now that $\mathbf{u}^R \in R_2$, where R_2 is bounded by the line $c = c^L$ and the curves Γ_K and $\mathcal{T}$. Let $\mathbf{u}^2 = (s^2, c^2)$ be the point of intersection of the c-rarefaction curve through $\mathbf{u}^R$ with $\Gamma_K \cup \{c = c^L\}$. There are two possibilities for this intersection. If $c^2 = c^L$, we have the sequence

$$\mathbf{u}^L \xrightarrow{s-wave} \mathbf{u}^2 \xrightarrow{c-rarefaction} \mathbf{u}^R \tag{B.30}$$

Here, $s^L < s^2$ and the point $(s^L, f(s^L, c^L)$ lies above the Welge tangent with respect to s^2, so that the only possible s-wave in an upward shock. The resulting sequence

$s_u^{sk} c_d^{rf}$ is qualitatively similar to the one found in Case 3B (see figure B.24). On the other hand, if $c^2 > c^L$, define $\mathbf{u}^1 = (s^1, c^2) \in \Gamma_R$ and consider the sequence

$$\mathbf{u}^L \xrightarrow{c-rarefaction} \mathbf{u}^1 \xrightarrow{s-wave} \mathbf{u}^2 \xrightarrow{c-rarefaction} \mathbf{u}^R \tag{B.31}$$

The s-wave must be an upward shock, so that the only possible solution sequence is $c_u^{rf} s_u^{sk} c_d^{rf}$. As an example, let's do the entire calculation with $u^L = (0.3, 0.1) \in \mathcal{L}$ and $u^R = (0.77, 0.7) \in \mathcal{R}$. Here, $c^* = 0.7434$, so that u^R lies in region R_2. The c-rarefaction curve through u^R intersects with Γ_K before hitting $c = c^L$. The point of intersection is $u^2 = (0.8140, 0.3962)$. This state is connected via an s-wave to the state $u^1 = (0.5334, 0.3962)$ lying on the left c-rarefaction curve. This s-wave will be an upward shock (the Welge tangent is at $s = 0.1890$ and thus well below s^1 and s^2). Figure B.33 shows a plot of the saturation profile. The shock is sandwiched between an upward and downward c-rarefaction. The numerics start capturing the correct profile only with a very high number of spatial grid-points (> 30000).

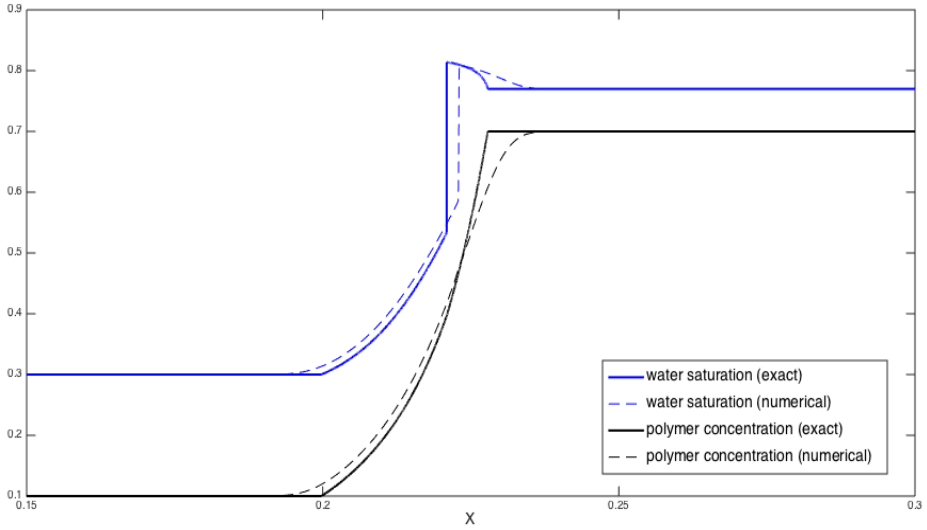

Figure B.33: $u^L = (0.3, 0.1)$ and $u^R = (0.77, 0.7)$

(C) Finally, assume that $\mathbf{u}^R \in R_3$, the region of $\mathcal{L}$ where $c > c^*$. Let $\mathbf{u}^T = (s^T, c^R)$ be the intersection of the line $c = c^R$ and $\mathcal{T}$. We can join $\mathbf{u}^T$ and $\mathbf{u}^R$ by an s-wave. Note that, since $a'(c) > 0$, the point $(s^T, f(s^T, c^R))$ on the graph of $f(s, c^R)$ always above the Welge tangent with respect to s^R. This prevents the formation of a single downward shock, leaving just two possibilities. Since $\mathbf{u}^T \in R_2$, Case 4B gives us a way of connecting $\mathbf{u}^L$ and $\mathbf{u}^T$. This yields the solution sequences $s_d^{rf} c_u^{rf} s_d^{rf}$, $s_u^{sk} c_d^{rf} s_d^{rf}$, $s_d^{rf} c_d^{rf} s_d^{rf} s_d^{sk}$ and $s_u^{sk} c_d^{rf} s_d^{rf} s_d^{sk}$. To demonstrate these, take $u^L = (0.27, 0) \in \mathcal{L}$ and

$u^R = (0.4, 0.6) \in \mathcal{R}$. The left c-rarefaction curve hits the transition curve at $c^* = 0.35695$, which means that $u^R \in R_3$. There will be an s-wave connecting u^R to $u^T = (0.7225, 0.6) \in \mathcal{T}$. This state lies in R_2 and is thus treated in the same way as was done in Case 4B. The c-rarefaction curve through u^T intersects Γ_K at $u^2 \approx (0.7930, 0.2690)$, which is then connected via another s-wave to the state $u^1 = (0.448711, 0.2690)$ on the c-rarefaction curve coming from u^L. The resulting saturation profile is shown in figure B.34. The first part looks the same as the solution plotted in figure 5.38. In this case, the last part is an s-wave consisting of a rarefaction and a shock. An s-rarefaction alone is also possible by adjusting s^R (see figure B.35).

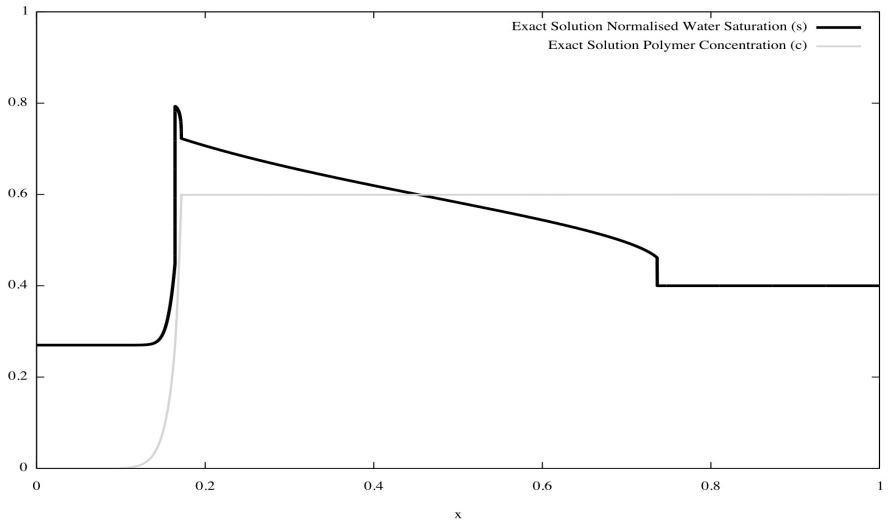

Figure B.34: $u^L = (0.27, 0)$ and $u^R = (0.4, 0.6)$

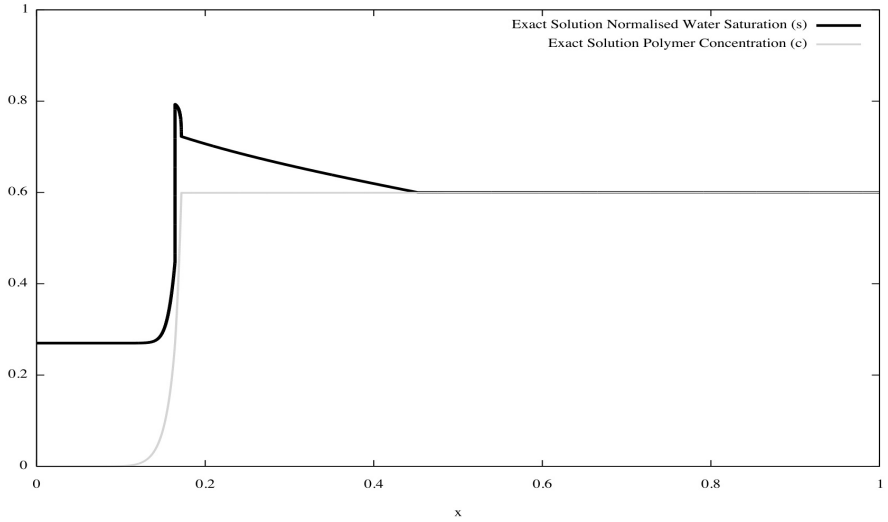

Figure B.35: $u^L = (0.27, 0)$ and $u^R = (0.6, 0.6)$

References

[1] Stiff, H.A., Davis, L.E., *A method for predicting the tendency of oil field waters to deposit calcium sulfate*, Journal of Petroleum Technology, Vol.195, p. 25-28 (1952)

[2] Miles, L., *A New Concept in Scale Inhibitor Formation Squeeze Treatments*, Society of Petroleum Engineers (1970)

[3] Meyers, K. O., Skillman, H. L., Herring, G. D., *Control of Formation Damage at Prudhoe Bay, Alaska, by Inhibitor Squeeze Treatment.*, Society of Petroleum Engineers, 37, p.1019-1034 (1985)

[4] King, G. E., Warden, S. L., *Introductory Work in Scale Inhibitor Squeeze Performance: Core Tests and Field Results*, Society of Petroleum Engineers (1989)

[5] Kerver, J. K., Heilhecker, J. K., *Scale Inhibition by the Squeeze Technique.*, Petroleum Society of Canada, 8, p.15-23 (1969)

[6] Vetter, O. J., *The Chemical Squeeze Process Some New Information on Some Old Misconceptions.*, Society of Petroleum Engineers, 25, p.339-353 (1973)

[7] Trogus, F.J., Sophany, T., Schechter, R.S., Wade, W.H., *Static and Dynamic Adsorption of Anionic and Nonionic Surfactants*, Society of Petroleum Engineers Journal, 17, p.337-344 (1977)

[8] Ramirez, W.F., Shuler, P.J., Friedman, F., *Convection, Dispersion, and Adsorption of Surfactants in Porous Media*, Society of Petroleum Engineers Journal, 20, p.430-438 (1980)

[9] Sorbie, K. S., Wat, R. M. S., Todd, A. C., *Interpretation and Theoretical Modeling of Scale-Inhibitor/Tracer Corefloods*, Society of Petroleum Engineers, 7, p.307-312 (1992)

[10] Sorbie, K.S. , Yuan, M.D., Todd, A.C., Wat, R.M.S., *The Modelling and Design of Scale Inhibitor Squeeze Treatments in Complex Reservoirs*, Society of Petroleum Engineers (1991)

[11] Sorbie, K. S., Gdanski, R. D., *A Complete Theory of Scale Inhibitor Transport, Adsorption/Desorption and Precipitation in Squeeze Treatments.*, Society of Petroleum Engineers (2005)

[12] Ayawei, N., Ebelegi, A.N., Wankasi, D., *Modelling and Interpretation of Adsorption Isotherms*, Hindawi Journal of Chemistry (2017)

[13] Kahrwad, M., Sorbie, K. S., Boak, L. S., *Coupled Adsorption/Precipitation of Scale Inhibitors: Experimental Results and Modeling*, Society of Petroleum Engineers, 24, p.481-491 (2009).

[14] Sorbie, K. S., *A General Coupled Kinetic Adsorption/Precipitation Transport Model for Scale Inhibitor Retention in Porous Media: I. Model formulation*, Society of Petroleum Engineers (2010)

[15] Vazquez, O., Sorbie, K. S., Mackay, E. J., *A General Coupled Kinetic Adsorption/Precipitation Transport Model for Scale Inhibitor Retention in Porous Media: II. Sensitivity Calculations and Field Predictions*, Society of Petroleum Engineers (2010)

[16] Sorbie, K. S., *A Simple Model of Precipitation Squeeze Treatments*, Society of Petroleum Engineers (2012).

[17] Zhang, H., Mackay, E. J., Chen, P., Sorbie, K. S., *Non-Equilibrium Adsorption and Precipitation of Scale Inhibitors: Corefloods and Mathematical Modelling*, Society of Petroleum Engineers (2000)

[18] Yuan, M. D., Sorbie, K. S., Todd, A. C., Atkinson, L. M., Riley, H., Gurden, S., *The Modelling of Adsorption and Precipitation Scale Inhibitor Squeeze Treatments in North Sea Fields*, Society of Petroleum Engineers (1993)

[19] Malandrino, A., Yuan, M. D., Sorbie, K. S., Jordan, M. M., *Mechanistic Study and Modelling of Precipitation Scale Inhibitor Squeeze Processes.*, Society of Petroleum Engineers (1995).

[20] Van Genuchten, M. Th., Alves, W. J., *Analytical Solutions of the One-Dimensional Convective-Dispersive Solute Transport Equation*, U.S. Department of Agriculture, Technical Bulletin No. 1661, p.151 (1982)

[21] Kumar, A., Jaiswal, D.K., Kumar, N., *Analytical solutions to one-dimensional advection-diffusion equation with variable coefficients in semi-infinite media*, J. Earth Syst. Sci. 118, No. 5, pp. 539-549 (2009)

[22] Prez Guerrero, J.S., Skaggs, T.H., *Analytical solution for one-dimensional advection-dispersion transport equation with distance-dependent coefficients*, Journal of Hydrology, 390, p.57-65 (2010)

[23] Hong, S.-A., Shuler, P. J., *A Mathematical Model for the Scale Inhibitor Squeeze Process.*, Society of Petroleum Engineers (1987).

[24] Shuler, P. J., *Mathematical Model for the Scale-Inhibitor Squeeze Process Based on the Langmuir Adsorption Isotherm.*, Society of Petroleum Engineers (1993)

[25] Bracewell, R., *Heaviside's Unit Step Function, H(x). The Fourier Transform and its Applications*, McGraw-Hill (2000)

[26] Rhee, H-K. , Aris, R. and Amundson, N.R., *First Order Partial Differential Equations, Vol. 2, Theory and Application of Hyperbolic Systems of Quasi-linear Equations*, Prentice Hall (1989)

[27] Buckley, S. E., Leverett, M. C., *Mechanism of Fluid Displacement in Sands.*, Society of Petroleum Engineers, 146, p.107-116 (1942)

[28] Allen, F.R., *A Note On Buckley-Leverett Theory*, AEE Winfrith (1979)

[29] Dake, L.P., *Fundamentals of Reservoir Engineering*, Elsevier Scientific Publishing Company (1978)

[30] Kenneth S. Sorbie, *Polymer-Improved Oil Recovery*, Blackie and Son Ltd (1991)

[31] Johansen, T., Winther, R.: *The solution of the Riemann Problem for a Hyperbolic System of Conservation Laws modelling Polymer Flooding*, Society for Industrial and Applied Mathematics (1988)

[32] Alinhac, S.: *Hyperbolic Partial Differential Equations*, Springer (2009)

[33] Ockendon, J., Howison,S., Lacey, A., Movchan, A., *Applied Partial Differential Equations*, Oxford University Press (2003)

[34] Holden, H, Risebro, N.H., *Front Tracking for Hyperbolic Conservation Laws*, Springer (2002)

[35] P.D. Lax, *Hyperbolic systems of conservation laws II*, Communications on pure and applied mathematics, 10, p.537-566 (1957)

[36] Smoller, J., *Shock-Waves and Reaction-Diffusion Equations*, Springer (1994)

[37] LeVeque, R.J., *Numerical Methods for Conservation Laws*, Birkhauser (1992)

[38] Tadmor, E., *A Review of Numerical Methods for Nonlinear Partial Differential Equations*, Bulletin of the American Mathematical Society, Vol. 49, p.507-554 (2012)

[39] Shapira, Y., *Solving PDEs in C++: Numerical Methods in a Unified Object-Oriented Approach*, Society for Industrial and Applied Mathematics (2012)

[40] Hirsch, M.W., Smale, S., Devaney, R.L.: *Differential Equations, Dynamical Systems & An Introduction to Chaos*, Elsevier (2004)

[41] Corless, R.M, Gonnet, G.H, Hare, D.E.G., Jeffrey, D.J., Knuth, D.E., *On the Lambert W function*, University of Waterloo Computing Centre (1993)

[42] Krantz, S.G. and Parks, H.R., *The Implicit Function Theorem*, Birkhauser, Springer Science and Business media (2012)

[43] Lake, L.W., *Enhanced Oil Recovery*, Prentice-Hall, Inc. (1989)